Order Number 9104742

Simulation of a high-speed hermetic compressor with special attention to gas pulsations in three-dimensional continuous cavities

Kim, Jonghyuk, Ph.D.

Purdue University, 1988

U·M·I
300 N. Zeeb Rd.
Ann Arbor, MI 48106

PURDUE UNIVERSITY

Graduate School

This is to certify that the thesis prepared

By Kim, Jonghyuk

Entitled Simulation of a High Speed Hermetic Compressor
with Special Attention to Gas Pulsations
in Three Dimensional Continuous Cavities

Complies with University regulations and meets the standards of the Graduate School for originality and quality

For the degree of Doctor of Philosophy

Signed by the final examining committee:

Werner Soedel, chair

James F. Doyle

James F. Hamilton

John M. Starkey

Approved by the head of school or department:

Jan. 29 1988 WMP/W. J. Wiedemann
School of Mechanical Engineering

This thesis ☒ IS NO LONGER ☐ ~~IS NOT~~ to be regarded as confidential

Werner Soedel
Major professor

Grad School
Form No. 9
Revised 9-85

7-16-90
LLV

SIMULATION OF A HIGH SPEED HERMETIC COMPRESSOR WITH SPECIAL ATTENTION TO GAS PULSATIONS IN THREE DIMENSIONAL CONTINUOUS CAVITIES

A Thesis

Submitted to the Faculty

of

Purdue University

by

Jonghyuk Kim

In Partial Fulfillment of the

Requirements for the Degree

of

Doctor of Philosophy

May 1988

This thesis is dedicated

to my wife Chula

ACKNOWLEDGEMENT

I wish to place on record my sincere thanks to Professor Werner Soedel for his careful guidance and constant encouragement throughout this research. I am also grateful to Dr. James F. Hamilton, Dr. Robert J. Bernhard, and Dr. James F Doyle for serving on my advisory committee.

Special thanks are expressed to the staff of Ray W. Herrick Laboratories, in particular Director Raymond Cohen for providing a stimulating work environment. Also, I am thankful to Necchi S.p.A., Italy, for their sponsorship of the research.

It is beyond my ability to find appropriate words to appreciate my parents, who have been far away in Korea, but have been always in my mind during the study. Finally, I express my deepest gratitude to my wife Chula and daughter Chris Seoyoung, not only for enduring through everything, but also their constant love and encouragement during the period of research.

TABLE OF CONTENTS

LIST OF TABLE

LIST OF FIGURE

LIST OF SYMBOLS

Symbol	Description
A,B,C,D	four pole parameters
A_i	Lame parameter of a general curvilinear coordinate
C_{eq}	equivalent damping coefficient
C_p	constant pressure specific heat
C_v	constant volume specific heat
J_n	Bessel function of the first kind
I_n	modified Bessel function of the first kind
K_n	modified Bessel function of the second kind
P	complex amplitude of the acoustic pressure
P_k	k^{th} natural mode in terms of pressure
Q	complex amplitude of the volume flow
R	gas constant
R(r)	radial direction natural mode
S	cross sectional area of a pipe
T	temperature
V_c	clearance volume of the compressor cylinder
V(t)	instantaneous cylinder volume
V_o	volume of an acoustic cavity
W_c	work done by the compressor piston

Y_n	Bessel function of the second kind
$Z(z)$	vertical direction natural mode
Z_o	input point impedance
Z_{soo}	impedance of the side branch
$f(\underline{r},\omega)$	pressure response of the system due to a unit input volume flow
g_c	gravity constant
h	enthalpy
k	adiabatic constant or wave number
m_{eq}	equivalent mass of the valve
$\dot{m}$	mass flow rate through the valve port
$\underline{r}$	position vector
t	time
$\underline{u}$	acoustic velocity of the gas particle
$\Theta(\theta)$	circumferential direction natural mode
β	coefficient of the performance of refrigeration system
γ	pressure ratio of the valve flow ($\frac{P_u}{P_d}$)
δ_{st}	static deflection of the valve
$\delta(\underline{r})$	Dirac delta function in the space
κ	frequency parameter of the annular cavity
η	thermodynamic efficiency of the compressor
$\eta_k(t)$	modal participation factor of the acoustic equation
ξ	displacement of the mass neck of the gas in a short pipe
ξ_k	nondimensional damping coefficient of the valve

ϕ	phase angle
ω	frequency in terms of rad/sec

SUBSCRIPTS IN GENERAL

Subscript	Description
an	anechoic termination
d	discharge condition or downstream
eq	equivalent
i	i^{th}
k	k^{th}
L	output condition
o	average or output condition
s	suction condition
u	upstream

ABSTRACT

Kim, Jonghyuk. Ph. D., Purdue University, May 1988. Simulation of High Speed Hermetic Compressor with Special Attention to Gas Pulsations in Three Dimensional Continuous Cavities. Major Professor : Werner Soedel, School of Mechanical Engineering

This study is on the modeling and analysis of hermetic refrigeration compressors for the prediction of thermodynamic performance and gas pulsations.

A computer simulation model of a hermetic, reciprocating compressor has been developed to study basic performance and gas pulsations of compressors. The mathematical models are based on the polytropic process assumption for the cylinder process and a linear acoustic model for gas pulsations. To supplement the theoretical model, pressure measurements and valve motion measurements were conducted as fundamental experiments. Thermodynamic and acoustic performances of a prototype compressor were studied using the computer simulation program.

A general procedure has been developed to analyze complex acoustic systems composed of multiply connected three dimensional continuous cavities. The four pole

parameter concept was used as a fundamental tool for the system analysis. An approach to obtain the four pole parameters of an acoustic system from its pressure response solutions was developed. Pressure pulsations in the suction gas path including the shell cavity resonance effect were analyzed as an application example. For the response solution of the hermetic shell cavity, the eigen-function expansion method was used to model the cavity as an annular cylinder.

Design parameter studies for the thermodynamic efficiency improvement of the prototype compressor were conducted using the developed computer simulation program. Special concept mufflers for passive noise control in the suction gas path were studied using advanced features of the simulation program.

CHAPTER 1 - INTRODUCTION

1.1 General

The development of a reliable and efficient design procedure has become very important in modern compressor engineering since the advent of high speed compressors. Numerous experimental and theoretical investigations have been done on compressors with this goal in mind. Areas of concern and interest of the research described in the following were :

1. Improvement of thermodynamic efficiency (gas pulsation, thermodynamics, fluid mechanics) ;
2. Reduction of noise level (acoustics, vibrations) ;
3. Design of compressor valves and critical parts (vibrations,dynamics,stressanalysis).

In general, a cycle of operation of a high speed positive displacement compressor can be viewed as a number of complicated phenomena which interact with each other in a short time period. Thermodynamic processes in the cylinder, gas pulsations in the gas path, or valve motions cannot be studied separately without considering mutual

effects. For this reason, computer simulation techniques have become an essential part of compressor research and development.

A computer simulation program based on a mathematical model which includes cylinder processes, valve dynamics, valve flow, and gas pulsations provides a valuable tool to the designer and the researcher. Piston work, thermodynamic efficiency and loss, volumetric efficiency and mass flow rate are basic information for performance research. Gas pulsations and muffler performance studies can be done as applications of the program to noise research. Also, excitation forces by the cylinder gas pressure and expected valve motions can be obtained as basic data for dynamics research.

Some basic experimental measurements are necessary to provide experimental parameters such as damping coefficients and polytropic coefficient for a reliable simulation. Also, experimental results are needed to verify the accuracy of the simulation model. In this research, dynamic pressures in cylinder, suction cavity, discharge cavity, and valve motions were measured. Experimental work is also important and useful in its own right because it gives valuable information on the prototype compressor such as measured indicator diagrams and valve motions.

It has been two decades since the computer simulation model with a gas pulsation model was developed[3]. In this research the gas pulsation model was extended to include continuous three dimensional cavities. A general method for the analysis of gas pulsations inside the shell cavity was developed and included in the simulation model for the first time.

Also, the gas pulsation models were made more efficient by utilizing the four pole technique for all acoustic elements. This was possible since a new iterative solution technique was developed that allows treatment of the thermodynamic and flow process in the time domain utilizing frequency domain information for the manifolds. The four pole technique is a very attractive method because it is computationally very efficient and it allows great flexibility for modeling of various gas path configurations[7]. The developed computer simulation program is able to handle virtually all practical gas manifold systems for both the suction and discharge side.

Gas pulsations in the hermetic shell cavity were observed as one of major noise sources by many investigators[4,5,6,7]. Therefore gas pulsations inside the shell cavity were investigated in conjunction with the simulation program development. For the formulation of four pole parameters, an eigenfunction expansion method was employed by idealizing the cavity as an annular cylindrical

geometry. However any general cavity can be formulated by the general procedure developed provided its natural frequencies and natural modes are available. The procedure was extended to multiply connected three dimensional cavities.

Although the prototype compressor for this research was a reciprocating type compressor, certain results can easily be applied to other types of compressor by way of minor modifications. Especially the procedure of formulating four pole parameters for three dimensional cavity and multiply connected three dimensional cavities can be applied to other product designs such as automotive mufflers and pump driven fluid filled reactor vessels.

1.2 Literature Review

1.2.1 Compressor Simulation

In the early stage of the compressor research, the cylinder process and gas pulsations were investigated separately[8,19]. The compression process in the cylinder was modeled without coupling the cavity and piping pulsation pressures, and the gas pulsation was analyzed vice versa. Wambsgans and Cohen[9] developed one of the first detailed simulation models, but without considering gas pulsation. It was based on the polytropic process assumption with detailed valve motions and mass flow models, and is still used as a basic procedure for the

simulation of compressors.

In fact, the cylinder process and gas pulsation in the compressor line should be combined together because there are strong dynamic interactions between them. Brablik[3] was the first who combined the cylinder process simulation and gas pulsation analysis in the compressor lines. The simulation program integrates the thermodynamic process in the cylinder based on the polytropic process assumption, valve dynamics equation, and nonsteady gas pulsation equations simultaneously.

In modeling gas pulsation, the linearized acoustic theory has been widely and successfully used for small compressors[1,8,10]. The linear theory is reported to give valid results for cases in which the amplitude of the perturbed pressure is smaller than 15% of the mean pressure[1,11]. This condition is satisfied for most compressor applications.

Most gas pulsation models of the compressor are based on one dimensional wave theory[1,3,10,11,25,26,27]. This is because typical components in the compressor gas manifold are small compared to the smallest wave length of general interest[1], and, the solution procedure becomes simple to use. Lumped parameter models were introduced and have been widely used for the modeling of small volumes in the compressor gas path, such as a discharge volume, not

necessarily of one dimensional shape but relatively small[1,11,13]. Padilla-Navas et al. first used the Helmholtz resonator model for the analysis of compressor gas manifolds[13]. It was a serial combination of two lumped parameter acoustic elements of small volume and short neck. It is a very useful model because it is simple to formulate and well suited for the geometry of many compressor gas manifolds. Mutyala and Soedel[14] applied this model to the analysis of a two stroke engine manifold. Also, there are many other application examples [1,15,16,24].

Several methods can be used to combine the gas pulsation equation and the cylinder equation. The intuitively simplest way is to integrate all related equations numerically in the time domain [17,18,20]. However, other methods may offer greater advantages. For example, the gas pulsation equations can be solved analytically by mode superposition without relying on time consuming numerical integration. The excitation of the gas pulsation is provided by volume flow rates through valve ports calculated from the cylinder process simulation. This approach gives better flexibility in the mathematical modeling and computer programimng because the gas pulsation model can be independently formulated. However, we need to employ the fast Fourier transform and inverse fast Fourier transform techniques to connect the frequency domain and

the time domain because the cylinder process is solved in the first and the gas pulsation equation is solved in the last.

Elson and Soedel[10] were the first to employ this method. They modeled the gas path of a discharge system with a long pipe using impedance approach and finite difference technique. They calculated the flow through valve port assuming constant discharge line pressure. The unsteady line pressure is obtained by solving the pulsation model in the frequency domain using the calculated mass flow as excitation functions. Then the whole procedure is repeated until convergence is achieved. In fact this method was used as one of basic procedures in this research except that it was somewhat extended and modified.

Singh[11],Miller and Hatten[21], and Abe et al.[22] used transfer matrices to formulate acoustic equations of the gas cavity. This procedure is attractive because it is computationally very efficient , and it allows an acoustic element to be attached to or removed from the system easily by simple matrix manipulations. Singh utilized the four pole parameters to formulate transfer matrices of a complex acoustic system.

Singh and Soedel[11] developed an experimental procedure to measure transfer matrices of general acoustic cavities which are difficult to model as a lumped element

or one dimensional acoustic element. This work was extended recently for three dimensional acoustic cavities by Kung and Singh[23].

For this work, four pole transfer matrices were developed and used exclusively for gas pulsation modeling. Typical elements of compressor gas manifolds, such as resonators, short pipes, finite length pipes, and long pipes with anechoic ends, and three dimensional cavities were formulated into four pole matrices. Some special techniques were developed to handle complex combinations of these elements such as side branches and multiply connected elements.

1.2.2 Gas Pulsations in the Annular Shell Cavity

A typical arrangement of the gas pulsation system of the compressor is shown in Figure 1.1. Obviously, the gas cavity in the cylinder shell is also subjected to acoustic pulsation. Therefore this cavity should be included in a complete modeling of gas pulsations. Acoustic waves will be reflected back to the system from this cavity, which affect the analysis of the system by some amount. In the past, it was assumed that this effect was negligible. Especially for traditional designs, the effect on the thermodynamic efficiency prediction was thought to be very small because the volume of the shell cavity is relatively much larger than the suction cavity volumes in the intake

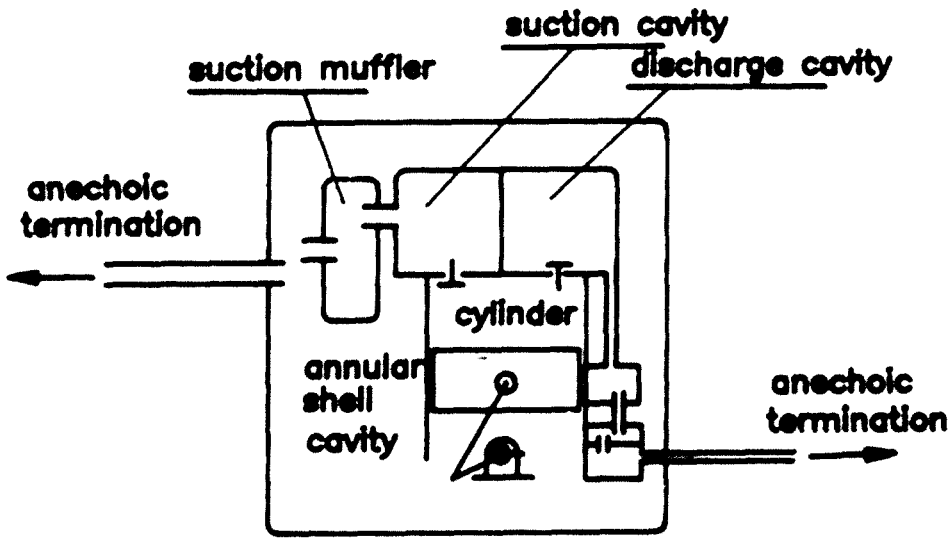

Figure 1.1 - Gas Pulsation Manifold in Compressor

manifold. For the novel design contemplated by the sponsor, this may not be true any longer.

No matter what design, the effect of gas pulsation in the shell cavity on noise generation has always been recognized as important[6,7,29,30]. Johnson and Hamilton[4,5] were the first who pointed out the importance of shell cavity resonances. They investigated cavity resonances using a two-dimensional annular model and attempted to interpret the effect on the measured sound level. This effect was also measured by Roys[7]. Recently, Noguchi, et al.[6] reported experimental results which show that the cavity resonance was the most important noise effect for their small rotary compressor. Experimentally, Kung and Singh[23,30] measured the transfer function of this type of cavity. Also they calculated transfer functions of annular-like cavities by the finite element method.

There is some literature concerning annular cavity acoustics problems applied to engineering problems not connected to compressor research. Au-Yang solved the free and forced vibration problem of an annular cavity container filled with fluid by the modal expansion method[31,32], but did not give four poles, Gazig solved an elastic wave propagation problem in an infinite cylinder and annular cylinder[33]. Also, there are some investigations of the rectangular cavity, its forced response, and interaction

with bounding structures [34,35].

1.3 Scope of Investigation

Chapter 2 is concerned with experimental work conducted during this research. Instrumentation and techniques of dynamic pressure and valve motion measurements are described in detail. The method to obtain experimental indicator diagrams and to extract the necessary information for the simulation model such as polytropic coefficients from measured data are discussed. The performance of the prototype is evaluated from measured data by calculating thermodynamic efficiencies and losses.

Major potential errors which may arise during the experiment are identified. Specifically, influences of pressure transducer gain errors and top dead center pick up error on performance evaluation of the compressor are discussed qualitatively and quantitatively.

In chapter 3, the mathematical model and the solution procedure of the computer simulation are presented. Basic mathematical models for the cylinder process, valve dynamics, and mass flow through the valve port are described. The modeling of gas pulsations of lumped parameter elements and one dimensional elements is presented in this chapter using the four pole parameter concept, while the three dimensional acoustic element is treated in the subsequent chapter.

Also there are discussions on the simulation algorithm that combines the frequency domain analysis (gas pulsation analysis) and the time domain analysis (cylinder process). A modified iteration scheme is used to overcome unstable convergence tendencies. Simulation results are compared to measured data for several cases in terms of indicator diagrams, pulsating pressures, and resulting thermodynamic efficiencies.

Chapter 4 is dedicated to the analysis of gas pulsations in the annular shell cavity. A general procedure for the formulation of four pole parameters of three dimensional cavities was established using an eigenfunction expansion method in curvilinear coordinates. Then, the compressor shell cavity is approximated as an annular cylindrical cavity and its four pole parameters are calculated as a specific example. Several application examples important for compressor noise control are demonstrated.

In chapter 5, the result of chapter 4 is extended to more complex acoustic systems. A general procedure is developed for the analysis of a system composed of two multiply connected large cavities. A large annular cylindrical cavity connected to a small lumped parameter volume is taken as an example. The response of the system which is connected to an anechoic pipe is obtained by utilizing the four pole parameter technique. Also, passive

noise control techniques to reduce pressure pulsations inside of the annular cavity are discussed.

In chapter 6, design improvements of the compressor are discussed. At first, various suction return systems and suction muffler designs are compared with each other in terms of volume flow transfer functions and excited pressure levels. Also, important design parameters which influence the thermodynamic performance of the compressor are identified and studied.

The achievements of the research are summarized in the last chapter.

CHAPTER 2 - EXPERIMENTAL MEASUREMENTS

2.1 Introduction

There are three major objectives for this experimental work. The first is to estimate the basic performances of a prototype compressor, such as overall thermodynamic efficiencies and losses. The second is to identify any existing design problems by examining experimental results. The last is to get useful informations for the later theoretical simulations, such as polytropic coefficients for the compression and expansion process.

Of all measurements, pressure volume diagrams which are converted from pressure time diagrams are the most important. Thus, the cylinder pressure and gas pulsation pressures at suction and discharge cavities were measured as function of time. Because these pressures are high frequency dynamic pressures, piezo-electric type transducers had to be used. Valve opening periods and instants were used as reference data to set absolute pressure levels. After setting absolute pressure levels, pressure-time diagrams were converted to pressure volume diagrams utilizing the crank position measurement and kinematic relationship of the compressor.

Like for all practical experiments, some amount of measurement error is unavoidable. The influence of these errors on the estimation of overall performance will be discussed in the last part of this chapter.

2.2 Pressure Measurements

2.2.1 Instrumentation

Measurement of pressure is the most important laboratory experiment. Pressures are measured as function of time in the cylinder, suction and discharge cavities. Measured pressure data with the information of crank angles and valve motions can be converted to P-V diagrams which enable us to visualize the thermodynamic losses due to gas pulsations and valve restrictions.

Because the prototype is a high speed type compressor (3600 rpm), piezo electric type pressure transducers had to be used to measure high frequency responses. But one difficulty of the piezo-electric type transducer is that it can measure only dynamic pressure. Therefore, a reference point is needed to get the absolute pressure levels of measured pressure. Discharge valve or suction valve opening time can be such a reference point, at which time the cylinder pressure is the same pressure as either the pressure in the suction or discharge plenum.

Pressure transducers and valve lift proximity probes were installed on different cylinder heads. Because the prototype is a small compact type compressor, two pressure transducers and two valve motion proximity probes could not be installed in the same cylinder head, without disrupting the original system significantly.

Six different operating conditions were selected for the experiment. At each condition, pressures and valve motions were measured separately using different cylinder heads. The conditions were kept as identical as possible. Suction and discharge pressure conditions of the experiment are listed in Table 2.1

The test set-up is illustrated in Figure 2.1. Suction, discharge, cylinder pressure and magnetic pick-up signals were recorded by a Nicolet Oscilloscope. Suction and discharge line temperatures and shell cavity temperatures were monitored to ensure that the compressor has steady state running conditions. All pressure transducers were mounted directly to the cavities using adaptors. The details of mounting are shown in Figure 2.2 and Figure 2.3.

Figure 2.4 shows the calibration curves for the pressure transducers. Due to the necessity of frequent opening of the compressor for instrumentations, the compressor shell was modified to have a flange. The

TABLE 2.1 - Operating Conditions of the Experiment

Experiment	Pressure (psig)		Temperature (^{o}F)		Experimental Polytropic Coefficient	1 Cycle time (m sec)
	Suction	Discharge	Suction	Discharge		
1	11	185	40.5	214.0	1.0461	17.6
2	10	200	39.0	220.5	1.0845	17.58
3	10	220	42.5	230.2	1.0944	17.6
4	20	185	36.5	231.5	1.1094	17.82
5	15	180	39.7	195.5	1.1761	17.5
6	15	160	41.1	204.0	1.0484	17.5

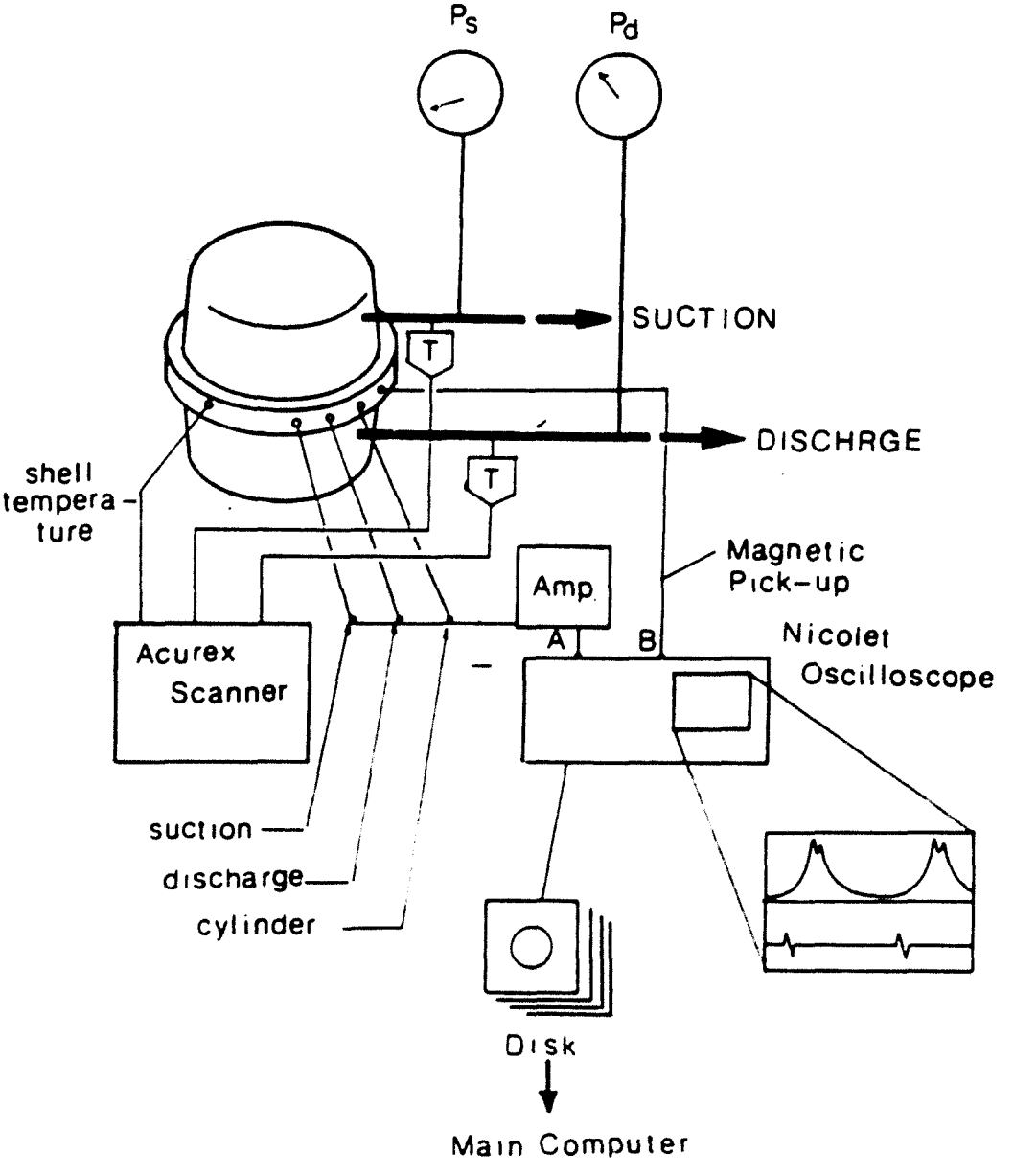

Figure 2.1 - Test Setup for the Pressure Measurement

Figure 2.2 - Pressure Transducers Installed

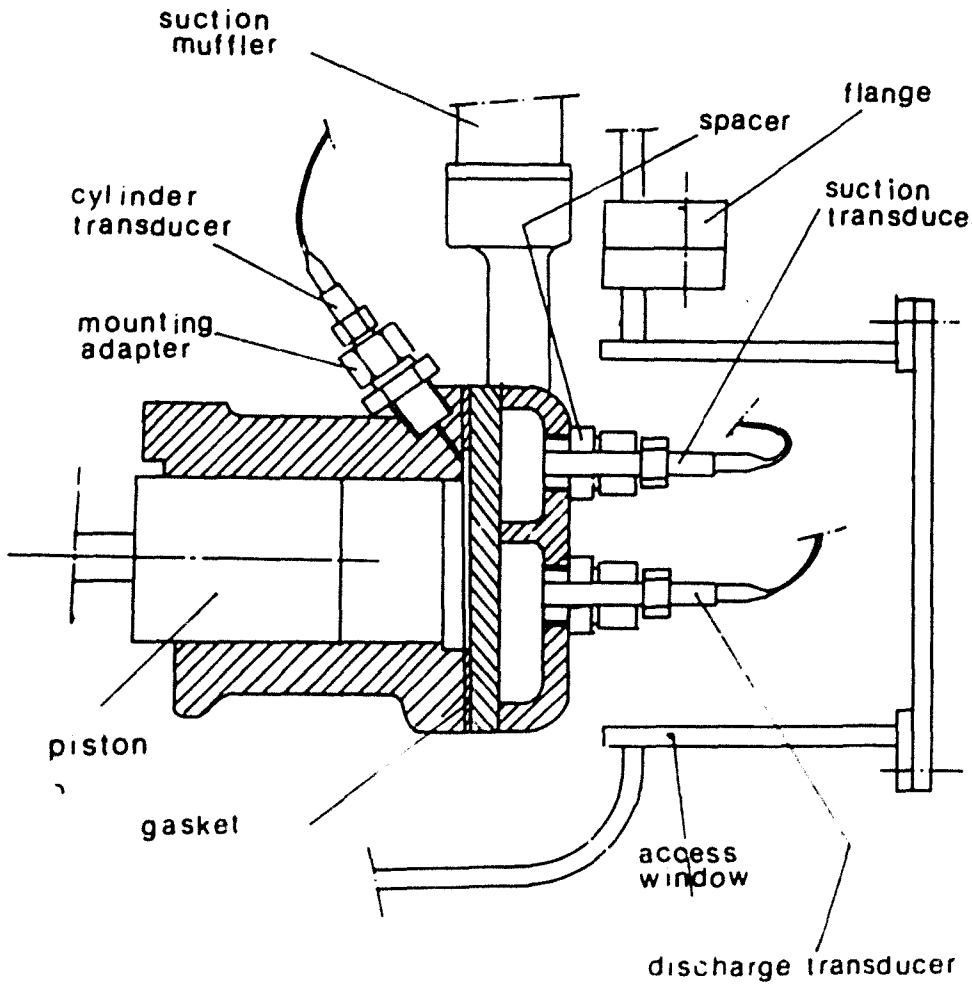

Figure 2.3 - Installation of Pressure Transducers

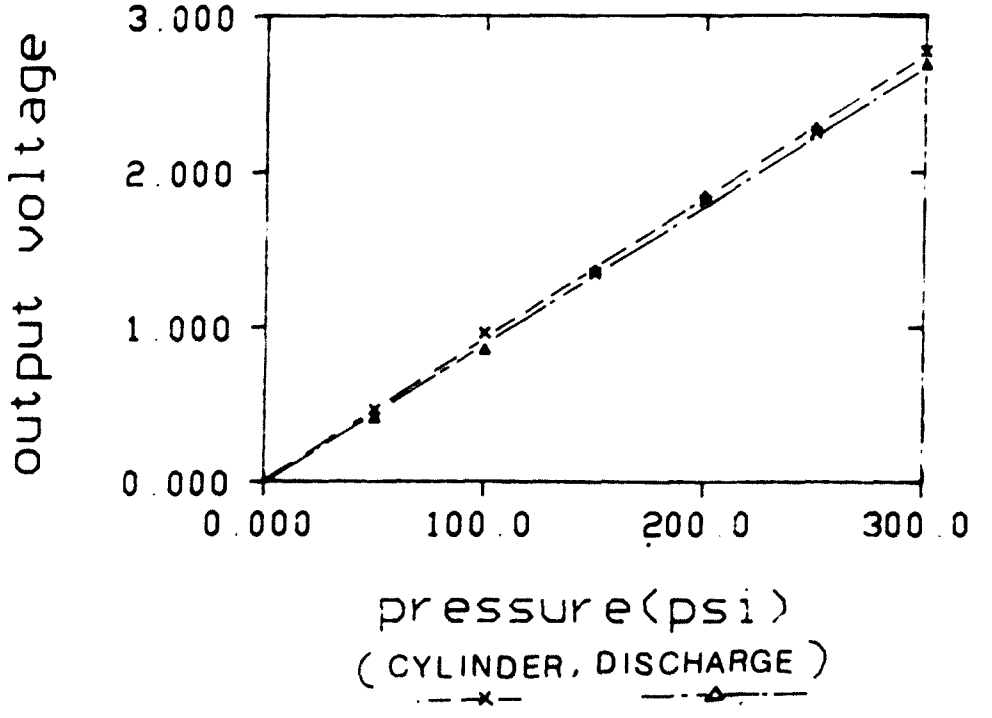

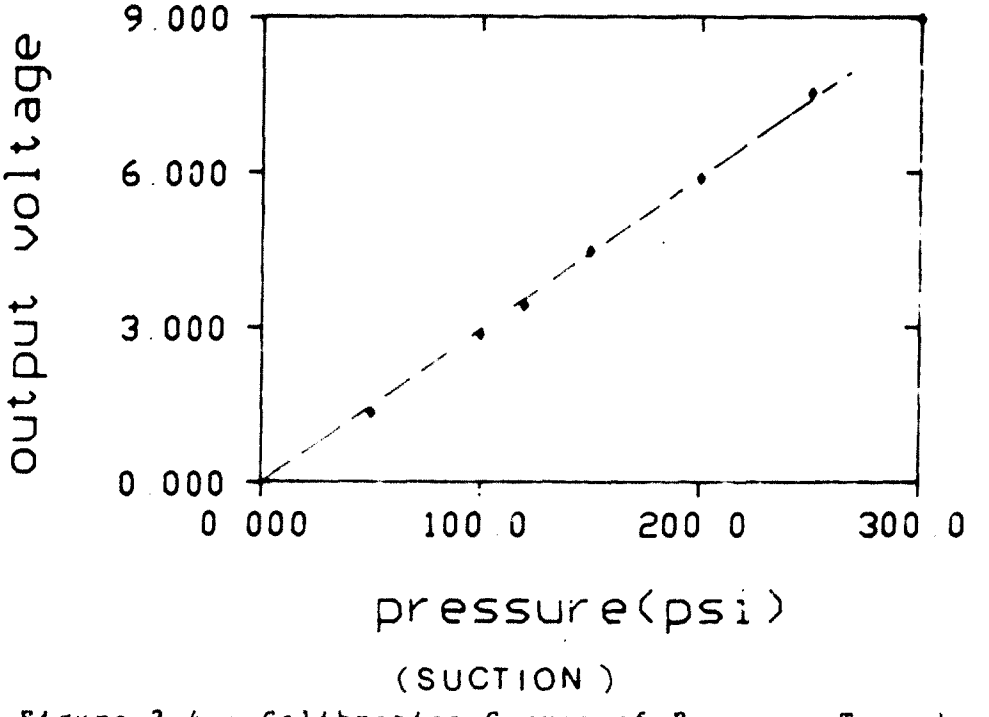

Figure 2.4 - Calibration Curves of Pressure Transducers

cylinder head on which pressure transducers are installed is shown in Figure ^.3. Because of limited space inside the compressor, an access window to the cylinder head and transducers was made. All transducers were mounted directly to the cavities.

The trigger pin for the magnetic pick up was installed on the top of the rotor and the pick up device was installed on the stator, as shown in Figure 2.5. However, the piston has very small displacement corresponding to rotations near the TDC or BDC, a small error when locating the TDC position may have occurred. The effect of TDC point measuring error can produce some interesting effects on the overall efficiency evaluation, as discussed in Section 2.5.

2.2.2 Measurement Results

Experimental results provide much useful information, even without the computer simulations. At first, the thermodynamic efficiency of the prototype can be directly calculated from the measured P-V diagram. Secondly, design problems can be found by careful examination of measured P-V diagrams and pressure pulsation traces.

Measured pressure-crank angle diagrams compared with simulation diagrams for two selected operating conditions from Table 2.1 are shown in Figure 3.22 and Figure 3.25. Absolute pressure levels were determined by the procedure

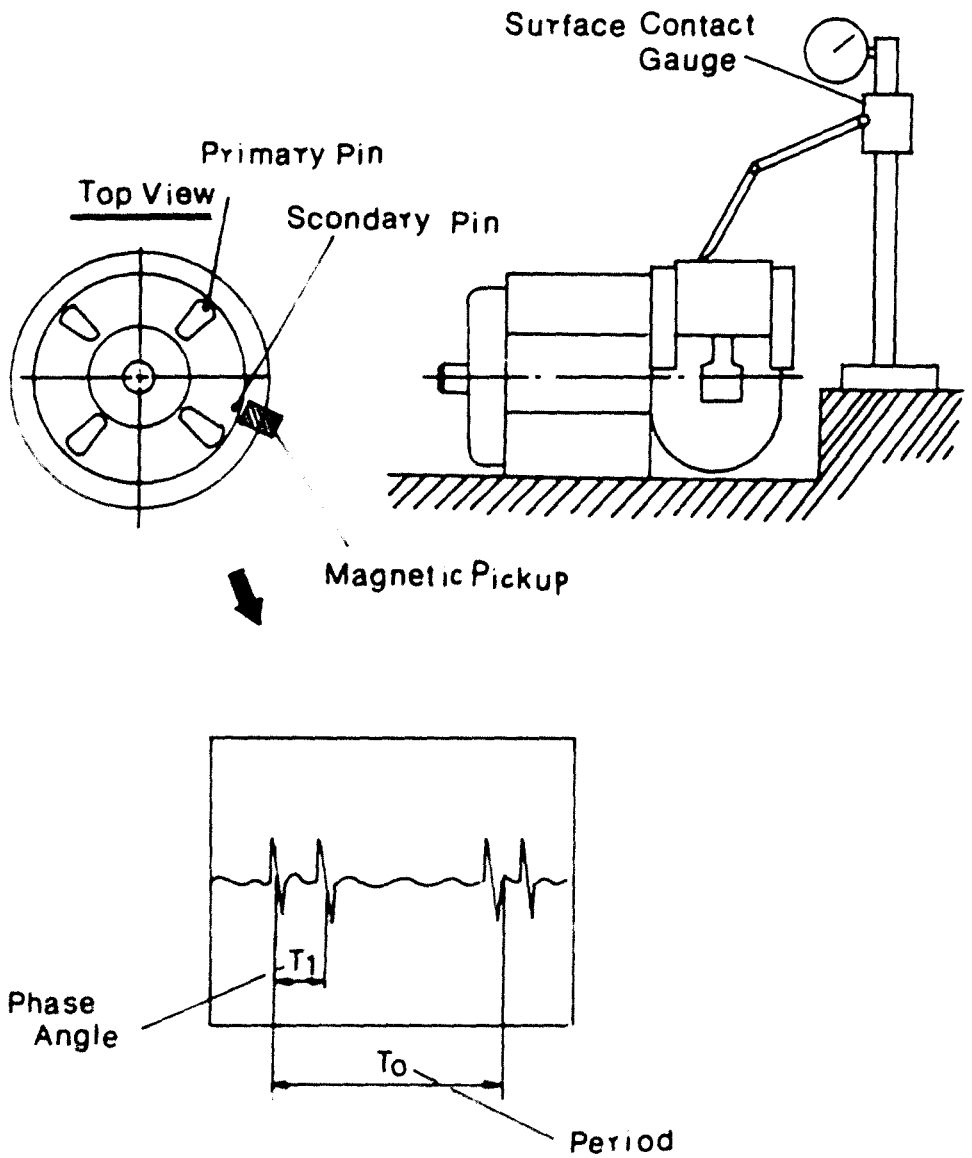

Figure 2.5 - Installation of the Magnetic Pickup Device

discussed in Section 2.4. For better insight, pressure-angle diagrams were drawn instead of pressure-time diagrams.

In general it can be seen that the discharge gas pulsation decays to almost zero during one operating cycle. It is introduced when the discharge valve opens. Gas rushes into the discharge cavity and causes an overpressure which will oscillate sinusoidally at a frequency approximately equal to five times the fundamental frequency of 60 cycles per second. This frequency is unchanged for the operating range investigated.

The suction pressure pulsations are much less pronounced, even while they are not negligible from an acoustics viewpoint. Fourier spectra of these pulsation pressures are shown in in Figure 2.6 and Figure 2.7. In the discharge pressure spectrum of Figure 2.7, the dominance of the fifth and sixth harmonic stems from the observed wave in the time trace of Figure 3.22 and Figure 3.26. For the suction cavity pressure, the time trace seems to indicate a wave of a frequency of approximately 480 Hz. The Fourier spectrum of Figure 2.6 shows several larger peaks in this vicinity. The actual time periods of one cycle of operation are listed in Table 2.1 for each experimental condition.

Figure 2.8 and Figure 2.9 are suction pressures and

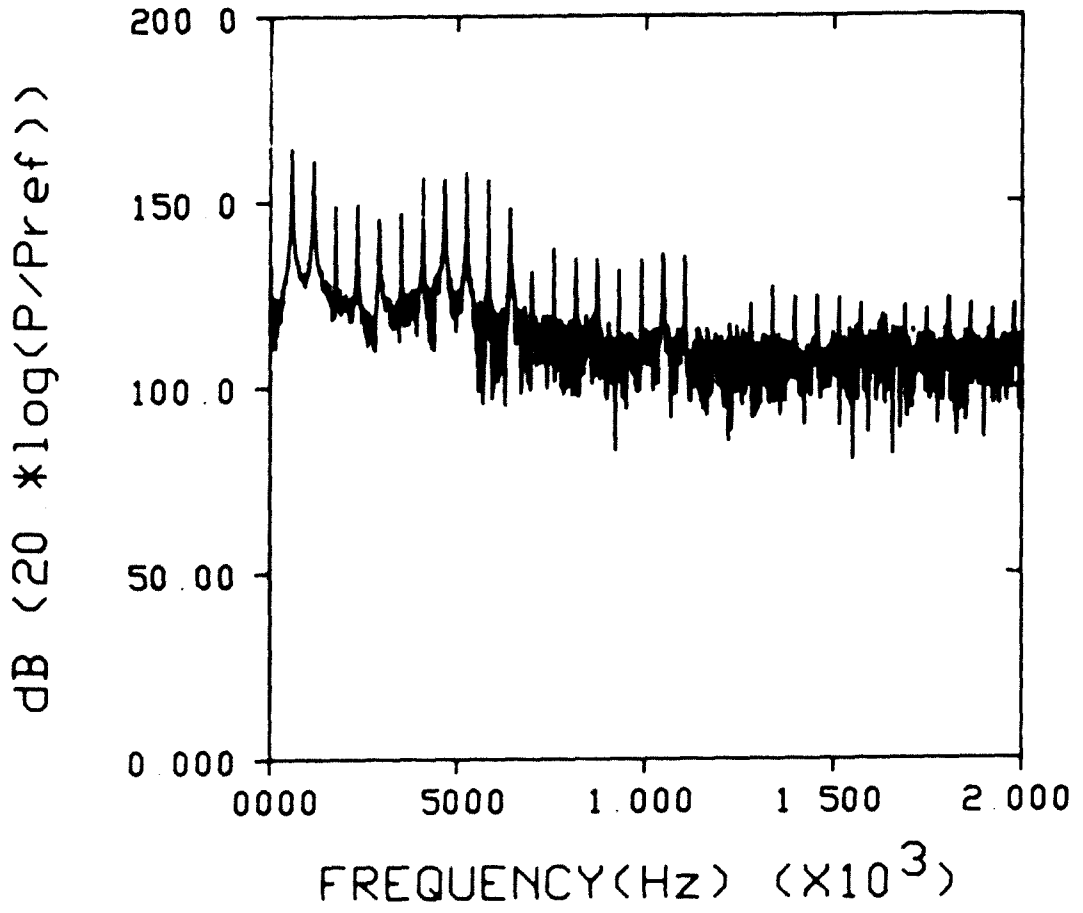

Figure 2.6 - Fourier Spectrum of the Suction Cavity Pressure

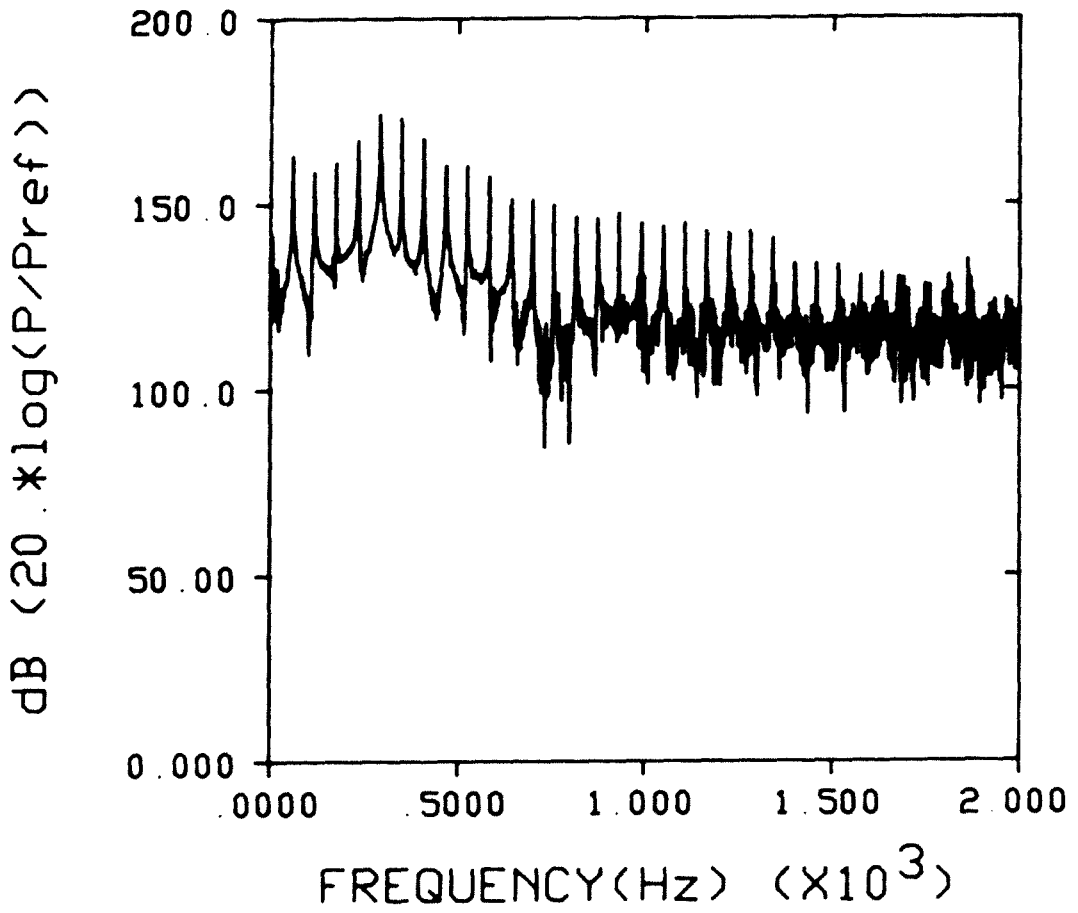

Figure 2.7 - Fourier Spectrum of the Discharge Cavity Pressure

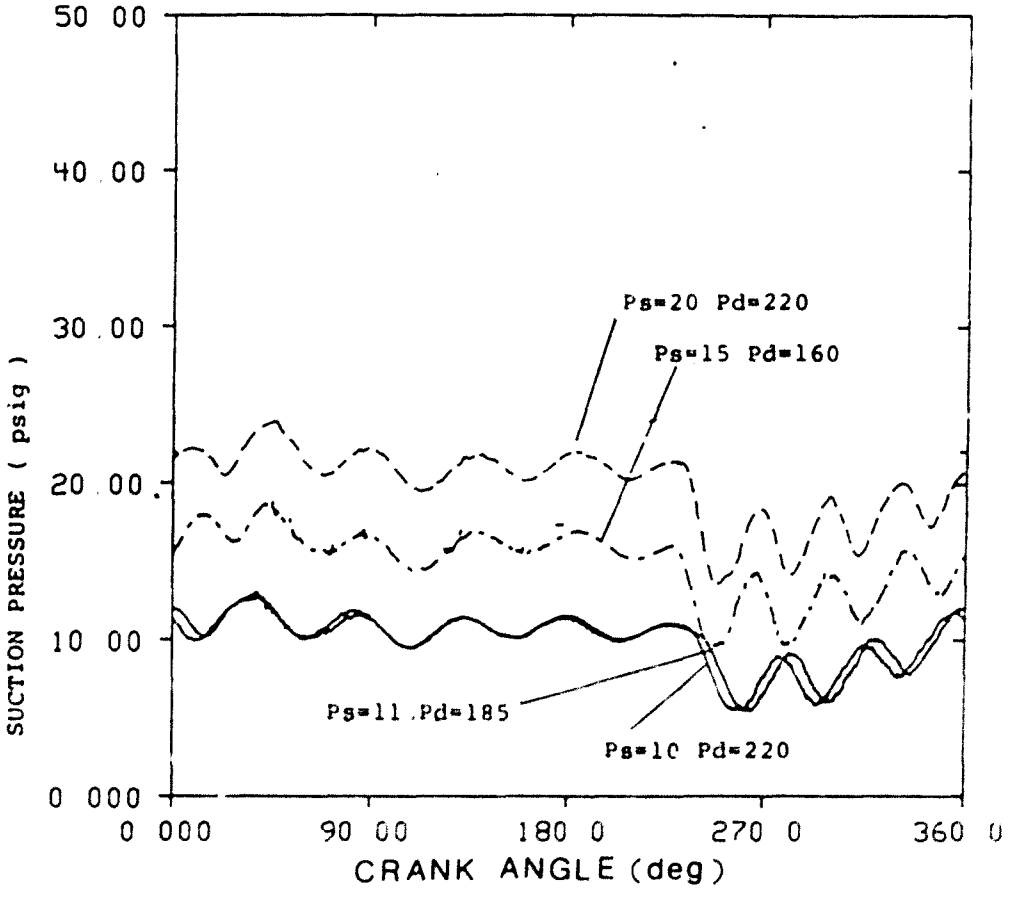

Figure 2.8 - Suction Pressures at Various Conditions

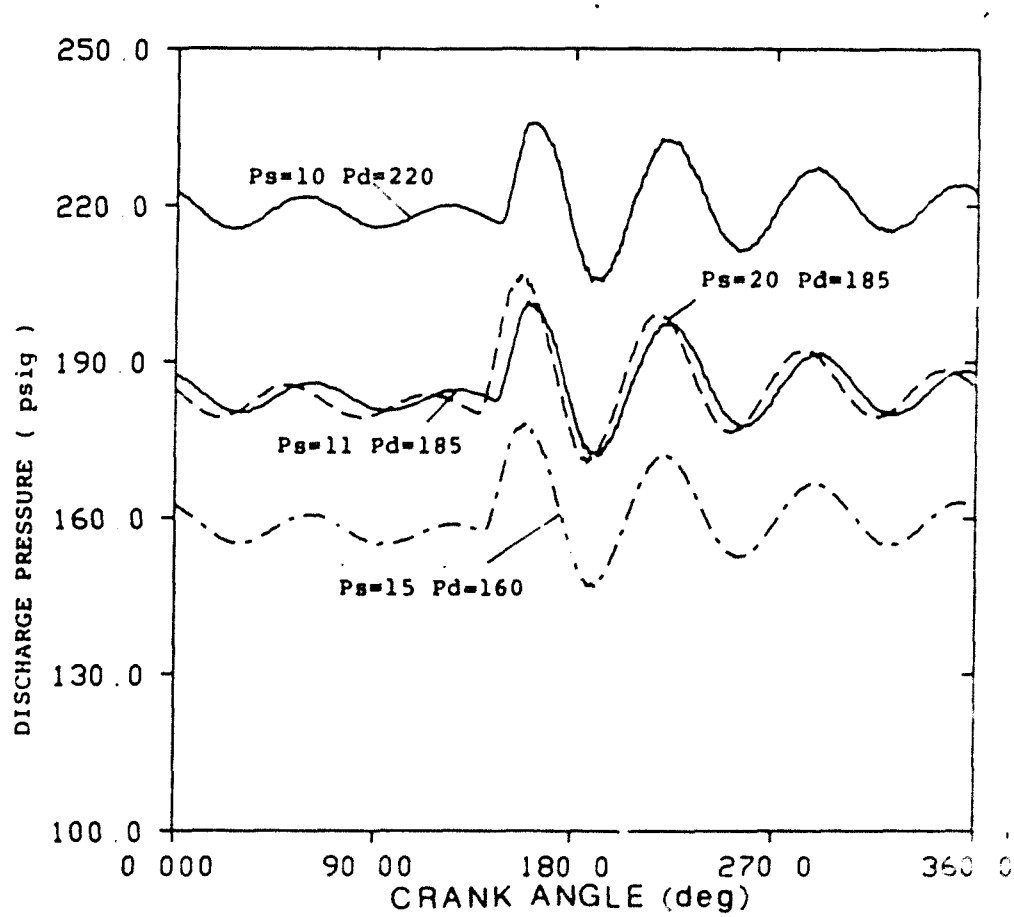

Figure 2.9 - Discharge Pressures at Various Conditions

discharge pressures at various operating conditions. It can be seen that the general qualitative behavior of the plenum pressures are not strongly affected by changes of operating conditions. That is, pulsation frequencies, and amplitude, and general shape remain very similar. Therefore, perturbations which may have been caused by modifications of the prototype design and certain inevitable small measurement errors will probably not contribute significantly to the interpretation of the overall pulsation characteristics of the system.

It is also of interest to obtain the Fourier spectrum of the cylinder pressure, since the cylinder pressure causes structural vibrations in the compressor housing that can be transmitted through the springs into the shell. Again, all harmonics are present as expected and as shown in Figure 2.10.

2.3 Valve Lift Measurements

Valve lift measurements on a prototype compressor are very informative. At first, the measured valve opening instant and the valve opening duration are used to set absolute pressure levels measured by piezo-electric transducers[18,27]. Secondly, possible problems in the valve design can be identified by examining the measured motion of valves.

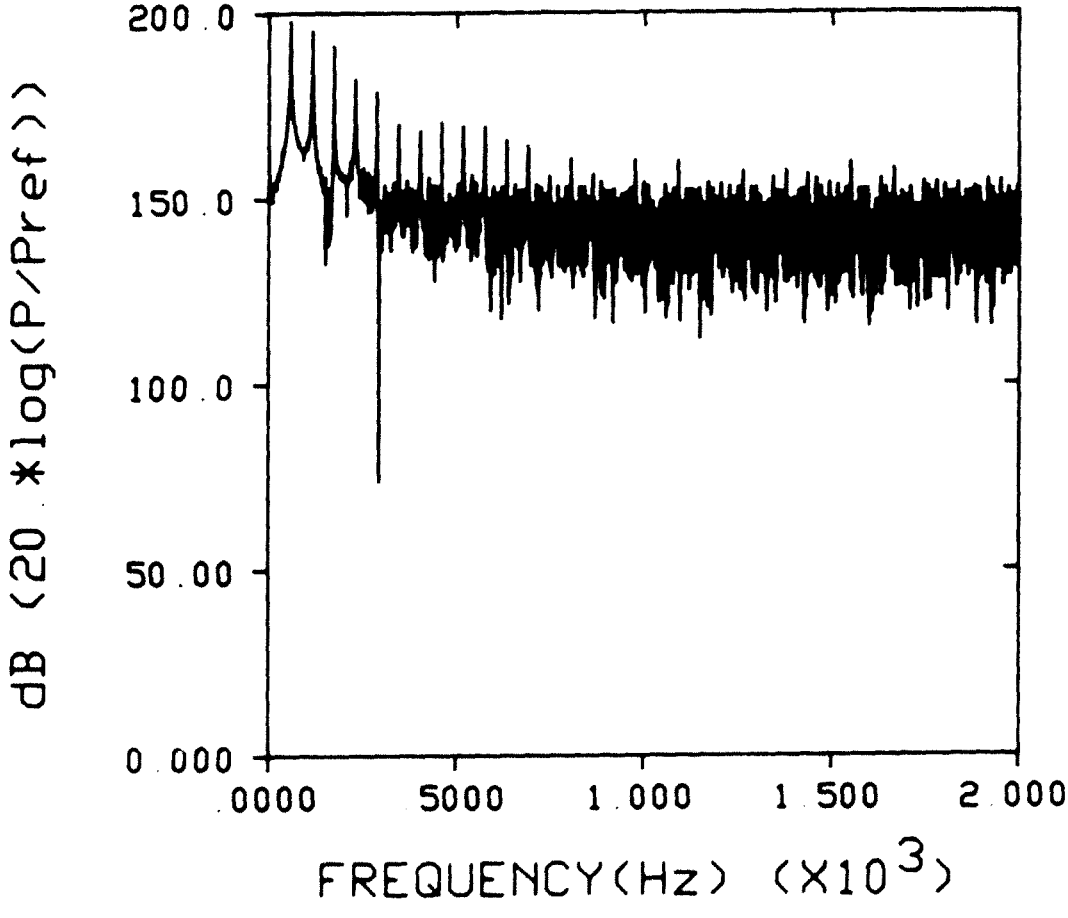

Figure 2.10 - Fourier Spectrum of the Cylinder Pressure

Unfortunately, valve motions are more difficult to be measured than pressures[2]. When they are measured, it is very difficult to avoid disruptions to the mass flow system. In this particular experiment, magnetic type proximity probes were used to measure valve lifts. For the instrumentation of the probes , some modifications had to be made.

2.3.1 Instrumentation

Bently-Nevada 190 type proximity probes were selected because they were the most compact size available. The installation for the calibration of the proximity probe is shown in Figure 2.11. Figure 2.12 is the illustration of the dynamic measurement principle of the proximity probe[36].

The probe operates on the principle that as the distance between the probe and measuring object changes, a magnetic field generated by the probe is changed. Usually the sensitivity of the proximity probe depends heavily on its installation condition. Therefore, quasistatic calibration was done after they were installed in the cylinder head. Figure 2.13 shows calibration curves.

Figure 2.14 is the photo of a cylinder head on which a proximity probe is installed. It shows the enlarged suction port through which the suction probe was installed. The net suction area was kept as close to the original

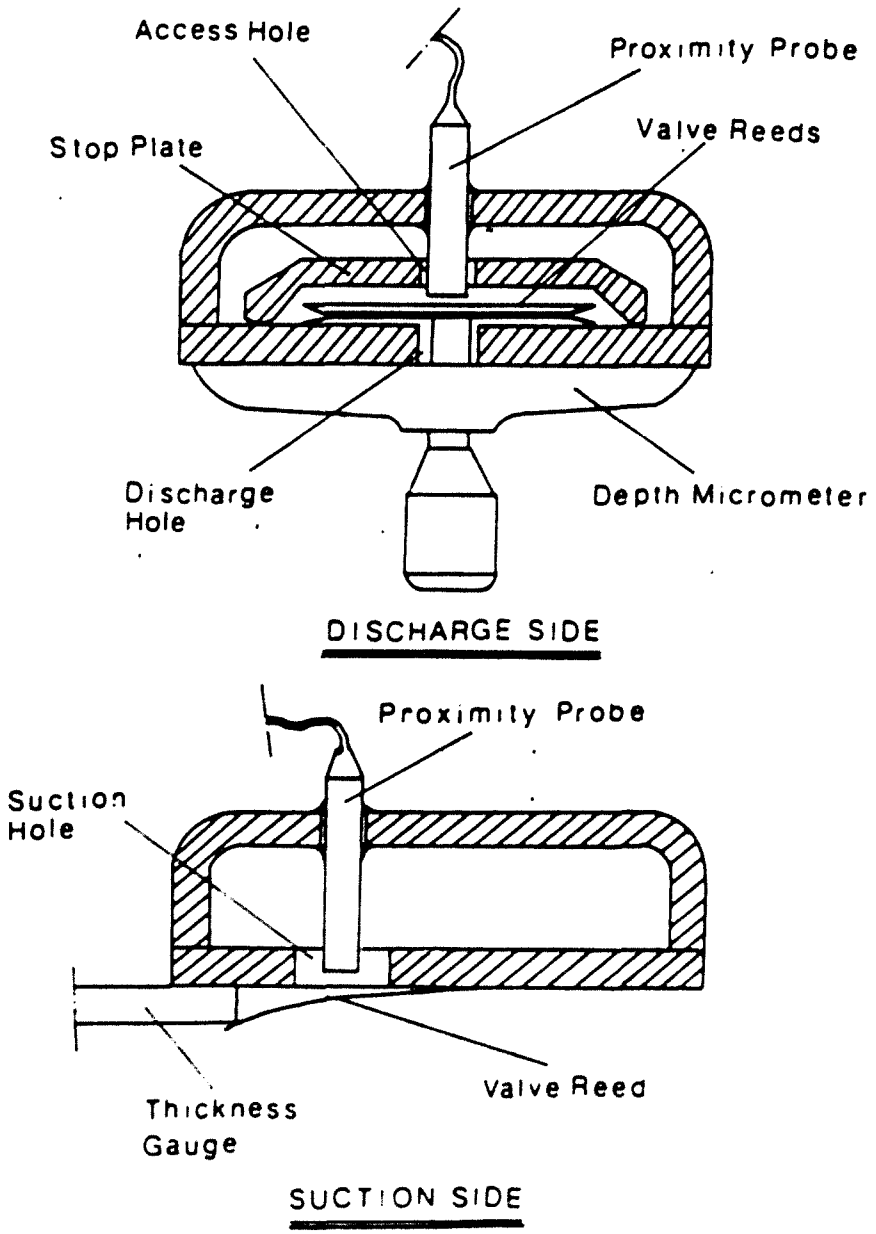

Figure 2.11 - Calibration Setup for the Valve Proximity Probe

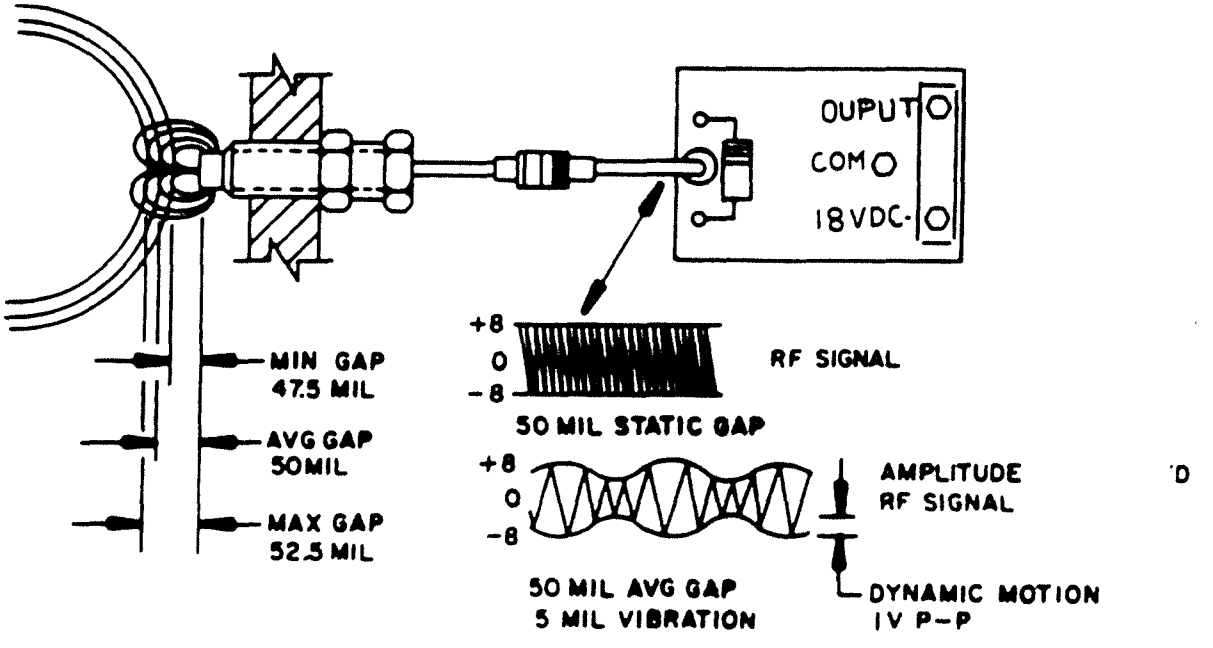

Figure 2.12 - Dynamic Measurement Principle of the Proximity Probe

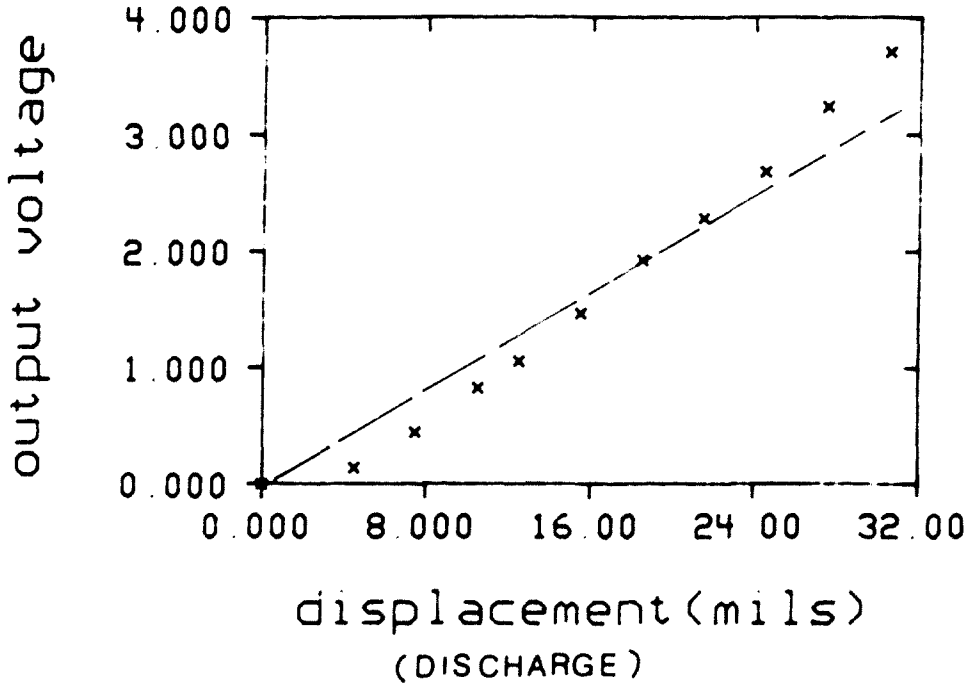

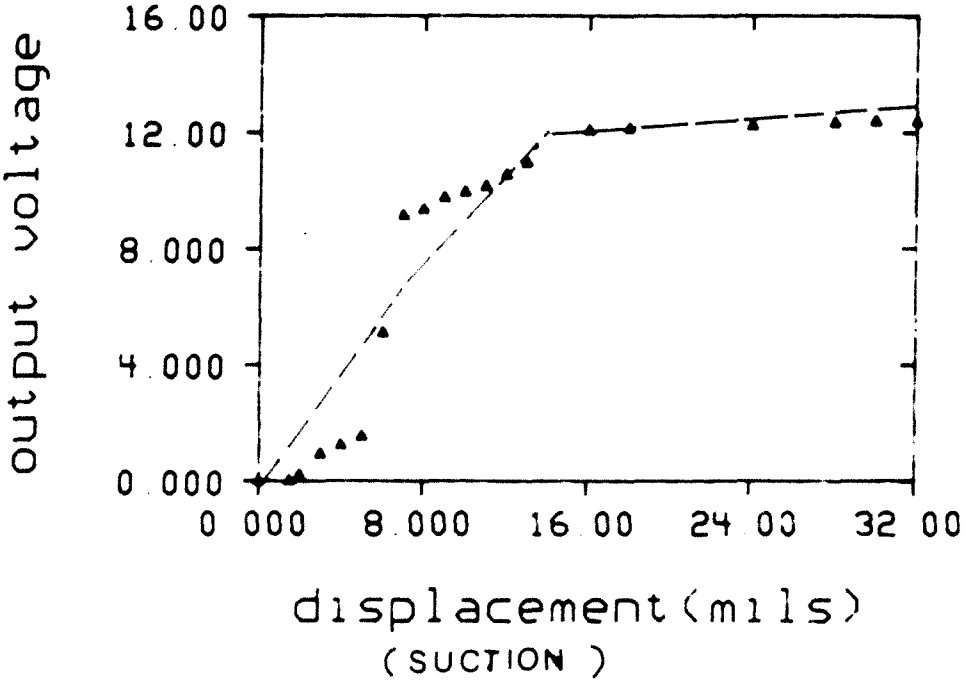

Figure 2.13 - Calibration Curves of Proximity Probes

Figure 2.14 - Modifications of the Suction Side to Install Proximity Probe

valve port area as possible by enlarging the valve boundaries. Obviously, the flow pattern through the suction port and thus the suction flow rate through the suction port must have been changed to some extent.

For the access of proximity probes to valve reeds, some modifications of the original system were unavoidable. At first, for the access of the proximity probe to the discharge valve reed, a hole was cut in the stop plate. It changes the stiffness of the valve stop plate, which in turn changes perhaps somewhat the valve stop height.

2.3.2 Measurement Results

Measured valve motions are shown in Figure 2.15 and Figure 2.16 , for the same two operating conditions as for the pressure measurements. To convert output voltage into displacement, calibration curves in Figure 2.13 were least square fitted to straight lines. A single straight line was sufficient for the discharge valve. Three different slopes were needed for the suction valve.

Valve opening durations are listed in Table 2.2 for each operating condition. Judging from the valve measurement data, it is believed that there is a small valve fluttering problem and some back flow phenomena in case of the suction valve. The flutter in the suction valve response is related to the gas pulsation in the suction manifold. The discharge valve seems to behave

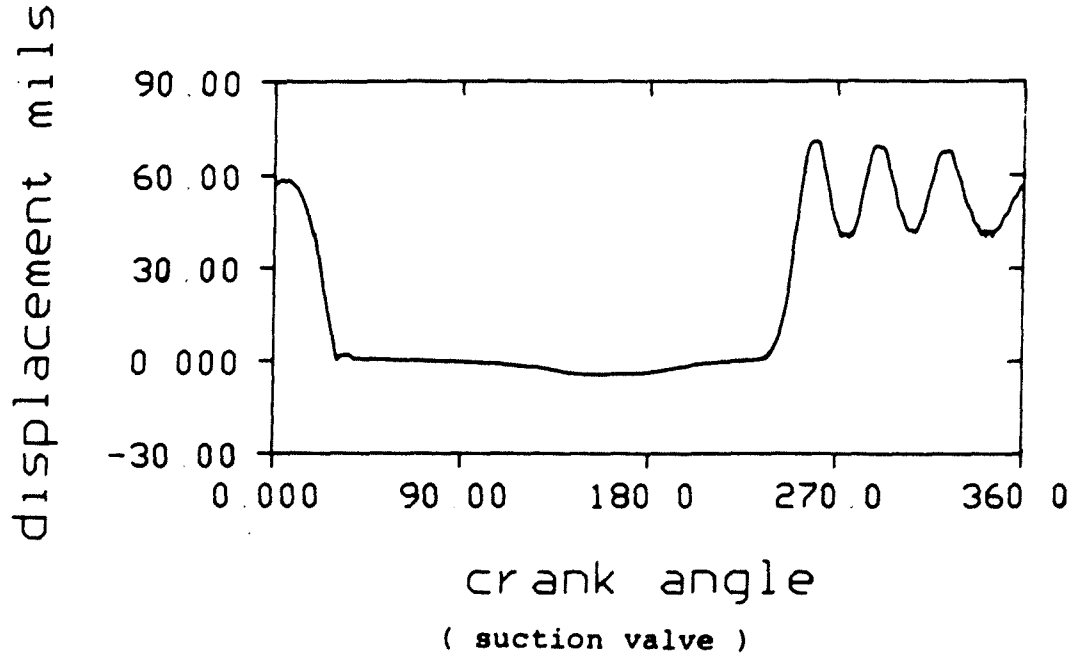

Ps=11 psig Pd=185 psig

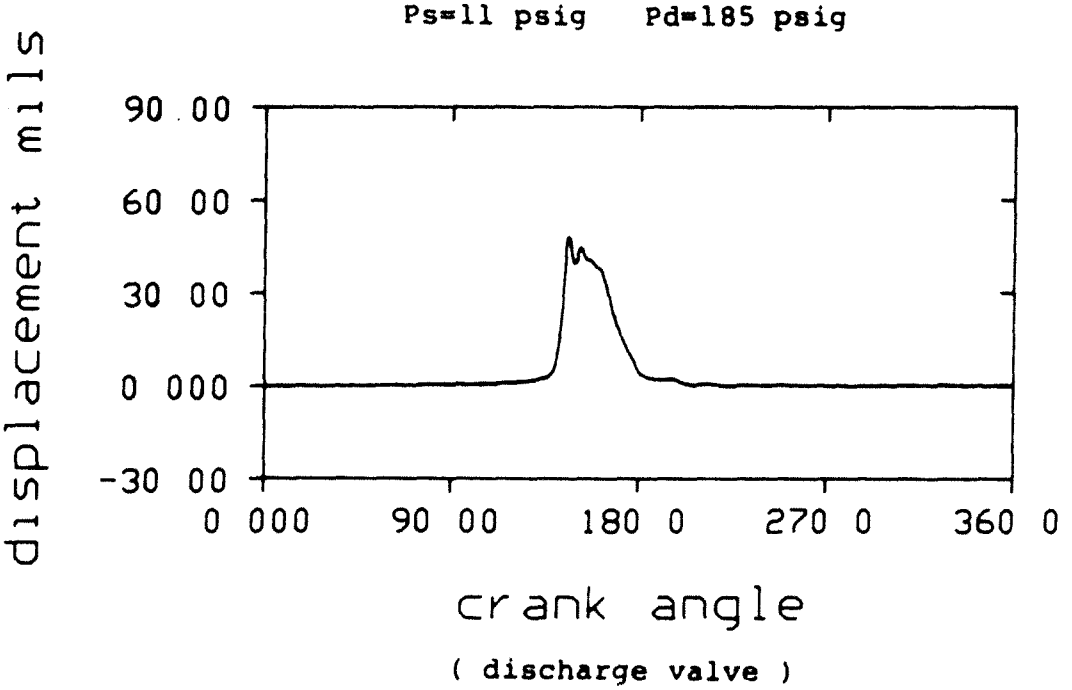

Figure 2.15 - Measured Valve Motions(1)

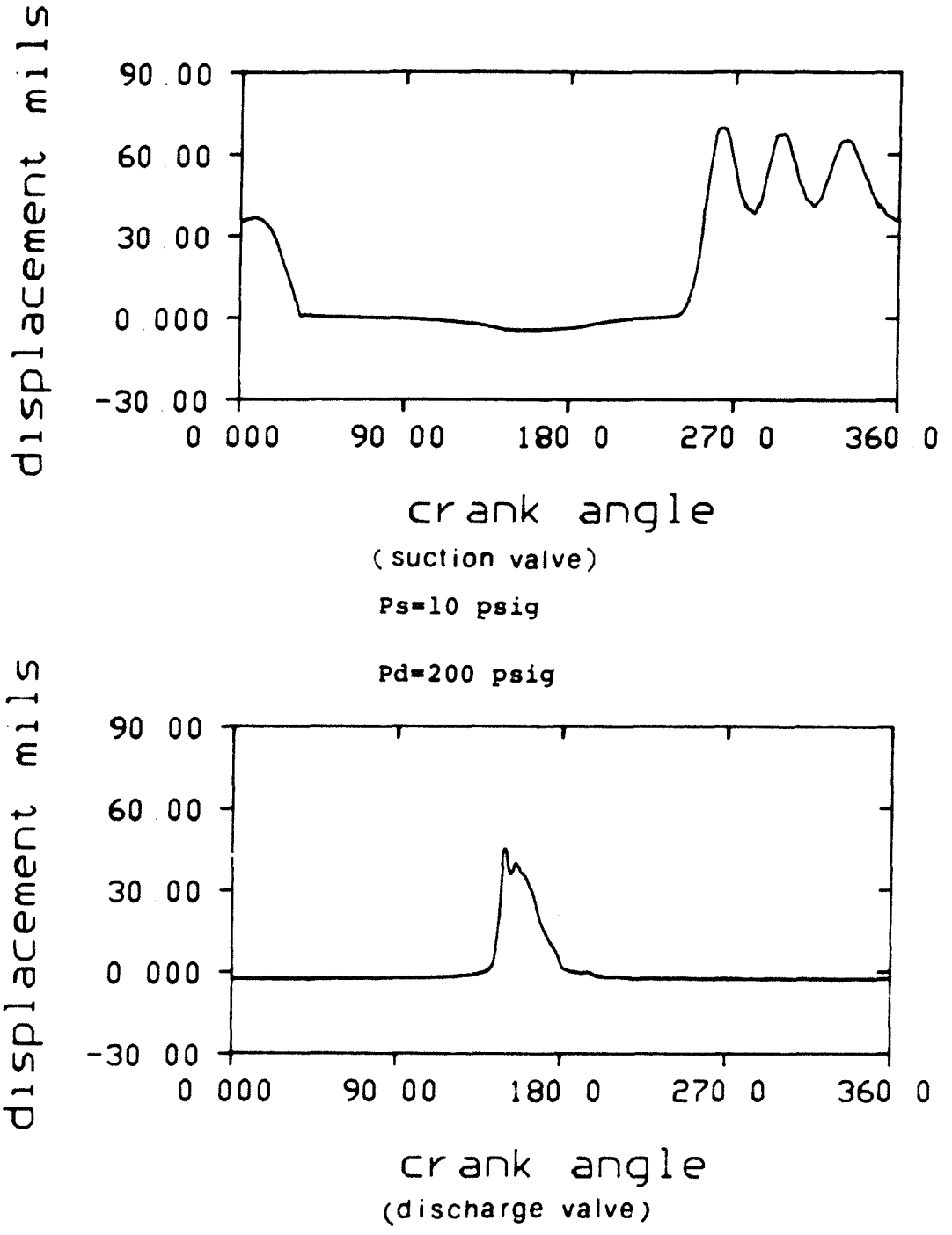

Figure 2.16 - Measured Valve Motions(2)

TABLE 2.2 - Duration of Valve Opening and Cylinder Pressure Transducer Gain

Experiment	Pressure (psig) Suction	Discharge	Valve Open duration (degree) Suction	Discharge	Cylinder Transducer Adjusted gain / Calibrated gain
1	11	185	152.5	47.0	0.975
2	10	200	152.05	40.3	0.989
3	10	220	151.5	40.4	1.0017
4	20	185	163.4	53.4	0.979
5	15	190	162.7	50.3	0.968
6	15	160	167.9	53.8	0.975

alright, except that it is too restrictive in flow area judging from the P-V diagrams. This indicates that more work will have to be done on the discharge valve and flow path design using a computer simulation program which includes the gas pulsation effect.

From an acoustics viewpoint, it is also of interest to examine the Fourier spectrum of the valve motions. They are shown in Figure 2.17 and Figure 2.18. They show clearly that the suction valve flutter comes through as the 9th harmonic at approximately 540 Hz. Because the acoustic investigation of Roys[7] for the same prototype compressor has shown a strong peak in the 500 Hz region, it is possible that the noise could perhaps be influenced by suppressing the valve flutter[2]. This does not mean, however, that the gas resonance inside the shell could not still be excited.

The discharge valve spectrum shows no particularly unusual features. Note that all valve spectra are normalized with respect to the maximum valve displacement.

2.4 Construction of P-V Diagrams

In the compressor, the area enclosed by a P-V diagram is the work performed by the piston as the gas is compressed. Therefore, a P-V diagram furnishes very useful information for the diagnosis of prototype compressors. Comparing the P-V diagram of the prototype with an ideal

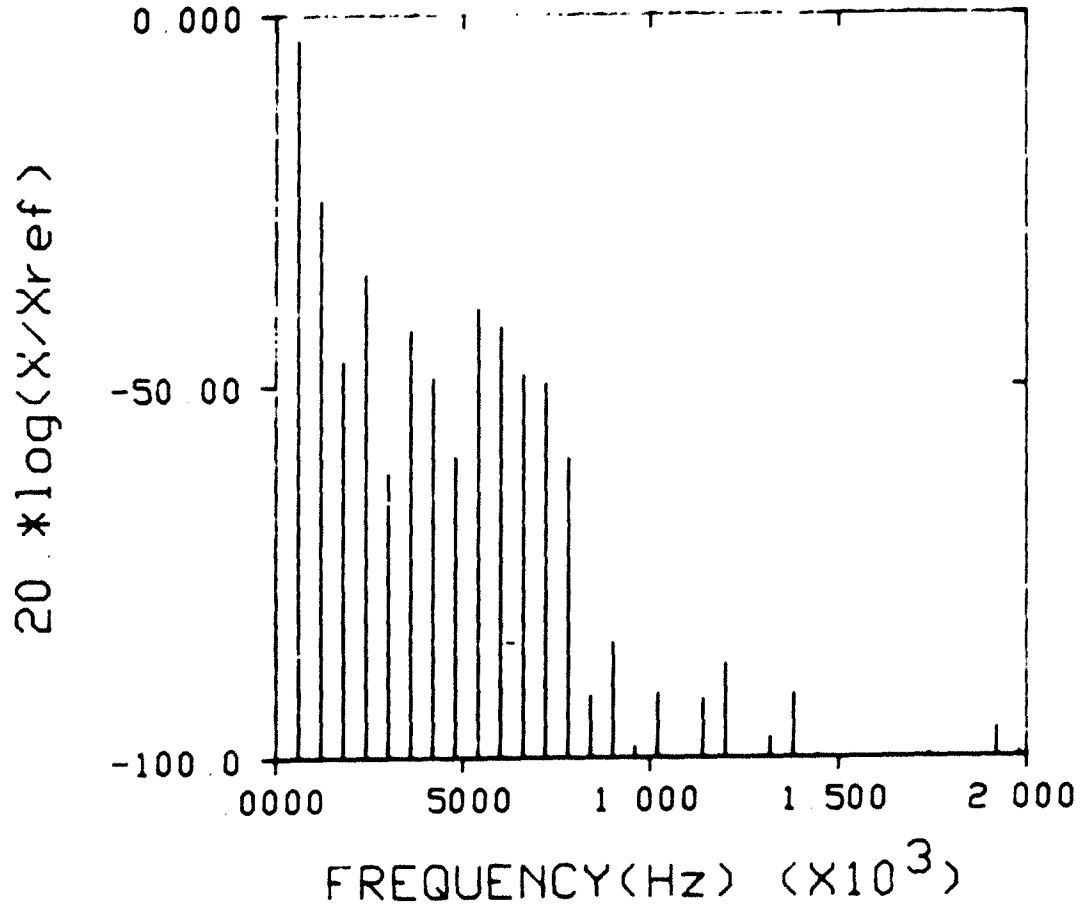

Figure 2.17 - Fourier Spectrum of the Suction Valve Motion

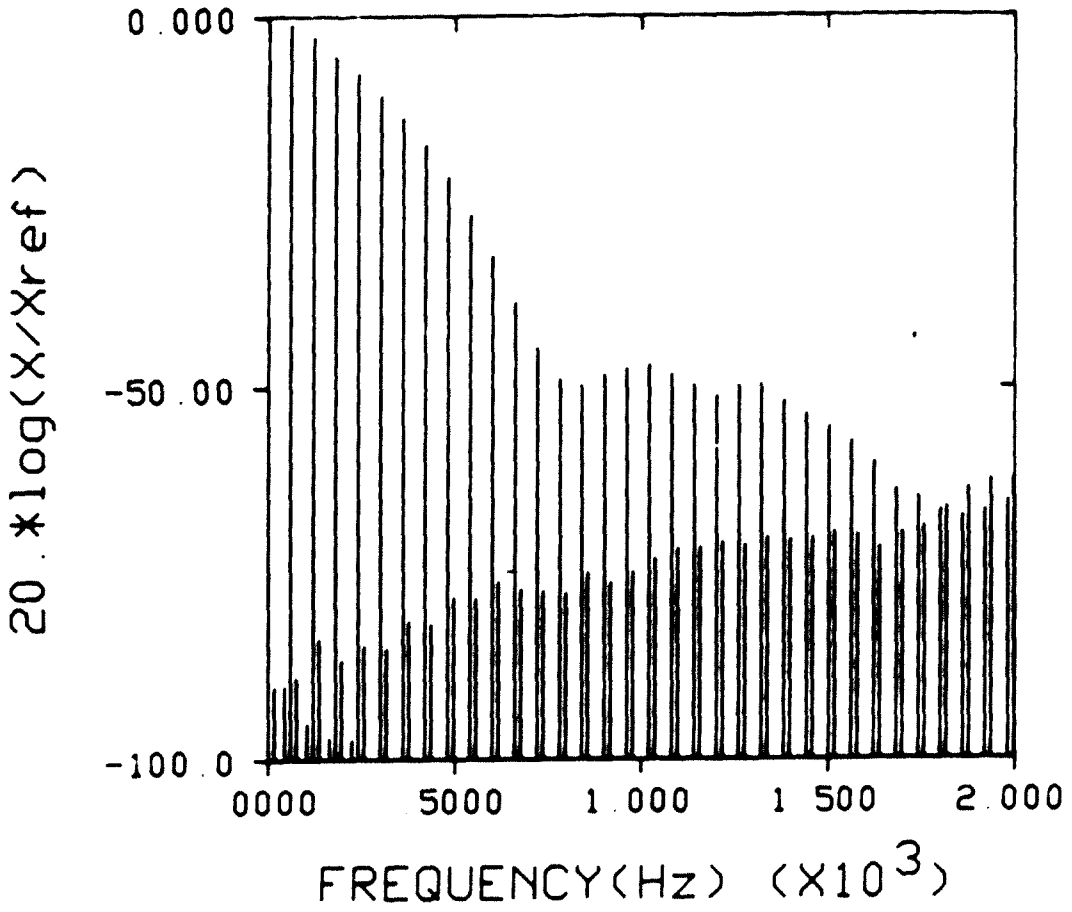

Figure 2.18 - Fourier Spectrum of the Discharge Valve Motion

P-V diagram allows us to identify the energy loss easily as it is illustrated in Figure 2.19. . Further, if pressure pulsations of both suction and discharge side are drawn as functions of volume, thermodynamic losses due to valves and gas pulsations can be separated[2].

To fold pressure time diagrams into pressure volume diagrams, two additional informations are necessary. The one is crank position as a function of time, by which time is converted to a corresponding volume utilizing the kinematic relationship in section 3.2.1. The other is valve motion measurement data. Because the pressure measured by piezo-electric pressure transducers is a dynamic relative pressure, a reference pressure level is necessary to set absolute pressure level.

In general, adjustment of the cylinder pressure level within practical accuracy is very difficult. In this process, various kinds of errors can be created which may reinforce each other. Nonlinearity, temperature dependence, and different behavior in the dynamic state from the quasi-static calibration state may be conceivable errors of the pressure transducer.

In valve lift measurements, modifications of the prototype are unavoidable in order to install the proximity probes. Such modifications will change the internal process of the compressor by some extent. Therefore,

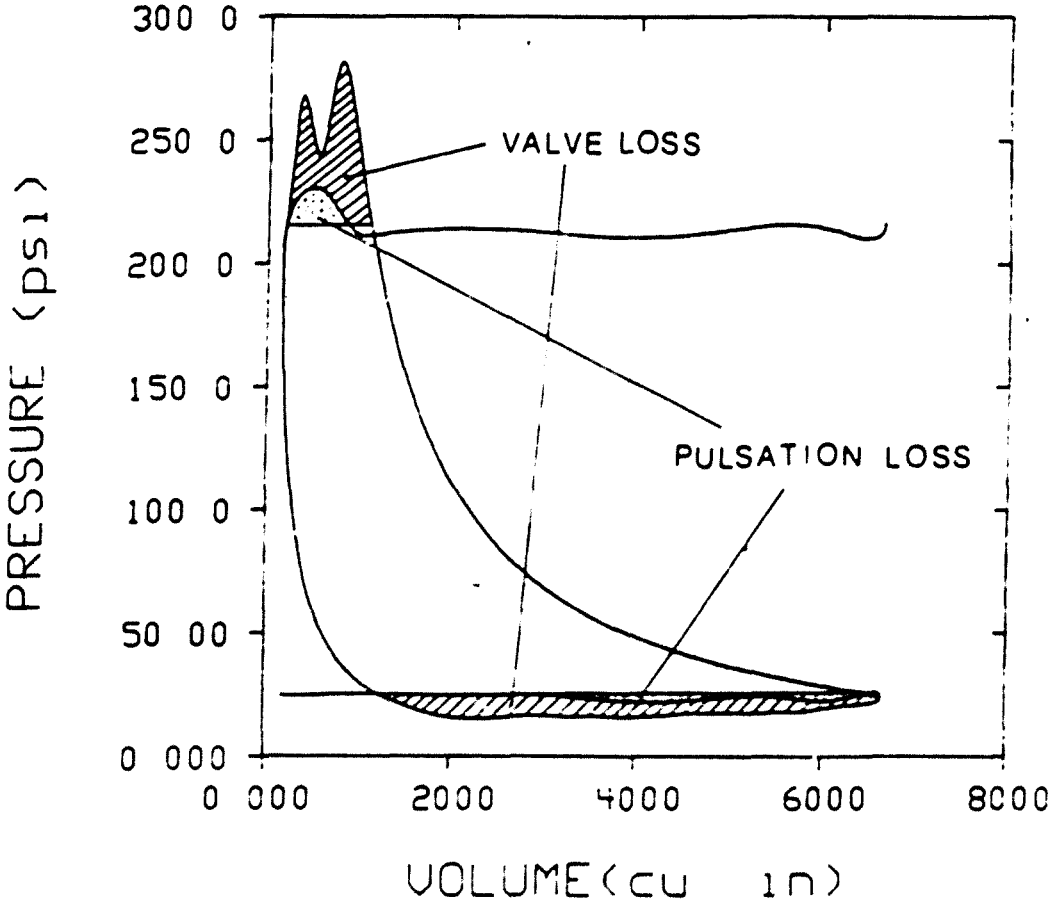

Figure 2.19 - Energy Losses in Compressor

measuring valve motions causes deviations from the actual valve motions. Also, a delayed response of the valve reed to the pressure changes can exist[2].

Even if the exact motion could be recorded, it is not easy to identify the exact starting point or end point of the valve motion because a valve reed is already in dynamic motion typically even while it is on the stop plate or valve seat, because it flexes into the port and starts moving as the pressure differential decreases. So, it was not possible to construct the pressure-crank angle diagrams and pressure volume diagrams relying only on calibrated pressure transducer gains and valve opening instants, but other considerations were taken into account.

Valve opening durations and the cylinder pressure curve were such additional reference data used to set absolute pressure levels. After the absolute pressure levels were determined, the pressure time data was converted to the pressure angle data with the aid of the magnetic pick up signal. Finally the pressure angle data was converted to the pressure volume data using the volume angle relationship. Resulting P-V diagrams showed consistent and reasonable results.

Suction and discharge pressures can be aligned with their absolute values because their average pressures can be thought of as being the suction and discharge line

pressures which are indicated by gages measuring the average pressure. It is assumed that the drop in average pressure between the suction and discharge manifold location and the location of the average line pressure measurement is negligible.

To set absolute cylinder pressure levels, more elaborate arguments are needed. If exact pressure transducer information and very accurate valve opening times are available, the cylinder pressure can be determined without too much difficulties by arguing that at the instant of valve opening, the cylinder pressure must be equal to the pressure in the valve manifold. This is true for either suction or discharge. However, the calibration of the pressure transducer is not expected to be that accurate. Figure 2.20 is an exaggerated illustration of what can happen if the P-V diagram is made only by using calibrated transducer gains and measured discharge valve opening time. Obviously, the suction process will not properly be described. Judgement is therefore necessary when fitting the various measurements together.

The method that was used in this application is to argue that the point at which cylinder pressure starts its polytropic expansion can be taken as the discharge valve closing time. (See point A in Figure 2.21.) The suction valve opening time was chosen such that the duration of valve opening agrees with the measured duration of valve

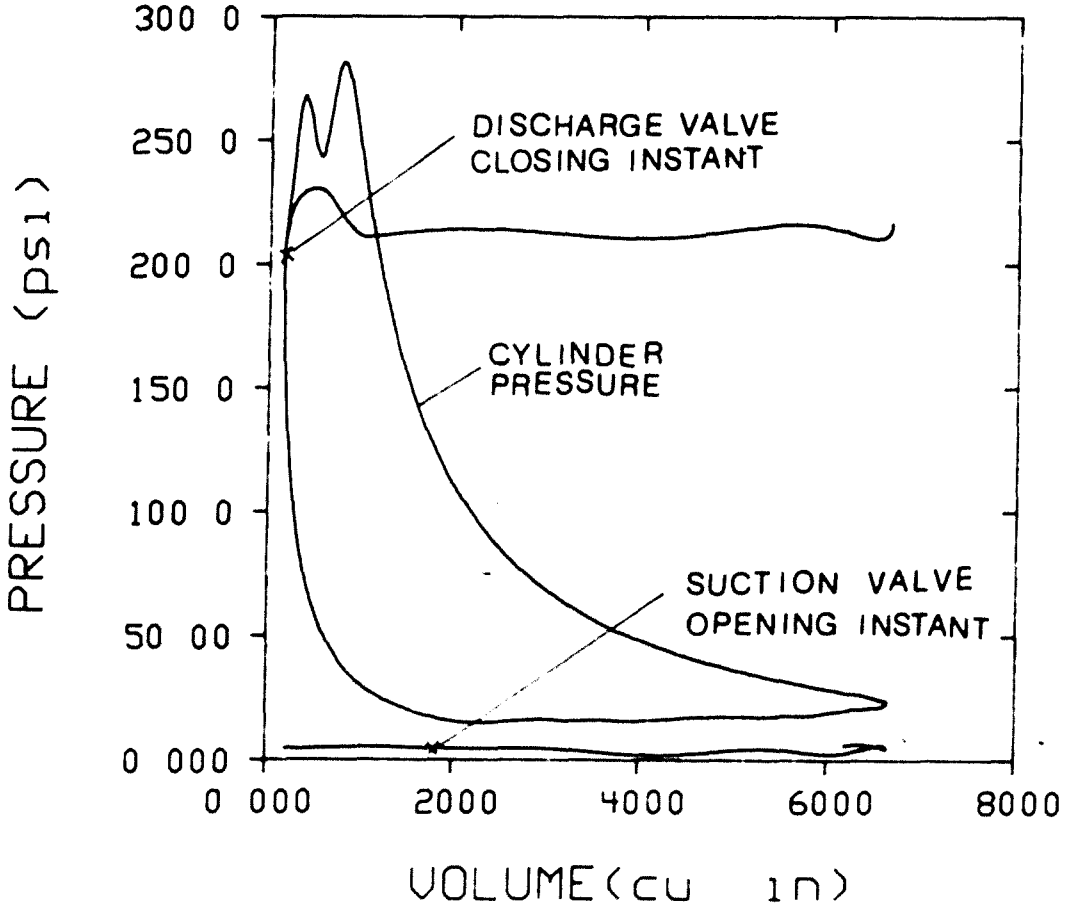

Figure 2.20 - An Example of Misfitted P-V Diagrams

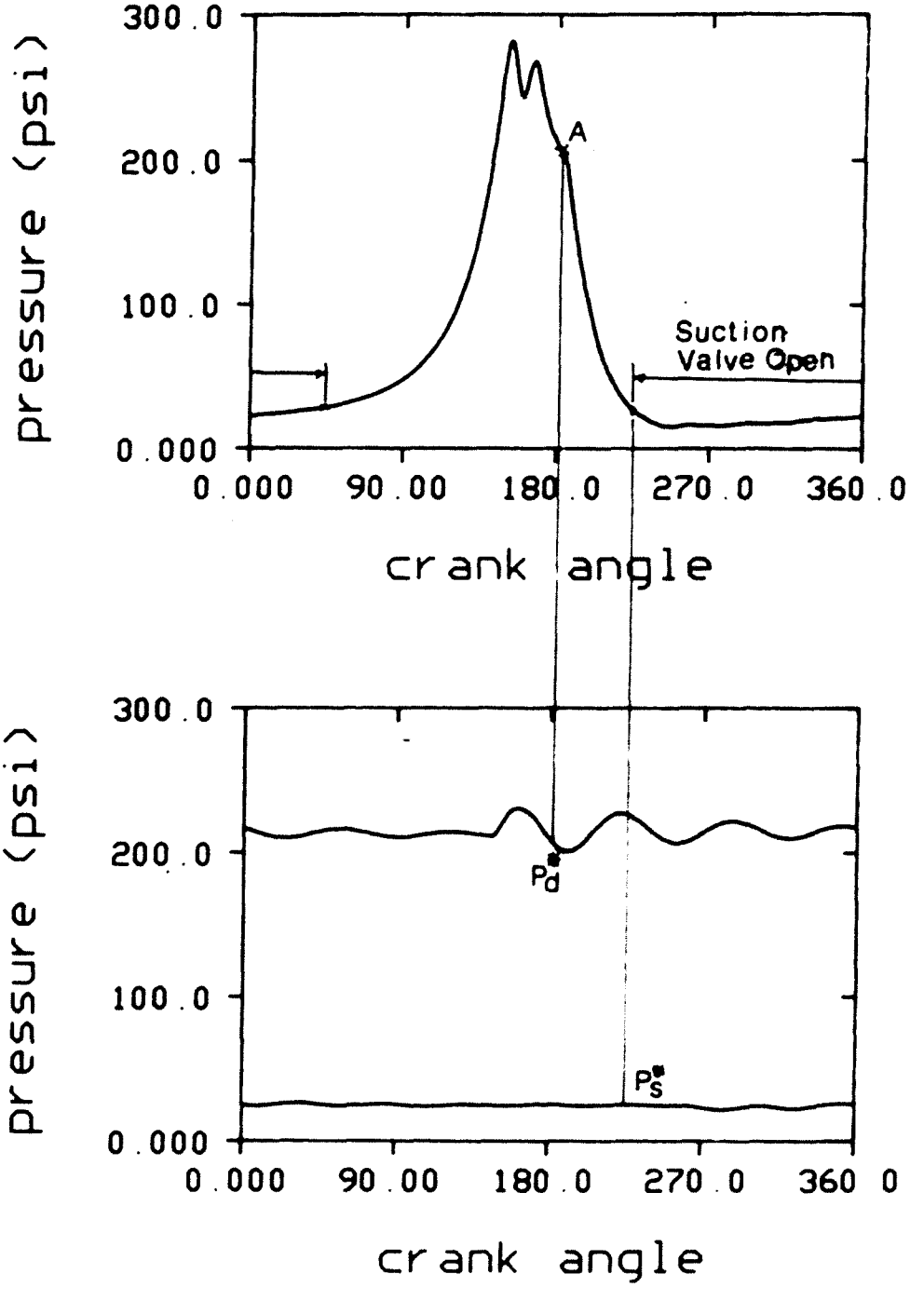

Figure 2.21 - Illustration of Absolute Pressure Setting Procedure

opening. The transducer gain was then calculated from the two points which are supposed to be the suction and discharge pressures. Using this gain and the reference pressure, cylinder pressure was determined.

Figure 3.23 and Figure 3.26 are selected P-V diagrams which were obtained by the procedure stated previously. Suction and discharge pressures which make a closed loop during one cycle were drawn only for the half cycle for which the valves are open. The thermodynamic efficiencies are shown in the result section in Table 2.3.

2.5 Estimation of Possible Experimental Errors [37]

The errors in the pressure transducer calibration ,in valve motion detection, and in crank position measurement are major potential errors in the evaluation of compressor performance.

2.5.1 Influence of Pressure Measurement Error

Gains of pressure transducers are calibrated by a quasi-static process, while the actual process is dynamic. Also, deviation from linearity (1% max) and temperature sensitivity (0.03% per degree Fahrenheit) may have to be considered. This can be partially eliminated by more involved calibration procedures[38]. Table 2.4 shows the effect of pressure transducer gains on the estimation of thermodynamic efficiencies and losses.

TABLE 2.3 - Effect of Errors in Pressure Transducer Gain Estimated for the Case of P_s = 10 psig and P_d = 200 psig

Case	Overall Efficiency	Thermodynamic Losses			
		Suction Valve Loss	Suction Side Pulsation Loss	Discharge Valve Loss	Discharge Side Pulsation Loss
Calibrated Gains	82.61%	8.298%	1.208%	6.277%	1.647%
(Both Calibrated Gains x 1.1)	83.109%	7.839%	1.338%	5.89%	1.824%
(Both Calibrated Gains x 1.2)	83.519%	7.456%	1.469%	5.552%	2.003%
(Both Calibrated Gains x 0.9)	82.275%	8.519%	1.080%	6.653%	1.473%
(Both Calibrated Gains x 0.8)	81.887%	8.843%	0.954%	7.015%	1.301%

TABLE 2.4 - Effect of Errors in Top Dead Center Measurement

*Estimated in case of P_s = 10 psig, P_d = 200 psig

Case	Overall Efficiency	Thermodynamic Losses: Suction Valve Loss	Suction Side Pulsation Loss	Discharge Valve Loss	Discharge Side Pulsation Loss	Polytropic Coefficient
Measured	82.61%	8.258%	1.208%	6.277%	1.647%	1.0845
$+2^{o*}$	82.172%	8.811%	1.268%	6.221%	1.529%	1.05625
$+4^{o}$	81.651%	9.467%	1.339%	6.155%	1.388%	1.01489
-2^{o}	82.985%	7.786%	1.158%	6.323%	1.749%	1.14579
-4^{o}	83.309%	7.377%	1.114%	6.361%	1.838%	1.1929

Positive angle error means, TDC comes that much earlier

2.5.2 Influence of Crank Angle Measurement Error

Because the linear displacement of the piston corresponding to the rotation of the crank is very small around the TDC or BDC, even a small error in detection of the TDC point when the triggering pin is installed may lead to significant errors in terms of angle. This will cause the P-V diagram to be distorted. An example is shown in Figure 2.22 and Figure 2.23 , where on purpose crank angle errors of TDC was introduced. It is remarkable that only 2 degrees of deviation makes such a difference in the P-V diagram shape. For comparison a P-V diagram of presumably zero error is also shown. Figure 2.22 and Figure 2.23 illustrates the influence of crank angle measurement errors.

Of even greater importance is the experimental polytropic coefficients. Numerical estimations of this effect on thermodynamic efficiencies and polytropic coefficient estimations are listed in Table 2.4.

2.5.3 Errors due to the Procedure of Setting Absolute Pressures

Pressure and valve lifts were measured at different times using different cylinder heads. Therefore, some deviations in operating condition must have existed although all controllable conditions were kept as equal as possible. Furthermore, flow paths were disrupted to

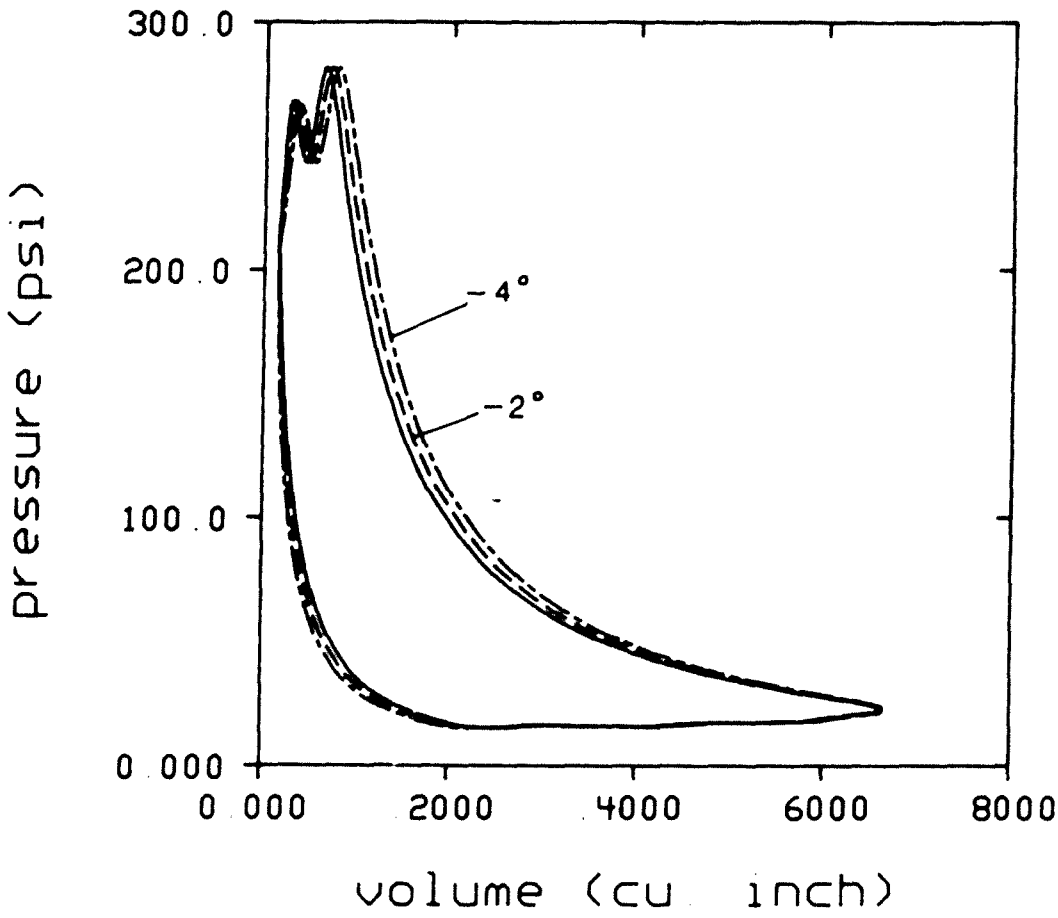

Figure 2.22 - Effect of TDC measurement Errors on the P-V Diagram (1)

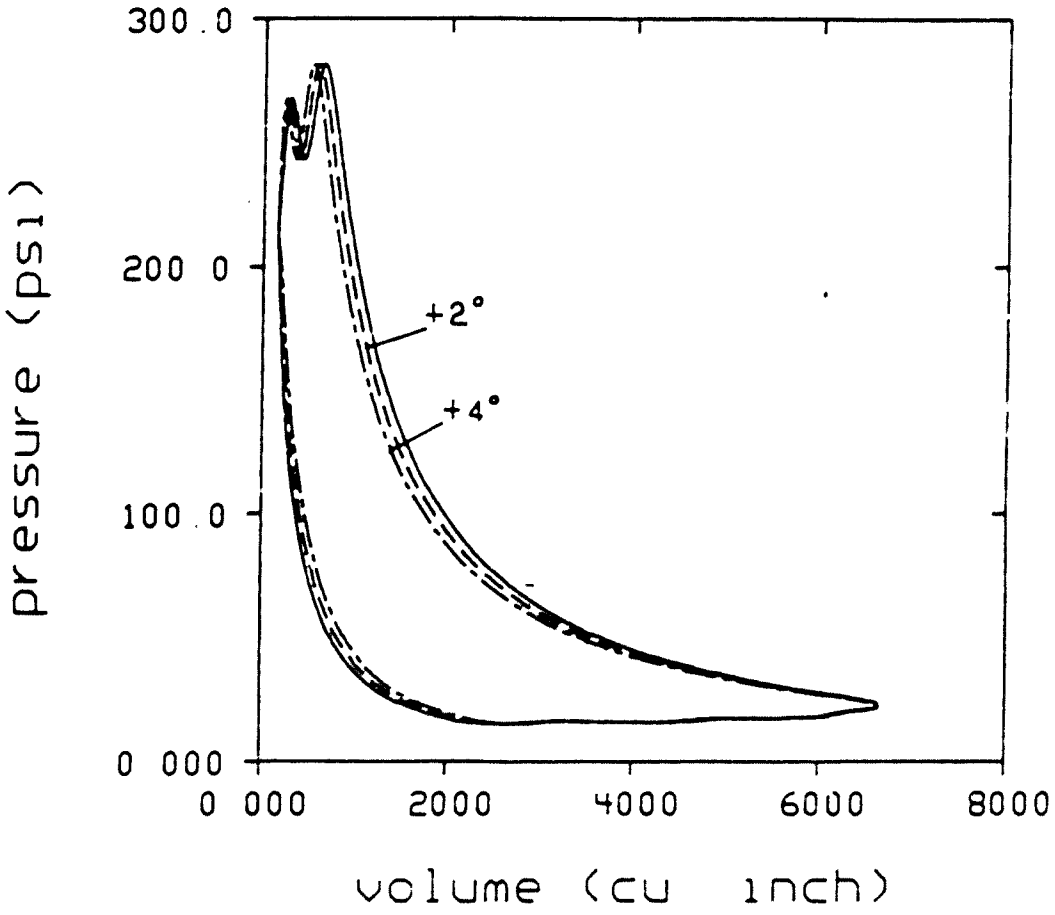

Figure 2.23 - Effect of TDC measurement Errors on the P-V Diagram (2)

install proximity probes, especially on the suction side. It is practically very difficult to decide the exact instant at which a valve opens, because of small dynamic responses prior to the actual opening. Ambiguous points which can be picked as the valve opening time span more than 2 degrees in terms of crank angle.

Also, oil stiction and Bernoulli effects have been found by some investigators to retard the valve opening [2,38]. It is possible that valve opening time errors are of the order of one degree which is a large error for fitting fast rising compressor pressures to discharge plenum pressures, although it was often done in the past.

In this experiment, the cylinder pressure transducer gain was calculated utilizing valve motion data. This had to be done for each experiment. The ratios of these gains to the calibrated gain are listed in Table 2.2. These variations can be thought to reflect the overall errors for the P-V diagram construction. The ratios are within 3 % from the calibrated value and less than 2 % from each other except for one case.

Calibrated gains were used for discharge and suction pressures because average values of those pressures were taken to be the suction and discharge line pressures. Also, errors in those gains cause much smaller relative differences in the overall efficiency, as well as for each

thermodynamic loss[37]. The effect on the overall efficiencies and on each loss is listed in Table 2.4 for one particular operating condition.

Therefore even with the possibility of errors, Table 2.4 shows that if we take the ideal situations to be the one where no valve or pulsation loss exist, roughly 8 % loss are attributable to suction valve flow loss and 1.5 % to suction pulsation, 6 % to the discharge valve flow loss and 1.5 % to the discharge pulsation loss. This gives a thermodynamic efficiency of about 83 %. Note that we have accepted the heat transfer in and out of the cylinder as unchangeable. Thus, this thermodynamic efficiency does not refer to an idealized isentropic or isothermal cycle, but the actual cycle with ideal valves. Discharge pressure transducers affect mainly the ratio of valve losses to pulsation losses, but not the overall efficiency.

2.6 Interpretation of Experimental Results

The performance of a refrigeration cycle is given in terms of the coefficient of performance β, which is defined for a refrigeration cycle,[39]

$$\beta = \frac{q_L}{W_c} \tag{2.1}$$

where,

$$q_L = h_1 - h_5 \tag{2.2}$$

and h_1, h_5 are enthalpies measured at points 1 and 5 shown

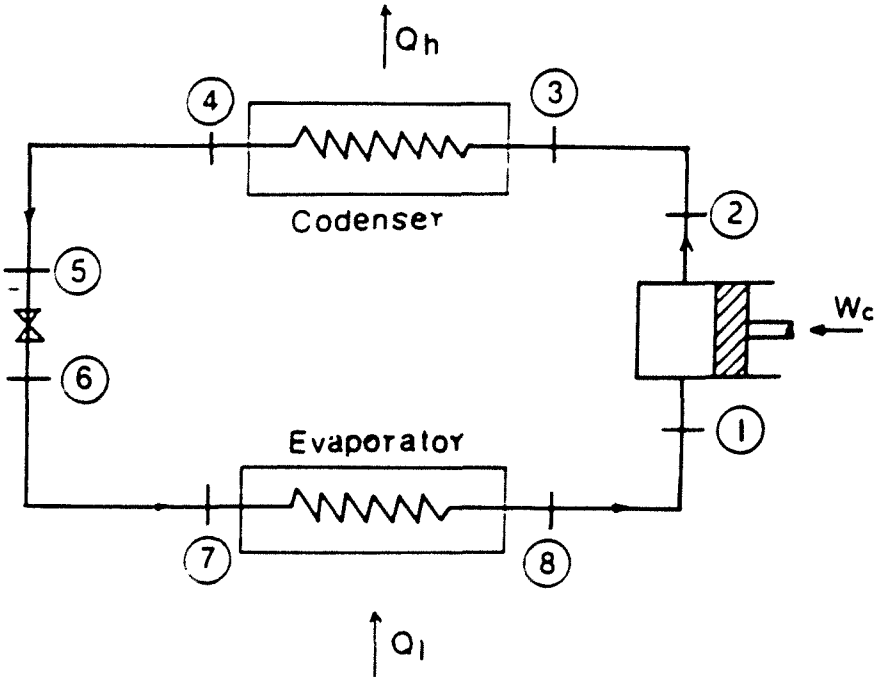

Figure 2.24 - A Schematic Diagram of Refrigeration System

in Figure 2.24. Therefore, to maximize the performance, work per one cycle should be minimized.

An actual P-V diagram and an ideal isentropic P-V diagram of a compressor are compared in Figure 2.25. Because the enclosed area of the P-V diagram indicates work supplied by the piston, the area difference can be thought of as a thermodynamic losses. There are two kinds of thermodynamic losses; one is caused by the difference between a polytropic constant and the reversible adiabatic gas constant $k = C_P/C_V$. The other is caused by over-compression and under expansion during valve action. The former is caused by heat transfer. A pseudopolytropic change also occurs due to leakage of gas during the compression and expansion process. The latter is caused by valve flow losses and gas pulsations. Therefore, two efficiencies were defined for our analysis.

The thermodynamic efficiency η_1 is

$$\eta_1 = \frac{W_{1s}}{W'_{act}} \tag{2.3}$$

where W_{1s} is the ideal isentropic work, equal to the area 1-2'-3'-4'-1, W'_{act} is the area of the actual P-V diagram, but with discharge and suction process losses subtracted. It is defined by 1-2-3-4-1 in Figure 2.25.

The thermodynamic efficiency η_2 is

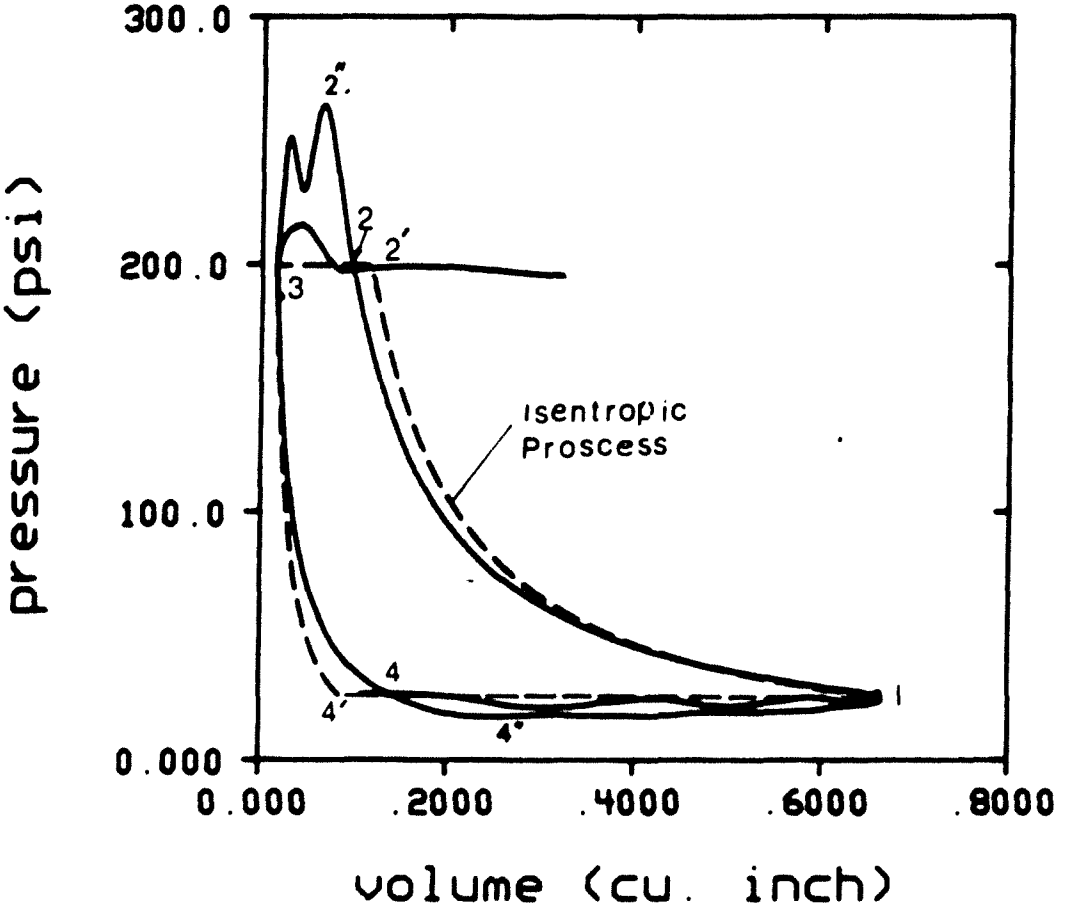

Figure 2.25 - An Actual vs. Ideal P-V Diagram

$$\eta_2 = \frac{W'_{act}}{W_{act}} \qquad (2.4)$$

Where W_{act} is the actual area of the total P-V diagram, all losses considered. It is defined in Figure 2.25 by 1-2-2"-3-4-4"-1.

The total thermodynamic efficiency η is therefore,

$$\eta = \eta_1 \eta_{2'} = \frac{W_{is}}{W_{act}} \qquad (2.5)$$

Note that the result of Fig. (2.25) seems to indicate that $\eta_1 > 1$.

For the compressor measured, it is felt that this is either caused by cooling of the cylinder walls by the suction gas or that the apparent gain in efficiency is due to leakage around the piston during compression. It is presumably very difficult to separate these two effects by experiment. It indicates that it is perhaps desirable to measure the actual mass delivered per unit piston work, but mass flow measurement is presently also unprecise. It would be impossible to separate out mass losses due to leakage.

If we agree that the valve designer has no influence on cylinder heat transfer and piston leakage, the thermodynamic efficiency η_2 is more important.

A computer program to implement the numerical integration to compute the efficiency η_2 was developed.

Using that program, η_2 was calculated for each operating conditions and listed in Table 2.5.

There are two kinds of energy losses; the one is energy loss by compression or expansion, the latter is valve systems loss. In this research, the latter part was studied because it is a more controllable or optimizable loss. The valve system loss is caused by valve and flow passage resistance and gas pulsations.

Experimental P-V diagrams were integrated numerically to calculate losses and the thermodynamic efficiency η_2 for each operating condition. They are shown in Table 2.5. As already mentioned, it appears that approximately 14 % loss is due to valve flow loss and 3 % loss is due to gas pulsation.

2.7 Summary

By studying the experimental P-V diagrams, the following intermediate conclusions could be made for the prototype compressor under study.

1. Energy losses due to valve flow losses seem to be a major part of the energy loss. Together suction and discharge valves consume between 12 % and 20 % of the piston work depending on the operating conditions.

2. Gas pulsations are not serious as far as the energy efficiency is concerned. However, they should be

TABLE 2.5 - Thermodynamic Efficiencies and Losses

Experiment	Pressure (psig) Suction	Discharge	Overall Efficiency	Valve Loss Suction Side	Valve Loss Discharge Side	Pulsation Loss Suction Side	Pulsation Loss Discharge Side	Total Power (kw)
1	11	185	82.53%	5.90%	6.90%	2.90%	1.77%	0.257
2	10	200	82.61%	8.26%	6.28%	1.12%	1.65%	0.270
3	10	220	83.66%	6.29%	6.10%	2.46%	1.49%	0.278
4	20	185	77.62%	11.32%	8.27%	0.11%	2.69%	0.333
5	15	180	79.19%	6.94%	8.07%	3.36%	2.45%	0.287
6	15	160	79.06%	6.24%	8.84%	3.49%	2.39%	0.272

traced in case modifications in flow passage design or muffler design will cause pulsation problems. It is best to anticipate this by theoretical simulation.

For both discharge and suction together, pulsation losses are between 2 % and 6 % of the piston work. From an acoustic viewpoint, however, it should be remembered that the energy contained in the sound waves is very small. Considering this, the gas pulsation found are very large as far as the noise control problem goes and should be reduced, if possible.

3. Valve flutter was observed for the suction valve, but no severe problem exists. The suction valve does not close properly at times. The discharge valve behaves well dynamically.

CHAPTER 3 - COMPUTER SIMULATION

3.1 Introduction

In general, a cycle of operation of a high speed positive displacement compressor can be described as a number of complicated phenomena, interacting and taking place in a short period of time[2]. The basic mathematical model in this research consists of five sets of coupled equations as shown in Figure 3.1. These are the volume equations of the cylinder, the thermodynamic equation of the cylinder process based on the polytropic process assumption, the mass flow equations through the valve, the valve dynamics equations, and the gas pulsation equations in the gas path.

In addition to theoretical equations, two sets of basic prototype measurements were conducted. Pressures in cylinder, suction and discharge valve plenums and valve motions were used to establish polytropic coefficients and valve dauping coefficients. Effective flow and effective force areas of the valve were calculated from the approximate equations obtained by Hamilton and Scwerzler[40].

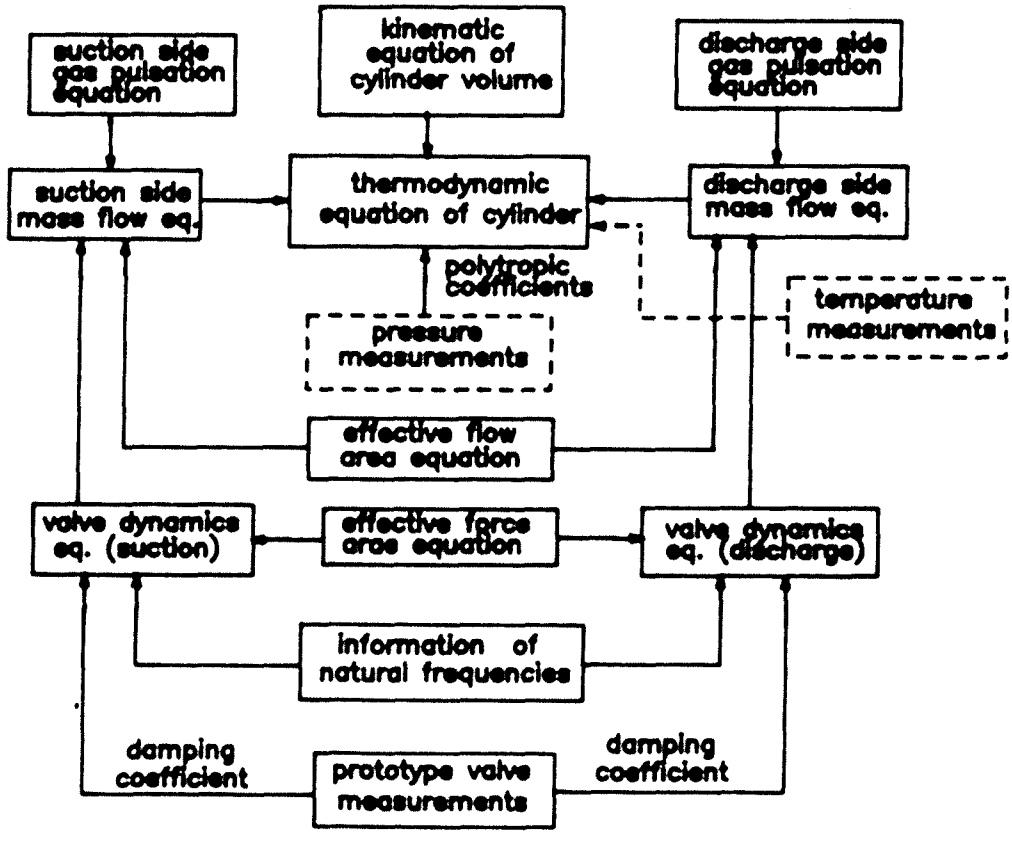

Figure 3.1 - Combination of Theoretical Informations with Laboratory Experiment for Compressor Analysis

Several simplifications and idealizations were made for the simulation model of this research. The main interests of this research were to determine thermodynamic efficiencies and gas pulsations behavior. Therefore relatively simplified valve motions and flow models were employed. Major characteristics of the simulation model can be identified as

1. A polytropic process model for the thermodynamic process of the cylinder was used.

2. An one dimension isentropic flow model was used for the valve flow. Quasi-state flow is assumed.

3. Detailed gas pulsation models were developed using lumped parameters, continuous one dimensional, and continuous three dimensional models.

4. The interaction between the cylinder process and the gas pulsation was calculated by a new iterative method.

5. The model has the capability to calculate the gas pulsations inside of the shell.

3.2 Mathematical Modeling of the System

In the following, the basic equations are summarized. They are derived in reference[18].

3.2.1 Kinematics of the Compressor

Instantaneous cylinder volume can be calculated from the following equation.

$$V(t) = V_c + \frac{\pi D^2 R_1}{4} \{ 1 + \cos\theta(t) + [\frac{R_2}{R_1} 1 - \sqrt{1 - (\frac{R_1}{R_2})^2 \sin^2\theta(t)}\ ] \} \qquad (3.1)$$

$$\text{and} \quad \theta(t) = \omega t \qquad (3.2)$$

where $V(t)$ = instantaneous cylinder volume, V_c = clearance volume, ω = angular velocity of crank. For the definition of D, R_1, R_2, see in Figure 3.2.

3.2.2 Thermodynamic Equation of Cylinder

Ideal gas, one dimensional flow, and a polytropic process are assumed. Mass conservation of the cylinder volume is assumed by

$$\dot{m}(t) = \dot{m}_{vs} - \dot{m}_{vd} \qquad (3.3)$$

where $m(t)$ = instantaneous mass in cylinder, $\dot{m}_{vs}$ = mass flow rate through suction valve, $\dot{m}_{vd}$ = mass flow rate through discharge valve.

The polytropic process equation is

$$P(t) = P_o (\frac{m(t)}{\rho_o v(t)})^n \qquad (3.4)$$

where P_o, ρ_o are initial conditions.

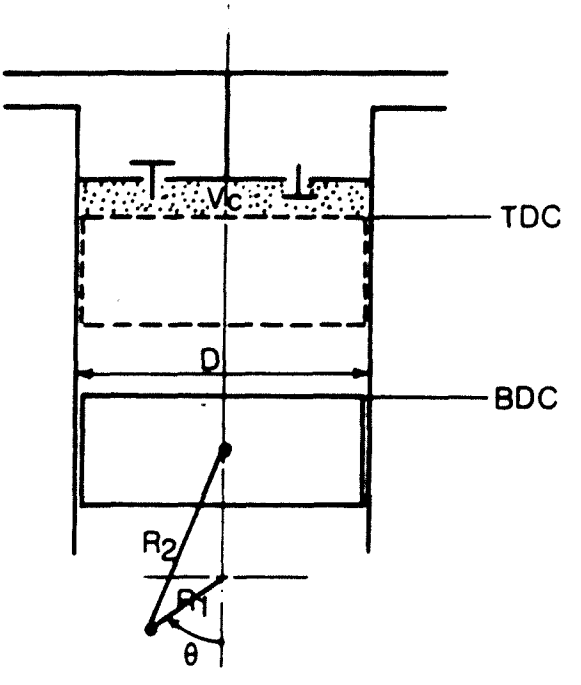

Figure 3.2 - Kinematics of Reciprocating Compressors

The instantaneous temperature is found from

$$T(t) = T_o \left(\frac{P(t)}{P_o}\right)^{\frac{n-1}{n}} \qquad (3.5)$$

where n is the polytropic constant

3.2.3 Valve Dynamics and Valve Flow

(1) Mass Flow through Valves

Basic assumptions are

1) One dimensional isentropic flow

2) Steady flow equations

3) Valve openings can be treated instantaneously as a simple orifice of equivalent effective cross-sectional area

4) Upstream conditions are assumed to be stagnation conditions

Mass flow through the valve is given by

$$\dot{m}_v = A_v P_u \sqrt{\frac{2kg_c}{(k-1)RT_u}} \sqrt{\gamma^{\frac{2}{k}} - \gamma^{\frac{k+1}{k}}} \qquad (3.6)$$

where

$$\gamma = \frac{P_d}{P_u} \quad \text{if} \quad \gamma > \frac{P_{crit}}{P_u} \text{ (unchoked)} \qquad (3.7)$$

$$\gamma = \gamma_c \quad \text{if} \quad \gamma < \frac{P_{crit}}{P_u} \text{ (choked)} \tag{3.8}$$

$$\gamma_c = \left(\frac{2}{k+1}\right)^{\frac{k}{k-1}} \tag{3.9}$$

and where, referring to Figure 3.3, A_v = effective flow area (in^2), P_u = upstream pressure (psi), k = C_p/C_v ratio of specific heats, R = Gas constant (ft-lbf/R/lbm), γ = P_d/P_u, T_u = upstream temperature (^oR), g_c = gravitational constant (32.2 ft/sec^2),

(2) Valve Dynamics Equation

In this case, suction and discharge valves were modeled as one-dimensional equivalent mass-spring system, as shown in Figure 3.4.

$$m_{eq}\ddot{x} + C_{eq}\dot{x} + k_{eq}\,x = (P_u - P_d) \cdot A_F \tag{3.10}$$

where A_F = effective area of the valve (in^2), m_{eq} = equivalent mass of the valve (lb sec^2 / in), C_{eq} = damping coefficient (will be adjusted to the experimental result) ($\frac{lbf\ sec}{in}$), and k_{eq} = equivalent stiffness of the valve (lbf/in), where

$$k_{eq} = \frac{F_{st}}{\delta_{st}} \quad \text{(see Figure 3.4)} \tag{3.11}$$

The equivalent mass can be obtained from

$$\omega_{eq} = \frac{k_{eq}}{\omega_n^2} \tag{3.12}$$

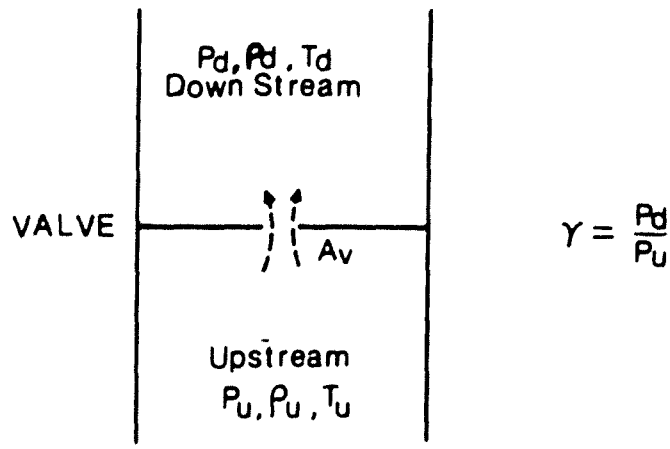

Figure 3.3 - Schematic Diagram of the Mass Flow through the Compressor Valve

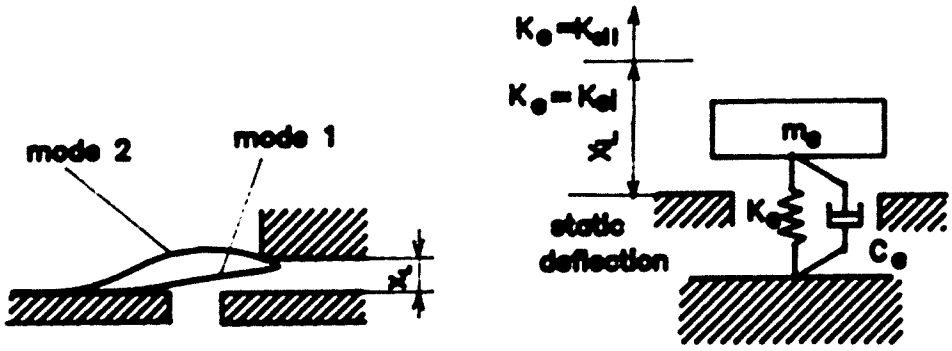

SUCTION VALVE

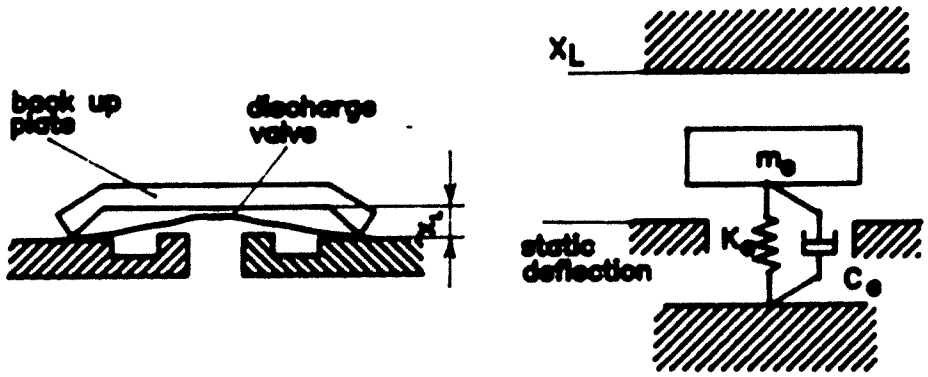

DISCHARGE VALVE

Figure 3.4 - Idealized One Dimensional Model for the Valve Motions

where ω_n is the measured 1st fundamental natural frequency of the valve.

(3) Auxiliary Equations[26]

1) Effective flow area. Referring to Figure 3.5,

$$KA_v = \frac{(KA)_o}{[1 + (\frac{(KA)_o}{(KA)_1})^2]^{1/2}} \qquad (3.13)$$

where K = contraction coefficient

2) Effective force area. Referring to Figure 3.6,

$$A_F = (KA_v)^2 \left(\frac{A_p}{A_r^2} + \frac{1}{A_o}\right) \qquad (3.14)$$

3.3 Analysis of Gas Pulsations

The four pole matrix is a very convenient concept for the analysis of a composite dynamic or acoustic system[40,41]. Four pole parameters of typical acoustic elements which comprise gas manifold of the compressor are derived in this section. Also, techniques to obtain the system solution using four pole matrices of its elements are discussed. A general method to obtain four pole parameters for a three dimensional cavity from pressure response solutions will be discussed in chapter 4.

The four pole equation of an acoustic system is defined as

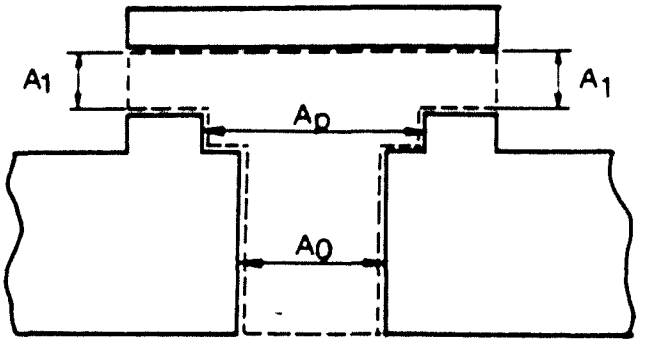

Figure 3.5 - Effective Flow Area of the Compressor Valve[17]

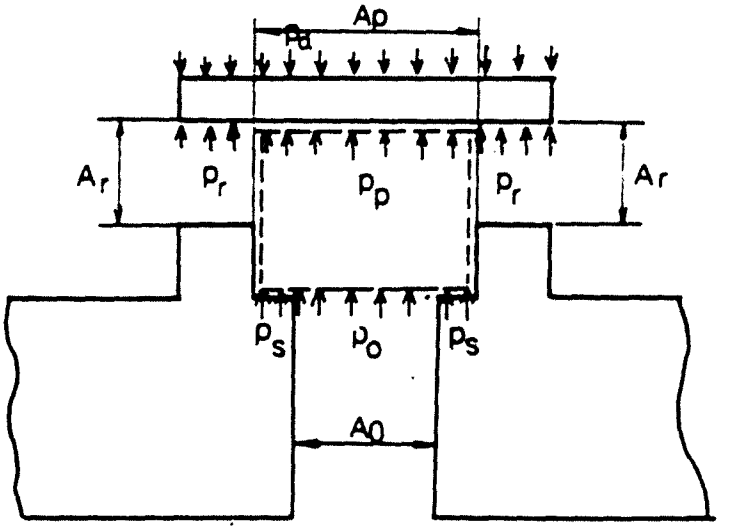

Figure 3.6 - Effective Force Area of the Compressor Valve

$$\begin{Bmatrix} Q_o \\ P_o \end{Bmatrix} = \begin{bmatrix} A & B \\ C & D \end{bmatrix} \begin{Bmatrix} Q_L \\ P_L \end{Bmatrix} \qquad (3.15)$$

where subscripts o and L stand for quantities at the input port and the output port as shown in Figure 3.7 , and Q and P are complex amplitudes of harmonic volume flow and acoustic pressure. For example, the pressure at the input point is

$$p(t) = P_o e^{j\omega t} \qquad (3.16)$$

A,B,C, and D designate complex four pole parameters throughout this thesis.

3.3.1 Four Pole Parameters of Acoustic Elements

(1) Four Poles of a Lumped Parameter Cavity

The acoustic pressure-volume relationship of a small cavity is according to reference[1],

$$P = - \rho_o C_o^2 \frac{\delta V}{V_o} \qquad (3.17)$$

where, C_o is the speed of sound

ρ_o is average density of the gas in cavity

V_o is volume of the cavity (see Figure 3.8.)

Therefore,

$$P = - \frac{\rho_o C_o^2}{V_o} \left[\int^t Q_L \, dt - \int^t Q_o \, dt \right]$$

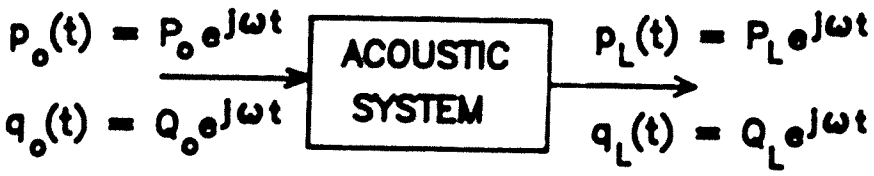

Figure 3.7 - An Acoustic Four Pole System

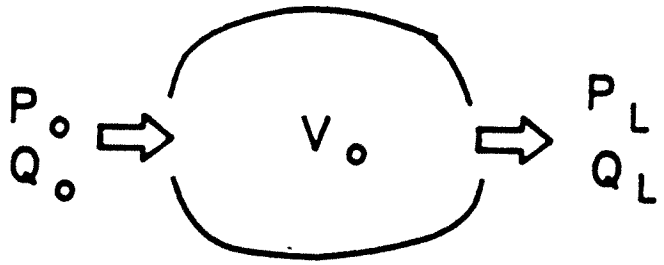

Figure 3.8 - A Lumped Parameter Acoustic Cavity

$$= \frac{\rho_o C_o^2}{j\omega V_o} (Q_o - Q_L) \qquad (3.18)$$

Because the cavity is being approximated as a lumped parameter acoustic element,

$$P = P_o = P_L \qquad (3.19)$$

By rearranging equation (3.18),

$$Q_o = \frac{P_L}{\rho_o C_o^2} j\omega V_o + Q_L \qquad (3.20)$$

Rewriting equations 3.19 and 3.20 in matrix form, the four pole equation is given by

$$\begin{Bmatrix} Q_o \\ P_o \end{Bmatrix} = \begin{bmatrix} 1 & \frac{j\omega V_o}{\rho C_o^2} \\ 0 & 1 \end{bmatrix} \begin{Bmatrix} Q_L \\ P_L \end{Bmatrix} \qquad (3.21)$$

(2) Four Pole of a Short Lumped Parameter Pipe

If a gas is contained in a relatively short pipe which is connected to a volume, the gas vibrates as if it is an incompressible mass connected to a spring[1]. The equilibrium equation of this mass is, referring to Figure 3.9,

$$(P_o - P_L) S_o - D\dot{\xi} = \rho_o S_o L_o \ddot{\xi} \qquad (3.22)$$

where D is the damping coefficient and S_o is cross section

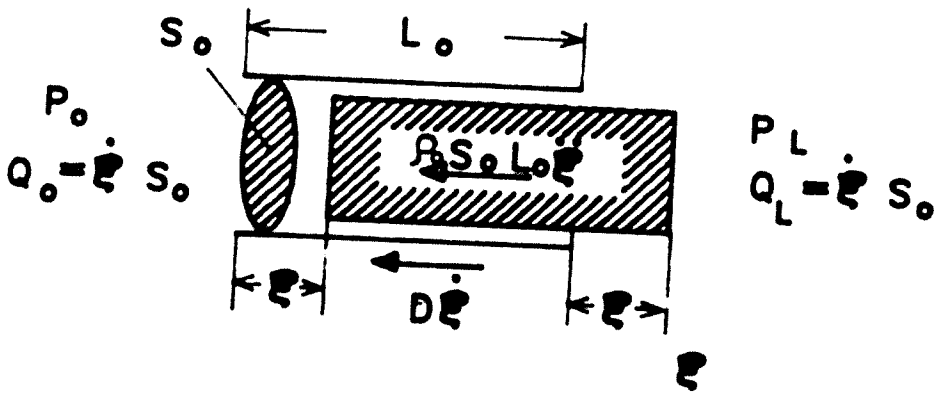

Figure 3.9 - Free Body Diagram of the Gas in a Short Pipe

area of the pipe.

Volume velocities are the same at both ends of the neck because the gas is assumed to be incompressible,

$$Q_o = Q_L \tag{3.23}$$

Since $S_o\dot{\xi} = Q_o = Q_L$, equation 3.20 becomes

$$P_o = \left(\frac{D}{S_o^2} + j\omega \frac{\rho_o L_o}{S_o}\right) Q_L + P_L \tag{3.24}$$

Therefore, the four pole equation becomes

$$\begin{Bmatrix} Q_o \\ P_o \end{Bmatrix} = \begin{bmatrix} 1 & 0 \\ \frac{D}{S_o^2} + j\omega\frac{\rho_o L_o}{S_o} & 1 \end{bmatrix} \begin{Bmatrix} Q_L \\ P_L \end{Bmatrix} \tag{3.25}$$

(3) A Finite Length Pipe

In case of a long pipe relative to the shortest acoustic wave length of interest, the gas in the pipe cannot be considered incompressible any more. One dimensional wave equation has to be solved to obtain the four pole relations.

The four pole equation is given as

$$\begin{Bmatrix} Q_o \\ P_o \end{Bmatrix} = \begin{bmatrix} \cosh\gamma L & \dfrac{j\omega S_o}{\rho_o C_o^2 \gamma \sinh\gamma L} \\ \dfrac{\rho_o C_o^2 \gamma \sinh\gamma L}{j\omega S_o} & \cosh\gamma L \end{bmatrix} \begin{Bmatrix} Q_L \\ P_L \end{Bmatrix} \qquad (3.26)$$

where $\gamma = a + jk$, and where the wave number $k = \frac{\omega}{C_o}$ The constant "a" represents the fluid damping term which is discussed in reference[1] in more detail.

3.3.2 Formulation of the Overall Four Pole Matrix

(1) Suction Gas Path

The suction side gas path of the prototype compressor is shown in Figure 3.10. It is composed of three volumes including a side branch -resonator(V_{3s}) connected to the first volume(V_{1s}) and an annular shell cavity. The annular cavity is connected to an anechoically terminated pipe.

The overall four pole matrix can be obtained by cascading four pole matrices of serially connected elements. For example

$$\begin{Bmatrix} P_i \end{Bmatrix} = \begin{bmatrix} A_{pi} & B_{pi} \\ C_{pi} & D_{pi} \end{bmatrix} = \begin{bmatrix} 1 & 0 \\ \dfrac{D_i}{S_{is}^2} + j\omega\dfrac{\rho_o L_{is}}{S_{is}} & 1 \end{bmatrix} \qquad (3.27)$$

is the four pole matrix of the i^{th} lumped parameter pipe. Notice that for pipes which are relatively long, equation

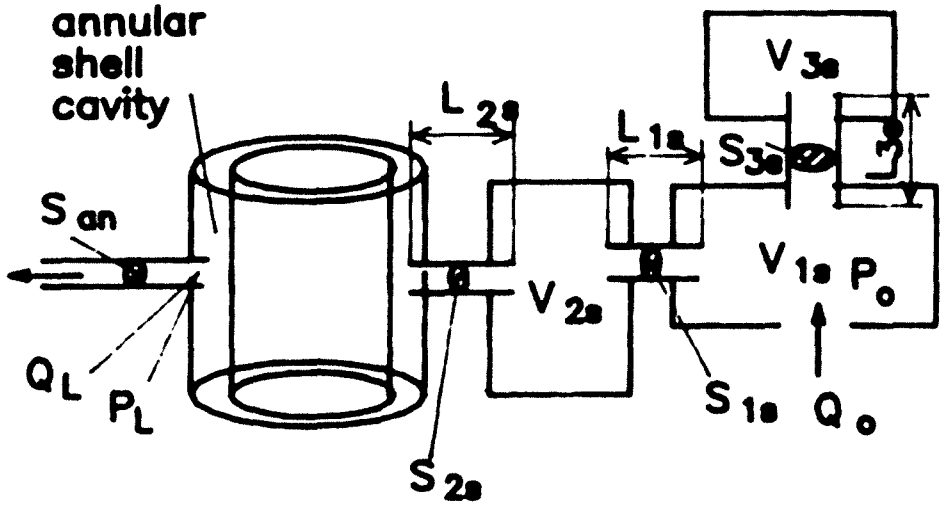

Figure 3.10 - Suction Gas Manifold of the Prototype Compressor

3.26 should be used. The four pole matrix of the i^{th} volume is

$$\begin{bmatrix} V_i \end{bmatrix} = \begin{bmatrix} A_{vi} & B_{vi} \\ C_{vi} & D_{vi} \end{bmatrix} = \begin{bmatrix} 1 & \frac{j\omega V_{is}}{\rho_o C_o^2} \\ 0 & 1 \end{bmatrix} \tag{3.28}$$

The four pole matrix of the annular cavity, which will be formulated in the next chapter for the continuous case, is in general

$$\begin{bmatrix} V_a \end{bmatrix} = \begin{bmatrix} A_a & B_a \\ C_a & D_a \end{bmatrix} \tag{3.29}$$

The resulting overall four pole matrix is defined as

$$\begin{bmatrix} T \end{bmatrix} = \begin{bmatrix} A_T & B_T \\ C_T & D_T \end{bmatrix} \tag{3.30}$$

This overall four pole matrix $\begin{bmatrix} T \end{bmatrix}$ can be obtained by multiplying five four pole matrices

$$\begin{bmatrix} A_T & B_T \\ B_T & D_T \end{bmatrix} = \begin{bmatrix} V_1' \end{bmatrix} \cdot \begin{bmatrix} P_1 \end{bmatrix} \cdot \begin{bmatrix} V_2 \end{bmatrix} \cdot \begin{bmatrix} P_2 \end{bmatrix} \cdot \begin{bmatrix} V_a \end{bmatrix} \tag{3.31}$$

where, $[\ V_1'\ ]$ stands for a modified four pole matrix of the first cavity to take account of the effect of the side branch resonator. According to reference[1],

$$\begin{bmatrix} V_1' \end{bmatrix} = \begin{bmatrix} A_{v1} & B_{v1} + \frac{1}{Z_{soo}} \\ C_{v1} & D_{v1} \end{bmatrix} \tag{3.32}$$

where Z_{soo} is the impedance of the input point of the side branch. To obtain Z_{soo}, let us consider the four pole equation of the side branch alone. Because the side branch is composed of a short pipe and a small cavity, the four pole equation of the side branch is given by,

$$\begin{Bmatrix} Q_{3s} \\ P_{3s} \end{Bmatrix} = \begin{bmatrix} A_s & B_s \\ C_s & D_s \end{bmatrix} \begin{Bmatrix} Q_{3L} \\ P_{3L} \end{Bmatrix}$$

$$= \begin{bmatrix} A_{p3} & B_{p3} \\ C_{p3} & D_{p3} \end{bmatrix} \cdot \begin{bmatrix} A_{v3} & B_{v3} \\ C_{v3} & D_{v3} \end{bmatrix} \begin{Bmatrix} Q_{3L} \\ P_{3L} \end{Bmatrix} \qquad (3.33)$$

$Q_{3L} = 0$ because the end of the side branch is closed, therefore, equation (3.33) tells us that

$$Z_{soo} = \frac{P_{3s}}{Q_{3s}} = \frac{1}{B_s} = \frac{1}{A_{p3} B_{v3} + B_{p3} D_{v3}} \qquad (3.34)$$

Now the four pole matrix of the suction gas path given by equation 3.31 can readily be calculated.

(2) Discharge Gas Path

The gas path of the discharge is composed of four serially connected volumes, with three short pipes as shown in Figure 3.11. Using similar conventions for the suction side, the four pole matrix is obtained by

$$\begin{Bmatrix} T \end{Bmatrix} = \begin{Bmatrix} V_1 \end{Bmatrix} \cdot \begin{Bmatrix} P_1 \end{Bmatrix} \cdot \begin{Bmatrix} V_2 \end{Bmatrix} \cdot \begin{Bmatrix} P_2 \end{Bmatrix} \cdot \begin{Bmatrix} V_3 \end{Bmatrix} \cdot \begin{Bmatrix} P_3 \end{Bmatrix} \cdot \begin{Bmatrix} V_4 \end{Bmatrix} \qquad (3.35)$$

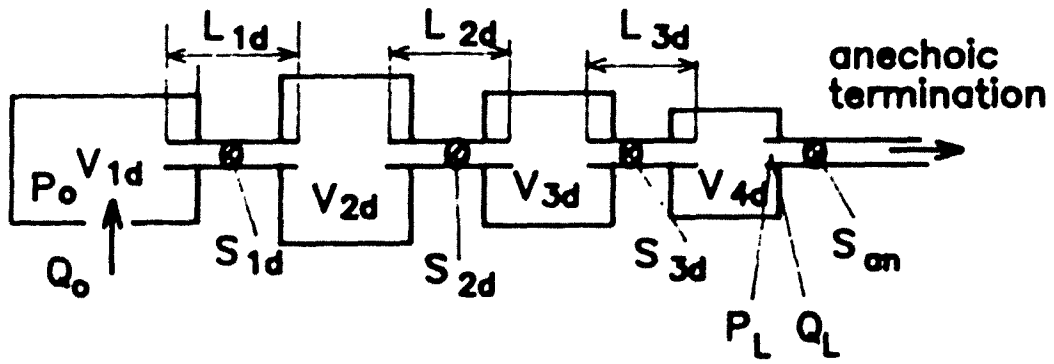

Figure 3.11 - Discharge Gas Manifold of the Prototype Compressor

3.3.3 Calculation of the Frequency Response Spectrum

The input point impedance is defined as

$$Z_o = \frac{P_o}{Q_o} \tag{3.36}$$

Physically, this is the pressure response of the first cavity of the system due to a unit input volume flow through the valve port. Let us take the suction side as the example, because the procedure can be applied to the discharge side in exactly the same way. The overall four pole equation of the suction side is

$$\begin{Bmatrix} Q_o \\ P_o \end{Bmatrix} = \begin{bmatrix} A_T & B_T \\ C_T & D_T \end{bmatrix} \begin{Bmatrix} Q_{sL} \\ P_{sL} \end{Bmatrix} \tag{3.37}$$

The system is anechoically terminated, therefore, Q_{sL} and P_{sL} are related by[1]

$$Q_{sL} = \frac{S_{an}}{C_o \rho_o} P_{sL} \tag{3.38}$$

Then, from equation 3.37

$$Q_{sL} = \left(A_T \frac{S_{an}}{C_o \rho_o} + B_T \right) P_{sL} \tag{3.39}$$

$$P_{so} = \left(C_T \frac{S_{an}}{C_o \rho_o} + D_T \right) P_{sL} \tag{3.40}$$

Therefore, the input point impedance is given by

$$Z_o = \frac{P_{so}}{Q_{so}} = \frac{C_T \frac{S_{an}}{C_o \rho_o} + D_T}{A_T \frac{S_{an}}{C_o \rho_o} + B_T} \qquad (3.41)$$

Obviously the same procedure can be applied for the discharge side.

At first, the effect of the continuous annular cavity is not included in the compressor simulation. Because the annular cavity is much larger than the other cavities, the pressure at the annular cavity was at first assumed to be constant. It is a good approximation if pulsating pressures in the suction cavity and thermodynamic efficiency are the major concerns. In such a case, the overall four pole matrix of the suction system is obtained by multiplying the first four element matrices except the matrix of the annular cavity in equation (3.31).

Because the acoustic pressure in the shell cavity is assumed to be zero, from equation (3.37),

$$Q_{so} = A_T Q_{sL} \qquad (3.42)$$

$$P_{so} = C_T Q_{sL} \qquad (3.43)$$

Therefore, the pressure response (or the input point impedance) is,

$$Z_o = \frac{P_{so}}{Q_{so}} = \frac{C_T}{A_T} \qquad (3.44)$$

The pressure response spectrum is obtained by calculating the pressure responses as a function of

frequency by equation (3.41) or (3.44). Figure 3.12 is the spectrum of the suction manifold which does not have a side branch resonator and Figure 3.13 is the spectrum of the discharge manifold of the prototype compressor.

3.4 Numerical Implementations

As discussed before, the total mathematical model for the compressor simulation involves the following equations

1. A kinematics equation which defines the cylinder volume (equation(3.1)).
2. The thermodynamic equation for the cylinder process (equation(3.4)).
3. Two mass flow equations (equation(3.6)).
4. Two simplified valve dynamics equations (equation(3.10)).
5. Suction and discharge gas pulsation equation.

These equations are coupled with each other. The pulsating pressures at the suction and discharge cavities are coupled with mass flow equations and valve dynamics equations because these pressures are the back pressure which valves see.

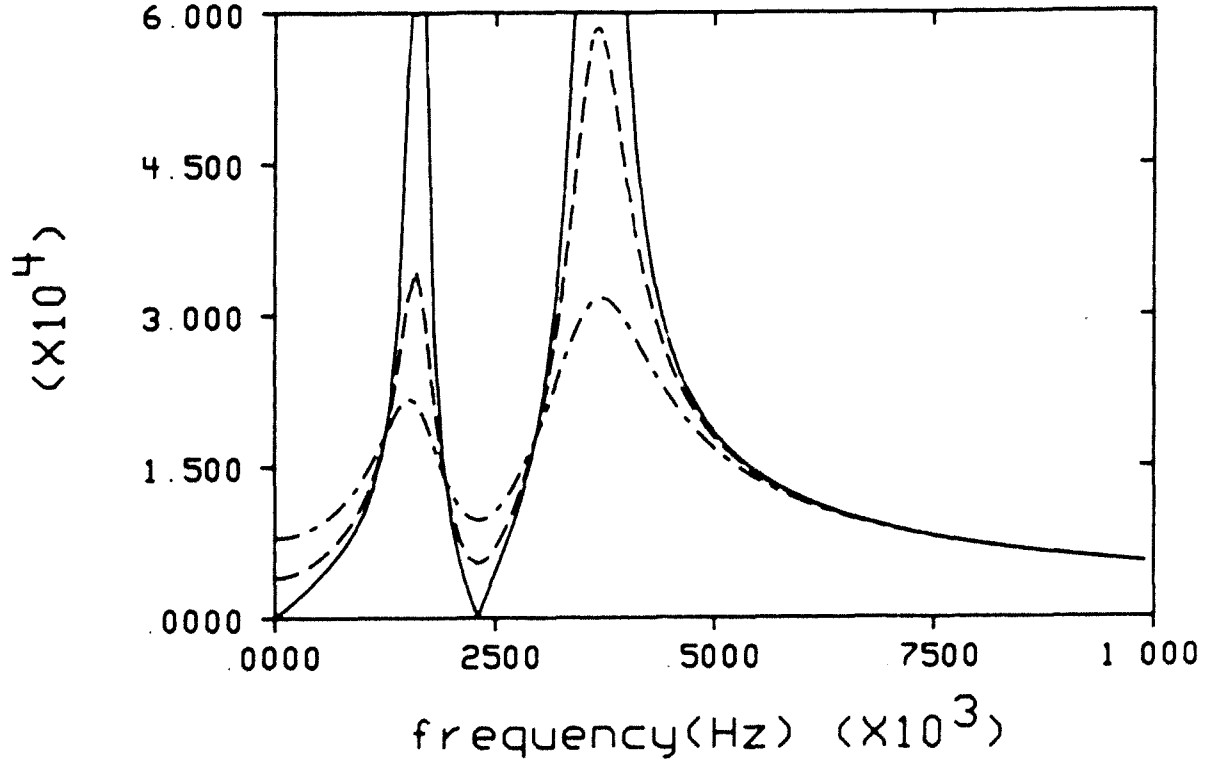

Figure 3.12 - Pressure Response Spectrum of the Suction Gas Manifold, _____ ξ = 0., ---- ,ξ = 0.1, —-—-— ,ξ = 0.2

3.4.1 Structure of the Simulation Program

The overall flow chart of the simulation program is shown in Figure 3.14. As shown in Figure 3.15, a P-V diagram is calculated with constant suction and discharge line pressures at the beginning. The P-V diagram is integrated for a given number of cycles for each pulsation pressure condition until the result is converged. At the end of each given iteration, the acoustic pressures at the suction and discharge cavities are calculated. These iterations, each of which is composed of a few cycles of P-V integration and one calculation of a new set of pulsation pressures, should be continued until converged results are obtained.

(1) Frequency Response Calculation (Step 1 in Figure 3.14)

At the beginning of the simulation, frequency response spectra of the suction manifold and the discharge manifold are calculated following the procedure in section 3.3. This step is conducted only once during the entire simulation and kept in an array form for later use.

(2) Calculation of Polytropic Expansion and Compression Procedure (Step 2, 5 in Figure 3.14)

When both the suction valve and the discharge valve are closed, there is no mass flow in or out of the compressor cylinder. Therefore, the cylinder process during

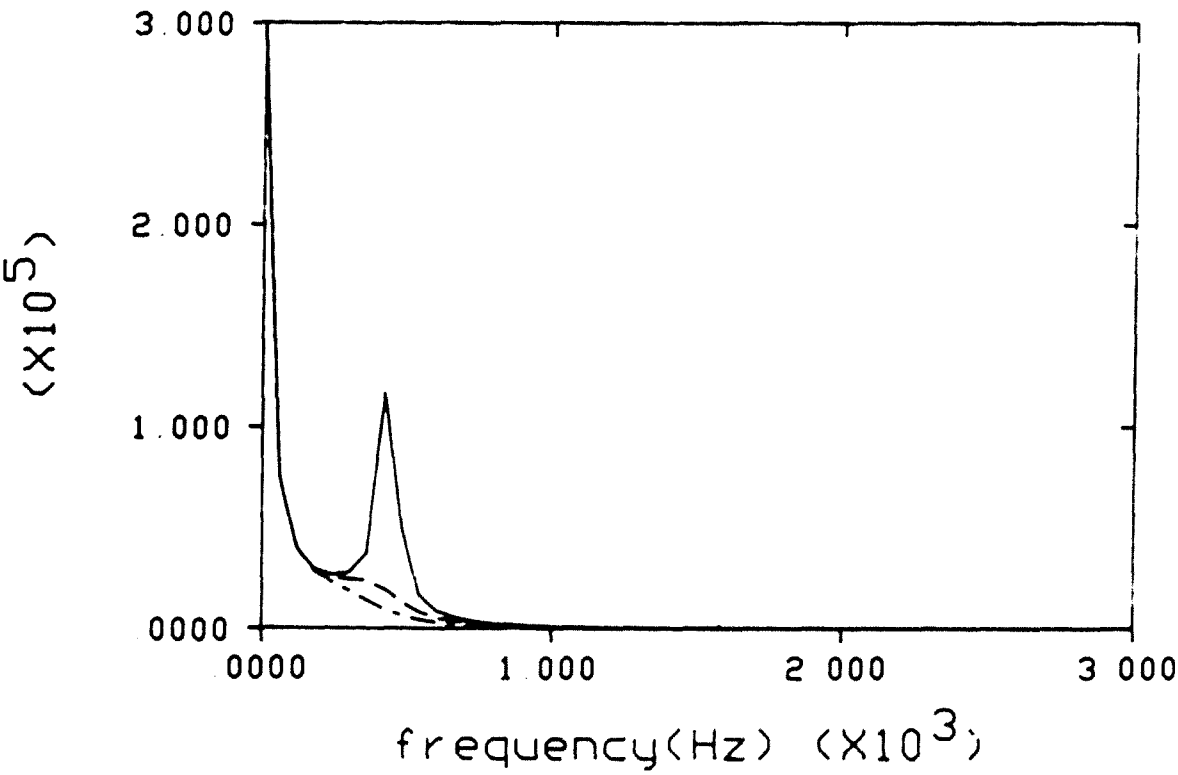

Figure 3.13 - Pressure Response Spectrum of the Discharge Gas Manifold, ——— ξ = 0., - - - - ,ξ = 0.1, —·—·—,ξ = 0.2 —··—,ξ = 0.2

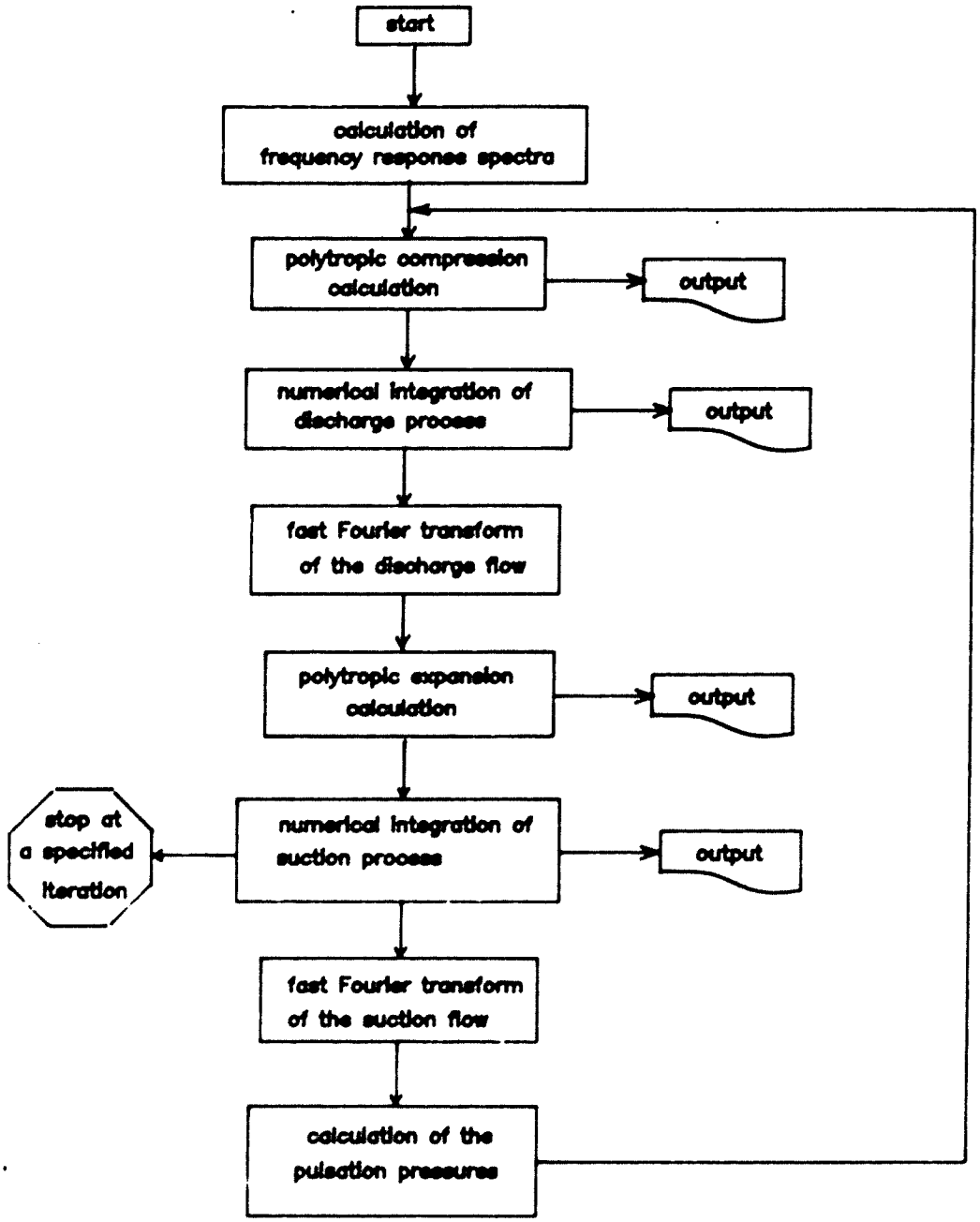

Figure 3.14 - Overall Structure of the Computer Simulation Program

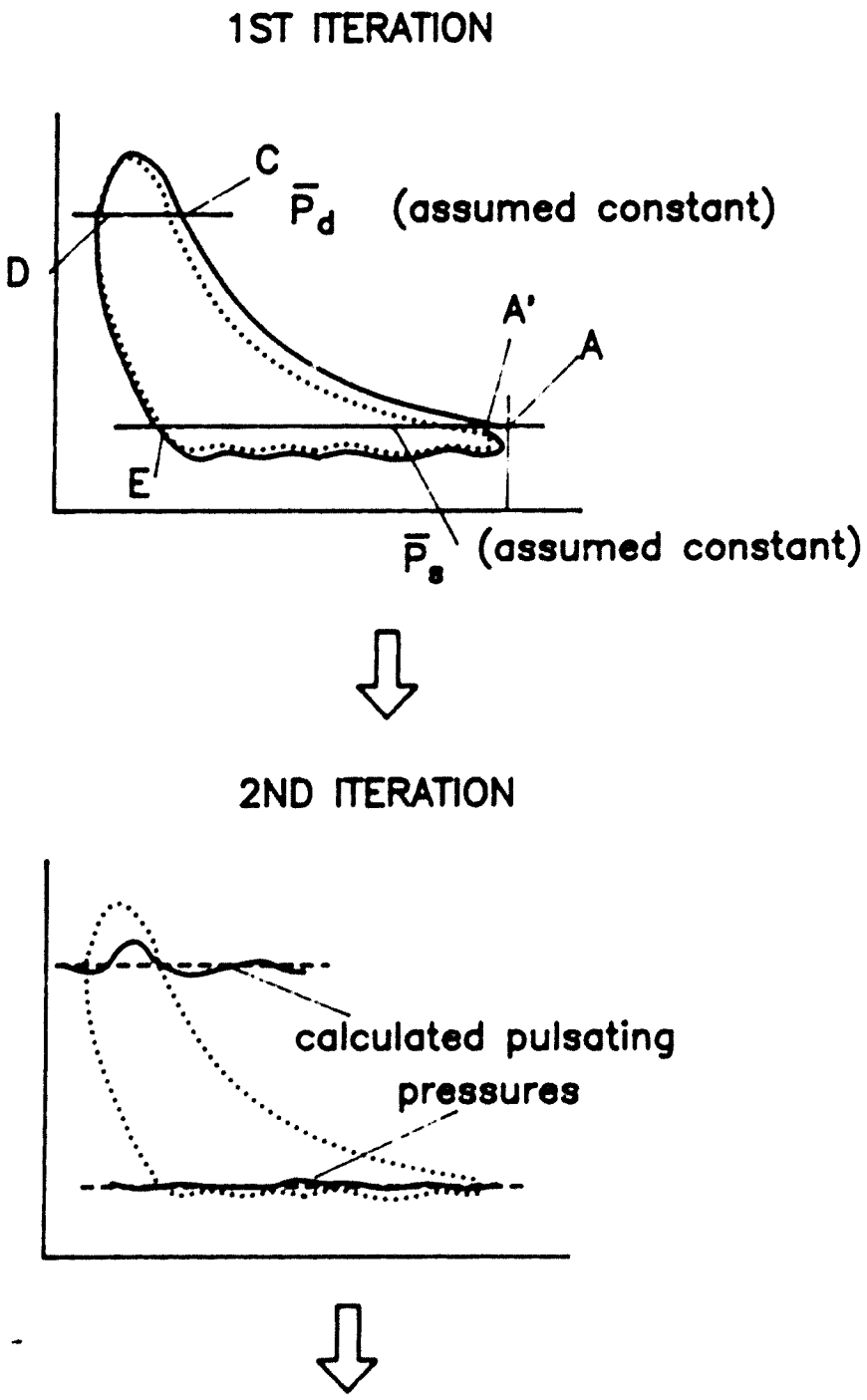

Figure 3.15 - Illustration of the Iterative Calculation of the P-V Diagram

the polytropic expansion and compression can be calculated from the polytropic equation.

$$p_c(t) = P_o \left(\frac{V_o}{V_c(t)}\right)^n \qquad \text{(equation(3.4))}$$

where P_o and V_o are the initial cylinder pressure and volume.

The polytropic index n has to be estimated or determined experimentally. The coefficient describes the average heat transfer between cylinder gas and cylinder wall. In the case of no heat transfer,

$$n = k = \frac{C_{p_o}}{C_{v_o}} \qquad (3.45)$$

If all the heat generated during the compression is removed, or all the heat loss during the expansion is supplied,

$$n = 1 \qquad (3.46)$$

For typical, small high speed compressors,

$$1 < n < k \qquad (3.47)$$

In general the coefficient n has different values for the compression process and for the expansion process[43].

(3) Numerical Integrations for the Suction Process and the Discharge Process (Step 3, 6 in Figure 3.14)

Once one of the valves is open, cylinder process equation, valve dynamics equations, and valve flow equations are solved simultaneously. The Runge-Kutta method is employed to solve the equation set. It is a forward numerical integration schema starting with given initial values.

The equations which are to be calculated at each time step are

1. The cylinder volume equation (equation(3.1))
2. The cylinder mass equation (equation(3.3))
3. The cylinder state equation (equation(3.4))
4. The mass flow equation (equation(3.6))
5. The valve dynamics equation (equation(3.10))

with auxiliary equations (3.13) and (3.14). The valve dynamic equation is decomposed into two first order differential equations. Starting with

$$m_{eq}\ddot{y} + c_{eq}\dot{y} + k_{eq}y = (P_u - P_d) \cdot A_F \quad \text{(equation}$$

and letting

$$y_1 = y \tag{3.48}$$

$$y_2 = \dot{y}_1 = \dot{y} \tag{3.49}$$

Then,

$$\dot{y}_2 = \ddot{y} = -\frac{c_{eq}}{m_{eq}}\dot{y} - \frac{k_{eq}}{m_{eq}}y + \frac{\Delta p}{m_{eq}}A_F$$

$$= -\frac{C}{m}y_2 - \frac{k}{m}y_1 + \frac{P_u - P_d}{m}A_F \qquad (3.50)$$

The mass flow is also a function of y_1 which determines the valve opening. Therefore,

$$\dot{m}_C = f_1(m_c, y_1, y_2; p_c, p_d, p_s, \ldots) \qquad (3.51)$$

$$\dot{y}_1 = f_2(m_c, y_1, y_2, ; p_c, p_d, p_s, \ldots) = y_2 \qquad (3.52)$$

$$\dot{y}_2 = f_3(m_c, y_1, y_2; p_c, p_d, p_s \ldots)$$

$$= -\frac{c_{eq}}{m_{eq}}y_2 - \frac{k_{eq}}{m_{eq}}y_1 + \frac{\Delta p}{m_{eq}}A_F \qquad (3.53)$$

By integrating equations(3.48) through (3.53), valve displacements (y_1) ,valve mass flows and cylinder mass (m_c) are obtained at each time step. The instantaneous cylinder pressure is determined from equation (3.4) with the calculated cylinder mass. Reference[42] gives a general discussions of the Runge-Kutta method and reference[11] can be consulted for the application of the method to the compressor simulation.

It is necessary to assume the initial conditions to start the numerical integration. For example, the values

for the discharge process are taken from the conditions at point C in Figure 3.15. The polytropic compression process starts from the point A , at which the cylinder pressure and temperature are the average suction line pressure and temperature, and the piston is at the bottom dead center. If the cylinder pressure is increased to the average discharge line pressure, the numerical integration procedure for the discharge process starts using the conditions at point C as initial conditions.

After a certain number of time steps of integration, the discharge valve closes because the cylinder pressure drops under the average discharge line pressure(point D in Figure 3.15). Then the numerical integration procedure stops and the polytropic expansion process calculation starts until the process reaches point D at which the cylinder pressure is the discharge pressure.

The integration of the suction process continues to point A´ in Figure 3.15. The whole cycle is repeated for the specified times until a converged indicator diagram is obtained for the given set of pulsation pressures.

The size of the time step has to be carefully determined. A smaller time step produces more accurate result at the cost of more computing time.

(4) Fast Fourier Transform

The volume flows through the valve ports are computed as a function of time, while Fourier components of these flows are needed for the calculation of the pulsating pressures in the frequency domain. Therefore, the volume flow data in the time domain are transformed to the frequency domain by discrete Fourier transformation.

The discrete Fourier transformation is derived in refence[10].

$$Q_k = \frac{1}{N} \sum_{r=0}^{N-1} q_r \, e^{-j(2\pi kr / N)}, \qquad (3.54)$$

Where, k = 0,1,2,...,(N-1). The actual computation is done by the fast Fourier transform algorithm.

(5) Calculation of the Pulsation Pressures (Figure 3.16)

The pulsation pressures in the discharge cavity and in the suction cavity are periodic functions with the fundamental period being the time it takes for one compressor cycle. Like all other periodic functions, these pressures can be represented by a Fourier series. For example, the Fourier series representation of the discharge pressure is

$$p_d(t) = a_o + 2 \sum_{n=1}^{\infty} \left(a_n \cos \frac{2\pi nt}{T} + b_n \sin \frac{2\pi nt}{T}\right) \qquad (3.55)$$

where

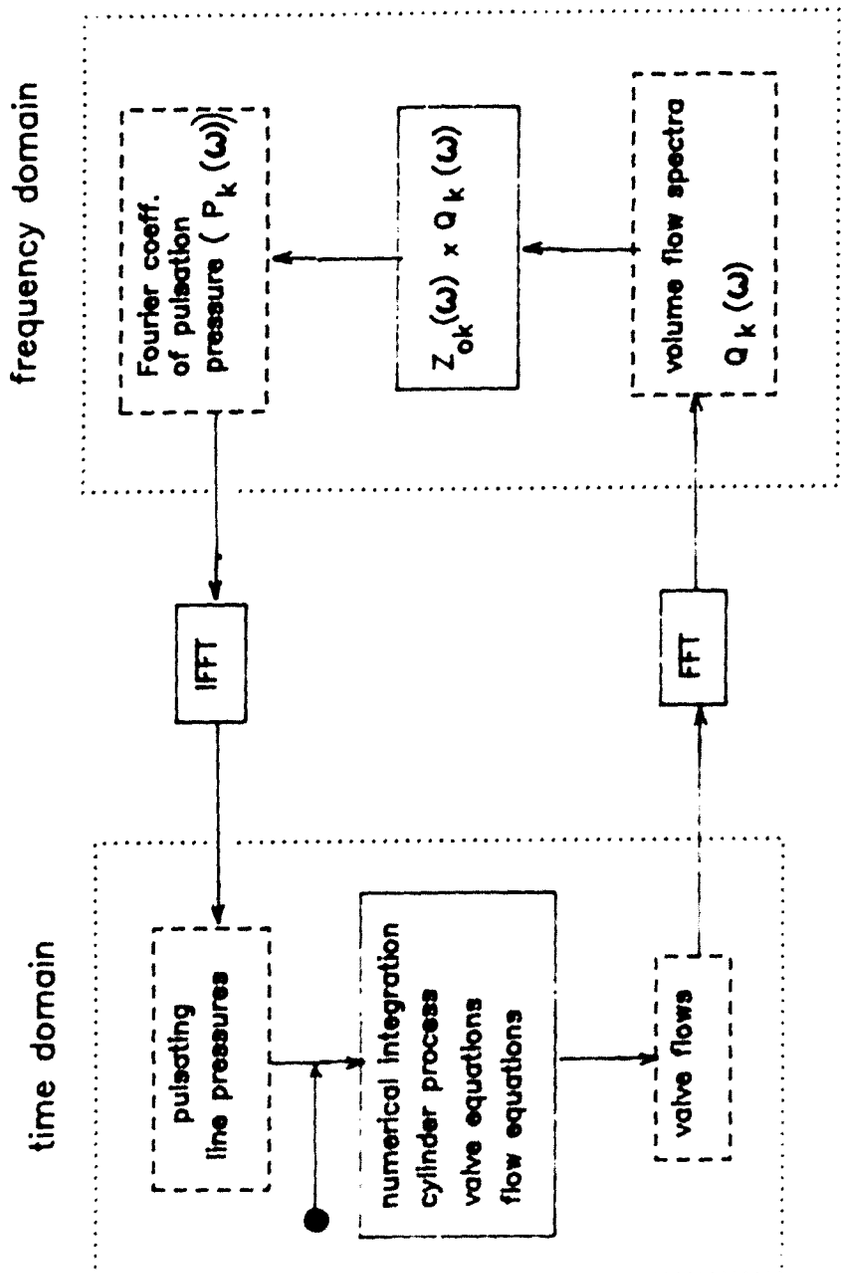

Figure 3.16 - Calculation of Pulsating Pressures

$$a_n = \frac{1}{T}\int_o^T p_d(t)\cos\frac{2\pi nt}{T}\,dt \qquad n = 0,1,2,\ldots \qquad (3.56)$$

$$b_n = \frac{1}{T}\int_o^T p_d(t)\sin\frac{2\pi nt}{T}\,dt \qquad n = 0,1,2,\ldots \qquad (3.57)$$

If equation (3.55) is summed to a sufficiently large number nrec, we obtain

$$p_d(t) = \sum_{n=0}^{nrec} P_n\, e^{j\frac{2\pi nt}{T}} \qquad (3.58)$$

$$\text{Where, } P_n = 2(a_n - jb_n) \qquad (3.59)$$

Therefore, equation (3.55) can be rewritten

$$p_d(t_r) = \sum_{n=0}^{nrec} P_n\, e^{j(2\pi nr/N)} \qquad (3.60)$$

where, r=0,1,2,..,N-1, and $t_r = \frac{T}{N}\cdot r$

Equation (3.60) is the inverse discrete Fourier transform which recovers a function of time from its frequency domain data. By using equation (3.60), the pulsation pressure $p_d(t)$ can be calculated as a discrete time series if we know the frequency amplitudes of the pulsating pressure P_n, n = 0, 1, 2,...,nrec. They can be calculated as

$$P_n = Z_o(\omega_n) \cdot Q_n \qquad (3.61)$$

where Q_n is the amplitude of input volume flow to the cavity, which is obtained by the Fourier transform of the volume flow calculated by the numerical integration of the valve flow process. Also, $Z_o(\omega_n)$ is the pressure response(or input point impedance) which is calculated from

equations (3.41) or (3.43) using the four pole parameters of section (3.3). P_o in equation (3.58) has to be taken as the average line pressure.

Again, it should be noted that the same procedure can be applied for the calculation of the suction pressure.

In summary, the pulsating pressure is calculated by the inverse Fourier transform of the pressure amplitudes which are computed by multiplying the volume flow amplitude of the input flow with the input point impedance (or pressure response) of the cavity. The volume flow amplitude is obtained by the Fourier transform of the volume flow which is calculated as a function of time during the numerical integration of the cylinder process.

3.4.2 Convergence Problem of the Simulation Program3.

The simulation program is an iteration of integrations starting from assumed initial conditions. Therefore the convergence of the routine has to be assured. Convergence can be checked by comparing the results of successive steps. In other words, the simulation result of each step has to show a tendency to converge to a stable value after enough iterations.

It was known from experience that suction cavity pressure and suction valve motion often had difficulty to converge in previous simulations. Therefore, those values

and the cylinder mass at each step are the best indicators for the convergence check.

Secondly, the program should give an accurate answer as well. Accuracy is dependent on the following parameters.

1. Number of integration time steps per cycle (n) (Symbols in brackets are variable names in the computer program).

2. Number of data points to be taken for the fast Fourier transform (nft).

3. Number of terms to be retained for the Inverse Discrete Fourier Transform (nrec).

It is obvious that more accurate results are obtained if larger numbers are used for those parameters. This is at the cost of longer computing time.

Figure 3.17 shows four suction pressures from the same data sets except different combinations of the above parameters. The curves are almost in complete agreement. From experience, the following values are recommended for compressors of the type that is being investigated.

n = 720

nft = 256

nrec = 21

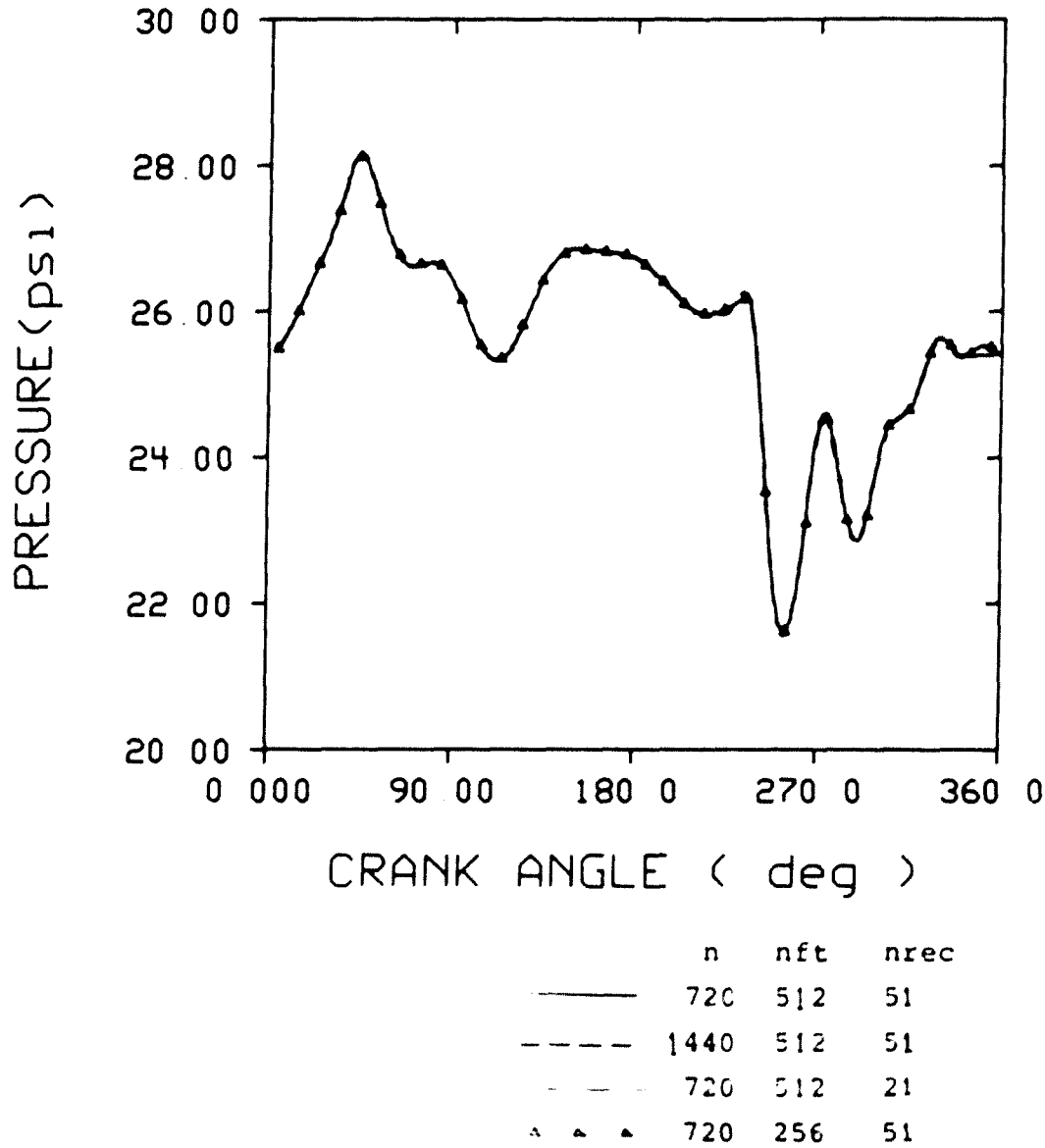

Figure 3.17 - Effect of Integration Step Size and Other Parameters on the Accuracy of Suction Pressure prediction

Parameters which control the convergence are number of iterations(niter2), number of cycles of P-V diagram integration per each iteration(niter1), and a parameter to slow down the converge speed. The latter parameter will be discussed below.

At each iteration, better simulated values are calculated by using the the results of the previous simulation step as new initial conditions. The role of niter1 and niter2 is to perform the iteration a sufficient number of times. However, in the actual applications, the suction pressure and suction valve motion was not converging consistently. Because the suction valve interaction time with the cylinder process is much longer than for the discharge valve, the Fourier spectrum of the suction volume flow which is calculated from the cylinder process simulation varies by a large amount at each step compared to the change in the discharge side. This seems to be the reason why the suction side simulation has more difficulty to attain a stably converged result.

Figure 3.18 - (a) shows suction pressures at two consecutive iterations (4th,5th) when no reduction factor was used. It shows fairy large variation for the suction valve. At this iteration, the discharge pressure has already converged as shown in Figure 3.18 - (b). An oscillating tendency of the suction valve closing time was observed during further iterations.

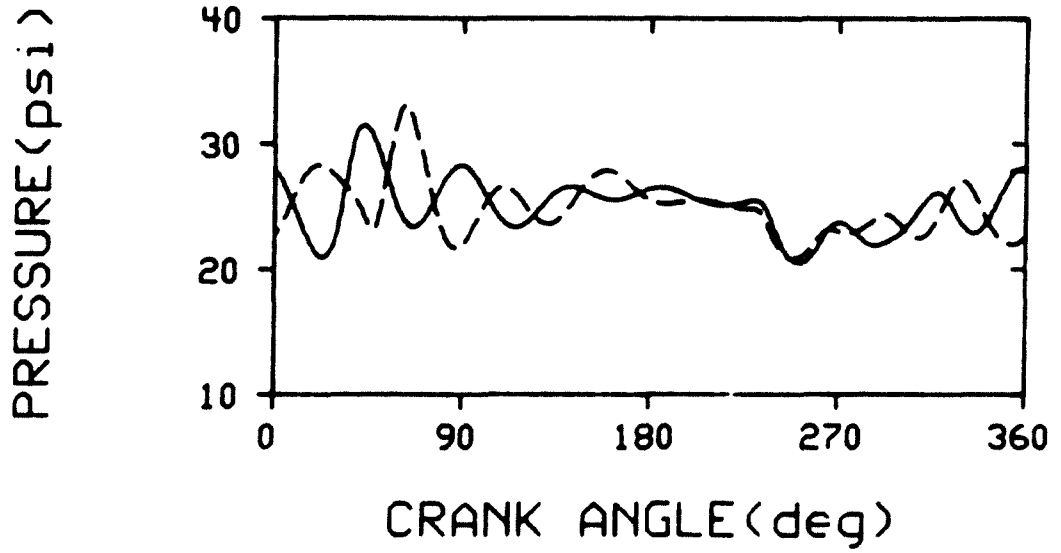

a) SUCTION PRESSURE

——— 4th iteration - - - - 5th iteration

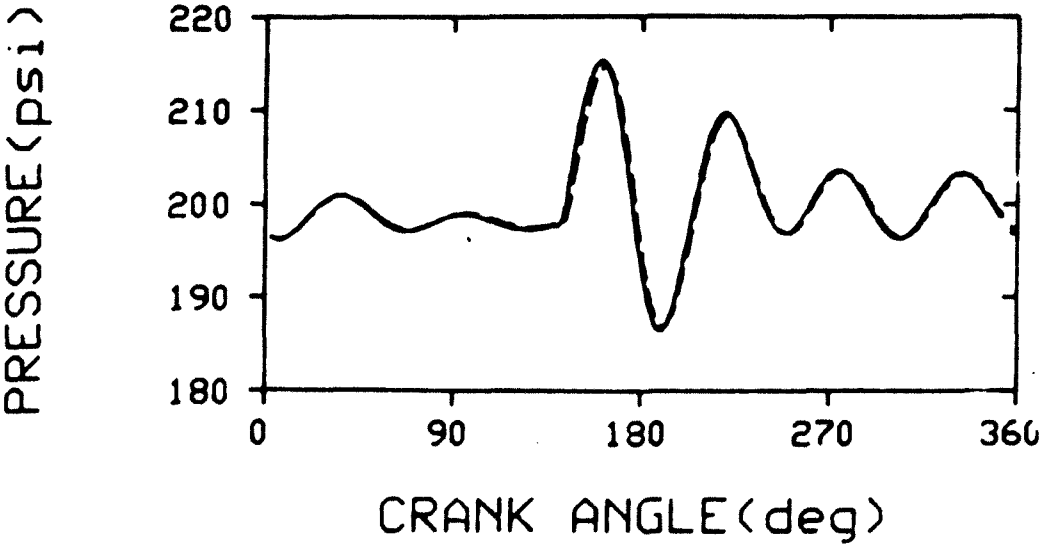

b) DISCHARGE PRESSURE

Figure 3.18 - Unstable Convergence Tendency of the Suction Pressure

This phenomenon can be viewed as follows:

1. Integration of the cylinder process produces a calculated volume flow data, which is deviating from the true value.

2. By solving the acoustic equation, a far more developed pulsation pressure is obtained than would normally occur.

3. The calculated pressure provides a very different initial condition for the next iteration, which increases the volume flow error, which increases the error of the acoustic calculation, and so on. This situation is partially caused by the suction side pressure drop through the suction valve being very small (less than a fifth of the discharge side pressure drop) and by the cylinder pressure having a very small slope at the suction valve closing time.

From the above speculation, the attempted convergence speed can be thought to be too fast. This problem has not been reported before. It does not occur for the case when full integration methods are employed. For the case of the impedance approach, which requires the combination of the integration and the acoustic response solution, most work was done for the discharge side[8,21], and no problems were encountered.

Similar iteration trouble was found in the simulation of the large deflection problem of a thin shell. Soedel[20] eliminated this problem by employing a modified iteration schema.

Because of the above reasons, the pressure for the ith iteration is modified as,

$$P'_{s,i} = \eta * P_{s,i} + (1-\eta)* P'_{s,i-1} \qquad (3.62)$$

where, η is a convergence factor such that $0 < \eta < 1$ and $P'_{s,i}$ is the suction pressure which will be used for the numerical procedure of the i th step. $P_{s,i}$ is the suction pressure calculated by the acoustic equation at the i th step. And $P'_{s,i-1}$ is the suction pressure which was used for the i-1 th iteration. That is, only a fraction of the new calculated pulsation pressures are used for the next iteration. Obviously, this schema requires more iterations. Therefore, it has to be studied further to determine an optimal value of the convergence speed factor, and the corresponding number of iterations.

Let us take an example operating conditions P_s = 11 psig and P_d = 185 psig with η = 0.2. Figure 3.19 shows the cylinder mass at each integration step. Figure 3.20 and Figure 3.21 show the pressure and valve lift diagrams at a few last iterations. It can be concluded that a satisfactory convergence was achieved.

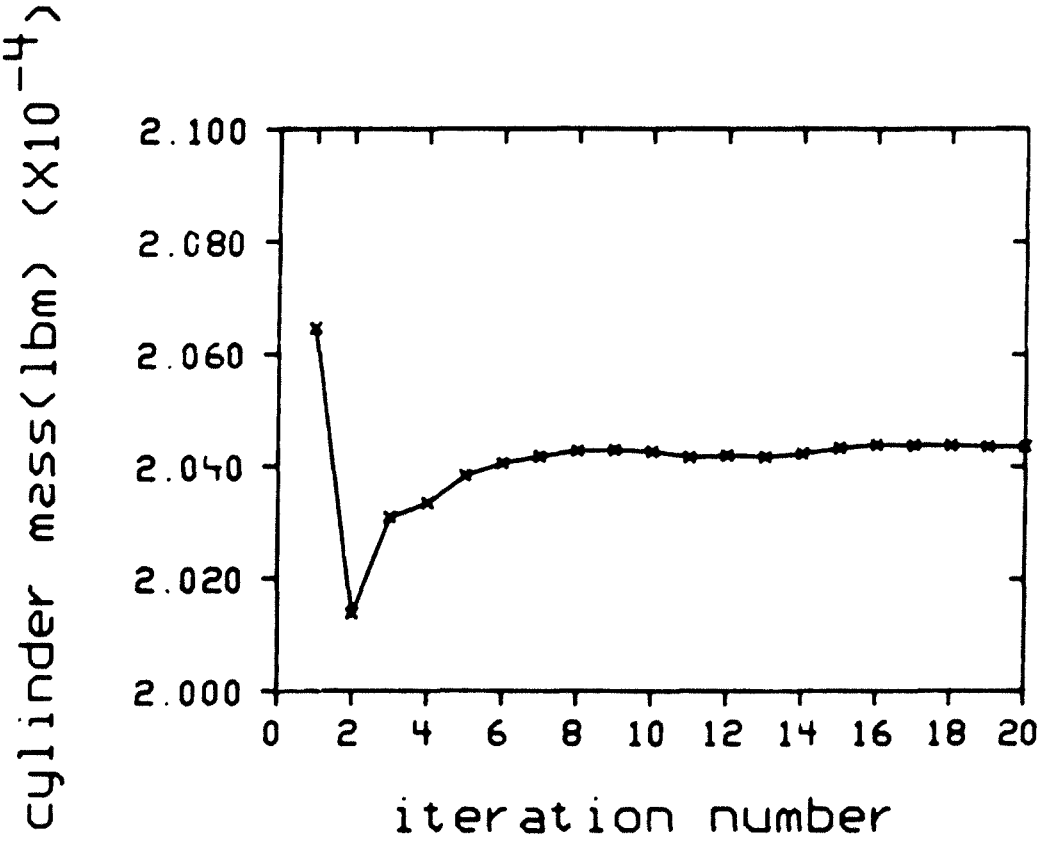

Figure 3.19 - Observation of the Convergence

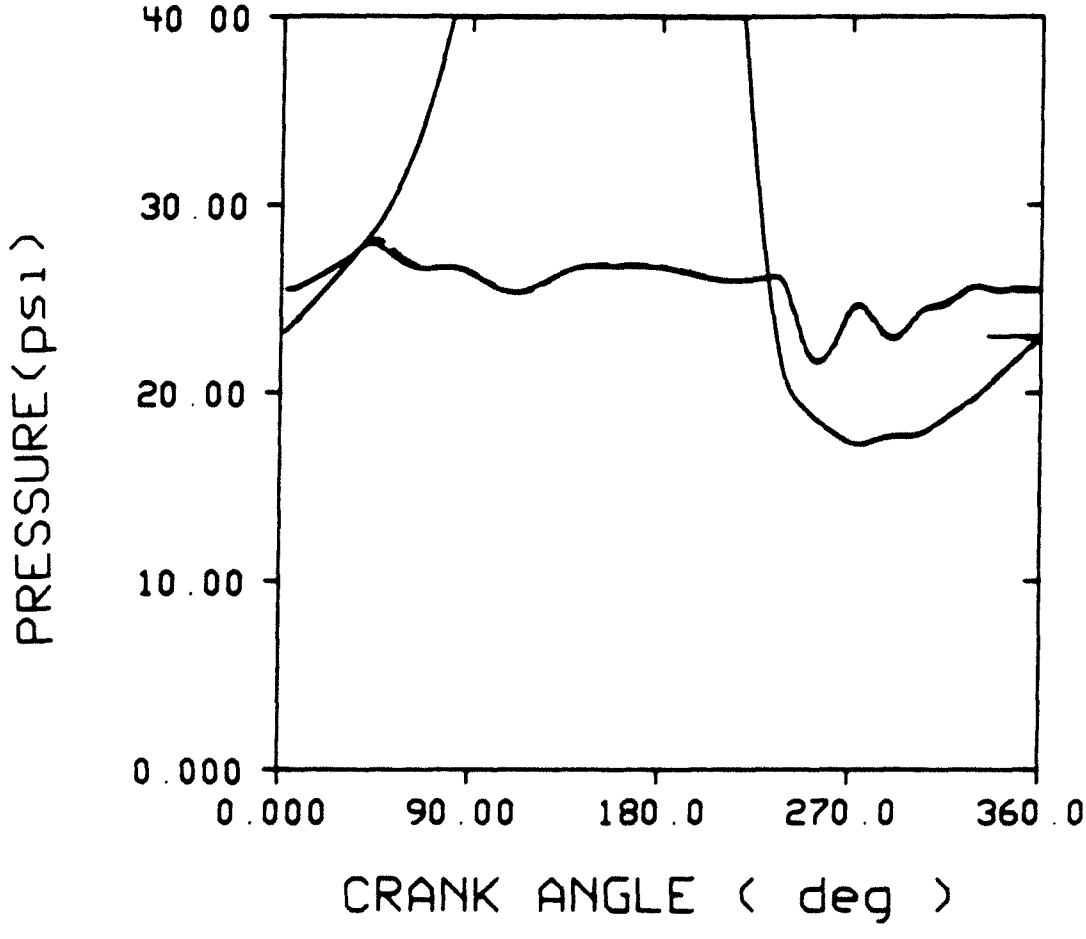

Figure 3.20 - Converged Suction Pressure with Modified Integration Schema, ——— ,11th iteration, – – – – ,13th iteration, —·—·—,15th iteration

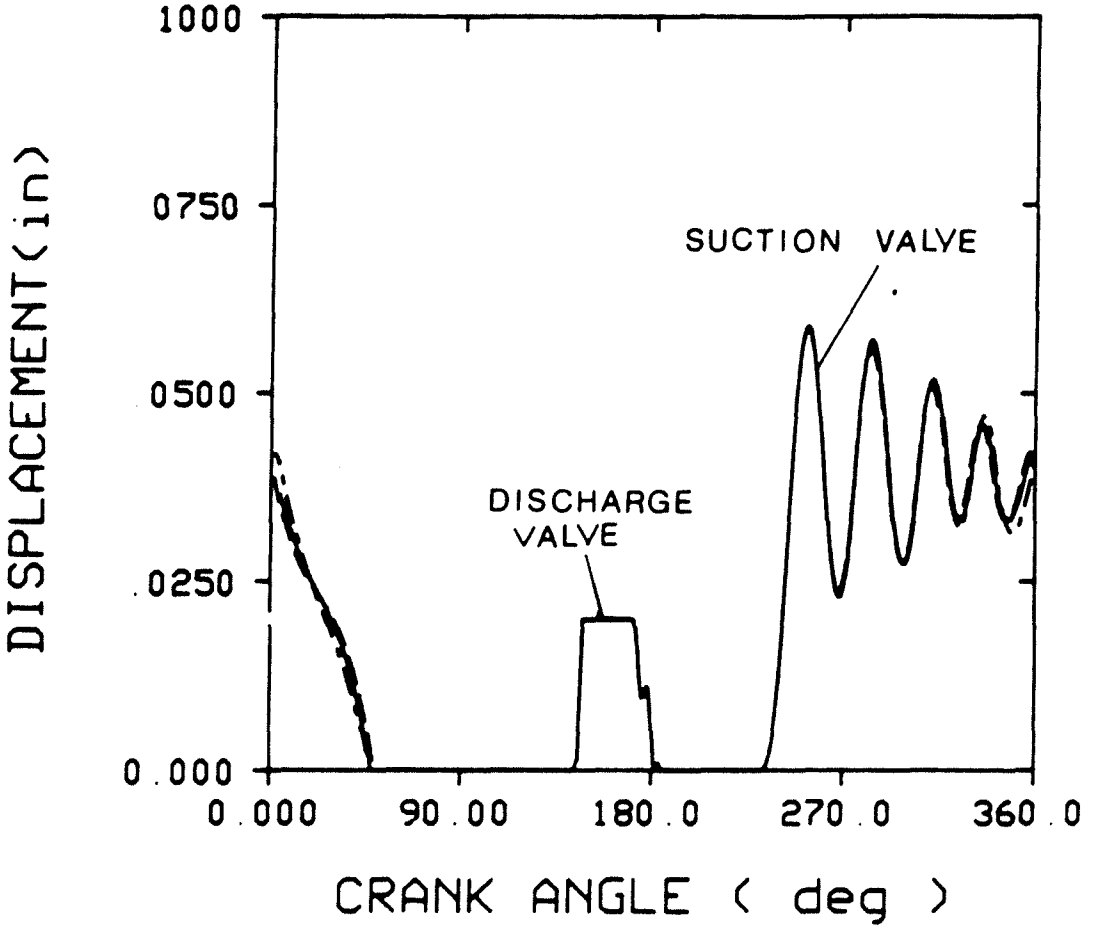

Figure 3.21 - Converged Valve Motions with Modified Integration Schema, ——— ,11th iteration, – – – – ,13th iteration, —·— ,15th iteration

In the actual use of the program, the total number of iterations has to be selected, relative to the value of the speed factor. The rule of thumb to determine the number of iterations is niter2 > $\frac{2}{\eta}$. It is better to check the convergence by comparing a few calculations. Recommendations for these parameters, from the experience, are

niter1 = 2

niter2 = 15

factor = 0.2

3.5 Simulation Results and Comparison to Experiments

Simulation results were compared to corresponding measurements for five operating conditions. (see Table 3.1)

Calculated pressures were compared to measured pressures in Figures 3.22 to 3.26 for two selected operating conditions. There were noticeable differences at the peak cylinder pressure, even while the general overpressure tendency is simulated. This is considered to be from the fact that a simple one degree of freedom valve model was used for the complex discharge valve. The other possible reason may be that there is perhaps a gas pulsation inside the cylinder induced by reflected waves from the cylinder head[27].

TABLE 3.1 - Simulated and Measured Thermodynamic Efficiencies and Losses

Case		Overall Efficiency (%)	Valve Loss (%)		Pulsation Loss (%)	
			Suction	Discharge	Suction	Discharge
1*2	A*1	82.53	5.90	6.90	2.9	1.77
	B	82.16	7.61	5.92	2.53	1.78
2	A	82.61	8.26	6.28	2.12	1.65
	B	82.79	7.35	5.71	2.54	1.62
3	A	83.66	6.29	6.1	2.46	1.49
	B	83.86	6.93	5.36	2.45	1.40
4	A	79.19	6.94	8.07	3.36	2.45
	B	78.47	8.71	7.77	2.84	2.22
5	A	79.06	6.24	8.84	3.49	2.39
	B	76.02	9.30	9.31	2.93	2.44
max. error (%)		3.8	32.9	12.3	14.6	9.4

*1. A: measured B: calculated

*2. Operating Conditions

Case	P_s (psig)	P_d (psig)
1	11	185
2	10	200
3	10	220
4	15	180
5	15	160

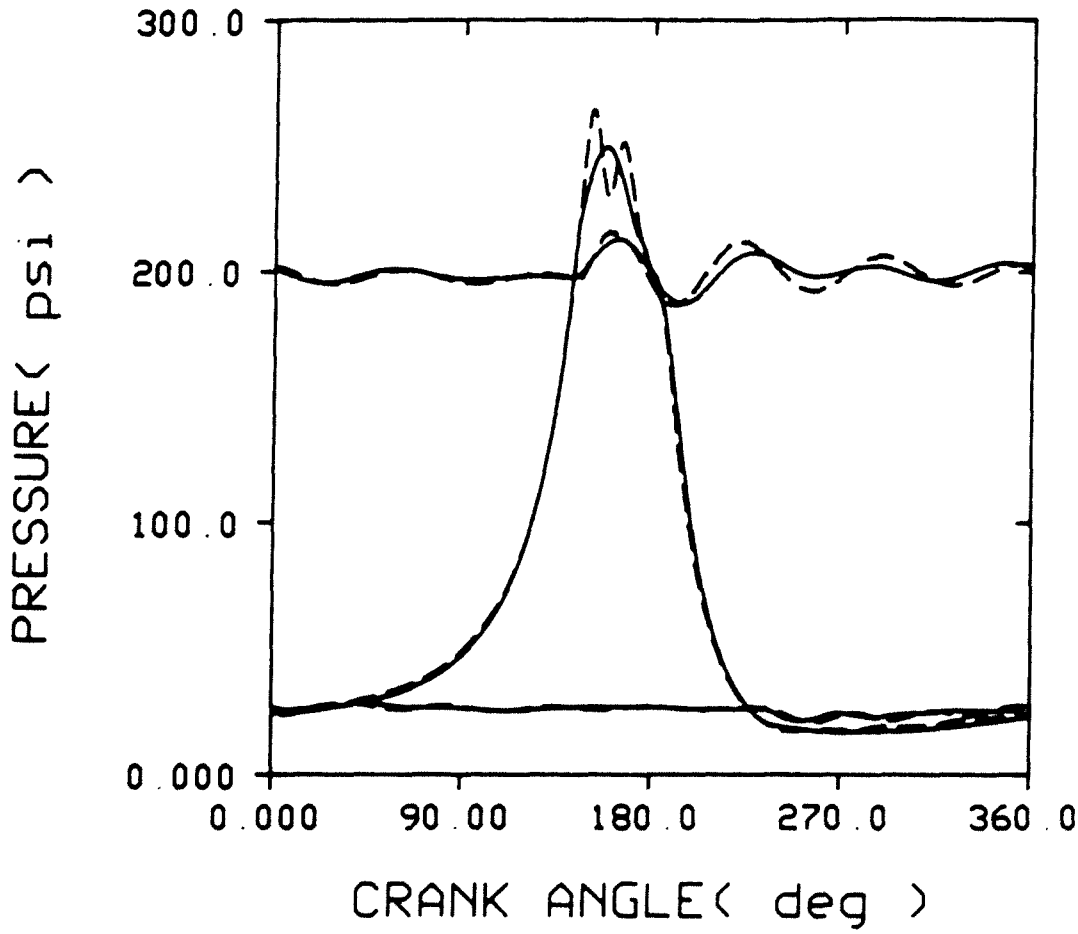

Ps = 11 psig Pd = 185 psig

Figure 3.22 - Pressure vs. Crank Angle Diagram(1), ---- ,measured, ——— ,calculated

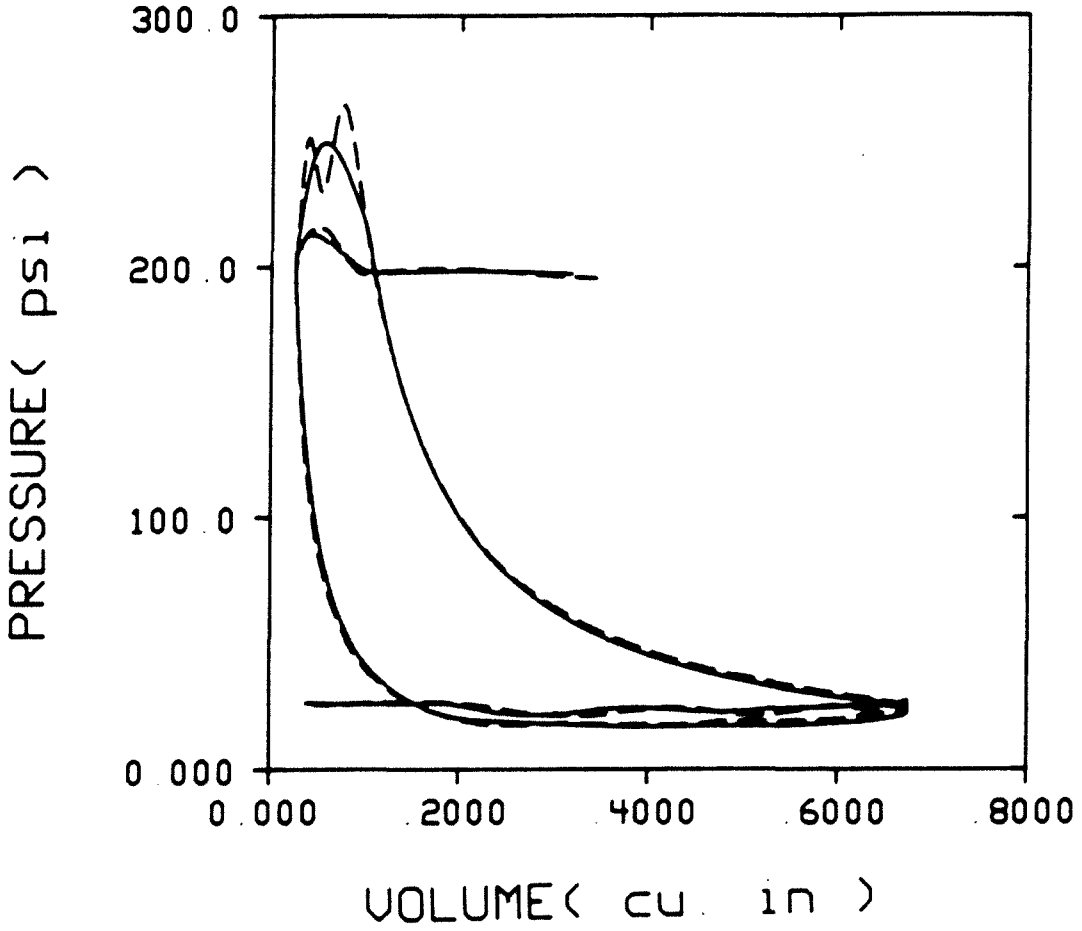

Ps = 11 psig Pd = 185 psig

Figure 3.23 - Pressure vs. Volume Diagram(1), ----- ,measured, ——— ,calculated

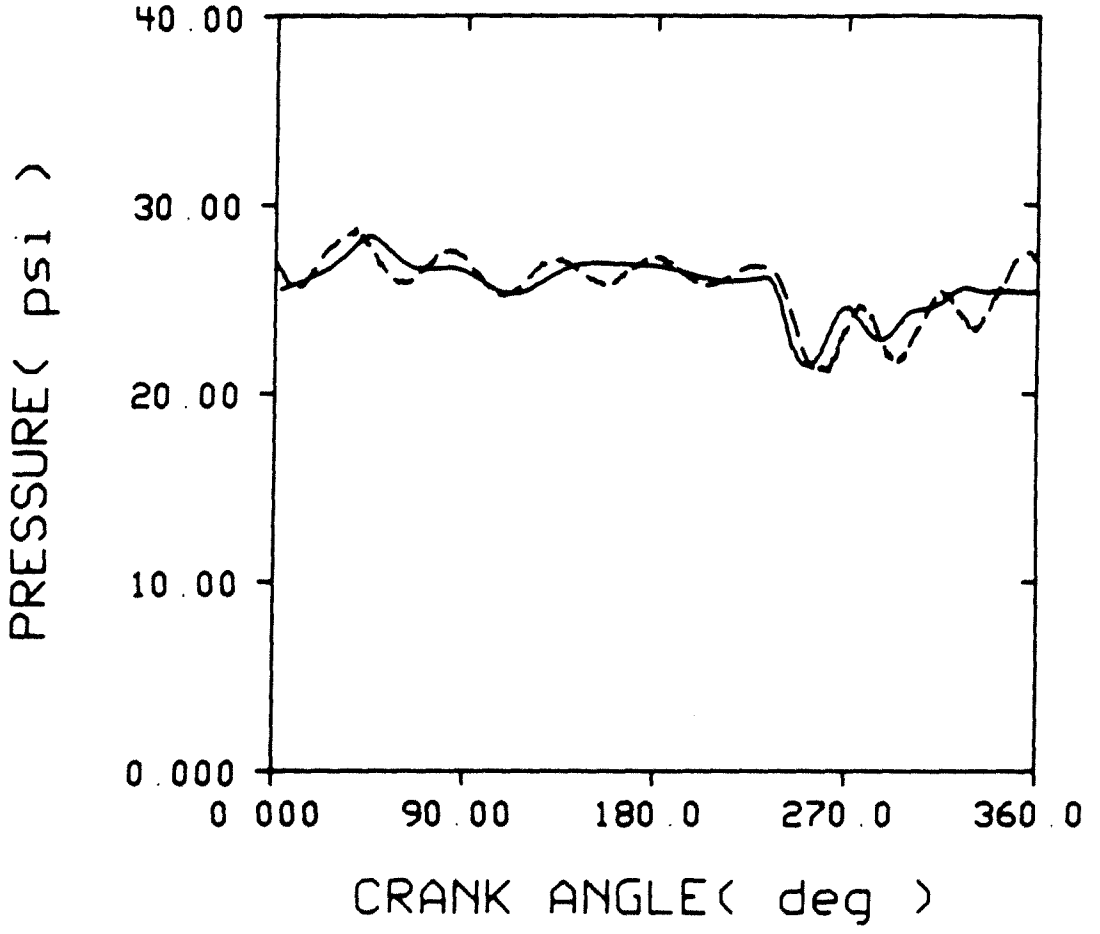

Ps = 11 psig Pd = 185 psig

Figure 3.24 - Suction Pressure vs. Crank Angle Diagram(1),
---- ,measured, ——— ,calculated

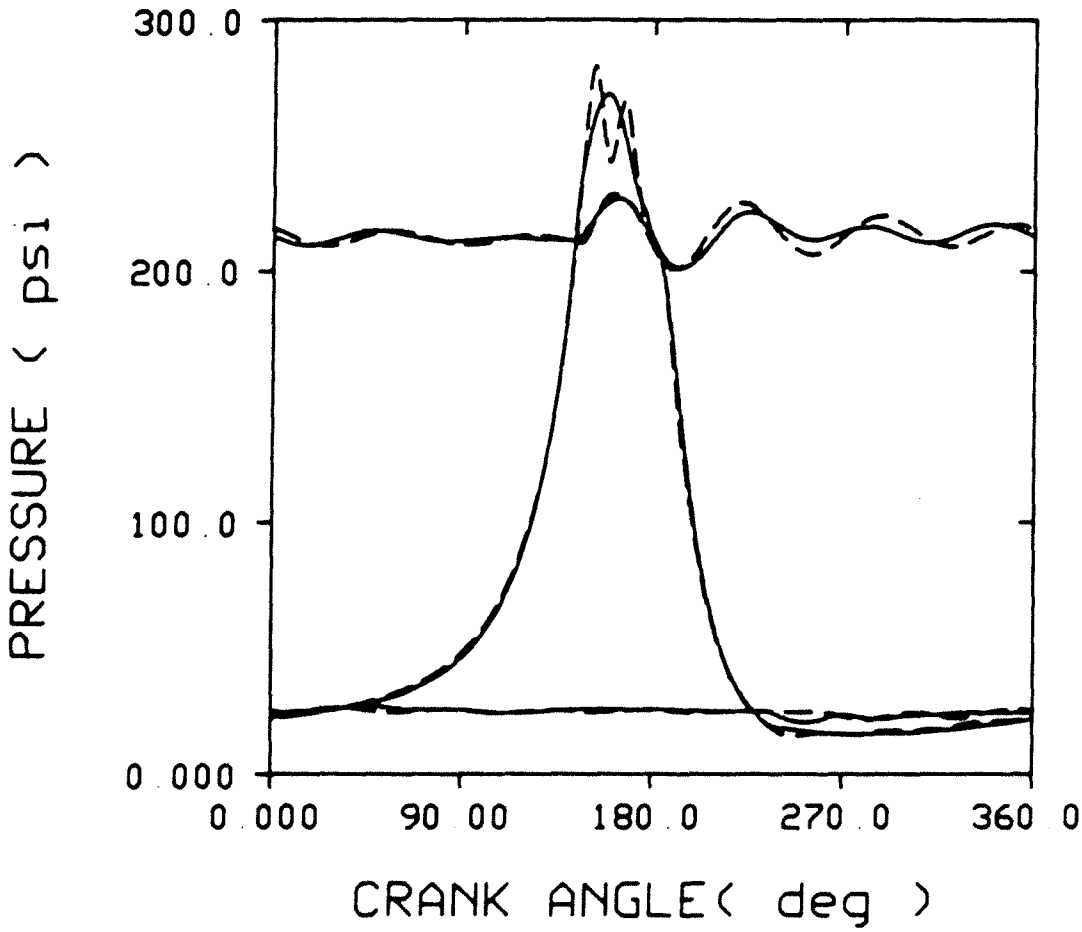

Figure 3.25 - Pressure vs. Crank Angle Diagram(2)
---- ,measured, ——— ,calculated

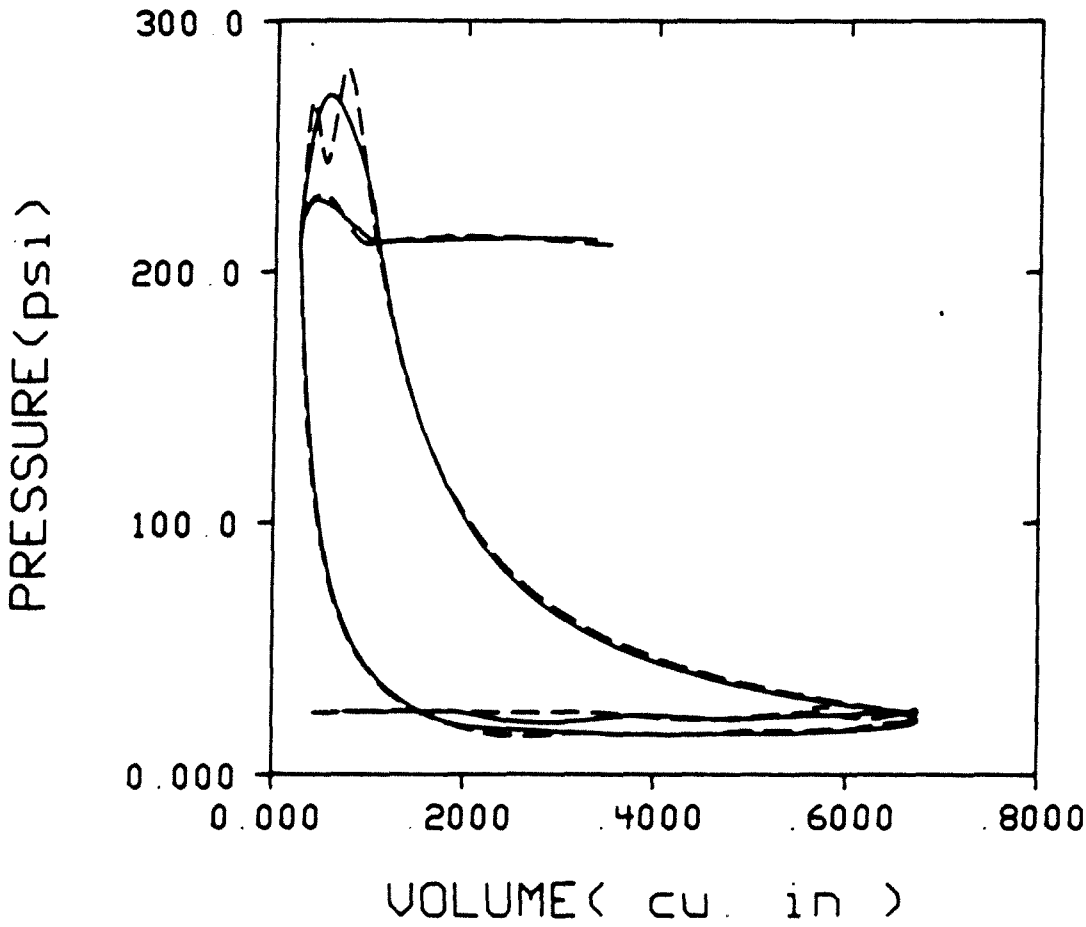

Ps = 10 psig Pd = 200 psig

Figure 3.26 - Pressure vs. Volume Diagram(2)
----,measured, ——— ,calculated

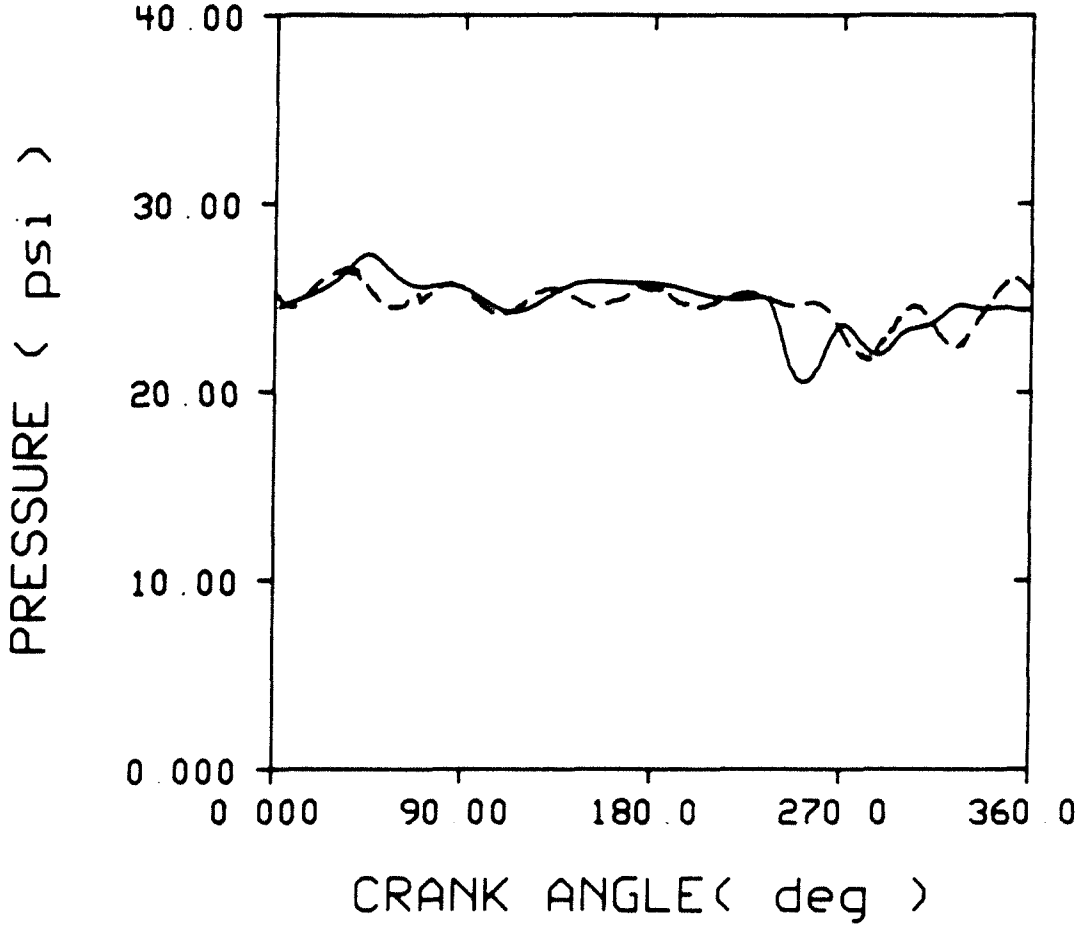

Ps = 10 psig Pd = 200 psig

Figure 3.27 - Suction Pressure vs. Crank Angle Diagram(2)
----,measured, ————,calculated

With current parameter sets for simulation, the discharge pressure is very closely predicted. For the suction side, more adjustment of the suction valve stiffness and the damping ratios may improve the accuracy of the prediction. For both sides, the qualitative aspect of the simulation, for example frequency and amplitude of the pulsation pressures and valve motions, was satisfactory.

Based on these graphs, thermodynamic efficiencies and losses of each set were calculated by integrating areas of P-V diagrams. The result is summarized in Table 3.1. For the definitions of these efficiencies and losses, section 2.6 has to be referenced.

Figure 3.28, Figure 3.29, Figure 3.30 are Fourier spectra of the cylinder, suction and discharge pressures. These figures were compared to the experimental results of the first report. They showed fairly good agreement. For example, dominant 6,7,8,9,10^{th} harmonics were observed in both pressure spectrums. Figure 3.31 shows simulated valve motions.

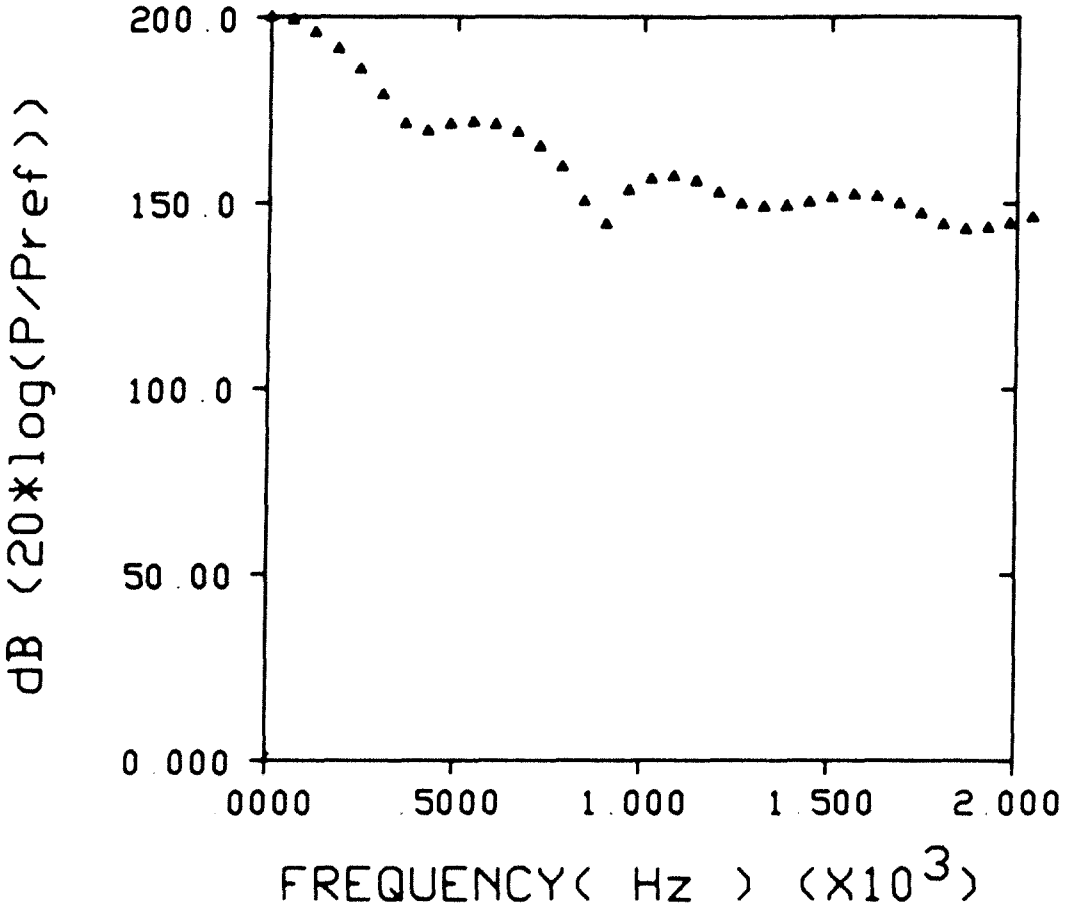

Ps = 11 psig Pd = 185 psig

Figure 3.28 - Fourier Spectrum of the Simulated Cylinder Pressure

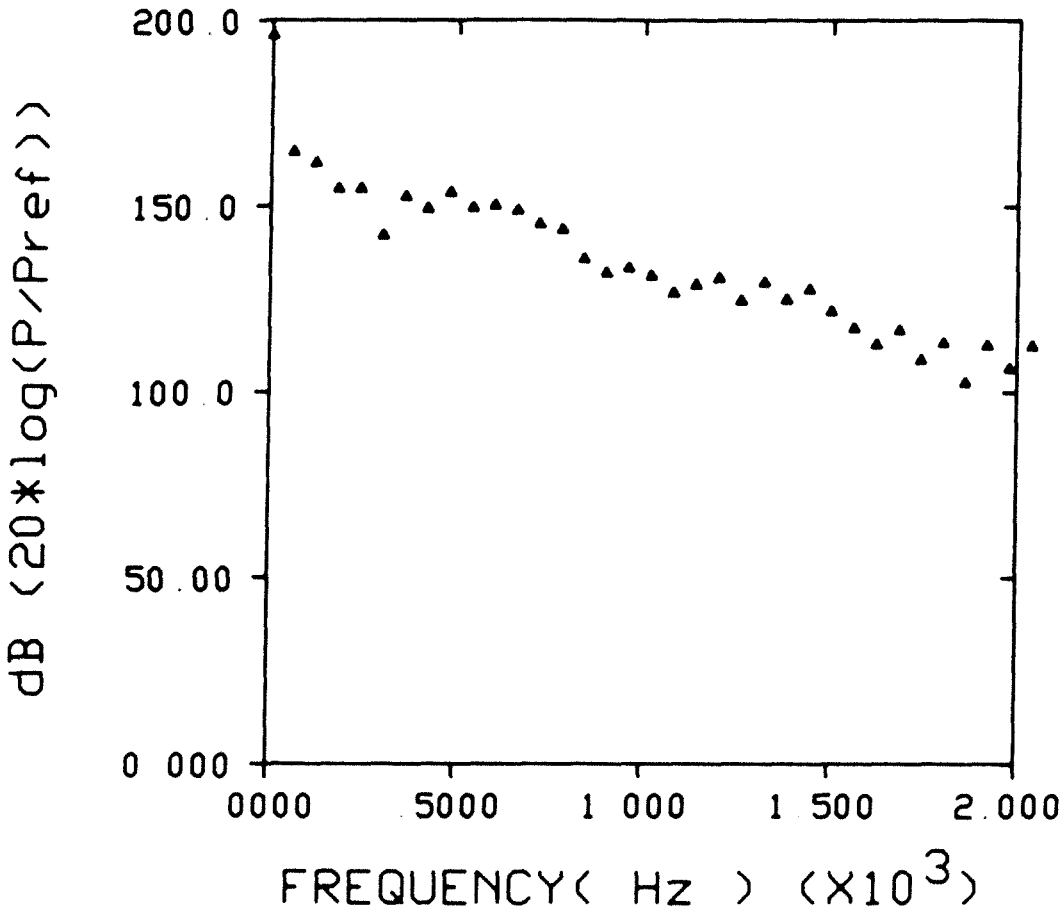

Ps = 11 psig Pd = 185 psig

Figure 3.29 - Fourier Spectrum of the Simulated Suction Pressure

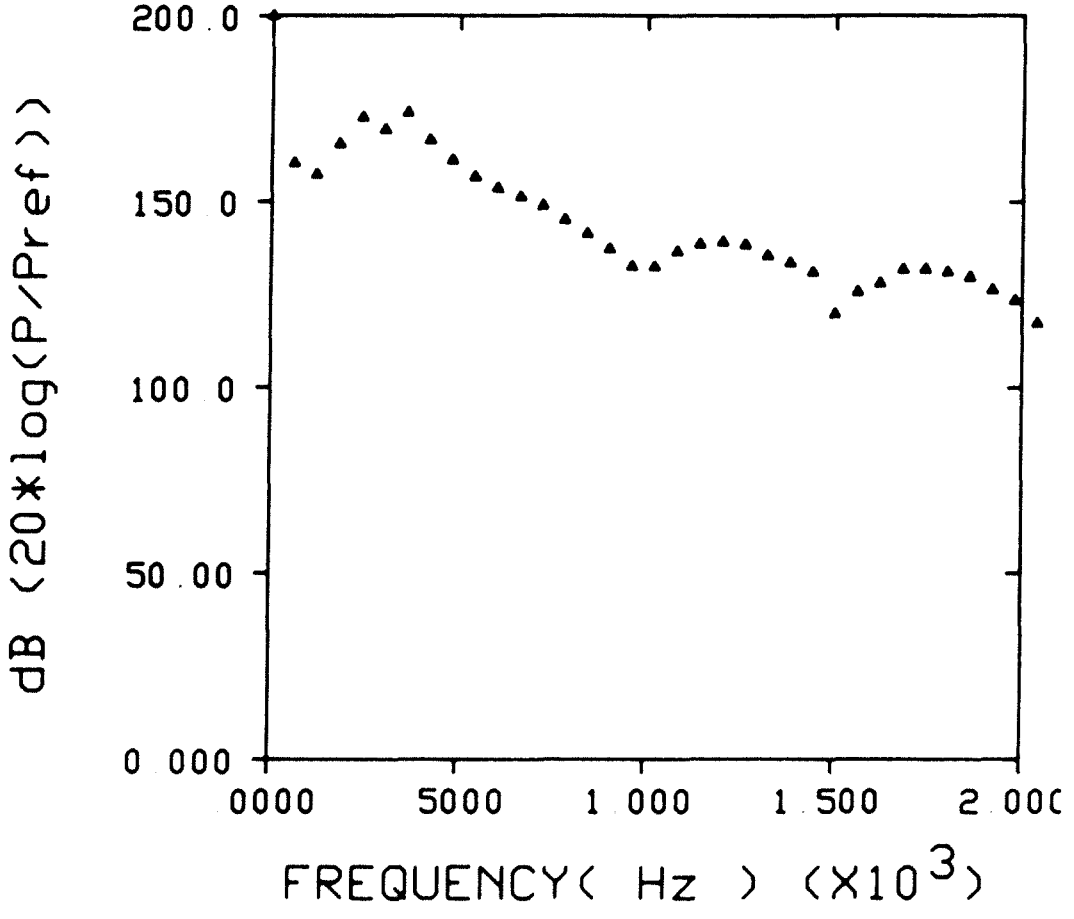

Ps = 11 psig Pd = 185 psig

Figure 3.30 - Fourier Spectrum of the Simulated Discharge Pressure

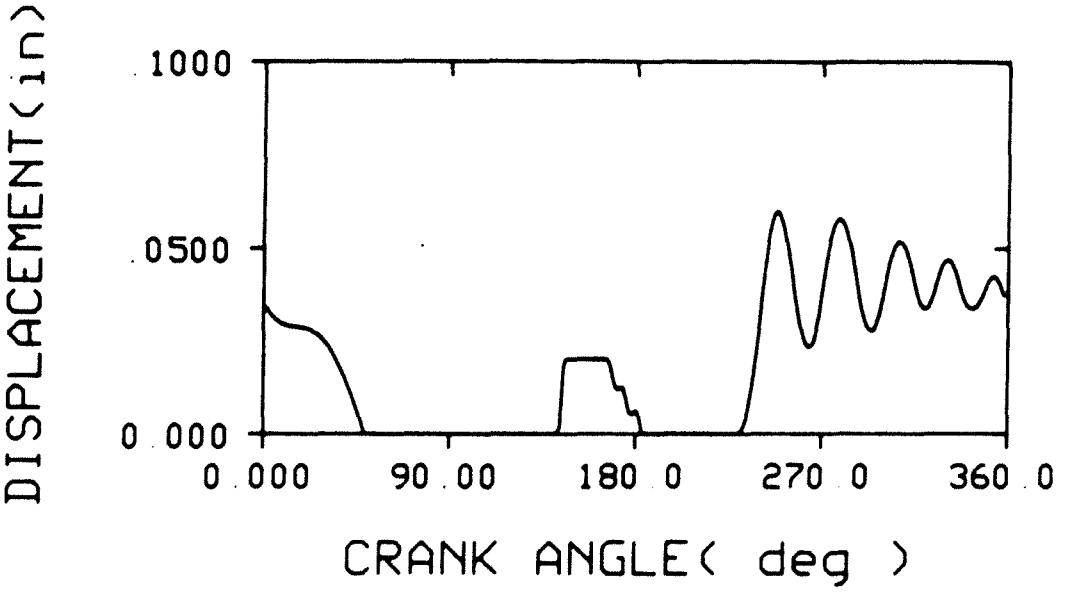

Figure 3.31 - Simulated Valve Motions

CHAPTER 4 - GENERAL FORMULATION OF FOUR POLE PARAMETERS FOR THREE DIMENSIONAL CAVITIES UTILIZING MODAL EXPANSION WITH SPECIAL ATTENTION TO THE ANNULAR CYLINDER

4.1 Introduction

Acoustic cavities that resemble an annular cylinder bounded by two concentric rigid cylindrical walls are often encountered in machinery. In this chapter, a general procedure is discussed to formulate four poles of an acoustic system and it is applied to an annular type cavity.

Four pole parameters are a very useful concept for the analysis of a composite acoustic system because of computational efficiency and flexibility. Good discussions on basic concepts of four poles of dynamic systems and their practical applications are found in references [1,40].

If the acoustic system has a large dimension compared to a wave length of interest, the pressure responses which are necessary to formulate four pole parameters have to be obtained by solving the continuous wave equation of the system. Typically, only one dimensional acoustic elements have been formulated analytically due to the difficulty of

the solution procedures involved in three dimensional cavities. In this chapter, four poles for a cylindrical annular cavity are obtained by the eigenfunction expansion method.

The free vibration analysis of the system is the first step to formulate four poles. An early attempt to obtain the resonance of an annular shell cavity of a refrigeration compressor and resulting noise radiation was made by Johnson [4,5]. He solved the free vibration problem of the annular cavity to obtain normal modes and resonant frequencies. Au-Yang conducted free vibration analysis and experiments of an annular cavity including the structural interaction effect [31]. Kung and Singh used the finite element method to obtain normal modes for more general shape cavities for which the inside wall is not a cylindrical shape [30].

Experimental or numerical work to obtain forced response solutions due to single or multiple volume flow inputs are found in several researcher's works [6,23,32], but four poles were not obtained. In this chapter, a general procedure to formulate acoustic four poles from forced response solutions is established and four poles of annular cavities are obtained from the analytical solution as an example. For the example of application, acoustic characteristics of the annular cavity connected to an anechoically terminated pipe were studied. Noise radiation

of enclosures of such cavities due to inside gas pulsations was observed to be one of the major sound sources in hermetic refrigeration compressors by several researchers [4,6,7].

The approach was checked against the special situation of one dimensional wave guide response solutions and excellent agreement was found as expected, but the comparison is not shown in this chapter.

4.2 General Four Pole Formulation in Curvilinear Coordinates

4.2.1 Formulation of Four Poles from Pressure Response Solutions

A linear acoustic system may be comprised of one or more lumped or continuous acoustic elements. The relationship between input pairs Q_1, P_1 and output pairs Q_2 and P_2 are expressed as;

$$Q_1 = AQ_2 + BP_2 \tag{4.1}$$

$$P_1 = CQ_2 + DP_2 \tag{4.2}$$

A, B, C, D are the four pole parameters [1]. The four pole parameters can be derived if the pressure response solution of the acoustic element is available.

Suppose the pressure solution is given by

$$P(\underset{\sim}{r})e^{j\omega t} = f_1(\underset{\sim}{r},\omega)\ Q_1 e^{j\omega t} - f_2(\underset{\sim}{r},\omega)\ Q_2 e^{j\omega t} \qquad (4.3)$$

In equation (4.3), if $Q_2 = 0$ and $\underset{\sim}{r} = \underset{\sim}{r}_2$,

$$P(\underset{\sim}{r}_2)\big|_{Q_2=0} = P_2\big|_{Q_2=0} = f_1(\underset{\sim}{r}_2,\omega)\ Q_1 \qquad (4.4)$$

Also, if $Q_2 = 0$ in equation (4.1),

$$Q_1 = BP_2\big|_{Q_2=0} \qquad (4.5)$$

Comparing equation (4.4) and equation (4.5), it is obtained that

$$B = \frac{1}{f_1(\underset{\sim}{r}_2,\omega)} \qquad (4.6)$$

Using equations (4.1), (4.2) and (4.3) in a similar way, it can be shown that

$$A = \frac{f_2(\underset{\sim}{r}_2,\omega)}{f_1(\underset{\sim}{r}_2,\omega)} \qquad (4.7)$$

$$C = -f_2(\underset{\sim}{r}_1,\omega) + \frac{f_1(\underset{\sim}{r}_1,\omega)}{f_1(\underset{\sim}{r}_2,\omega)} \cdot f_2(\underset{\sim}{r}_2,\omega) \qquad (4.8)$$

$$D = \frac{f_1(\underset{\sim}{r}_1,\omega)}{f_1(\underset{\sim}{r}_2,\omega)} \qquad (4.9)$$

From the above discussion, four poles of an acoustic system can be obtained if the pressure response of the system at the input point and the output point to a harmonic volume flow is known. Therefore, any analytical or numerical method can be employed as long as it can give correct pressure response solutions.

4.2.2 Formulation of Response Solutions for a General Three Dimensional Cavity

Utilizing the wave equation of general continuous media with pressure and volume flow sources as given by Doak [44], one obtains for negligibly small mean flow velocities and viscosity

$$\nabla^2 p - \frac{1}{C_0^2} \frac{\partial^2 p}{\partial t^2} = - \frac{\partial}{\partial t} (\dot{m}(\underline{r})) \tag{4.10}$$

where p is the acoustic pressure, C_0 is the sound velocity in the medium, and $\dot{m}(\underline{r})$ is the mass flow source distribution function. ∇^2 is the Laplacian operator in general curvilinear coordinates:

$$\nabla^2 = \frac{1}{A_1 A_2 A_3} \left[\frac{\partial}{\partial \alpha_1} \left(\frac{A_2 A_3}{A_1} \frac{\partial}{\partial \alpha_1} \right) + \frac{\partial}{\partial \alpha_2} \left(\frac{A_3 A_1}{A_2} \frac{\partial}{\partial \alpha_2} \right) + \frac{\partial}{\partial \alpha_3} \left(\frac{A_1 A_2}{A_3} \frac{\partial}{\partial \alpha_3} \right) \right] \tag{4.11}$$

where α_1, α_2, α_3 are the curvilinear coordinates and A_1, A_2, A_3 are the Lamé parameters.

As discussed in the previous section, four pole parameters can be obtained if the pressure responses to unit input volume flow are known. If the flow source has relatively small dimensions compared to the overall size of the cavity and to the wave length corresponding to the highest frequency of interest, it is reasonable to approximate the source as a point source using a Dirac delta function description.

$$\dot{m}(\underline{r}) = \rho_0 \, Q e^{j\omega t} \, \delta(\underline{r}-\underline{r}^*) \tag{4.12}$$

where, $j = \sqrt{-1}$ and $\delta(\underline{r}-\underline{r}^*)$ is the Dirac delta function which is, in general curvilinear coordinates (Figure 4.1)

$$\delta(\underline{r}-\underline{r}^*) = \frac{1}{A_1}\delta(\alpha_1-\alpha_1^*) \cdot \frac{1}{A_2}\delta(\alpha_2-\alpha_2^*) \cdot \frac{1}{A_3}\delta(\alpha_3-\alpha_3^*) \tag{4.13}$$

The solution of equation (4.10) can be obtained by the eigenfunction expansion method if the natural frequencies and normal modes are available. It is of the form

$$P(\underline{r},t) = \sum_{k=0}^{\infty} \eta_k(t) \, P_k(\underline{r}) \tag{4.14}$$

where $P_k(\underline{r})$ is the k^{th} normal mode of the system. Note that $P_0(\underline{r})$ is a constant pressure mode and corresponds to a zero natural frequency.

Substituting equations (4.12) and (4.14) in equation (4.10), we obtain

$$\sum_{k=0}^{\infty} [\eta_k(t) \, \nabla^2 P_k(\underline{r}) - \frac{1}{c_0^2} \ddot{\eta}_k(t) \, P_k(\underline{r})] = -j\omega \rho_o \, Q \, \delta(\underline{r}-\underline{r}^*) \, e^{j\omega t} \tag{4.15}$$

Because the $P_k(\underline{r})$ are natural modes, it can be shown that

$$\nabla^2 P_k(\underline{r}) = -\frac{\omega_k^2}{c_0^2} P_k(\underline{r}) \tag{4.16}$$

Therefore equation (4.15) becomes

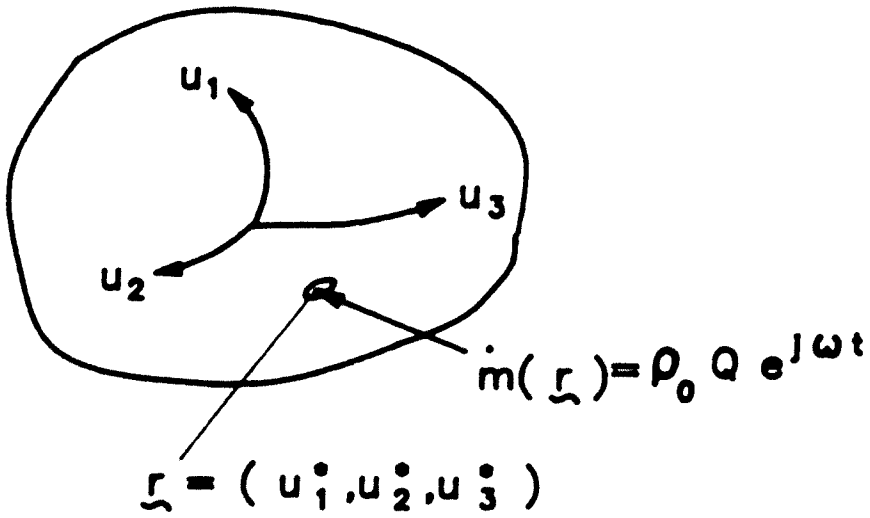

Figure 4.1 - An Acoustic Cavity with an Input volume Flow Source

$$\sum_{k=0}^{\infty} [\ddot{\eta}_k(t) + \omega_k^2 \eta_k(t)] P_k(\underline{r}) = j \omega \rho_0 C_0^2 Q \delta(\underline{r}-\underline{r}^*) e^{j\omega t} \quad (4.17)$$

If we multiply both sides of equation (4.17) by $P_n(\underline{r})$ and integrate over the domain, we obtain decoupled equations by utilizing the orthogonality property of eigenfunctions.

$$\ddot{\eta}_k(t) + \omega_k^2 \eta(t) = \frac{j \omega \rho_0 C_0^2 Q P_k(\underline{r}^*) e^{j\omega t}}{\int\int\int P_k^2(\underline{r}) A_1 A_2 A_3 d\alpha_1 d\alpha_2 d\alpha_3} \quad (4.18)$$

where k=0, 1, 2, 3, ..., each of which stands for one natural mode number: $\omega_0 = 0$, ω_k = the k^{th} natural frequency, and $P_k(\underline{r})$ are the natural modes. Further, if we introduce modal damping in equation (4.18), and if we define

$$N_k = \int\int\int P_k^2(\underline{r}) A_1 A_2 A_3 d\alpha_1 d\alpha_2 d\alpha_3 \quad (4.19)$$

then equation (4.18) becomes

$$\ddot{\eta}_k(t) + 2 \xi_k \omega_k \dot{\eta}_k(t) + \omega_k^2 \eta_k = \frac{j \omega \rho_0 C_0^2 P_k(\underline{r}^*)}{N_k} \cdot Q e^{j\omega t} \quad (4.20)$$

The steady state solution of equation (4.20) is

$$\eta_k(t) = \frac{j \omega \rho_0 C_0^2 P_k(\underline{r}^*) Q e^{j\omega t}}{N_k [(\omega_k^2-\omega^2) + 2j \omega \omega_k \xi_k]} \quad (4.21)$$

Therefore, the pressure response is, from equation (4.14),

$$P(\underline{r},t) = \sum_{k=0}^{\infty} \frac{j \omega \rho_0 C_0^2 P_k(\underline{r}^*) P_k(\underline{r}) Q}{N_k [(\omega_k^2-\omega^2) + 2j \omega \omega_k \xi_k]} \cdot e^{j\omega t} \quad (4.22)$$

Comparing equation (4.3) to equation (4.22), $f_1(\underline{r},\omega)$ is

obtained by letting $Q = 1$, $r^* = r_1$.

$$f_1(r,\omega) = \sum_{k=0}^{\infty} \frac{j\,\omega\,\rho_0\,C_0^2\,P_k(r_1)\,P_k(r)}{N_k\,[(\omega_k^2-\omega^2) + 2j\,\omega\,\omega_k\,\xi_k]} \qquad (4.23)$$

$f_2(r,\omega)$ is obtained by letting $Q = 1$, $r^* = r_2$.

$$f_2(r,\omega) = \sum_{k=0}^{\infty} \frac{j\,\omega\,\rho_0\,C_0^2\,P_k(r_2)\,P_k(r)}{N_k\,[(\omega_k^2-\omega^2) + 2j\,\omega\,\omega_k\,\xi_k]} \qquad (4.24)$$

Four pole parameters are obtained by applying equations (4.6) to (4.9):

$$A = \frac{\sum_{k=0}^{\infty} \frac{j\,\omega\,\rho_0\,C_0^2\,P_k^2(r_2)}{N_k\,[(\omega_k^2-\omega^2) + 2j\,\omega\,\omega_k\,\xi_k]}}{\sum_{k=0}^{\infty} \frac{j\,\omega\,\rho_0\,C_0^2\,P_k(r_1)\,P_k(r_2)}{N_k\,[(\omega_k^2-\omega^2) + 2j\,\omega\,\omega_k\,\xi_k]}} \qquad (4.25)$$

$$B = \frac{1}{\sum_{k=0}^{\infty} \frac{j\,\omega\,\rho_0\,C_0^2\,P_k(r_1)\,P_k(r_2)}{N_k\,[(\omega_k^2-\omega^2) + 2j\,\omega\,\omega_k\,\xi_k]}} \qquad (4.26)$$

$$C = -\sum_{k=0}^{\infty} \frac{j\omega\rho_0 C_0^2 P_k(r_2) P_k(r_1)}{N_k [(\omega_k^2-\omega^2) + 2j\omega\omega_k\xi_k]} + \sum_{k=0}^{\infty} \frac{j\omega\rho_0 C_0^2 P_k^2(r_1)}{N_k [(\omega_k^2-\omega^2) + 2j\omega\omega_k\xi_k]} \cdot \sum_{k=0}^{\infty} \frac{j\omega\rho_0 C_0^2 P_k(r_1) P_k(r_2)}{N_k [(\omega_k^2-\omega^2) + 2j\omega\omega_k\xi_k]} \sum_{k=0}^{\infty} \frac{j\omega\rho_0 C_0^2 P_k^2(r_2)}{N_k [(\omega_k^2-\omega^2) + 2j\omega\omega_k\xi_k]} \quad (4.27)$$

$$D = \frac{\sum_{k=0}^{\infty} \frac{j\omega\rho_0 C_0^2 P_k^2(r_1)}{N_k [(\omega_k^2-\omega^2) + 2j\omega\omega_k\xi_k]}}{\sum_{k=0}^{\infty} \frac{j\omega\rho_0 C_0^2 P_k(r_1) P_k(r_2)}{N_k [(\omega_k^2-\omega^2) + 2j\omega\omega_k\xi_k]}} \quad (4.28)$$

It was shown that four pole parameters can be derived for any type of acoustic system from the forced response solution. Modal expansion was used to obtain this solution. This means that if natural frequencies and modes are available as a result of analytical, numerical or experimental approaches, four poles can be formulated.

In this chapter, four poles of an annular cavity with rigid concentric walls will be obtained as an example, using analytically obtained natural modes and frequencies. The four pole formulation is valid for both gas filled cavities and fluid filled cavities.

4.3 Example : Formulation of Four Poles of an Annular Cavity

4.3.1 Natural Modes and Frequencies

Annular cavities are encountered in many applications, for examples in hermetic refrigeration compressors, or in water jackets of reactors. Four pole parameters of such cavities are needed to combine the cavity with a model of the overall system so that the simulation and analysis of the induced pressure response of the system is possible. Figure 4.2 shows an annular cavity which is connected to a long pipe.

As it was mentioned, natural frequencies and normal modes have to be found first. The homogeneous wave equation and boundary conditions are, referring to Figure 4.2,

$$\nabla^2 p - \frac{1}{c_0^2} \frac{\partial^2 p}{\partial t^2} = 0 \qquad (4.29)$$

$$\frac{\partial p}{\partial r} = 0 \quad \text{at} \quad r = a, \quad r = b \qquad (4.30)$$

$$\frac{\partial p}{\partial z} = 0 \quad \text{at} \quad z = 0, \quad z = h \qquad (4.31)$$

also, the continuity condition is imposed in the circumferential direction. ∇^2 is the Laplacian operator of equation (4.11), but specialized to cylindrical coordinates so that $A_1=1$, $A_2=r$, $A_3=1$, $\alpha_1=r$, $\alpha_2=\theta$, $\alpha_3=z$.

The fact that in a practical situation intake and outlet pipes occupy the cavity space presents no problem as

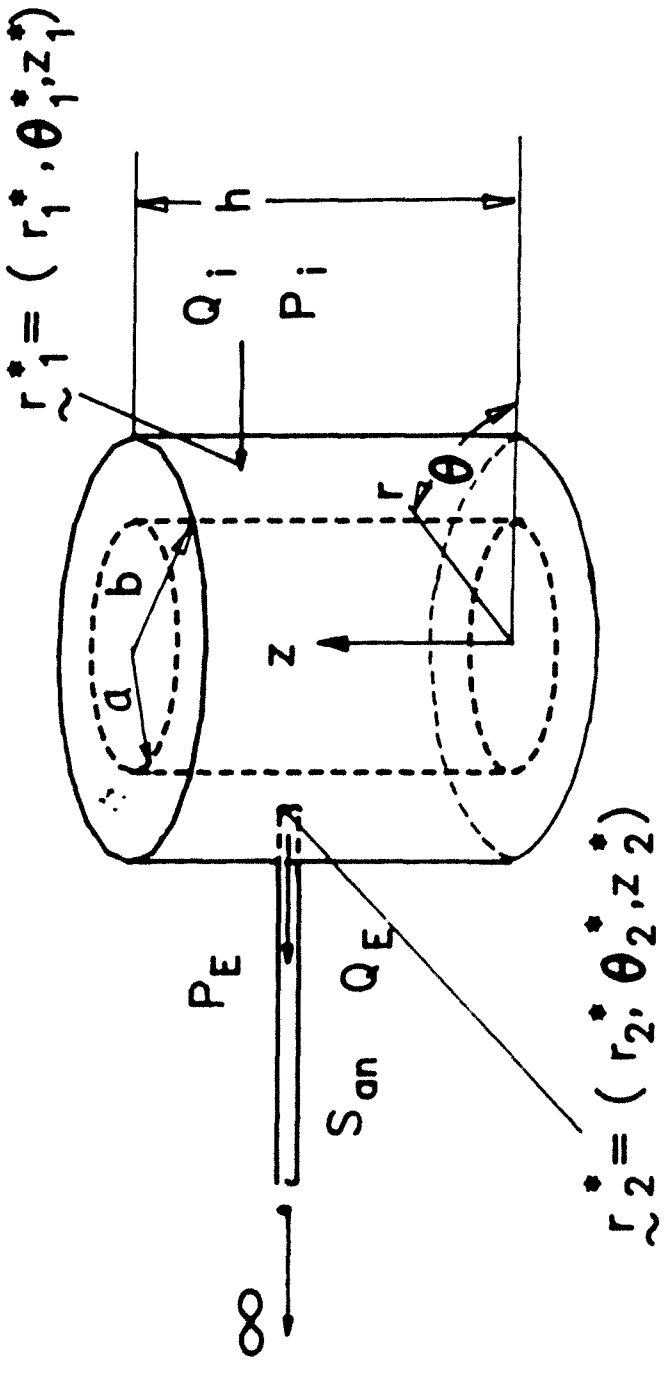

Figure 4.2 - Annular Cylindrical Cavity

long as the diameters of these pipes are small compared to the cavity dimensions and the wavelength of the highest frequency of interest. For example, in fractional horsepower refrigeration compressors, pipe diameters are of the order of 6mm, while cavity dimensions are typically of the order of 200mm height, 100mm outer diameter and 75mm inner diameter. The highest frequency of interest is approximately 1000 Hz, with a typical speed of sound of refrigeration gas of 160 m/sec. Thus, the smallest wavelength of interest is of the order of 160mm. Therefore, the space taken up by these pipes can be neglected. Of course, the basic approach of this research is not limited to such a simplification. More exact natural modes could be determined numerically or by experiment.

Without claiming originality, only for the sake of completeness of discussion, we solve this standard value boundary problem by separating variables.

$$P(r,\theta,z,t) = R(r)\,\Theta(\theta)\,Z(z)\,e^{j\omega t} \qquad (4.32)$$

Boundary conditions become

$$\frac{d}{dr}R(r)\Big|_{r=a} = \frac{d}{dr}R(r)\Big|_{r=b} = 0 \qquad (4.33)$$

$$\frac{d}{dz}Z(z)\Big|_{z=0} = \frac{d}{dz}Z(z)\Big|_{z=h} = 0 \qquad (4.34)$$

and $\Theta(\theta)$ has to satisfy the continuity condition. Substituting equation (4.32) in equation (4.29) and utilizing boundary conditions, we obtain.

$$\Theta(\theta) = \cos(n(\theta-\phi)) \qquad (4.35) \qquad n = 0,1,2,\ldots$$

and where ϕ is an arbitrary phase angle. Also

$$Z(z) = \cos \frac{m\pi}{h} z \qquad (4.36) \qquad m = 0,1,2,\ldots$$

In radial direction, an ordinary differential equation is obtained as

$$r^2 \frac{d^2}{dr^2} R(r) + r \frac{d}{dr} R(r) + \left\{\left[k^2 - \frac{m^2\pi^2}{h^2}\right] r^2 - n^2\right\} R(r) = 0 \qquad (4.37)$$

where $k = \frac{\omega}{C_0}$.

Solutions of equation (4.37) are given in terms of Bessel functions for $k > \frac{\omega\pi}{h}$,

$$R(r) = A_n J_n(\kappa r) + B_n Y_n(\kappa r) \qquad (4.38)$$

where $\kappa^2 = k^2 - \frac{m^2\pi^2}{h^2}$, J_n and Y_n are Bessel functions of the first kind and the second kind.

If $k < \frac{m\pi}{h}$, then

$$R(r) = A_n I_n(\chi r) + B_n K_n(\chi r) \qquad (4.39)$$

where, $\chi^2 = \frac{m^2\pi^2}{h^2} - k^2$, I_n and K_n are modified Bessel functions of the first kind and the second kind.

If equation (4.39) would be applied to the boundary conditions (equation (4.33)), the resulting characteristic equation would not have real roots. Therefore, this part of the solution can be ignored [4].

Applying boundary conditions (equation (4.33)) to equation (4.38), characteristic equations are obtained as follows:

$$J_n'(\kappa a)\, Y_n'(\kappa b) - J_n'(\kappa b)\, Y_n'(\kappa a) = 0 \qquad (4.40)$$

where primes denote differentiation with respect to r.

Using recurrence relationships for Bessel functions, equation (4.40) can be written as

$$[nJ_n(\kappa a)-\kappa a\, J_{n+1}(\kappa a)][nY_n(\kappa b)-\kappa b\, Y_{n+1}(\kappa b)] -$$
$$[nY_n(\kappa a)-\kappa a\, Y_{n+1}(\kappa a)][nJ_n(\kappa b)-\kappa b\, J_{n+1}(\kappa b)]=0 \qquad (4.41)$$

The roots of equation (4.41) are found as follows. We select values for n and seek the κ that satisfy the equation. There will be an infinite number of them. Each value is designated as κ_{nq} where q = 1,2,3,... denotes the q^{th} root of equation (4.41) for a given n. The natural frequencies in rad/sec are then obtained from

$$\omega_{mnq} = C_0 \sqrt{\kappa_{nq}^2 + \frac{m^2\pi^2}{h^2}} \qquad (4.42)$$

The mode function R(r) becomes

$$R(r) = J_n(\kappa_{nq} r) + C_{nq}\, Y_n(\kappa_{nq} r) \qquad (4.43)$$

where

$$C_{nq} = \frac{n\, J_n(\kappa_{nq} a) - \kappa_{nq} a\, J_{n+1}(\kappa_{nq} a)}{n\, Y_n(\kappa_{nq} a) - \kappa_{nq} a\, Y_{n+1}(\kappa_{nq} a)} \qquad (4.44)$$

Equations (4.35), (4.36) and (4.43) determine the natural modes. However, since $\Theta(\theta)$ is given as equation (4.35), we have to use two sets of mutually independent

natural modes, which is similar to the case when one solves for the vibration response of a closed ring or closed cylinder [10]. The reason is that the modes have no preferred orientation as far as θ direction is concerned. In order to allow for any orientation, as it might be excited in the forced case, we have to select two values of ϕ that give mode distributions that are orthogonal to each other. Selecting $\phi = 0$ and $\phi = \pi/2n$ gives $\Theta_{n1} = \cos n\theta$ and $\Theta_{n2} = \sin n\theta$. This gives the following two sets of pressure modes for $n,m = 0,1,2,\ldots$, and $q = 1,2,3\ldots$

$$P_{(mnq)1}(r,\theta,z) = [J_n(\kappa_{nq} r) + C_{nq} Y_n(\kappa_{nq} r)] \cdot \cos n\theta \cos \frac{m\pi}{h} z \tag{4.45}$$

$$P_{(mnq)2}(r,\theta,z) = [J_n(\kappa_{nq} r) + C_{nq} Y_n(\kappa_{nq} r)] \cdot \sin n\theta \cos \frac{m\pi}{h} z \tag{4.46}$$

Note that a constant pressure mode satisfies boundary conditions in r and z direction (equations (4.33) and (4.34)), and the continuity condition in θ direction. The corresponding natural frequency is obtained as zero if we substitute $P(r,\theta,z,t) = \text{const} \cdot e^{j\omega t}$ in equation (4.29). It is better to define this natural mode in addition to equations (4.45) and (4.46) in the following way.

$$P_{(0,0,0)1} = 1 \tag{4.47}$$

$$P_{(0,0,0)2} = 0 \tag{4.48}$$

$$\omega_{(0,0,0)} = 0 \tag{4.49}$$

This mode describes a spatially constant pressure change,

which has to be part of any forced solution that covers cases where gas is accumulated in the cavity.

An example of the natural mode for $n = m = q = 1$ is shown in Figure 4.3. The mode is one of which are typically strongly excited in practical machinery such as refrigeration compressor shells.

For a specific case of $a = 0.06$ m, $b = 0.08$ m, $h = 0.185$ m, $C_0 = 162.9$ m/sec (see Figure 4.2), and $\rho_0 = 6.04$ Kg/m^3, natural frequencies for various m, n, q are shown in Figure 4.4. From Figure 4.4, it can be seen that the lower natural frequencies correspond to q=1.

It is of some interest to discuss the radial distribution of natural modes of q=1. From equation (4.45) or (4.46), the mode is

$$R_{mnq}(r) = J_n(\kappa_{nq} r) + C_{nq} Y_n(\kappa_{nq} r) \qquad (4.50)$$

Figure 4.5 shows the radial distribution of natural modes for q=1 for various n numbers. As it is seen in equation (4.50), m numbers do not change the shape of these natural modes. The radial distribution is of almost constant value for $n = 1,2,3,...$ However, the mode has a nodal point in radial direction for n=0 and q=1, which is a higher mode (corresponds to the 53rd, 54th natural frequencies).

The cross sectional views of natural modes are schematically shown in Figure 4.6 for various n,q

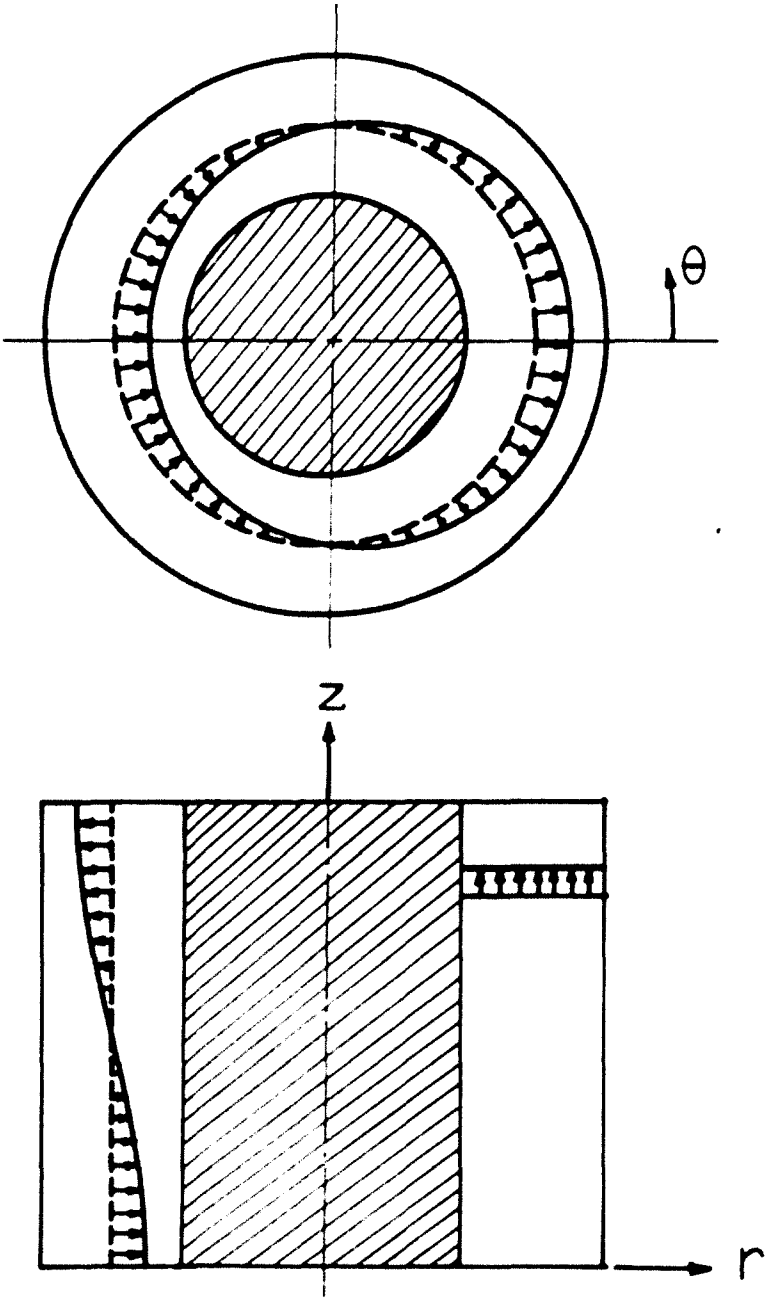

Figure 4.3 - Natural Modes in Terms of Pressure, $P_{(111)1}$

combinations. As it is shown, the mode for n=0 and q=1 has a similar shape to the mode for n=1, q=2, which is also a higher mode.

4.3.2 Four Poles

The four pole parameters are ready to be formulated, following the procedure of section 4.2. Since there are two normal modes at one natural frequency as shown in equations (4.45) and (4.46), it is convenient to modify some of the general equations, using an additional subscript 1 to assure that all mode components are summed up.

The functions $f_1(\underline{r},\omega)$ and $f_2(\underline{r},\omega)$, which define the four poles according to equations (4.6) to (4.9), become

$$f_1(r,\theta,z,\omega) = j\omega\rho_0 c_0^2 \sum_{l=1}^{2} \sum_{q=0}^{\infty} \sum_{n=0}^{\infty} \sum_{m=0}^{\infty} \frac{P_{(mnq)l}(r,\theta,z)\, P_{(mnq)l}(r_1,\theta_1,z_1)}{N_{mnq}\left[(\omega_{mnq}^2-\omega^2) + 2j\,\omega\,\omega_{mnq}\,\xi_{mnq}\right]} \tag{4.51}$$

$$f_2(r,\theta,z,\omega) = j\omega\rho_0 c_0^2 \sum_{l=1}^{2} \sum_{q=0}^{\infty} \sum_{n=0}^{\infty} \sum_{m=0}^{\infty} \frac{P_{(mnq)l}(r,\theta,z)\, P_{(mnq)l}(r_2,\theta_2,z_2)}{N_{mnq}\left[(\omega_{mnq}^2-\omega^2) + 2j\,\omega\,\omega_{mnq}\,\xi_{mnq}\right]} \tag{4.52}$$

where

$$N_{mnq} = \int_0^h \int_0^{2\pi} \int_a^b r\, P^2_{(mnq)l}(r,\theta,z)\, dr d\theta dz \tag{4.53}$$

Figure 4.7 to 4.10 show four pole parameters calculated for the specific case of the cavity which has the same dimension as that of Figure 4.4, and input point $r_1^* = (0.065m, 0^o, 5h/7)$, and output point $r_1^* = (0.075m, 180^o, 5h/7)$. Damping was taken to be $\xi_{mnq} = 0.01$. This example case corresponds approximately to a compressor shell volume for a small refrigeration compressor, filled with refrigerant gas at suction condition.

4.4 Application to System Problems

As example of an application of the derived four poles, consider an annular cavity which is connected to an anechoic pipe and subjected to a harmonic input volume flow source as shown in Figure 4.2.

The relationship between the volume velocity and the pressure of the pipe entrance is [1]:

$$Q_E = \frac{S_{an}}{\rho_0 C_0} P_E \tag{4.54}$$

where, S_{an} is the cross sectional area of the pipe. Therefore, the four pole equation relating input Q_i, P_i to output Q_E becomes

$$\begin{Bmatrix} Q_i \\ P_i \end{Bmatrix} = \begin{bmatrix} A & B \\ C & D \end{bmatrix} \begin{Bmatrix} 1 \\ \frac{\rho_0 C_0}{S_{an}} \end{Bmatrix} Q_E \tag{4.55}$$

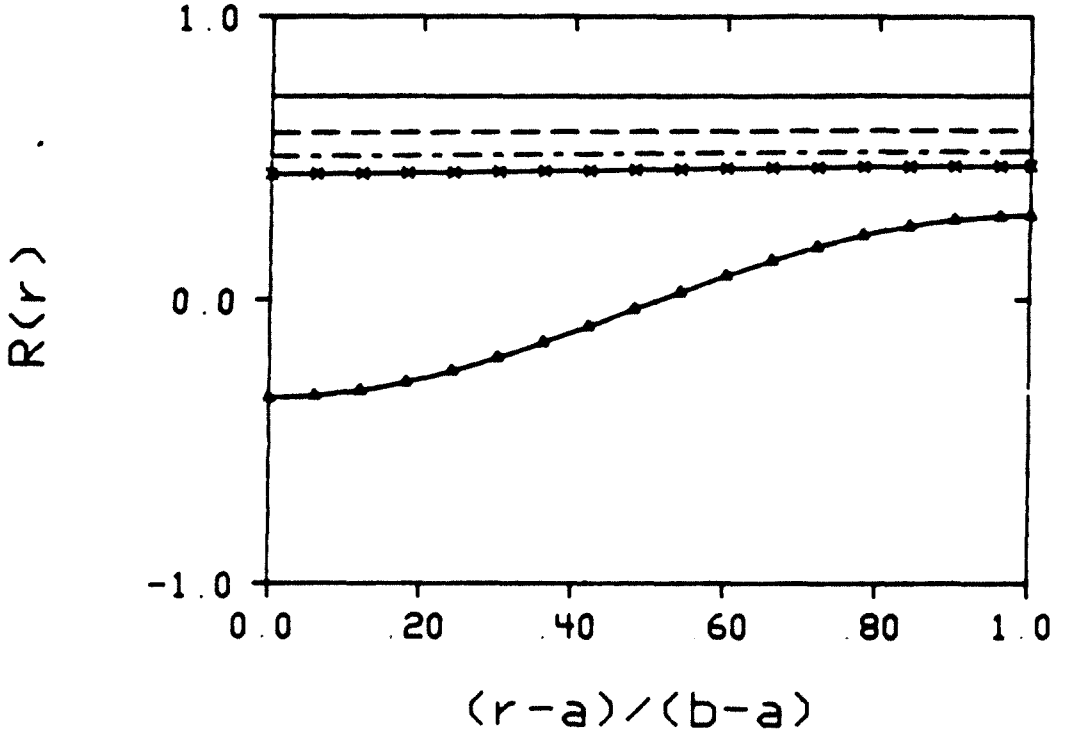

Figure 4.5 - Radial Direction Natural Modes, (q=1,n=1) ——— , (q=1,n=2) – – – – ,(q=1,n=3) — – — ,(q=1,n=4) —×— ,(q=1,n=0) —▲— .

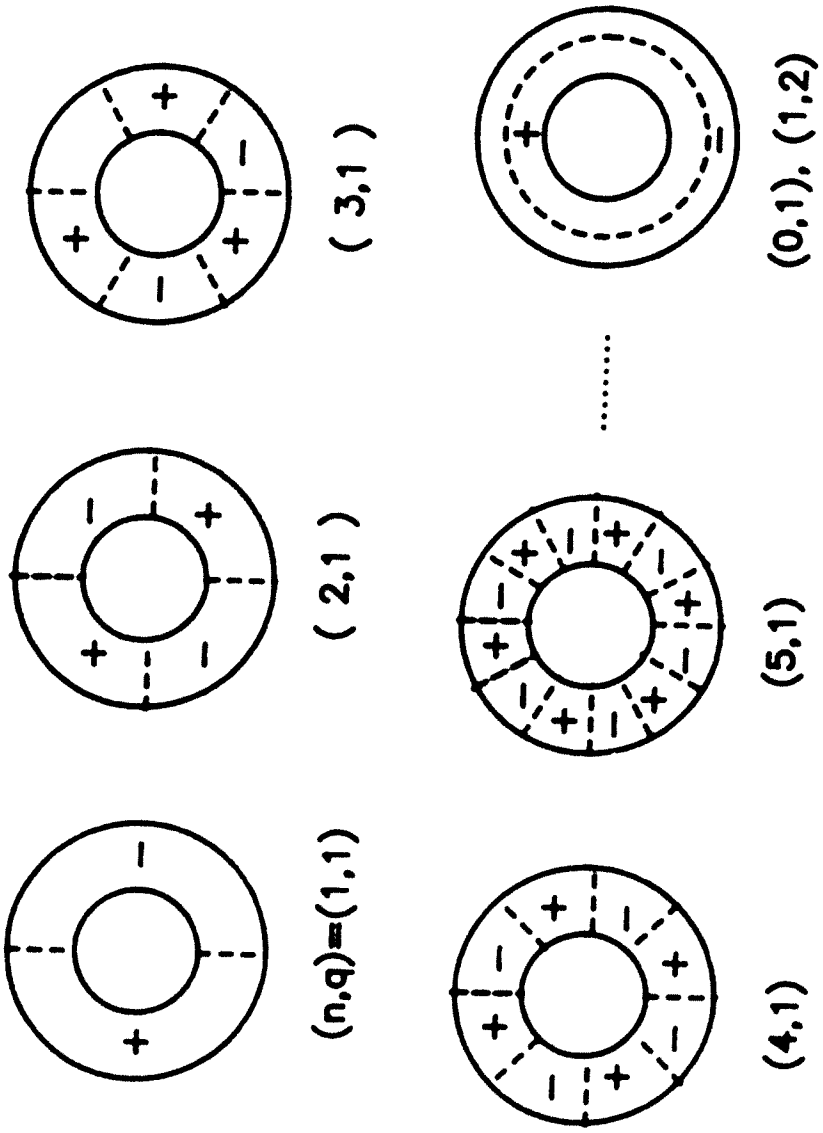

Figure 4.6 - Cross Sectional Natural Modes

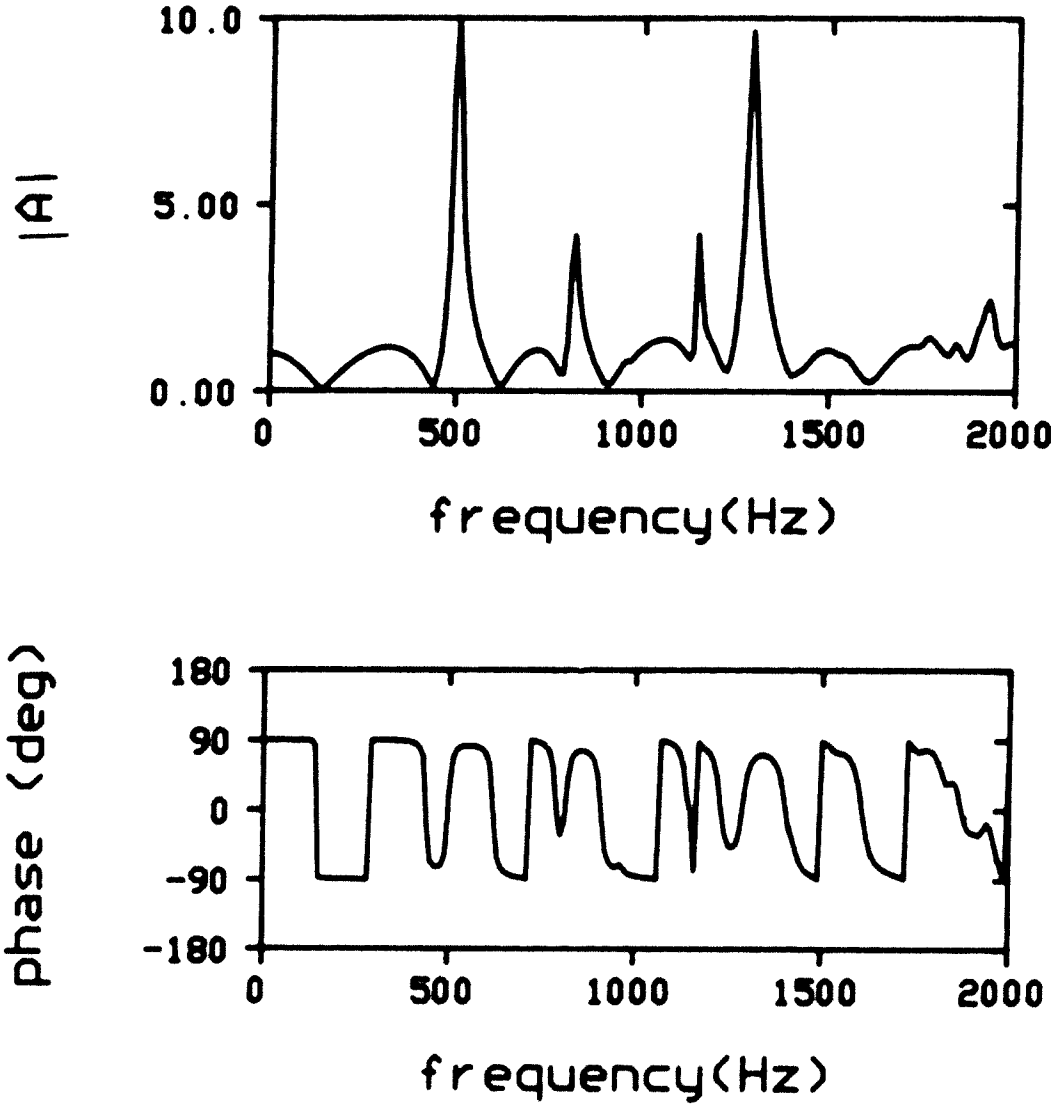

Figure 4.7 - Pole A

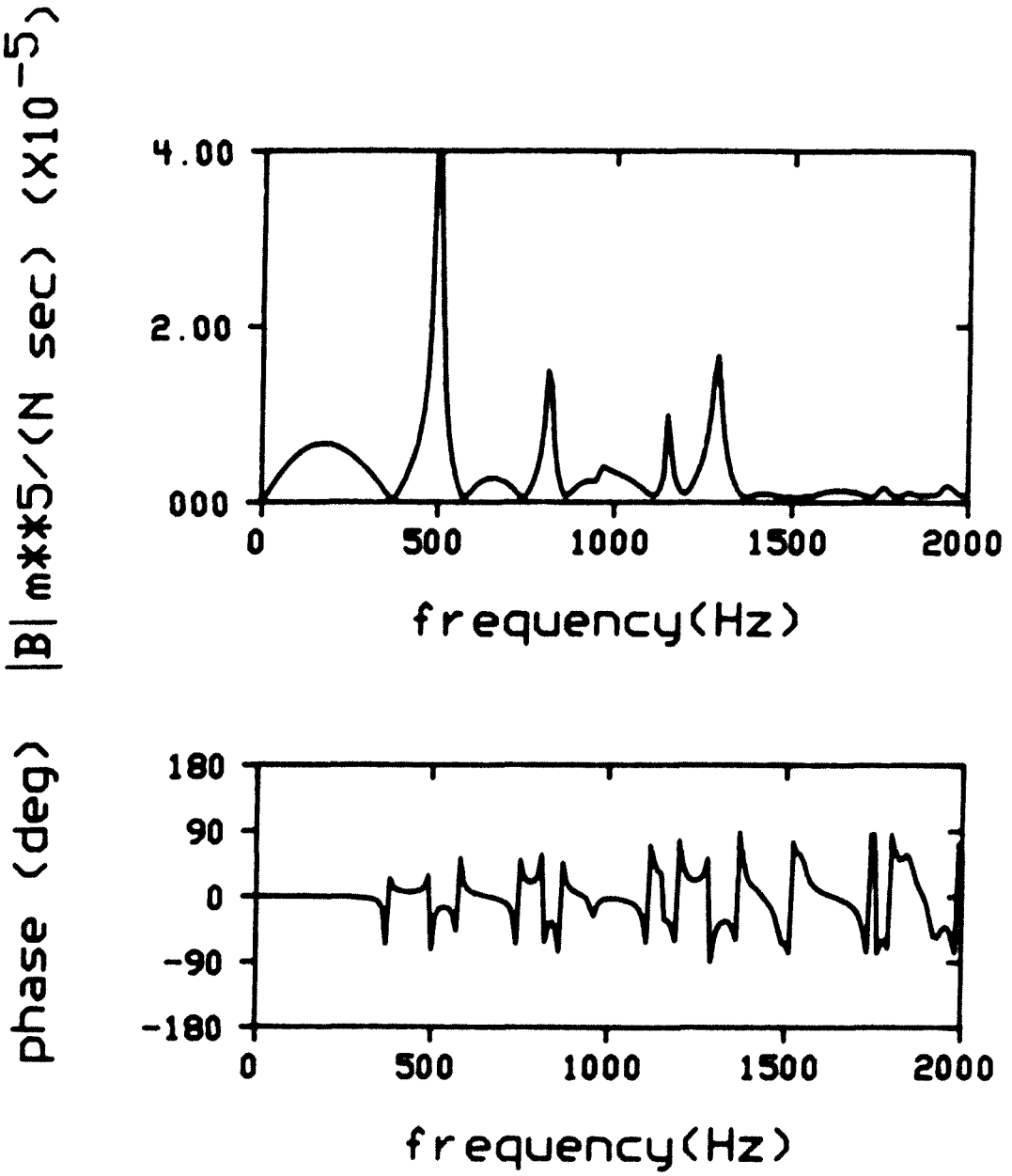

Figure 4.8 - Pole B

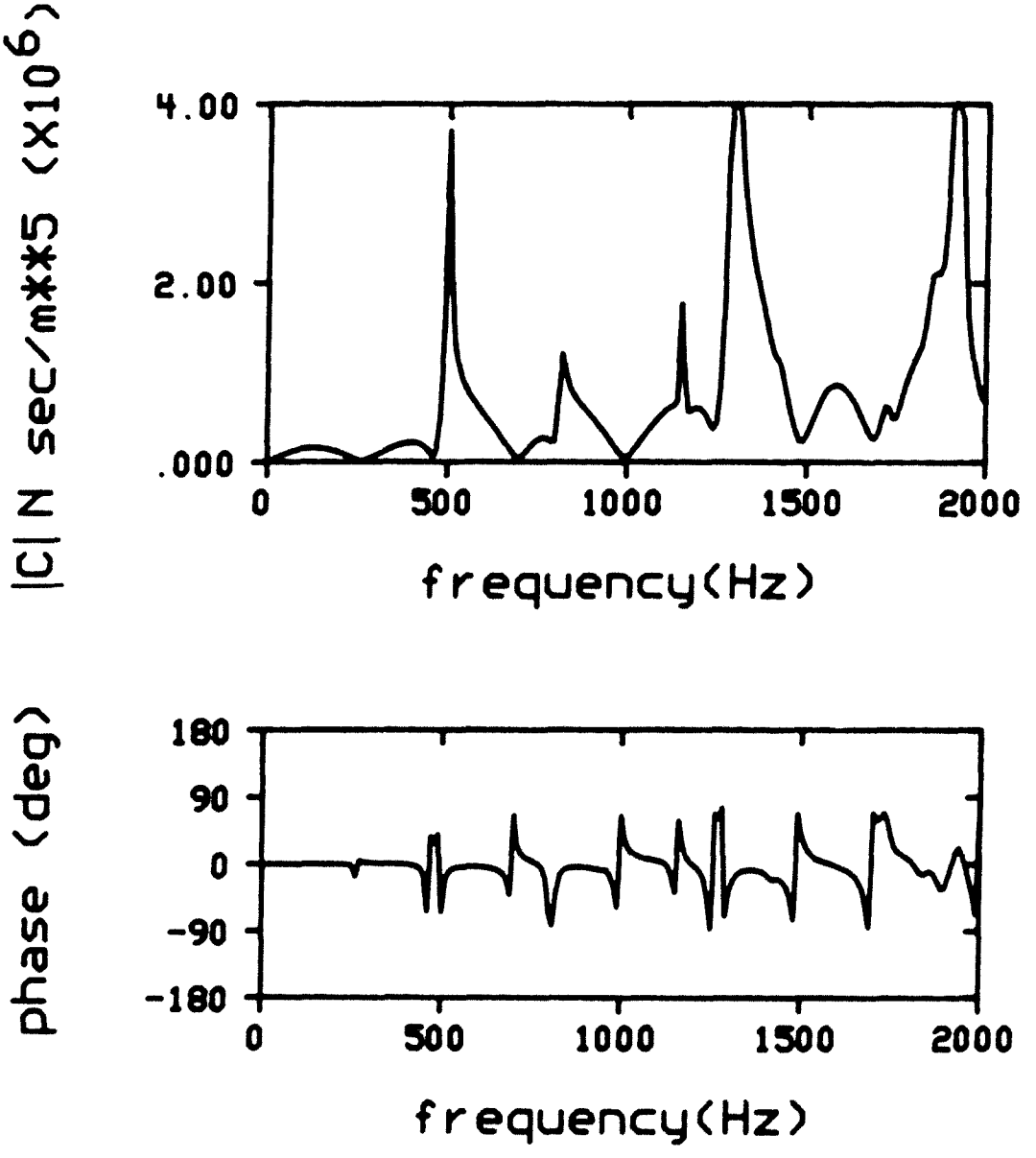

Figure 4.9 - Pole C

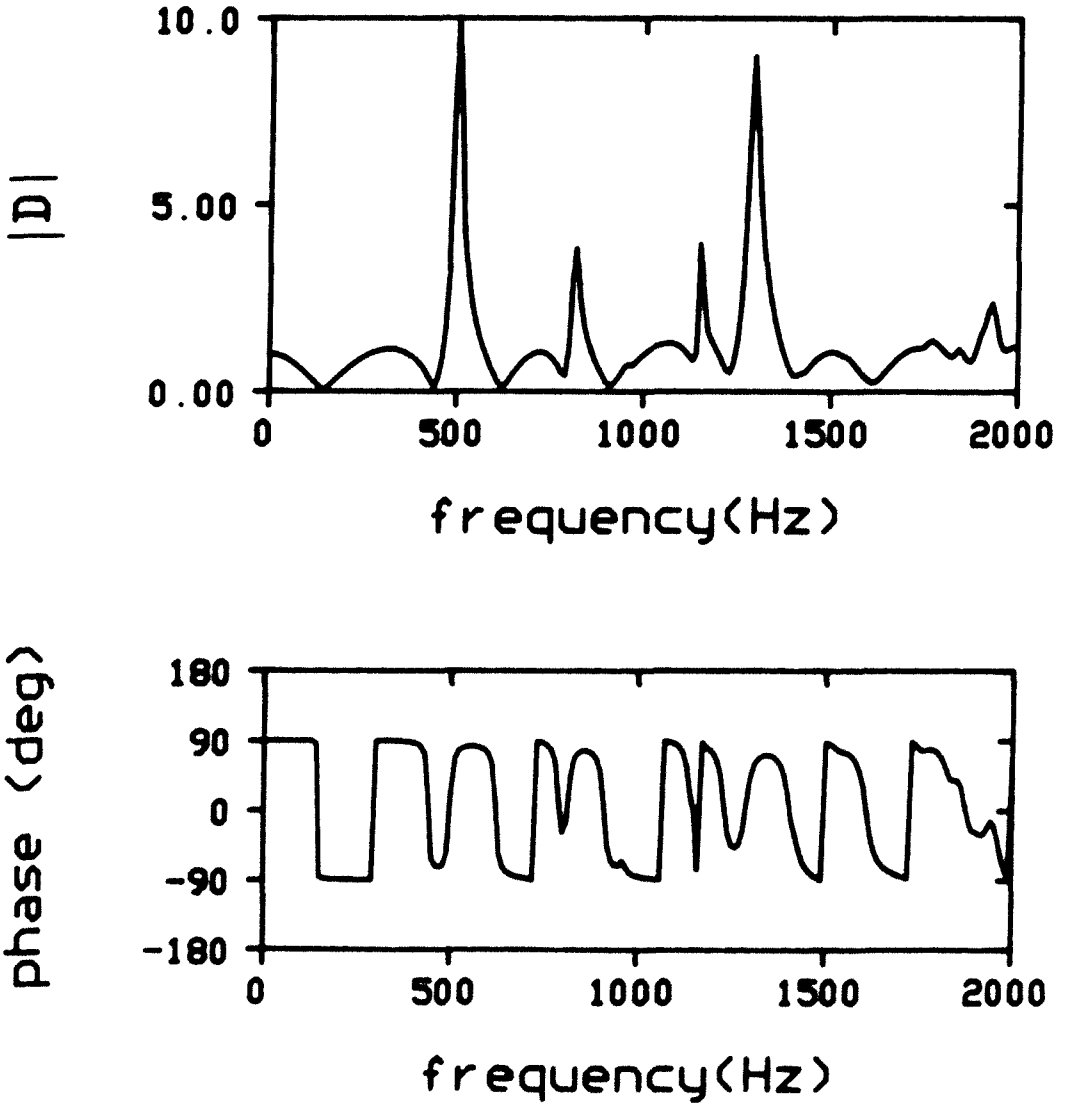

Figure 4.10 - Pole D

where, A, B, C and D are four poles of the annular cavity.

From equation (4.57), the driving point impedance is obtained as

$$\frac{P_i}{Q_i} = \frac{C \dfrac{S_{an}}{\rho_0 C_0} + D}{A \dfrac{S_{an}}{\rho_0 C_0} + B} \tag{4.56}$$

Also, transfer functions are

$$T_Q(\omega) = \frac{Q_E}{Q_i} = \frac{\dfrac{S_{an}}{\rho_0 C_0}}{A \dfrac{S_{an}}{\rho_0 C_0} + B} \tag{4.57}$$

$$T_P(\omega) = \frac{P_E}{Q_i} = \frac{1}{A \dfrac{S_{an}}{\rho_0 C_0} + B} \tag{4.58}$$

Volume transfer functions are shown in Figure 4.11 for four types of input/output port arrangements. The cavity has the same dimensions as the cavity of Figure 4.5, and $S_{an} = 0.3\times10^{-4}\,m^2$. Damping coefficients are taken as $\xi_{mnq} = 0.01$.

The position of input port is taken the same as for Figures 4.7 to 4.10 and the output port positions are $r^* = (r_E, \theta_E, z_E) = (0.075m, 180^\circ, 0.1321m)$ for case C_1, $(0.075m, 180^\circ, 0.0925m)$ for case C_2, $(0.075m, 0^\circ, 0.1321m)$ for case C_3 and $(0.075m, 0^\circ, 0.0925m)$ for case C_4.

If the dimension of the concentric gap is small compared to the height and the radius, as in many practical

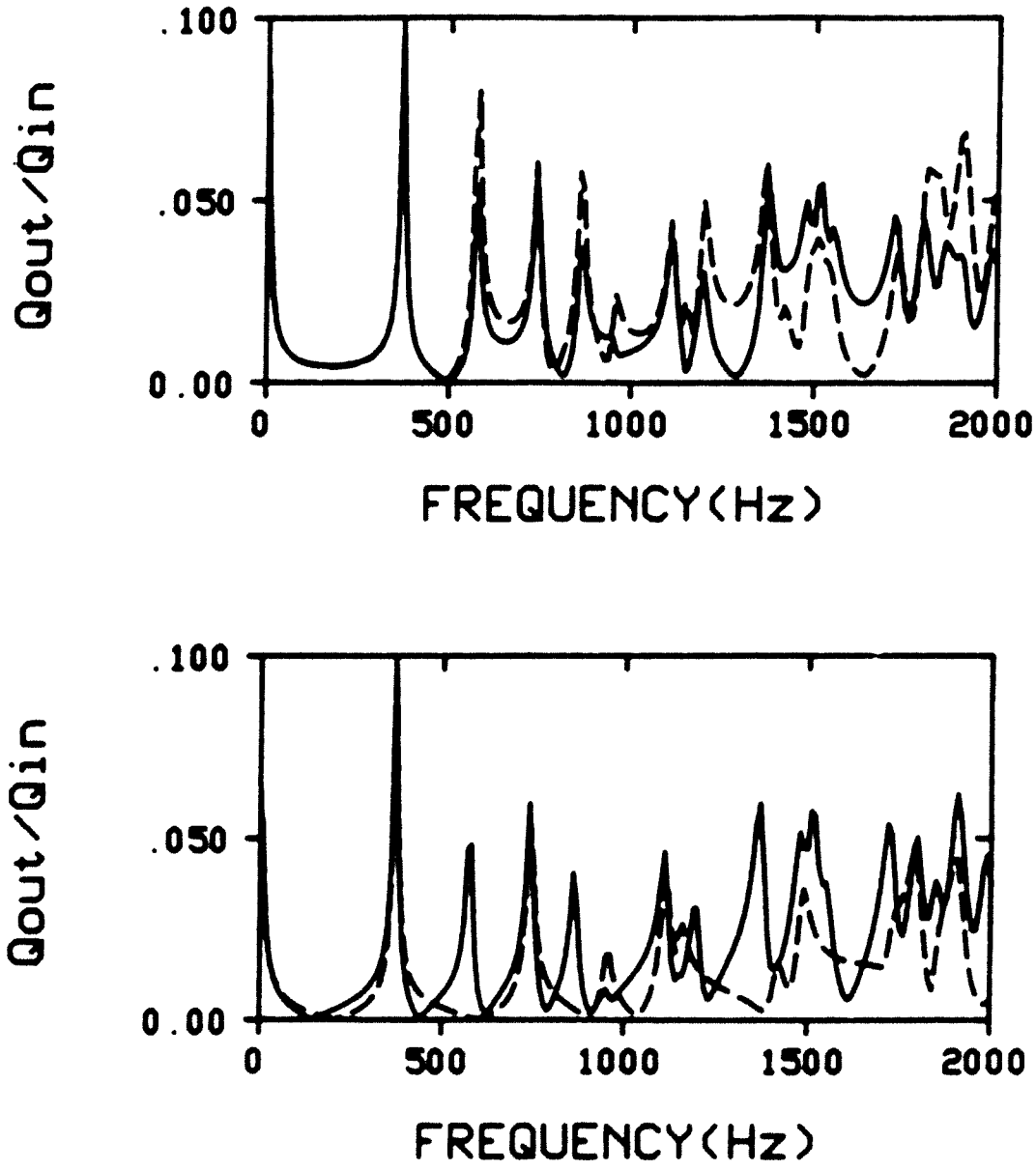

Figure 4.11 - Volume Flow Transfer Functions for Different Input-Output Geometry, Case C1, —— (top), Case C2, – – – (top), Case C3, —— (bottom), Case C4, – – – (bottom)

applications, modes where circumferential and axial motion dominates are usually excited. For the dimension of the example of a refrigeration compressor in Figure 4.2, the first circumferential motion dominated mode is shown to be the most important, which agrees with practical experience [7].

Figure 4.12 shows the volume flow transfer function at the first, the second and third lowest natural frequencies as function of the position of the output port. It is expected that the transfer function variation resembles each corresponding natural mode. As a practical application, if certain frequency components are found to be important to be controlled as the result of a sound measurement, the input port position can be designed to minimize the transfer function.

The output volume flow velocity is, from equation (4.57),

$$Q_E = T_Q(\omega)\, Q_i \tag{4.59}$$

The pressure due to Q_E and Q_i is, from equation (51),

$$p(\underline{r},t) = j\omega\rho_0 C_0^2\, e^{j\omega t} \sum_{l=1}^{2} \sum_{q=0}^{\infty} \sum_{n=0}^{\infty} \sum_{m=0}^{\infty} P_{mnq(l)}(r,\theta,z)$$

$$\frac{P_{mnq(l)}(r_1,\theta_1,z_1) - P_{mnq(l)}(r_2,\theta_2,z_2) T_Q(\omega)}{N_{mnq}\left[(\omega_{mnq}^2 - \omega^2) + 2j\,\omega\,\omega_{mnq}\,\xi_{mnq}\right]}\, Q_i \tag{4.60}$$

The magnitude of the excited pressure of the annular cavity due to a unit volume flow input at $\theta = 30^{\circ}$ is

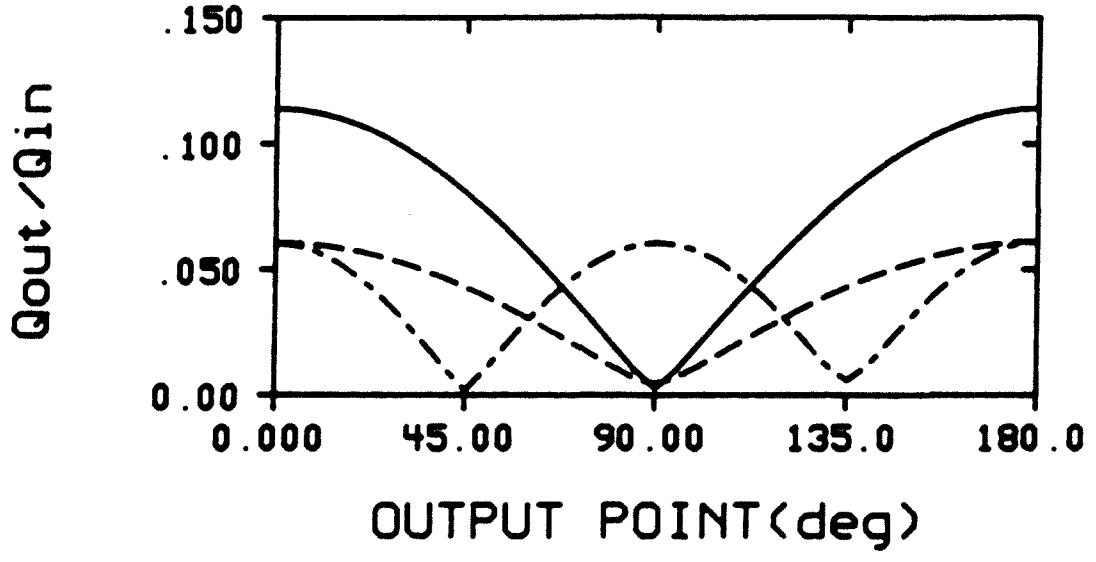

(a)

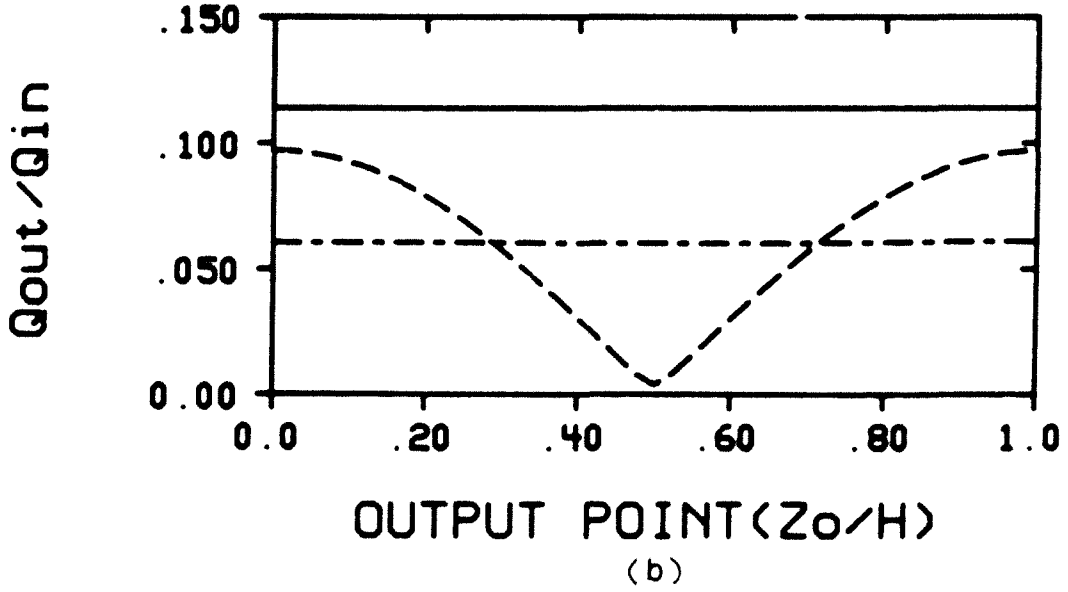

(b)

Figure 4.12 - Change of Transfer Functions due to the Output Port Location for the First Resonance, ——— , the Second, ——— and the Third, ———— . (a) Circumferential Variation for Z /H = 5/7, (b) Axial Variation for $\theta = 180^{o}$

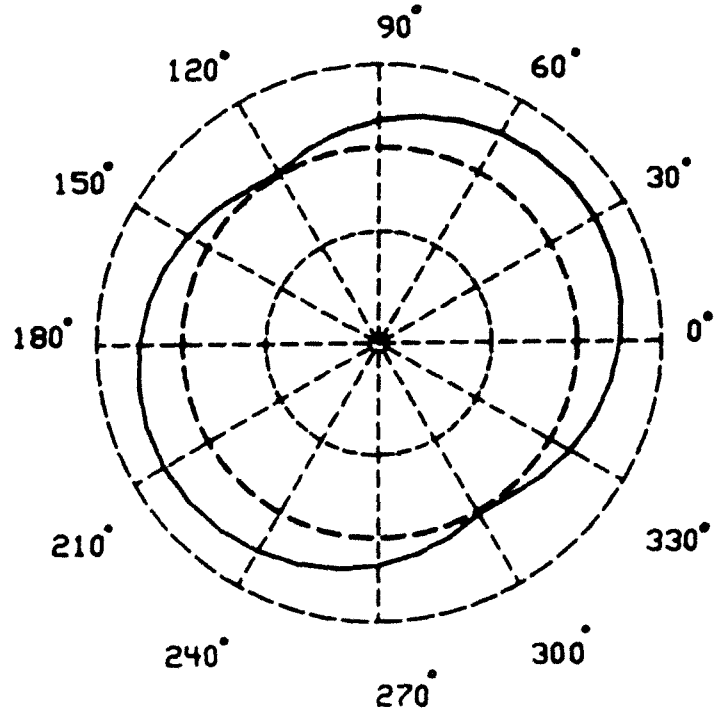

Figure 4.13 - Excited Pressure Shape (Magnitude)

plotted in Figure 4.13.

The particle velocities of the cavity can be obtained by integrating Euler's equation.

$$\underline{u} = -\frac{1}{\rho_0} \int \nabla p \, dt \tag{4.61}$$

where

$$\nabla = \frac{\partial}{\partial r} \underline{e}_r + \frac{1}{r} \frac{\partial}{\partial \theta} \underline{e}_\theta + \frac{\partial}{\partial z} \underline{e}_z \tag{4.62}$$

and where $\underline{e}_r$, $\underline{e}_\theta$, $\underline{e}_z$ are unit vectors in r, θ, z direction.

It can be nondimensionalized by dividing it by the particle velocity in the anechoic pipe.

$$\underline{u}^* = \frac{\underline{u}}{Q_E / S_{an}} \tag{4.63}$$

Each component of $\underline{u}^*$ was plotted against nondimensional coordinates in Figure 4.14 for a unit volume flow input of 540 Hz. The position of the input port was taken as $\underline{r}^* = (0.065\text{m}, 30^\circ, 0.1321\text{m})$, while all other dimensions are the same as case C1 of Figure 4.11. Figure 4.15 defines the lines along which velocities in Figure 4.14 were calculated. As can be seen at the cylinder wall, the radial component of the velocity is zero, which complies with the boundary condition. Tangential and axial velocity components exist at the walls, since wall friction and resulting boundary layers are assumed to be negligible when using the linear wave equation theory.

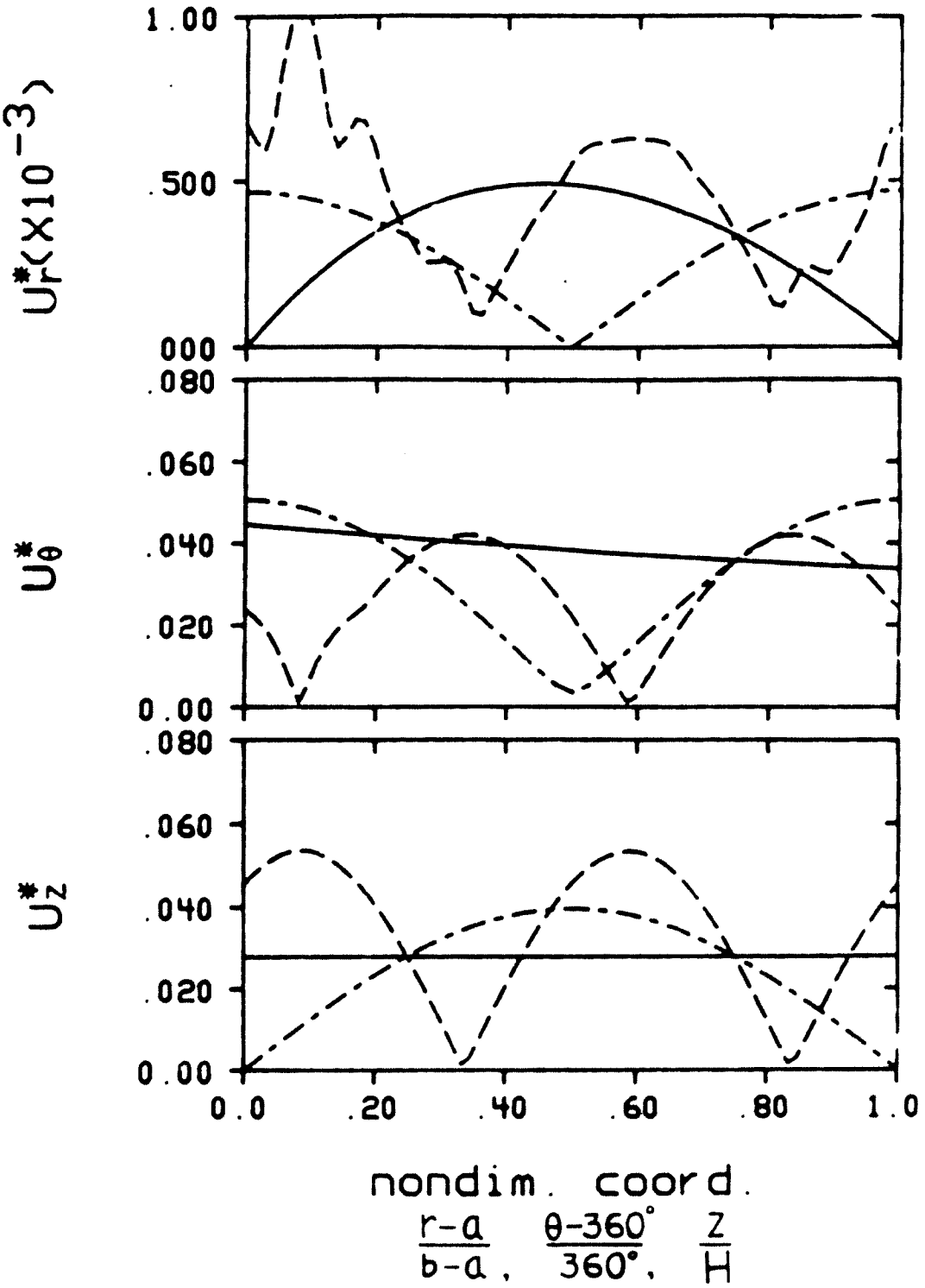

Figure 4.14 - Nondimensional Particle Velocities in an Annular Cavity, Velocity along Path I, ——— ,along path II, – – – – , along path III, —·— , in Figure 15

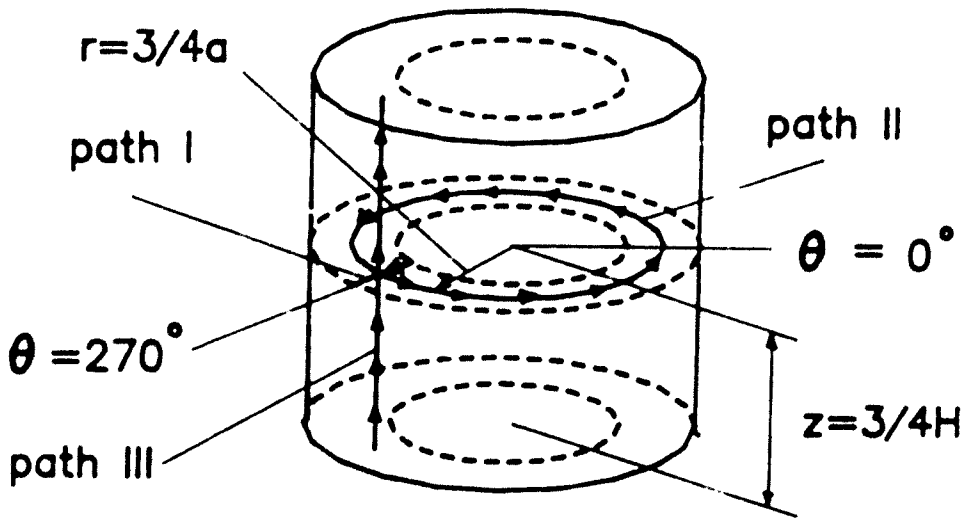

Figure 4.15 - Illustration for the Velocity Calculation Path

It can also be seen that tangential and vertical velocity components are dominating the motion as expected for lower mode frequencies.

4.5 Forced Response of the Cavity to Multiple Inputs

The previous development can be extended to an annular cavity subjected to multiple inputs shown in Figure 4.16.

If we define T_{Q1} and T_{P1} as

$$T_{Q1} = \frac{Q_{E,1}}{Q_{in,1}} \tag{4.64}$$

$$T_{P1} = \frac{P_{E,1}}{Q_{in,1}} \tag{4.65}$$

where $1 = 1,2,\ldots,n$, $Q_{E,1}$ and $P_{E,1}$ are the output volume flow and the output pressure due to input volume flow at point 1. Then T_{Q1} and T_{P1} are

$$T_{Q1} = \frac{\frac{S_{an}}{\rho_0 C_0}}{A_1 \frac{S_{an}}{\rho_0 C_0} + B_1} \tag{4.66}$$

$$T_{P1} = \frac{1}{A_1 \frac{S_{an}}{\rho_0 C_0} + B_1} \tag{4.67}$$

where, A_1, B_1 are pole parameters between the input point r_1^* and output point r_E^*.

The output volume velocity is given by

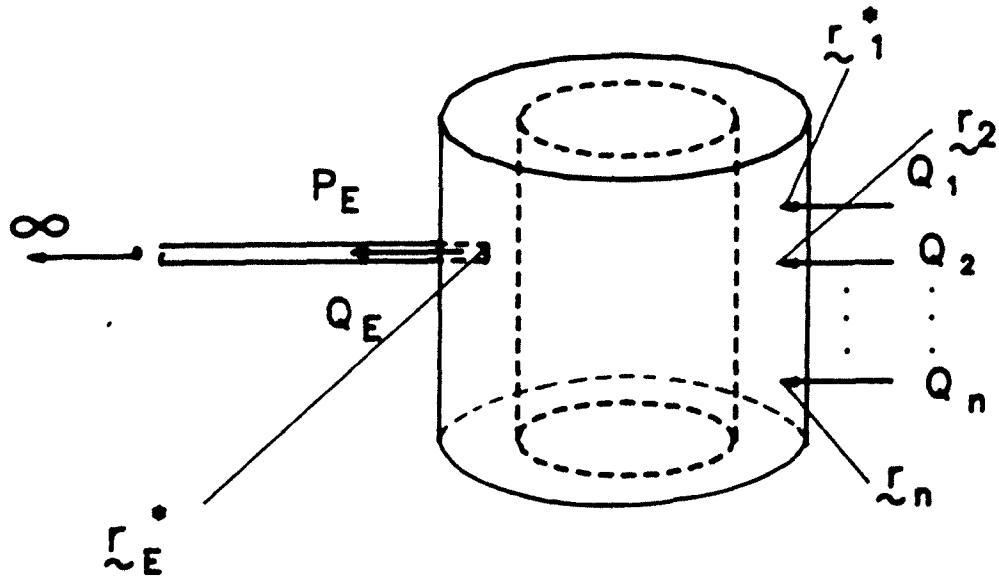

Figure 4.16 - An Annular Cavity with Multiple Inputs

$$Q_{TE}(t) = \sum_{l=1}^{n} Q_{El}\, e^{j\omega_l t}$$

$$= \sum_{l=1}^{n} T_{Ql}\, Q_l\, e^{j\omega_l t} \qquad (4.68)$$

For the special case where

$$\omega_1 = \omega_2 = \ldots = \omega_n$$

we obtain

$$Q_{TE}(t) = Q_E\, e^{j\omega t} = \sum_{l=1}^{n} T_{Ql}\, Q_l\, e^{j\omega t} \qquad (4.69)$$

The output point pressure is

$$P_{TE} = \sum_{l=1}^{n} P_{El}\, e^{j\omega t}$$

$$= \sum_{l=1}^{n} T_{Pl}\, Q_l\, e^{j\omega t} \qquad (4.70)$$

As an example, if we take two inputs that are located in circumferential direction as shown in Figure 4.17, of equal frequency ω and magnitude, but out of phase such that $Q_2 = Q_1\, e^{j\phi}$,

$$Q_{TE}(t) = (T_{Q1} + T_{Q2}\, e^{j\phi})\, Q_1\, e^{j\omega t} \qquad (4.71)$$

When $T_{Q1} = T_{Q2}$, which occurs if the inlets are arranged symmetrically with respect to outlet, then

$$Q_{TE}(t) = Q_1 T_{Q1}\, (1 + e^{j\phi})\, e^{j\omega t} \qquad (4.72)$$

From equation (4.74), it can be argued that the output flow pulsation is eliminated if the phase difference between two inputs is 180° for all frequencies, although it

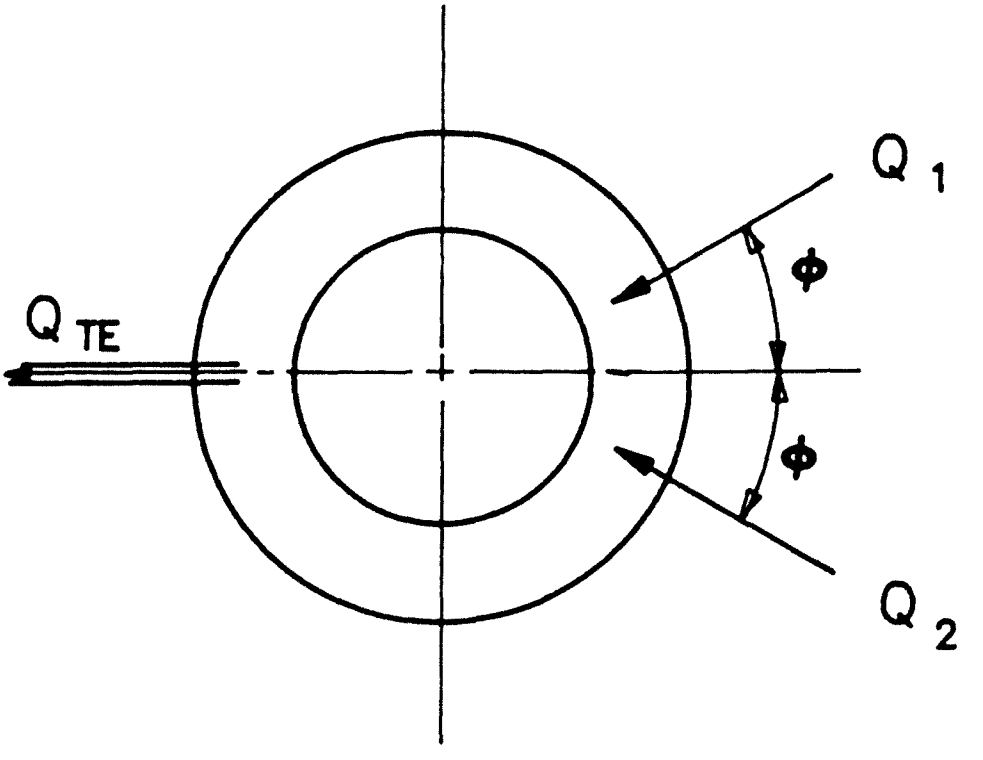

Figure 4.17 - An Annular Cavity with two Symmetric Inputs

may be difficult to achieve this in practical application.

If the two input frequencies are slightly different, a beating phenomenon is observed. The pressure at the output port when ω_1 = 315 Hz, ω_2 = 285 Hz, r_1^* = (0.065 m , 0^o, 0.13214 m) and r_2^* = (0.065 m , 0^o, 0.0925 m) is shown in Figure 4.18.

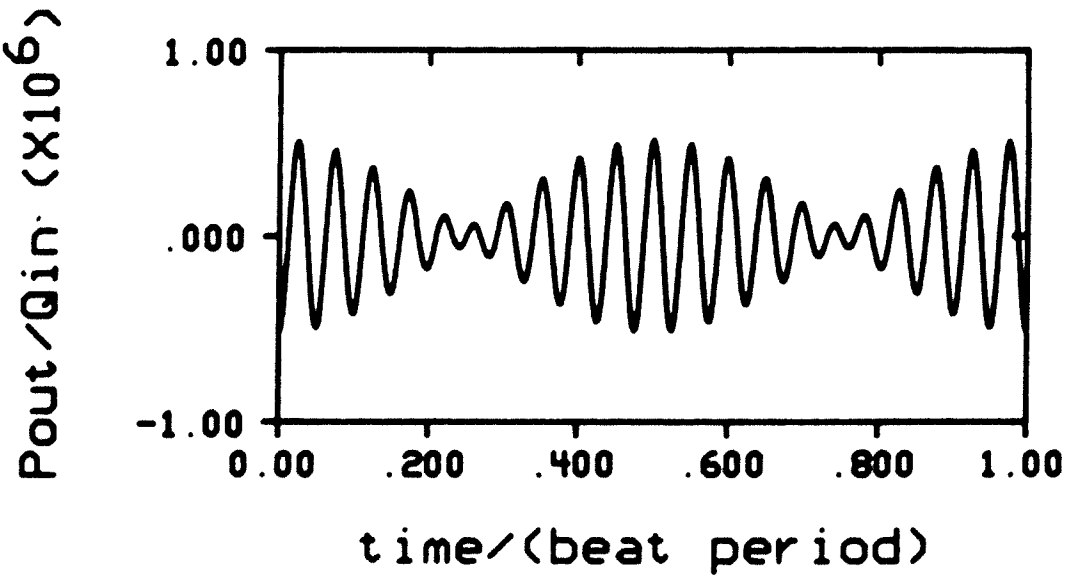

Figure 4.18 - Beating Phenomenon of the Output Pressure

CHAPTER 5 - ANALYSIS OF GAS PULSATIONS IN MULTIPLY CONNECTED ACOUSTIC CAVITIES

5.1 Introduction

5.1.1 Review of the Problem

Most work in the area of pressure pulsation analysis of complex fluid manifolds is based on the lumped parameter model. This method has been widely used for the compressor and engine manifold analysis because it is relatively simple[13,14,15]. However the method gives reasonable results only for elements which are small compared with the shortest wave length of interest[1]. Large cavities which have multiple connections cannot be treated by the lumped parameter model because it does not allow spatial variations of the pressure in the cavity.

An acoustic element of large dimension relative to the shortest wave length of interest has to be modeled as a continuous parameter model[1,47]. There have been investigations on the analysis of continuous parameter systems by several researchers for various geometries [30,32,46], however, most of them were on isolated acoustic elements. Literature survey revealed no attempt to analyze an acoustic system composed of multiply connected continuous acoustic elements.

Insights obtained from a simply connected cavity analysis cannot be extended to multiply connected manifolds because dynamic interactions between cavities become more complicated.

In this chapter, a general procedure is developed for the analysis of a system composed of two multiply connected large cavities. A cylindrical annular cavity connected to a small lumped parameter volume by double pipes is taken as an example, although the result can be applied to more general cases without any difficulty.

The four pole parameter technique was used as a fundamental tool of the analysis. It was used to build up the system solution from solutions of its elements as well as to study the response of the system when it is integrated with other acoustic elements, for example an anechoically terminated pipe. The authors have developed an approach to obtain four pole parameters of an acoustic system from its pressure response solutions and have applied it to the analysis of an annular cylindrical cavity[47]. In this chapter, the method is further extended and generalized to treat more complicated acoustic systems.

5.1.2 Four Pole Parameters

Four pole parameters of an acoustic system can be formulated if its pressure responses are known[47].

$$A = \frac{f_2(\underline{r}_2,\omega)}{f_1(\underline{r}_2,\omega)} \tag{5.1}$$

$$B = \frac{1}{f_1(\underline{r}_2,\omega)} \tag{5.2}$$

$$C = -f_2(\underline{r}_1,\omega) + \frac{f_1(\underline{r}_1,\omega)}{f_1(\underline{r}_2,\omega)} \cdot f_2(\underline{r}_2,\omega) \tag{5.3}$$

$$D = \frac{f_1(\underline{r}_1,\omega)}{f_1(\underline{r}_2,\omega)} \tag{5.4}$$

where, $f_1(\underline{r},\omega)$ and $f_2(\underline{r},\omega)$ are the pressure responses of the system at $\underline{r}$ due to a unit volume flow input at $\underline{r}_1$ and a unit volume flow input at $\underline{r}_2$, and $\underline{r}_1$ and $\underline{r}_2$ are the positions of the input port and output port of the system. For example, $f_1(\underline{r}_2,\omega)$ is the pressure response of the system at the output port due to a unit volume flow input at the input port. Therefore, knowing a general form of the pressure responses of the system, four pole parameters are readily calculated by the relationship in equations (5.1) to (5.4).

5.2 General Formulations

The acoustic system shown in Figure 5.1 has two large cavities connected to each other by n long pipes, which can

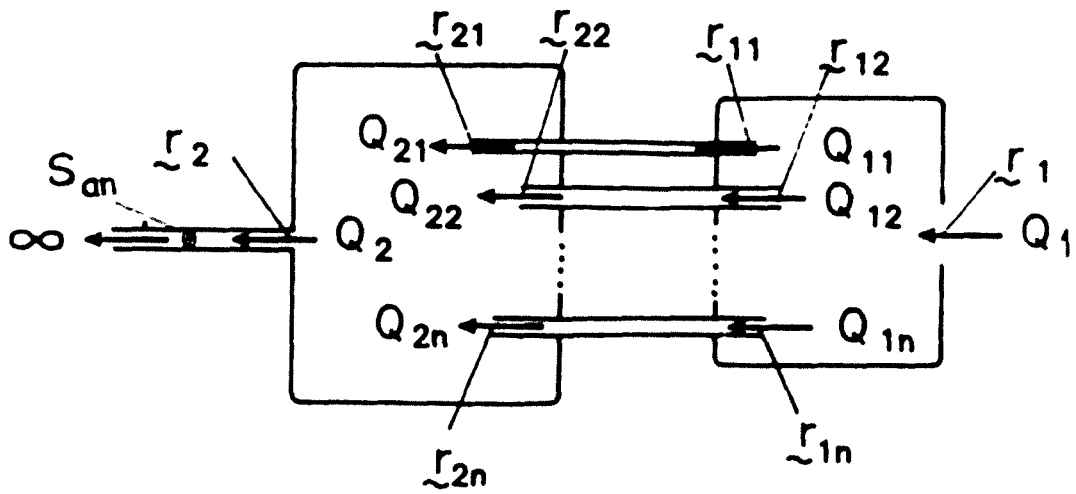

Figure 5.1 - Two Multiply Connected Acoustic Cavities

be found in various types of fluid machinery such as compressor gas manifolds or automobile mufflers.

Only for the purpose of conciseness in subsequent discussions, let us define the following terms for the system shown in Figure 5.1.

1. The first cavity and the second cavity mean the cavity which has the input port and the cavity which has the output port.

2. $\underset{\sim}{r}_1$ and $\underset{\sim}{r}_2$ are the position vectors of the input port and the output port of the system as it was mentioned above, and $\underset{\sim}{r}_{1i}$ and $\underset{\sim}{r}_{2i}$ are the connection points of the i^{th} pipe to the first and the second cavity.

3. Q_{1i} and Q_{2i} are complex amplitudes of the volume flows and P_{1i} and P_{2i} are complex amplitudes of the acoustic pressures at $\underset{\sim}{r}_{1i}$ and $\underset{\sim}{r}_{2i}$.

4. A_i, B_i, C_i, and D_i are four pole parameters of the i^{th} pipe.

5. $g(\underset{\sim}{r})$ and $h(\underset{\sim}{r})$ are pressure responses of the first cavity and the second cavity. The subscript denotes the position of the corresponding input volume flow to the cavity. For example, $g_{13}(\underset{\sim}{r}_1)$ stands for the pressure response of the first cavity at $\underset{\sim}{r}_1$ due to a unit volume flow input at $\underset{\sim}{r}_{13}$.

5.2.1 Formulation of Fundamental System Equations

Four pole equations of the i^{th} pipe are,

$$Q_{1i} = A_i\, Q_{2i} + B_i\, P_{2i} \tag{5.5}$$

$$P_{1i} = C_i\, Q_{2i} + D_i\, P_{2i} \tag{5.6}$$

where, $i = 1,2,3,\cdots,n$. Then the pressure response of the first cavity in Figure 5.1 is expressed as follows

$$P_1(\underline{r},\omega) = g_1(\underline{r})\, Q_1 - \sum_{j=1}^{n} g_{1j}(\underline{r})\, Q_{1j} \tag{5.7}$$

The pressure of the second cavity is

$$P_2(\underline{r},\omega) = \sum_{j=1}^{n} h_{2j}(\underline{r})\, Q_{2j} - h_2(\underline{r})\, Q_2 \tag{5.8}$$

Substituting equations (5.7) and (5.8) in equations (5.5) and (5.6) and by rearranging the results, we obtain

$$Q_{1i} - \sum_{j=1}^{n} \left(A_i\delta_{ij} + B_i h_{2j}(\underline{r}_{2i}) \right) Q_{2j} = -B_i h_2(\underline{r}_{2i}) Q_2 \tag{5.9}$$

$$\sum_{j=1}^{n} g_{1j}(\underline{r}_{1i}) Q_{1j} + \sum_{j=1}^{n} \left(C_i\delta_{ij} + D_i h_{2j}(\underline{r}_{2i}) \right) Q_{2j} = g_1(\underline{r}_{1i}) Q_1 + D_i h_2(\underline{r}_{2i}) Q_2 \tag{5.10}$$

where, $i = 1,2,3,\cdots,n$, and δ_{ij} is the Kronecker delta function.

Equations (5.9) and (5.10) are 2n equations which enable us

to solve 2n unknown internal volume flows Q_{1j} and Q_{2j}, j=1,2, ··, n, for a given set of input and output volume flows Q_1 and Q_2.

5.2.2 Derivation of the Four Pole Parameters

Pressure responses of the overall system $f_1(\underline{r},\omega)$ and $f_2(\underline{r},\omega)$ are necessary to be known to calculate four pole parameters. Considering the definition of $f_1(\underline{r})$, the corresponding volume flows are $Q_1 = 1$ and $Q_2 = 0$.

Therefore from equation (5.7),

$$f_1(\underline{r}_1,\omega) = P_1(\underline{r}_1,\omega)\big|_{Q_1=1,Q_2=0}$$
$$= g_1(\underline{r}_1) - \sum_{j=1}^{n} g_{1j}(\underline{r}_1)Q_{1j} \qquad (5.11)$$

and from equation (5.8),

$$f_1(\underline{r}_2,\omega) = P_2(\underline{r}_2,\omega)\big|_{Q_1=1,Q_2=0}$$
$$= \sum_{j=1}^{n} h_{2j}(\underline{r}_2)Q_{2j} \qquad (5.12)$$

where Q_{1j} and Q_{2j}, j=1,2, ···, n, should be obtained by solving equations (5.9) and (5.10) taking $Q_1 = 1$ and $Q_2 = 0$.

$f_2(\underline{r},\omega)$ can be obtained similarly :

$$f_2(\underline{r}_1,\omega) = P_1(\underline{r}_1,\omega)\big|_{Q_1=0,Q_2=-1}$$

$$= -\sum_{j=1}^{n} g_{1j}(\underline{r}_1)Q_{1j} \tag{5.13}$$

$$f_2(\underline{r}_2,\omega) = P_2(\underline{r}_2,\omega)\big|_{Q_1=0,Q_2=-1}$$

$$= \sum_{j=1}^{n} h_{2j}(\underline{r}_2)Q_{2j} + h_2(\underline{r}_2) \tag{5.14}$$

Notice that Q_2 is taken as negative because $f_2(\underline{r},\omega)$ is defined as the system response to a unit volume flow input at the output port, while an output flow is taken as positive for Q_2 during the formulation of equations (5.7) to (5.10). Again, Q_{1j} and Q_{2j} should be solved from equations (5.9) and (5.10) taking $Q_1 = 0$ and $Q_2 = -1$.

Now the four pole parameters are ready to be calculated from equations (5.1) to (5.4). In the actual calculations, one can utilize the reciprocal properties of the pressure response as follows.

$$f_1(\underline{r}_2,\omega) = f_2(\underline{r}_1,\omega) \tag{5.15}$$

$$g_{1i}(\underline{r}_{1j}) = g_{1j}(\underline{r}_{1i}) \tag{5.16}$$

$$h_{2i}(\underline{r}_{2j}) = h_{2j}(\underline{r}_{2i}) \tag{5.17}$$

where, $i,j = 1,2,3,\cdots,n$

5.2.3 Application to the System Analysis

Analysis of the system response is done by utilizing the derived four pole parameters. If the acoustic system

shown in Figure 5.1 is connected to an anechoically terminated pipe of cross sectional area S_{an}, the transfer functions are given as[1,47]

$$T_Q(\omega) = \frac{Q_2}{Q_1} = \frac{\dfrac{S_{an}}{\rho_o c_o}}{A\,\dfrac{S_{an}}{\rho_o C_o} + B} \tag{5.18}$$

$$T_p(\omega) = \frac{P_2}{Q_1} = \frac{1}{A\,\dfrac{S_{an}}{\rho_o C_o} + B} \tag{5.19}$$

where, $T_Q(\omega)$ is the volume flow transfer function , $T_p(\omega)$ is the pressure transfer function of the system, and A,B,C,D are four pole parameters of the overall system obtained by the procedure in the previous section. Also, the input point impedance of the system is given by

$$Z_o(\omega) = \frac{P_1}{Q_1} = \frac{C\,\dfrac{S_{an}}{\rho_o C_o} + D}{A\,\dfrac{S_{an}}{\rho_o C_o} + B} \tag{5.20}$$

Volume flows at the end of connecting pipes Q_{1i} and Q_{2i}, i= 1,2, $\cdots$, n, can be calculated from equations (5.9) and (5.10) by taking $Q_1 = Q_1$ and $Q_2 = T_Q(\omega)Q_1$. Therefore pressures at $\underline{r}_1$, $\underline{r}_2$,$\underline{r}_{1j}$, $\underline{r}_{2j}$, j = 1,2, $\cdots$, n, can be obtained from either equation (5.7) or (5.8). For example, the pressure at the output point is, from equation (5.8),

$$P_2 = P_2(\underline{r}_2)\big|_{Q_1=Q_1,\,Q_2=T_Q Q_1}$$

$$= \sum_{j=1}^{n} h_{2j}(\underline{r}_2)\, Q_{2j} - T_Q h_2(\underline{r}_2)\, Q_1 \qquad (5.21)$$

From equations (5.19) and (5.21), the following relation should be satisfied for a properly solved case,

$$\frac{Q_1}{A\frac{S_{an}}{\rho_o C_o} + B} = \sum_{j=1}^{n} h_{2j}(\underline{r}_2) Q_{2j} - T_Q\, h_2(\underline{r}_2) Q_1 \qquad (5.22)$$

Therefore, this relation can serve as a check of the numerical computations.

5.3 Example ; A Large Annular Cavity Connected to a Small Volume by Two Pipes

5.3.1 Pressure Responses of the System

As a special example of the previous general discussion, let us consider the system shown in Figure 5.2. The first volume is small enough to be approximated as a lumped parameter element in which excited pressure is assumed to be spatially constant. The second volume is a large annular cylindrical shape which is often seen in actual products such as a hermetic refrigeration compressors. The two volumes are connected to each other by two pipes which can be of different lengths and cross section.

Fundamental equations for this system can be reduced from developments of the previous section. Because the

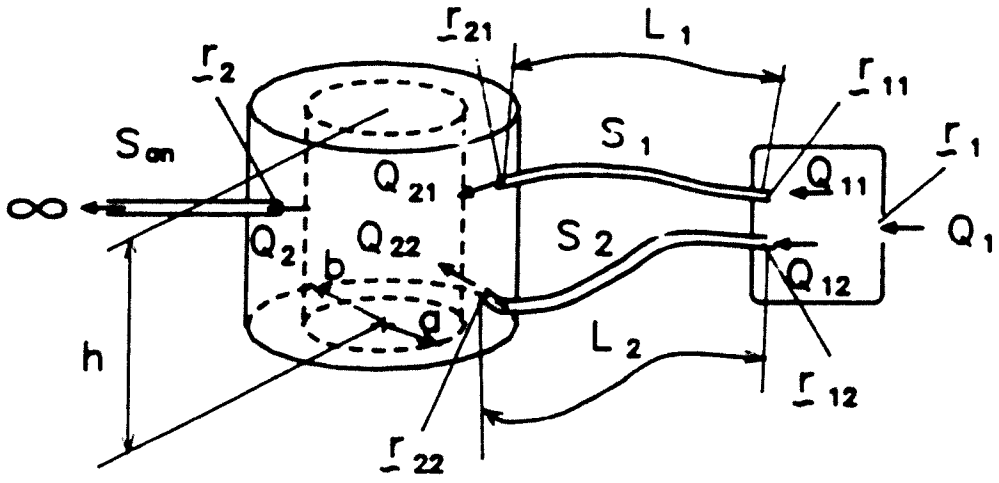

Figure 5.2 - An Annular Cavity Connected to a Small Lumped Parameter Cavity by Two Pipes

pressure is constant in the first cavity, let us define $g = g_i(\underset{\sim}{r}_j)$ where j,k=1,2,11,12.

Equations (5.9) and (5.10), used for the solution of the unknown volume flows, are modified as

$$Q_{11} - \left(B_1 h_{21}(\underset{\sim}{r}_{21}) + A_1\right)Q_{21} - B_1 h_{22}(\underset{\sim}{r}_{21})Q_{22} = -B_1 h_2(\underset{\sim}{r}_{21})Q_2 \tag{5.23}$$

$$Q_{12} - B_2 h_{21}(\underset{\sim}{r}_{22})Q_{21} - \left(B_2 h_{22}(\underset{\sim}{r}_{22}) + A_2\right)Q_{22} = -B_2 h_2(\underset{\sim}{r}_{22})Q_2 \tag{5.24}$$

$$g\,(\,Q_{11} + Q_{12}\,) + \left(D_1 h_{21}(\underset{\sim}{r}_{21}) + C_1\right)Q_{21} + D_1 h_{22}(\underset{\sim}{r}_{21}) = g\,Q_1 + D_1 h_2(\underset{\sim}{r}_{21})Q_2 \tag{5.25}$$

$$g\,(\,Q_{11} + Q_{12}\,) + D_2 h_{21}(\underset{\sim}{r}_{22})Q_{21} + \left(D_2 h_{22}(\underset{\sim}{r}_{22}) + C_2\right)Q_{22} = g\,Q_1 + D_2 h_2(\underset{\sim}{r}_{22})Q_2 \tag{5.26}$$

For the pressure response $f_1(\underset{\sim}{r})$, equations (5.11) and (5.12) are modified as

$$f_1(\underset{\sim}{r}_1,\omega) = g\,(\,1 - Q_{11} - Q_{12}\,) \tag{5.27}$$

$$f_1(\underset{\sim}{r}_2,\omega) = h_{21}(\underset{\sim}{r}_2)Q_{21} + h_{22}(\underset{\sim}{r}_2)Q_{22} \tag{5.28}$$

where, Q_{11}, Q_{12}, Q_{21}, and Q_{22} should be solved from

equations (5.23) to (5.26) with $Q_1 = 1$ and $Q_2 = 0$.

For the pressure response $f_2(\underline{r})$, equations (5.13) and (5.14) are modified as

$$f_2(\underline{r}_1,\omega) = - g\ (Q_{11} + Q_{12}) \tag{5.29}$$

$$f_2(\underline{r}_2,\omega) = h_{21}(\underline{r}_2)Q_{21} + h_{22}(\underline{r}_2)Q_{22} - h_2(\underline{r}_2) \tag{5.30}$$

Again, internal volume flows should also be obtained from equations (5.23) to (5.26) with $Q_1 = 0$ and $Q_2 = -1$.

5.3.2 Actual Calculation of Four Poles

For the actual calculation of four pole parameters of the system, it is necessary to know the pressure response solutions for the cavities, g and $h(\underline{r})$, and the four poles of the connecting pipes. Four poles of the finite length pipe can be derived from one dimensional wave propagation theory. Following reference[1], four pole parameters of the i^{th} pipe are given as

$$A_i = D_i = \cosh \gamma_i L_i \tag{5.31}$$

$$B_i = \frac{j\omega S_i}{\rho C_o^2 \gamma_i} \cdot \sinh \gamma_i L_i \tag{5.32}$$

$$C_i = \frac{\rho_o C_o^2 \gamma_i}{j\omega S_i} \cdot \sinh \gamma_i L_i \tag{5.33}$$

where, ρ_o is the average density of the gas of the system,

S_i, L_i are the cross sectional area and length of the i^{th} pipe, and C_o is the average speed of sound. γ_i is given as

$$\gamma_i = a_i + jk \tag{5.34}$$

where, k is the wave number defined as $\frac{\omega}{C_o}$, and a_i represent the damping effect of the i^{th} pipe which is defined as,

$$a_i = \frac{\zeta_i \sqrt{\nu\omega}}{2C_o d_i} \tag{5.35}$$

In equation (5.35), ζ_i is a correction coefficient that is adjusted for particular manifold geometries ,ν is the kinematic viscosity of the gas, and d_i is the diameter of the i^{th} pipe.

The pressure - input volume flow relationship of a small, lumped cavity is given as[1],

$$P = \frac{\rho_o C_o^2}{j\omega V_o} Q_o \tag{5.36}$$

Therefore, we obtain

$$g = P|_{Q_o=1} = \frac{\rho_o C_o^2}{j\omega V_{o1}} \tag{5.37}$$

where, V_{o1} is the volume of the first cavity.

The pressure response of the annular cavity was derived in chapter 4 using the eigen function expansion method. The general response is written as

$$h_{2j}(\underline{r}^*) = j\omega\rho_0 C_0^2 \sum_{l=1}^{2} \sum_{q=0}^{\infty} \sum_{n=0}^{\infty} \sum_{m=0}^{\infty}$$

$$\left[\frac{P_{(mnq)l}(\underline{r}^*)\, P_{(mnq)l}(\underline{r}_{2j})}{N_{mnq}\left[(\omega_{mnq}^2 - \omega^2) + 2j\,\omega\,\omega_{mnq}\,\xi_{mnq}\right]} \right] \qquad (5.38)$$

where $\underline{r}^*$ is (r^*, θ^*, z^*) because the cylindrical coordinate is being used, $P_{(mnq)l}$ is a natural mode of the annular cavity gas, ω_{mnq} is the corresponding natural frequency, and ξ_{mnq} is a modal damping coefficient. Reference [4] should be consulted for equations for $P_{(mnq)l}(\underline{r})$, N_{mnq}, and ω_{mnq}.

Equation (5.38) is a general form of the pressure response of the second cavity. For example, $h_{22}(\underline{r}_{21})$ can be obtained from equation (5.38) as follows.

$$h_{22}(\underline{r}_{21}) = h_{2j}(\underline{r}^*)\Big|_{j=2,\,\underline{r}^*=\underline{r}_{21}} = j\omega\rho_0 C_0^2 \sum_{l=1}^{2} \sum_{q=0}^{\infty} \sum_{n=0}^{\infty} \sum_{m=0}^{\infty}$$

$$\left[\frac{P_{(mnq)l}(\underline{r}_{21})\, P_{(mnq)l}(\underline{r}_{22})}{N_{mnq}\left[(\omega_{mnq}^2 - \omega^2) + 2j\,\omega\,\omega_{mnq}\,\xi_{mnq}\right]} \right] \qquad (5.39)$$

Now, the four pole parameters of the system shown in Figure 5.2 are ready to be calculated numerically using the procedures of the previous two sections.

5.3.3 Calculation of System Responses

Figure 5.3 shows the transfer functions $T_Q(\omega)$ which was calculated for the system shown in Figure 5.2 with dimensions a=0.06m, b=0.08m, h=0.185m, $V_{o1}=16 \times 10^{-6}\ m^3$,

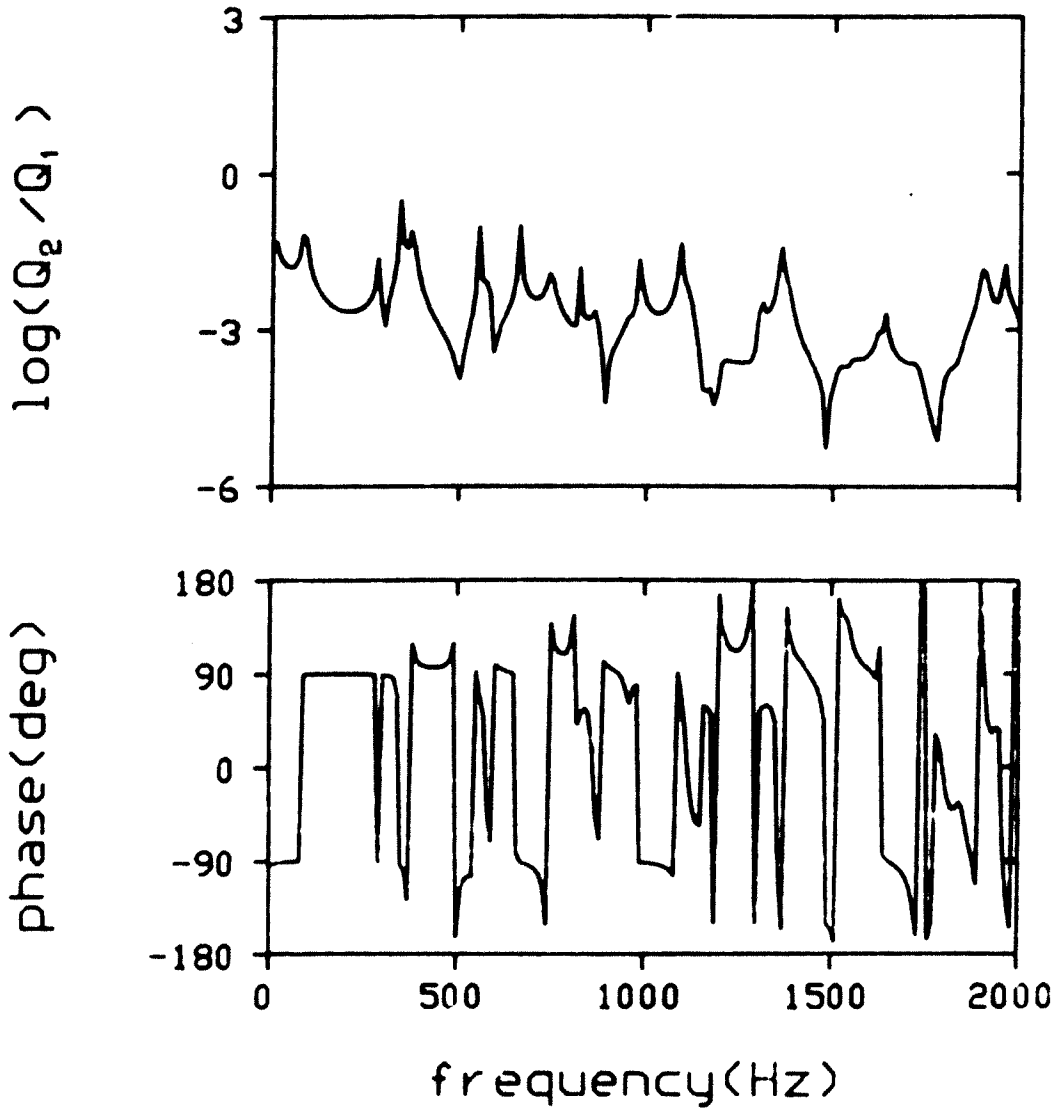

Figure 5.3 - Transfer Function of the Annular Cavity Doubly Connected to a Small Lumped Parameter Cavity

L_1=0.3m, L_2 =0.25m, r_{21}=(0.065m, 0^o, $\frac{3h}{4}$), r_{22} = (0.065m, 0^o, $\frac{3h}{4}$), and S_{an} = 0.3×10^{-4} m^2. Cross sectional areas of connecting pipes S_1 = S_2 = 0.32×10^{-3} m^2. Sound velocity and density were taken as C_o = 162.9 m, ρ_o = 6.04 kg/m^3, which is a typical suction line condition of the fractional horse power refrigeration compressor.

Figure 5.4 shows internal volume flows in the annular cavity Q_{21} and Q_{22} due to a unit volume flow input to the system, for the same case as Figure 5.3. Damping effects of the connecting pipes were not considered, but very low damping (1 % of the critical damping at each mode) was introduced in the annular cavity analysis.

The pressure in the first cavity can be obtained from the input point impedance Z_o in equation (5.20). General expressions for pressures at points inside of the annular cavity can be obtained from equation (5.38) with Q_1, Q_2 = $T_Q Q_1$ as follows.

$$P(\underline{r}) = j\omega\rho_o C_o^2 \sum_{l=1}^{2} \sum_{n=0}^{\infty} \sum_{m=0}^{\infty} \sum_{q=0}^{\infty} \frac{P_{mnq(l)}(r,\theta,z)}{N_{mnq}[(\omega_{mnq}^2-\omega^2) + 2j\omega\omega_{mnq}\xi_{mnq}}$$

$$\cdot \left[P_{mnq(1)}(r_{21},\theta_{21},z_{21})Q_{21} + P_{mnq(1)}(r_{22},\theta_{22},z_{22})Q_{22} - P_{mnq(1)}(r_2,\theta_2,z_2)Q_2 \right] \qquad (5.40)$$

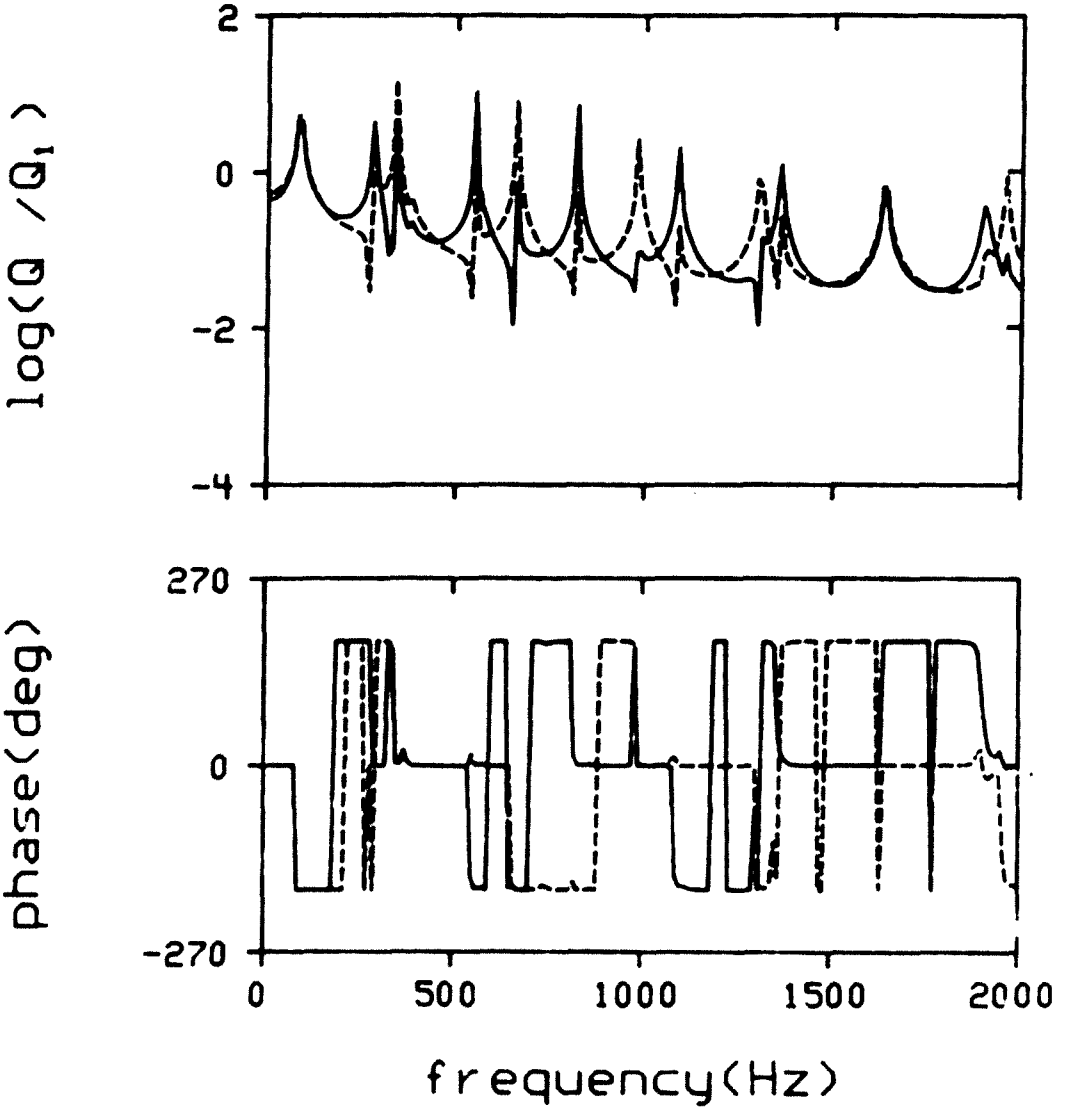

Figure 5.4 - Volume Flows in the Annular Cavity Doubly Connected to a Small Lumped Parameter Cavity. Q_{21}, ——— Q_{22} – – – –

5.4 Passive Control of the System Response

The response of the system in Figure 5.2 can be controlled by designing the connection pipes and locations appropriately.

The first method is based on the concept of mode elimination, which requires designing the two pipe connections to the annular cavity such as to take advantage of natural mode shapes. As it was shown in chapter 4 for most typical compressor shell configurations, the lowest natural frequencies belong to n = 1 or n = 2 modes (see Figure 5.5), where n specifies the natural mode number in the circumferential direction. As we can see in Figure 5.5, a pulsation dominated by the n = 1 mode can be eliminated by designing two ports located 180° apart. This design has little effect on the n=2 circumferential mode response.

Figure 5.6 shows the comparison of pulsations in the output line for the cases of $\theta=0^{\circ}$, which corresponds to a single connection design with a pipe of twice the area of an individual pipe, $\theta = 90^{\circ}$. L_1 and L_2 were taken as 0.25 m while other conditions are kept the same as for the case of Figure 5.4. It can be seen that the level of pulsations was reduced considerably by eliminating the excitation of the n=1 mode.

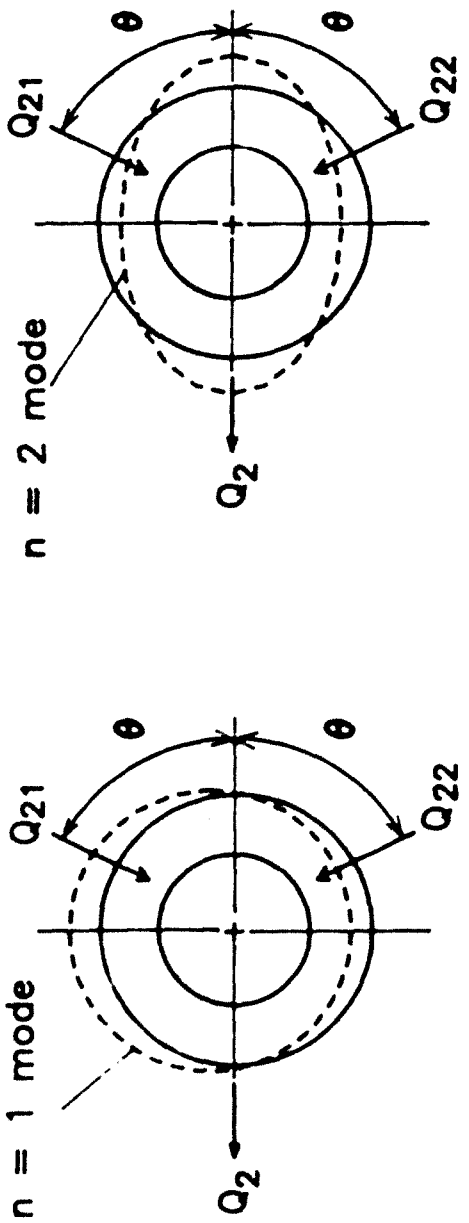

Figure 5.5 - Two Lowest Modes in Circumferential Direction and Design of Connection Ports

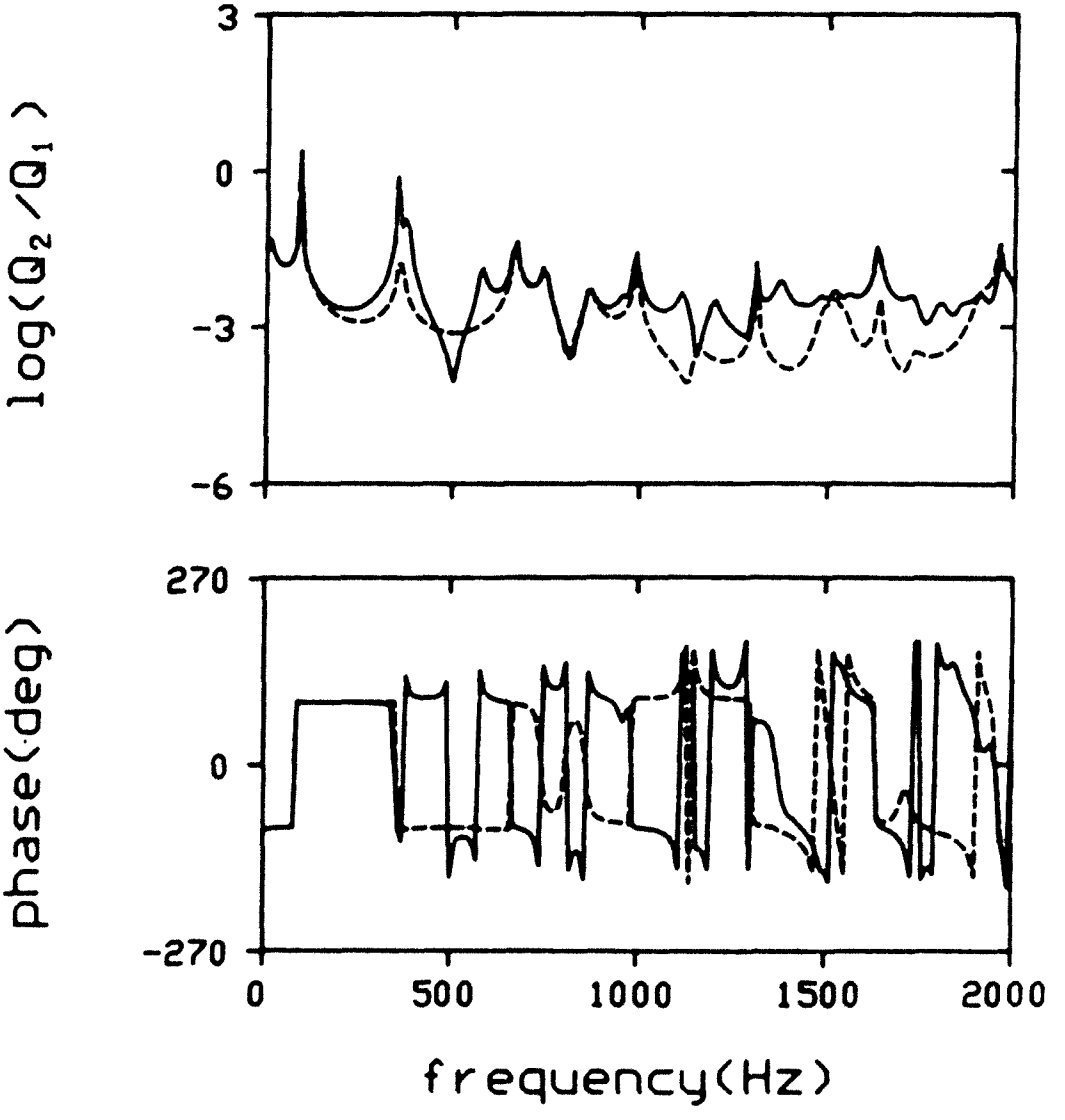

Figure 5.6 - Reduction of the Output Pulsation by Mode Eliminations, Original Design ——— , θ = 90° – – – –

The second method is based on the concept of wave cancellation, which utilizes the wave interference effect of input flows to the annular cavity from two connecting pipes. If connecting pipes of different lengths are located at the same point in the annular cavity, the output volume flow is expressed in terms of Q_{21} and Q_{22} as follows.

$$Q_2 = T_{Q1}\, Q_{21} + Q_{22}\, T_{Q2} =$$

$$T_{Q1}\,[Q_{21}\,(1 + e^{j(\phi_2-\phi_1)}) + (|Q_{22}|-|Q_{21}|)e^{j\phi_2}] \quad (5.41)$$

where, T_{Q1} is the transfer function between the connection point and the output point of the annular cavity, and ϕ_1 and ϕ_2 are phase angles of the flows Q_{21} and Q_{22}. Looking at equation (5.41), most of the pulsations can be eliminated if we can make $\phi_1 - \phi_2$ equal to 180° while keeping $|Q_{21}|$ and $|Q_{22}|$ close. This can be obtained by using two connecting pipes having half wave length differences in length.

The effect of wave cancellation is illustrated as function of the nondimensional difference of pipe lengths in Figure 5.7 for L_1 = 0.3 m, $Z_{21} = Z_{22}$ = (0.065m, 0°, $\frac{3h}{4}$). All the other dimensions are the same as in Figure 5.3. As it is expected, the pulsation flow possesses the minimum magnitude at $|L_2-L_1| = 0.5\lambda$. Figure 5.8 shows the effect of wave cancellations in terms of frequency when L_1

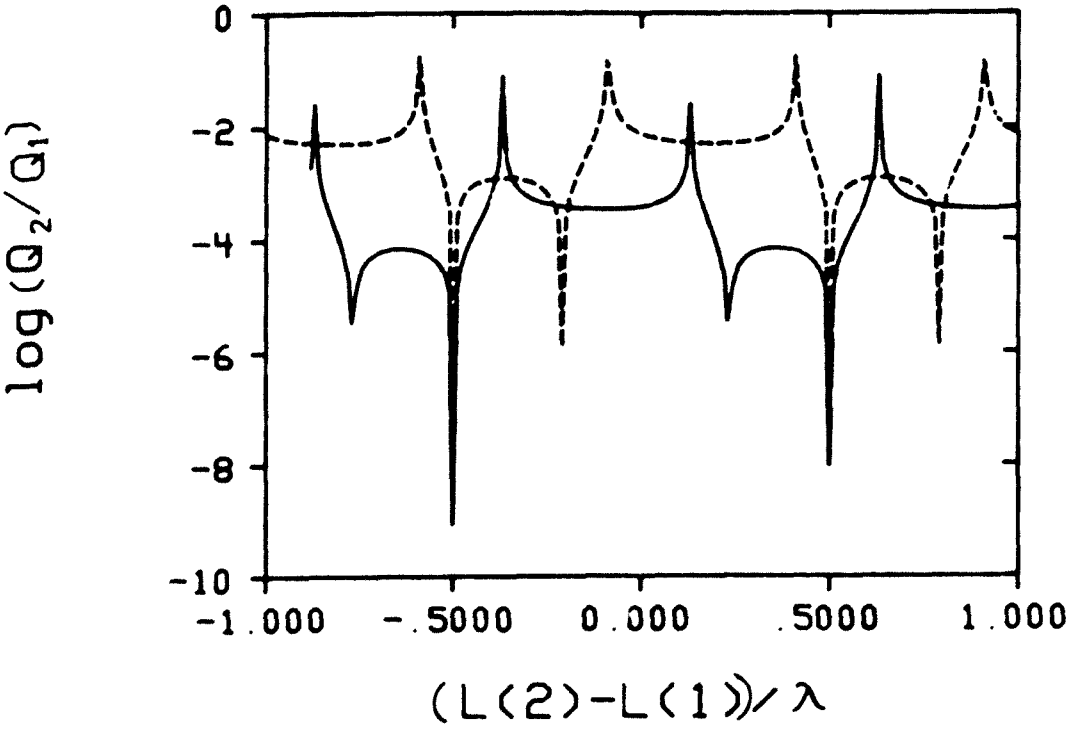

Figure 5.7 - Wave Cancellation Effect at Various Pipe Length Difference, 480 Hz ——— , 600Hz ----

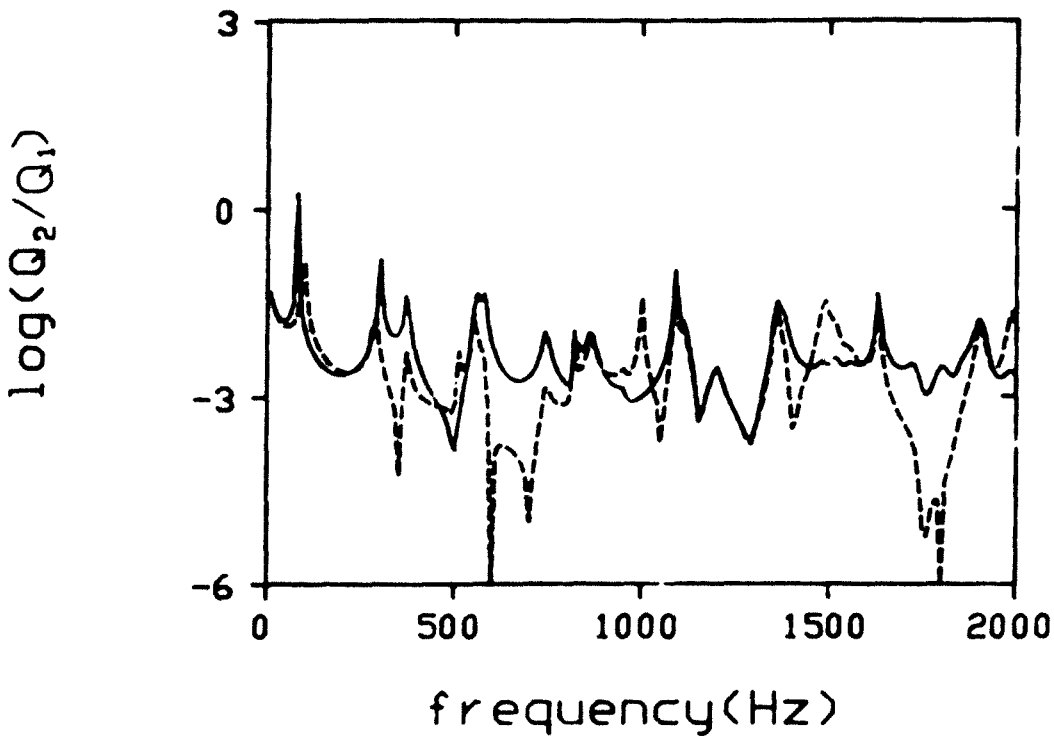

Figure 5.8 - Wave Cancellation Effect at 600 Hz, Original Design ——— , Wave Cancellation Design - - - - -

= 0.3m and L_2 is a half wave length shorter than L_1 at 600 Hz.

Comparing Figure 5.9 with Figure 5.6, one can find that the first method has a relatively broad band effect while the second method is more effective in reduction magnitude but over narrower frequency bands centered at the frequencies corresponding to $L_2-L_1 = \frac{\lambda}{2}, \frac{3\lambda}{2}, \cdots$.

Based on the above observations, one can devise a design to utilize the advantages of both methods by using four connection pipes as shown in Figure 5.9. This design can lower the frequency response of the system over a broad frequency range by eliminating excitations corresponding to the n=1 modes and can decrease the frequency response over certain narrow frequency bands which may be designed to coincide with the objectionable frequency of a spectrum. From a practical viewpoint, such a design may be difficult to apply to small machinery such as fractional horsepower hermetic compressors because of cost and space required. It will be more feasible for larger systems, for example for a pump driven nuclear reactor jacket filled with cooling water.

5.5 Concluding Remarks

The intent of this chapter is to study acoustic characteristics of multiply connected continuous acoustic elements. It is distinctive from previous investigations

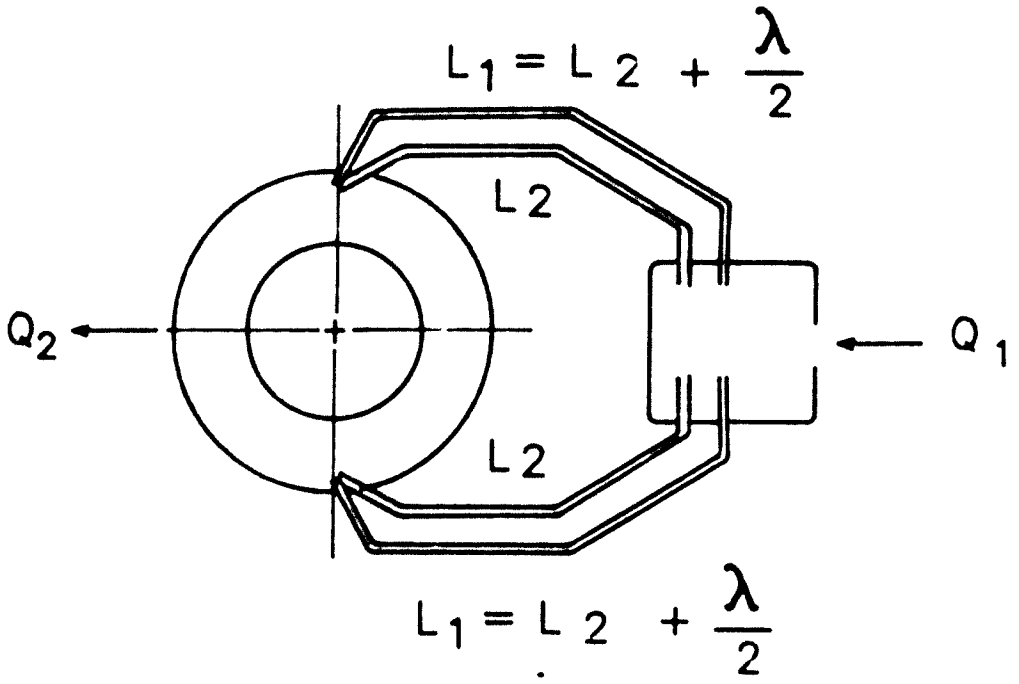

Figure 5.9 - Possible Design for the Lower System Pulsations

in which either lumped parameter models were used for complex manifolds[13,14,15] or continuous parameter models were used for relatively simple manifolds[32,46,47]. A general solution procedure was developed for two continuous cavities which are multiply connected by one dimensional continuous pipes. The fundamentals of the procedure can be applied to the analysis of even more general manifold system involving many cavities. The results have been used for a specific case of a continuous annular cavity connected to a small lumped parameter cavity by two continuous pipes. The system analysis was done utilizing four pole concepts to obtain acoustic responses in terms of pulsating pressure and volume flow. As an example of practical application, manifold connections were designed to passively control the system response by using natural mode elimination and phase cancellation concepts. Both methods are considered to be potentially very useful for the design of actual products. The analytical method developed in this work can be applied to other complex acoustic manifold, such as automotive mufflers or pulsing liquid systems.

CHAPTER 6 - EXPLORATION OF DIRECTIONS FOR DESIGN IMPROVEMENT

6.1 Design of the Suction Gas Manifold

6.1.1 General

The purpose of this section is not the development of a general theory of muffler design but the investigation of existing alternatives to pursuit designs and some new attempts of suction gas path design for the noise reduction of refrigeration compressors. General discussions of the identification and control of compressor noise sources can be found in references [4,7,8,48]. The approach of this section is based on the assumption that a general decrease of the noise level can be made if prominent peaks in the measured noise spectrum can be reduced. Roys[7] conducted sound power measurements on the same type of prototype compressor and reported dominant peaks in the 400 - 550 Hz frequency range(7^{th},8^{th},9^{th} peaks).

Figure 6.1 shows designs of suction gas manifold which are discussed in this section. Case A is the present design which has a standard expansion volume type suction muffler. A side branch resonator is attached to the suction head for case B. Designs shown in C and D are special arrangements of the suction gas return system to

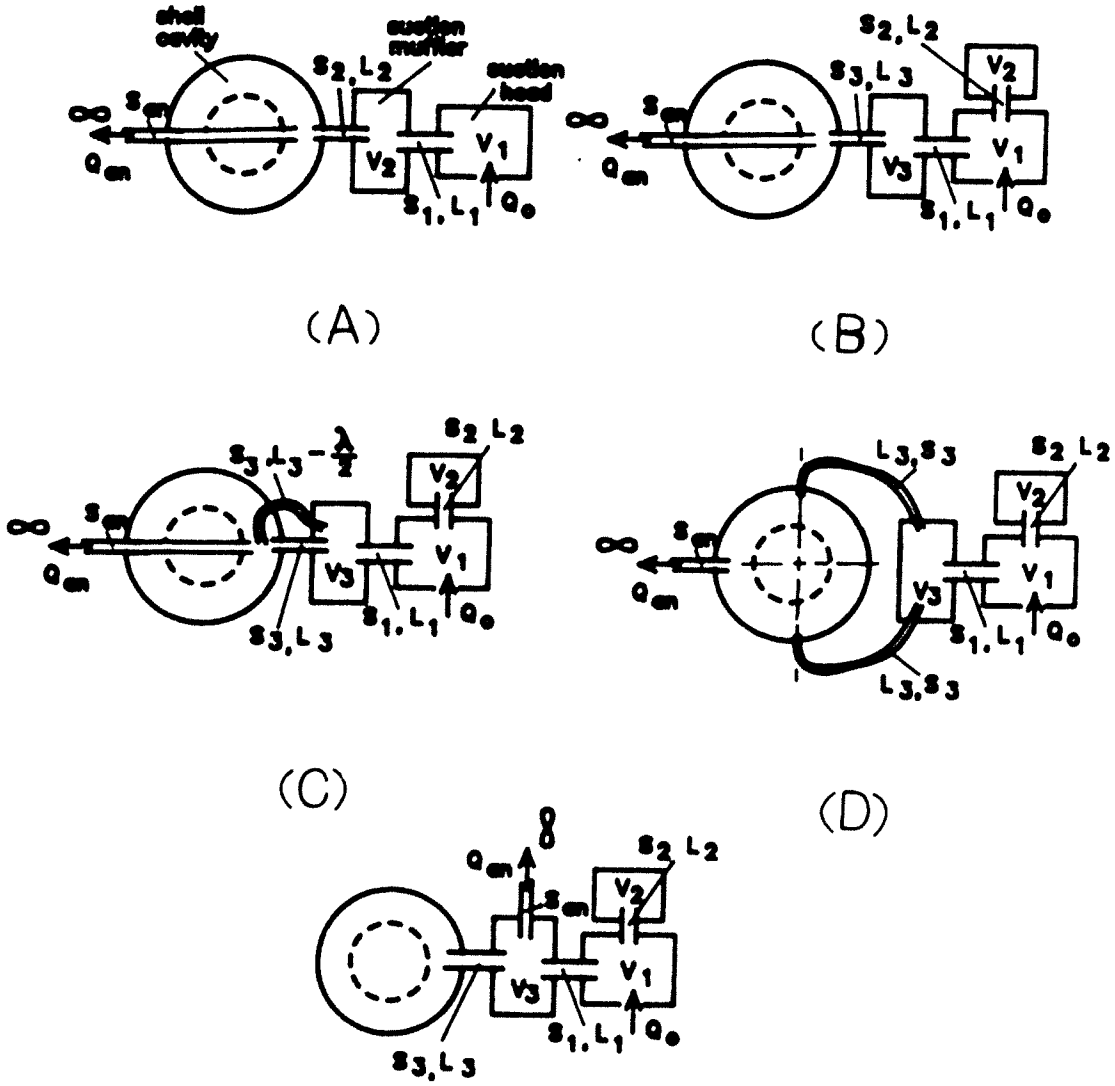

Figure 6.1 - Various Suction Manifold Designs

reduce pressure pulsations inside the hermetic shell cavity. Case E is the illustration of a special type of the suction system which was originally suggested by Roys[7]. It uses the compressor shell cavity itself as a side branch resonator.

6.1.2 Design of the Suction Muffler

Performances of the standard muffler(case A of Figure 6.1) and the muffler with a side branch resonator(case B of Figure 6.1) are compared in Figure 6.2 in terms of the volume flow transfer function. In order to provide a better insight, the transfer function of the suction system from which the standard muffler is removed is shown in curve C. The suction muffler acts as a low pass filter which reduces the transfer function in relatively high frequency range. The side branch resonator has a band filter effect as curve B shows. The center frequency of the filtering effect is the natural frequency of the resonator [49], which is

$$f^* = \frac{C_o}{2\pi}\sqrt{\frac{S_3}{L_3 V_3}} \qquad (6.1)$$

f^* should be designed to be close to the frequency of the noise peak which has to be eliminated. 440 Hz was used for this trial calculation. The two cases were the side branch resonator is located either off the first volume (suction head) or off the second cavity (suction muffler) are

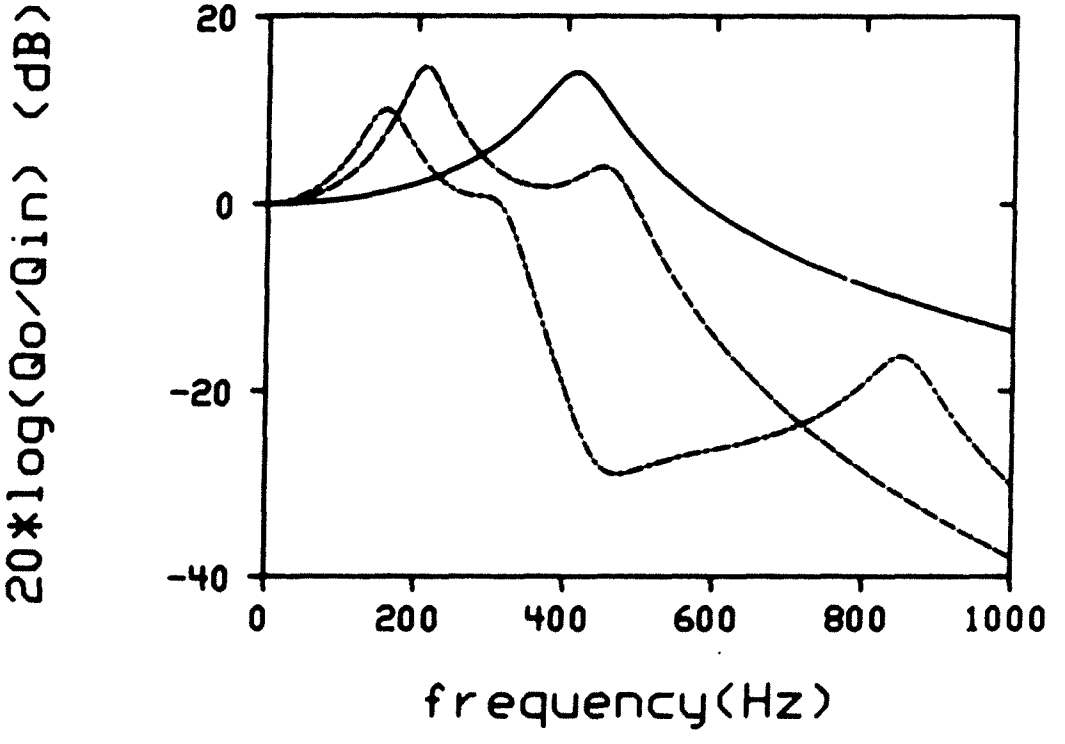

Figure 6.2 - Comparison of the Performances of Suction Mufflers, A : Standard Muffler ---- , B : Muffler with Side Branch —·—·— ,C : Suction Muffler Removed ——

compared in Figure 6.3. (It could also be located off a pipe.) Both design have the same filtering frequency f^*, however the attenuation effect is much stronger when the side branch is attached to the first cavity, which confirms common sense that tells one to locate a noise control device as near to the noise source as possible.

The comparison in Figure 6.2 can be misleading because the three curves do not represent completely equivalent conditions. For example, part of the attenuation effect of the muffler with the side branch resonator may have come from the increased overall volume of the system. Figure 6.4 is the illustration of the size effect of the first cavity under equivalent conditions. Curve A is the current prototype design which is shown in Figure 6.1-A, for which V_1 (suction head) is 0.1731 in^3 and V_2 (suction muffler) is 0.9764 in^3. Curve B and C are the volume flow transfer functions of the systems when V_1 is increased to 50 % and 70 % of the total volume which is kept as the same volume of 1.1495 in^3. The results show that the first cavity should be kept as large as possible even at the cost of the muffler volume.

Is this true for the side branch also? Figure 6.5 is the comparison of transfer functions of the standard muffler and the muffler with the side branch at the same total volume condition. It shows that the side branch has a beneficial effect for its designed band frequency even with

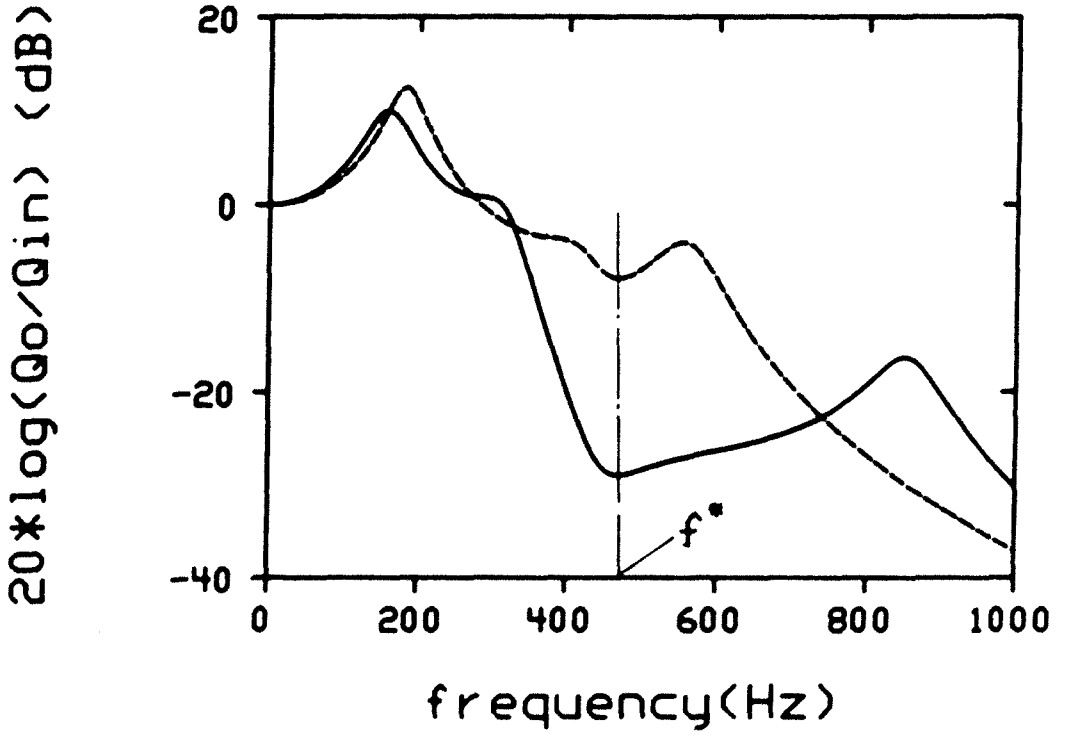

Figure 6.3 - The Effect of the Side Branch Location, at the Suction Head ——— ,at the Suction Muffler - - - -

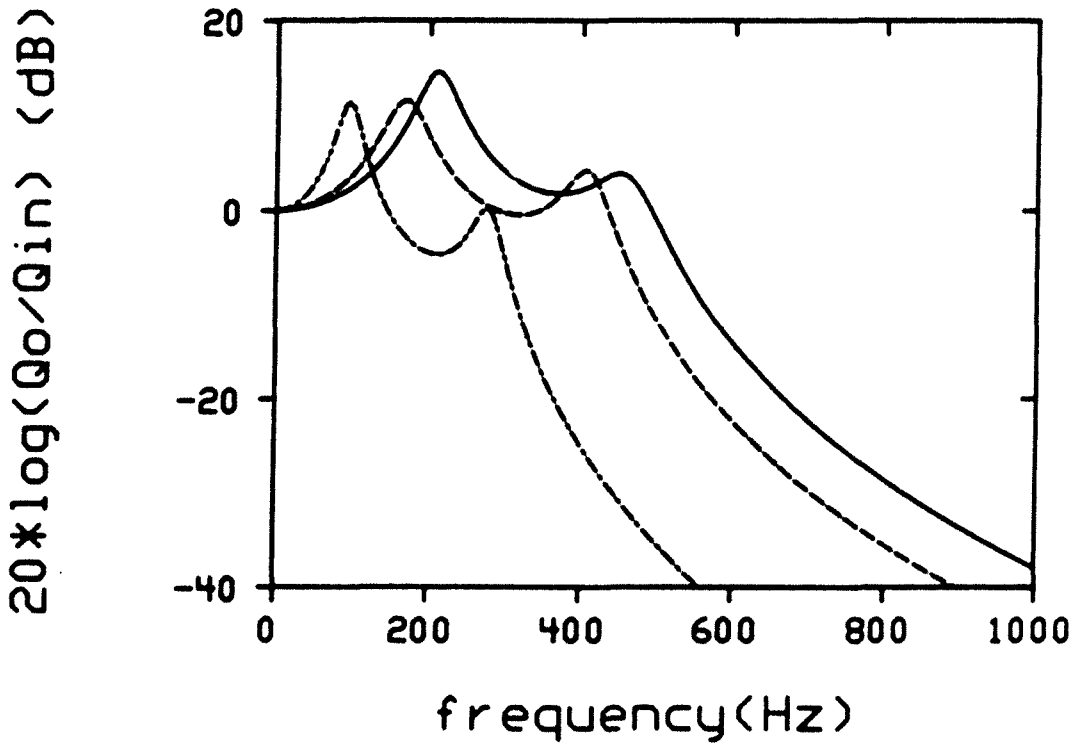

Figure 6.4 - Comparison of the First Cavity Size Effect under Equivalent Conditions, A : ——— , B : - - - , C: —·—·—

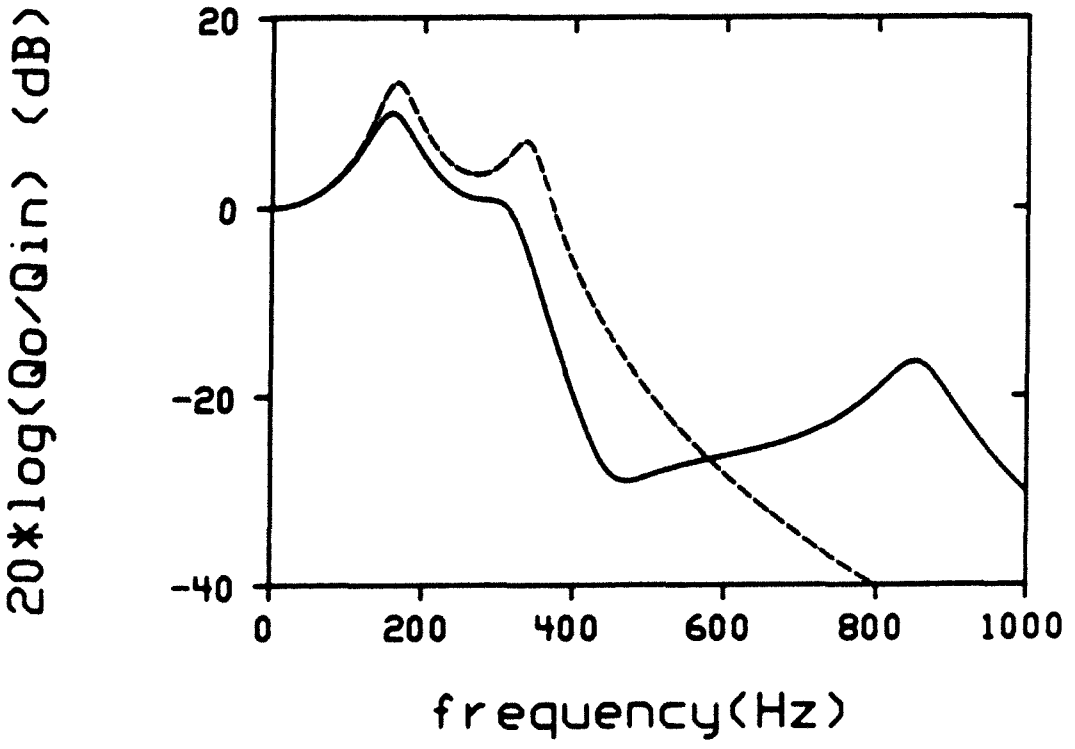

Figure 6.5 - Comparison of the Side Branch Resonator Effect at the Equivalent Condition, with Side Branch ——— , w/o Side Branch ----

the constant total volume constraint. Therefore, it can be concluded that the side branch is useful if most objectionable peaks in the measured noise spectrum are closely located within a relatively narrow frequency band. Figure 6.6 and Figure 6.7 show the simulated volume flows at the suction muffler exit and at the suction line outlet of the shell cavity, each of which induces the driving forces of pressure pulsations inside of the shell cavity and vibrations of the evaporator line of the refrigeration system. For these calculations, the computer simulation program which was developed in this research was used with the annular cylindrical acoustic cavity model which idealizes the shell cavity. The effect of the side branch is well observed around the center frequency of 440 Hz.

6.1.3 Design of the Suction Gas Return System

The suction gas pulsation inside of the shell cavity is one of the major noise sources of the hermetic compressors. Based on the studies in chapter 4 and chapter 5, two special designs of the suction gas return system were selected for the purpose of reduction of pressure pulsations in the shell cavity. They were named as the "wave cancellation design" (Figure 6.1-C) and the "mode elimination design"(Figure 6.1-D). Figure 6.1-E is also a special suction return design originally suggested by Roys[7], which uses the shell cavity as a side branch volume and lets the suction gas return directly to the

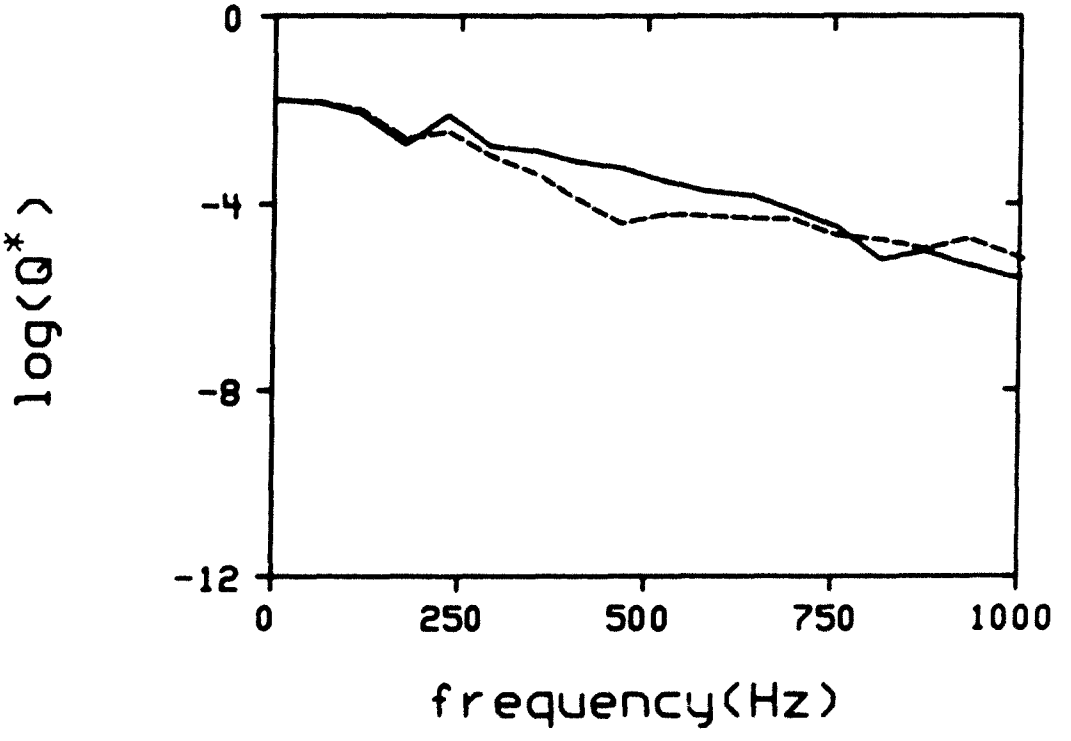

Figure 6.6 - Simulated Volume Flows at the Suction Muffler Exit ——— : Standard Muffler, - - - - : Muffler with Side Branch Resonator

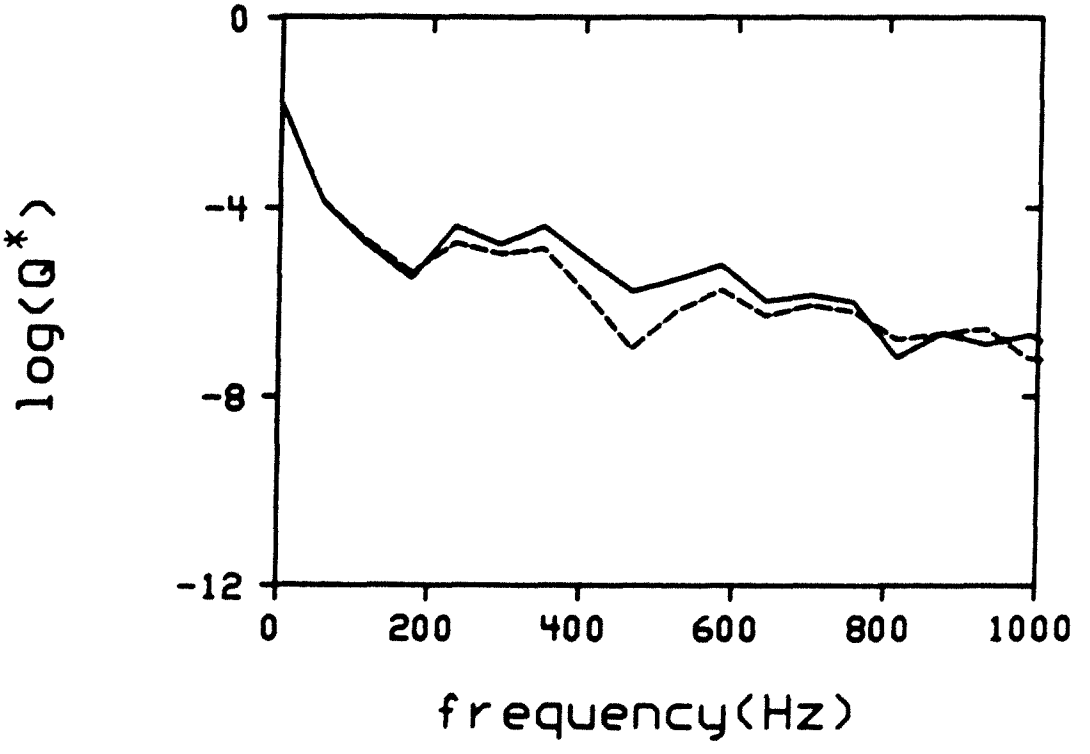

Figure 6.7 - Simulated Volume Flows at the Suction Line
——— : Standard Muffler, - - - - : Muffler with Side Branch

suction muffler from the suction line. This design was named "unconventional muffler".

Three designs are compared in terms of volume flows at the anechoic line in Figure 6.8. Because the unconventional muffler is designed for the suction port to connect directly to the anechoic line, it has the highest pulsation flow level which is even heigher than the standard case shown in Figure 6.7. Significant reductions in the volume flow level is observed in the frequency range up to 800 Hz for the wave cancellation design and the mode elimination design.

Figure 6.9 is the narrow band spectrum of the shell cavity pressure at a point $x^* = (0.07\ m, 0^o, \frac{3h}{4})$ for the compressors with the standard muffler and with the side branch muffler. Figure 6.10 is the one third octave band diagram of the Figure 6.9. The side branch effect is observed to reduce the pressure level in the 250 Hz and 800 Hz range visibly.

Narrow band diagrams of the shell cavity pressure at the same point as Figure 6.9 and Figure 6.10 are shown for the three special suction gas return systems in Figure 6.11. By comparing Figure 6.11 with Figure 6.9, it can be shown that the mode elimination design and the wave cancellation design have beneficial effects in the frequency range of 300 Hz to 700 Hz. The one third octave

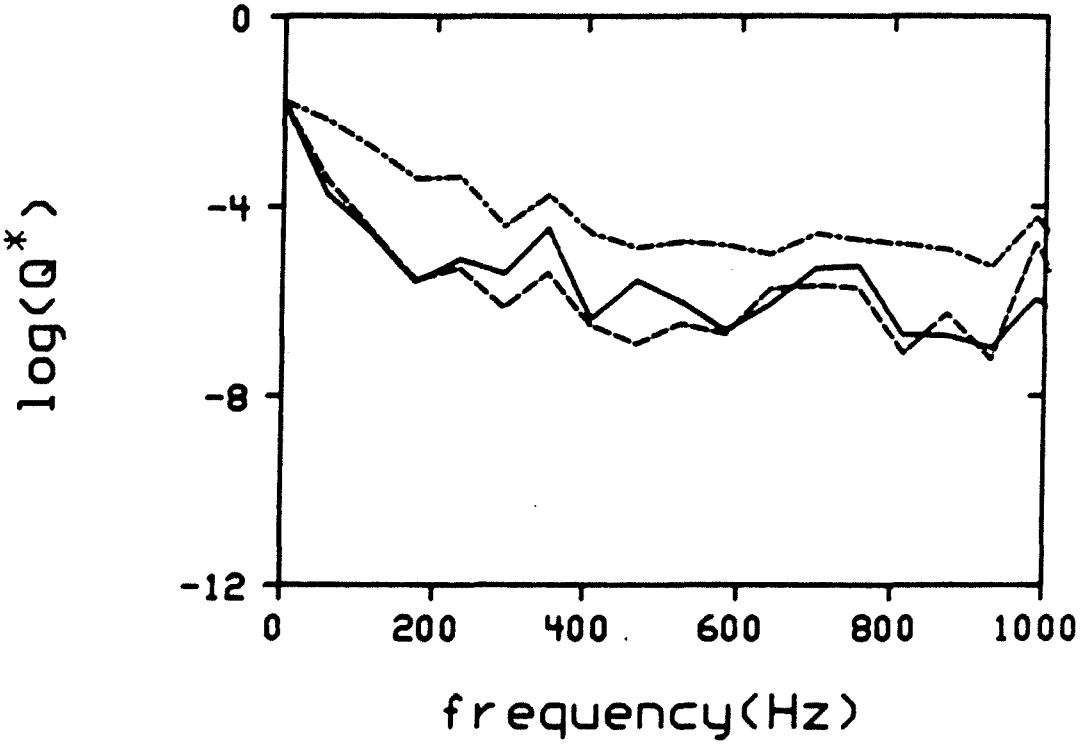

Figure 6.8 - Simulated Volume Flows at the Suction Anechoic Line ——— : Wave Cancellation Design — — — : Mode Elimination Design —·——·— : Unconventional Muffler

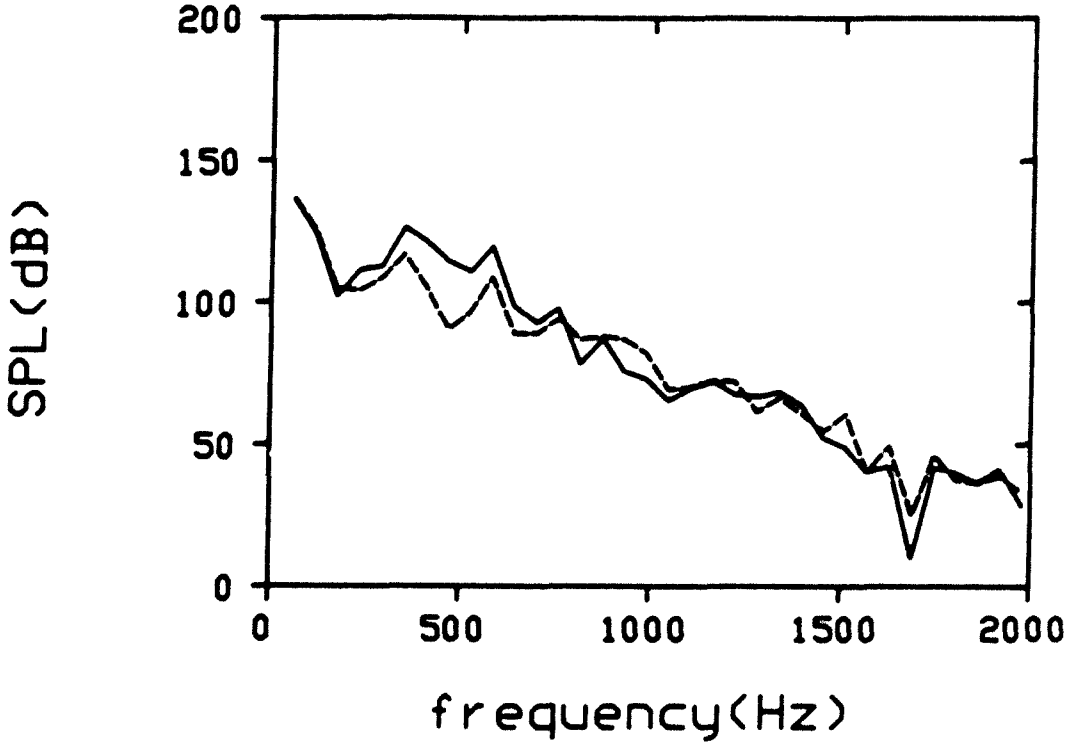

Figure 6.9 - Narrow Band Spectrum of the Shell Cavity Pressure ——— : System with Standard Muffler
---- : System with Side Branch Muffler

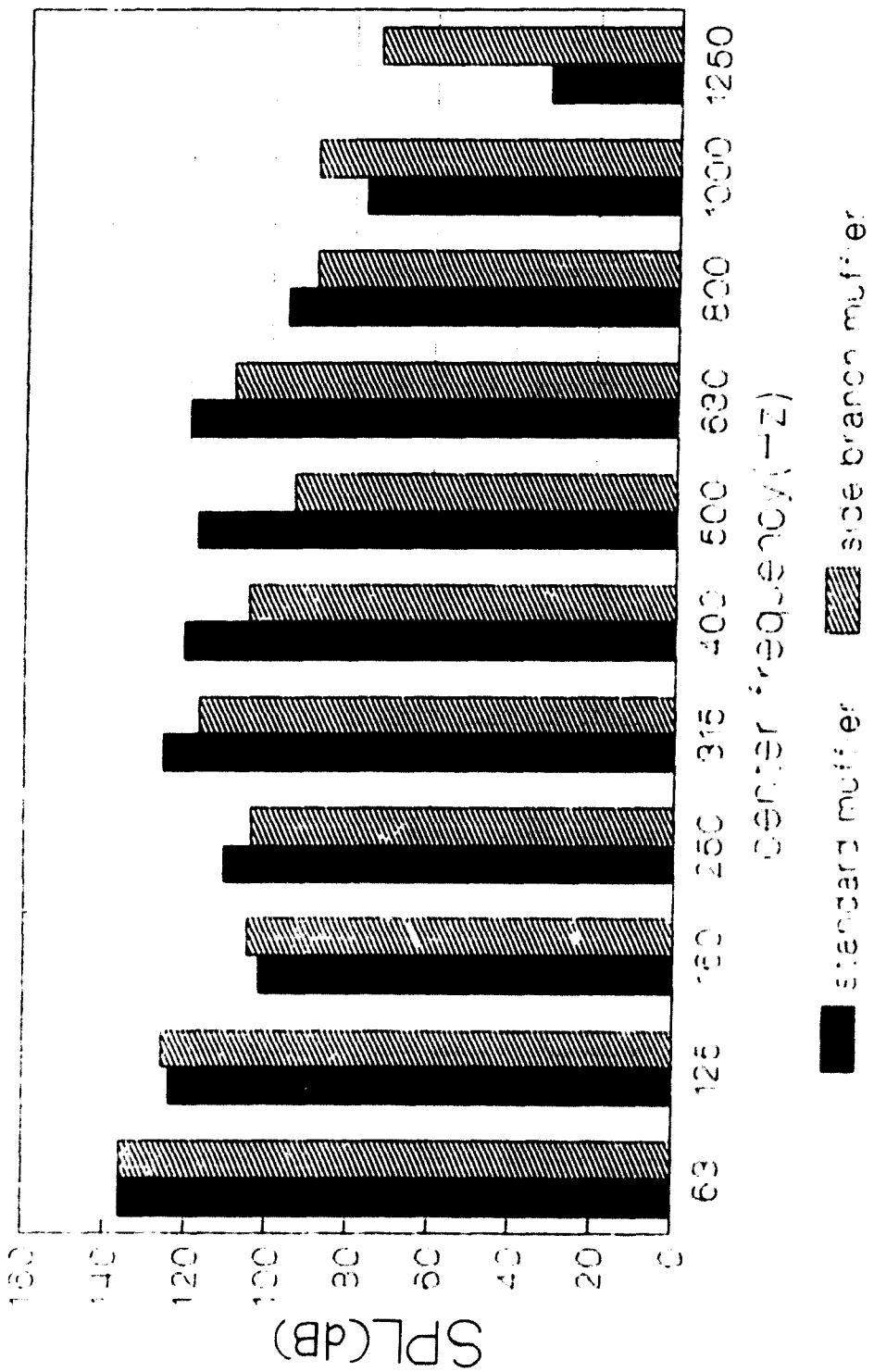

Figure 6.10 - One Third Octave Band Spectrum of the Shell Cavity Pressure

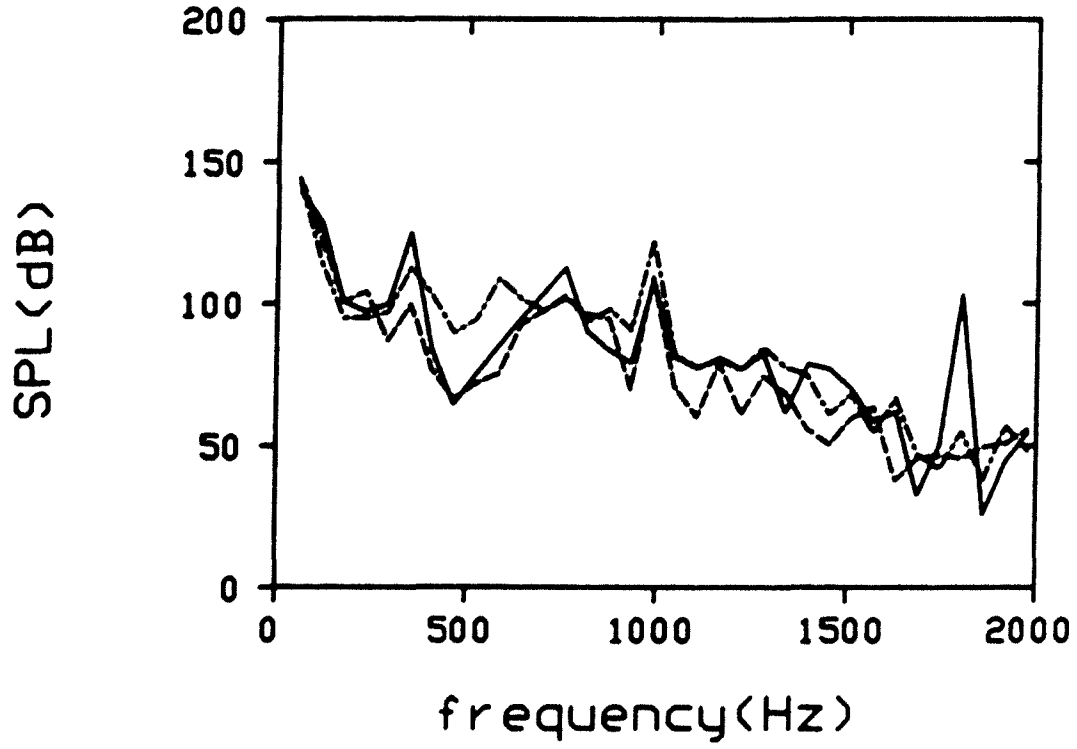

Figure 6.11 - Narrow Band Spectrum of the Shell Cavity Pressure ——— : System Wave Cancellation
- - - - : System with Mode Elimination
—·—: System with Unconventional Muffler

band diagrams of the Figure 6.11 are shown in Figure 6.12. The third octave band diagrams of the wave cancellation design and the mode cancellation design show lower pressure levels by 10 to 20 dB at 400 Hz and 500 Hz bands compared with the suction system with side branch muffler.

6.1.4 Summary and Recommendations

For the study in this section, effects of the designs on thermodynamic efficiencies were not considered. Because the acoustic impedance of the shell cavity is very small compared to the impedances of the suction head or suction muffler, no major efficiency change is expected by introducing an additional impedance of the special design. However, the rise of the suction gas temperature during the suction gas return process will affect the thermodynamic efficiency[50,51]. The mode elimination design would probably cause a temperature rise and therefore loss of efficiency, because it uses the suction inlet and outlet which are 90 degrees separated from each other. In this regard, the wave cancellation design appears to be a better solution. One potential problem of this method is that the performance will be relatively sensitive to the operating temperature change, because it is effective in relatively narrow bands as shown in Figure 5.8. The effective frequency band will be changing as the temperature change varies the speed of sound.

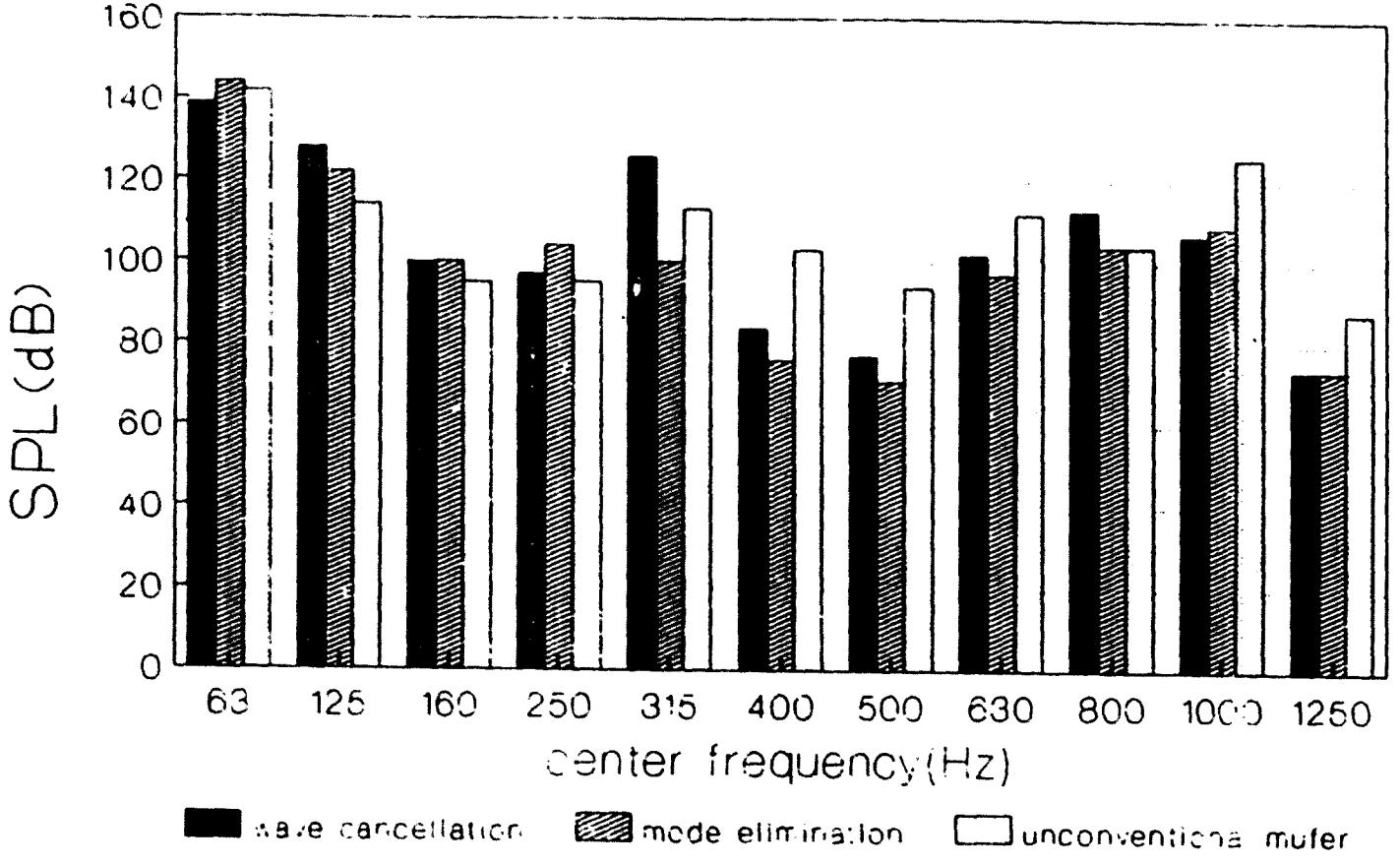

(with side branch muffler)

Figure 6.12 - One Third Octave Band Analysis of Special Suction Return Systems

The following practical recommendations can be made based on the results of this section.

1. The suction head volume should be designed as large as possible.

2. A side branch resonator can effectively eliminate some prominent noise peaks if it is designed properly.

3. To control the shell cavity pressure pulsations, the wave cancellation type design is considered to be the best method.

6.2 Design Parameter Study for Efficiency Improvement

To obtain some insight in the effect of major design changes on compressor performance, several variations of important design parameters were investigated. Selected design parameters were,

1. Stiffness of the suction and discharge valves

2. Size of the suction and discharge valve ports

3. Discharge valve stop height

4. Size of the suction and discharge cavities

5. Volume of the suction muffler

Explorations were made on the basis of single

parameter variation, which means only one parameter was changed from the original design. Large variations were taken intentionally to see corresponding effects more clearly. Table 6.1 is the summary of the parameter study. Figure 6.13 gives an overview for all the eleven cases that are presented. Figure 6.13-(A) shows the required work per unit circulation mass of refrigerant for each trial case. Thermodynamic efficiencies which are integrated from the P-V diagram cannot be directly compared with each other because mass flow per cycle is different for each case. Therefore, the curve in Figure 6.13-(A) shows the specific work of the system.

Figure 6.13-(B) shows the volumetric efficiencies for each test case. Based on Figure 6.13, the adjustment of valve port area is considered the most effective way to improve the thermodynamic efficiency ,although more comprehensive investigation will be necessary at the design change stage.

6.2.1 Variation of the Valve Stiffness

As it is expected, the valve stiffness change had effects both on the pressures and the valve motions. However, a significant decrease of the volumetric efficiencies with increase of stiffness was observed as shown in Figure 6.13.

TABLE 6.1 - Summary of the Parameter Study

Case	Description	Major Interests
1	Suction valve stiffness was doubled	Suction pressure, valve behavior
2	Discharge valve s .ffness was doubled	Discharge pressure
3	Discharge valve stiffness x 0.5	Discharge pressure
4	Suction port size x 2	Suction pressure, cylinder pressure
5	Suction port size x 0.8	Ditto
6	Discharge port size x 2	Discharge pressure peak cylinder pressure
7	Discharge valve stop height x 2	Discharge pressure, peak cylinder pressure discharge valve behavior
8	Discharge valve stop height x 0.5	Ditto
9	Suction cavity size x2	Suction pressure
10	Discharge cavity x 2	Discharge pressure, peak cylinder pressure
11	Suction muffler size x 1.5	Suction pressure volume flow

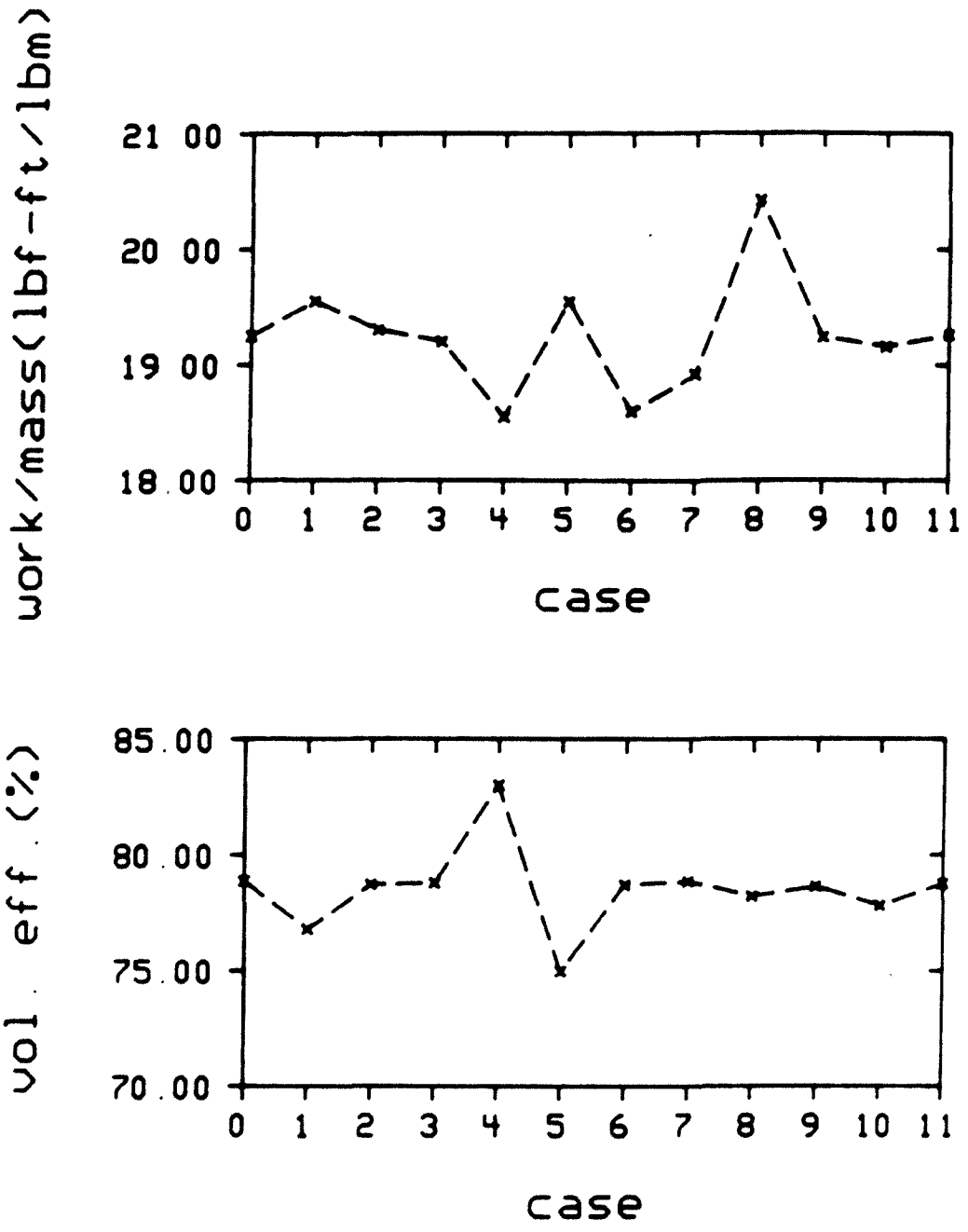

Figure 6.13 - Performance of the Prototype at Each Parameter Variations

Generally, it is known that the stiffer valve makes the valve close more quickly, which prevents undesirable back flows of the refrigerant gas. It is thought that the increased flow resistance negates this advantage in this case. It is interesting also that a suction valve stiffness change has a much stronger effect than a discharge valve stiffness change.

6.2.2 Variation of the Valve Port Size

This parameter had the strongest beneficial effect on the thermodynamic performance. Figure 6.14 and Figure 6.15 show effects of this parameter on the pressures. Figure 6.13 shows that increasing the valve port area improves the efficiency substantially.

However, it is reported in the literature that port area too large can create valve fluttering and noise problems[11]. Therefore, prior to the actual design change, effects on the volume flow spectrum and valve motions should be examined more closely.

6.2.3 Variation of Cavity Size

Calculations were made by changing suction and discharge cavity sizes to 200 % and 50% of the original size. There was no significant change in the cylinder pressure or efficiency as it was expected. Primarily, this variation caused an amplitude change of the pulsating

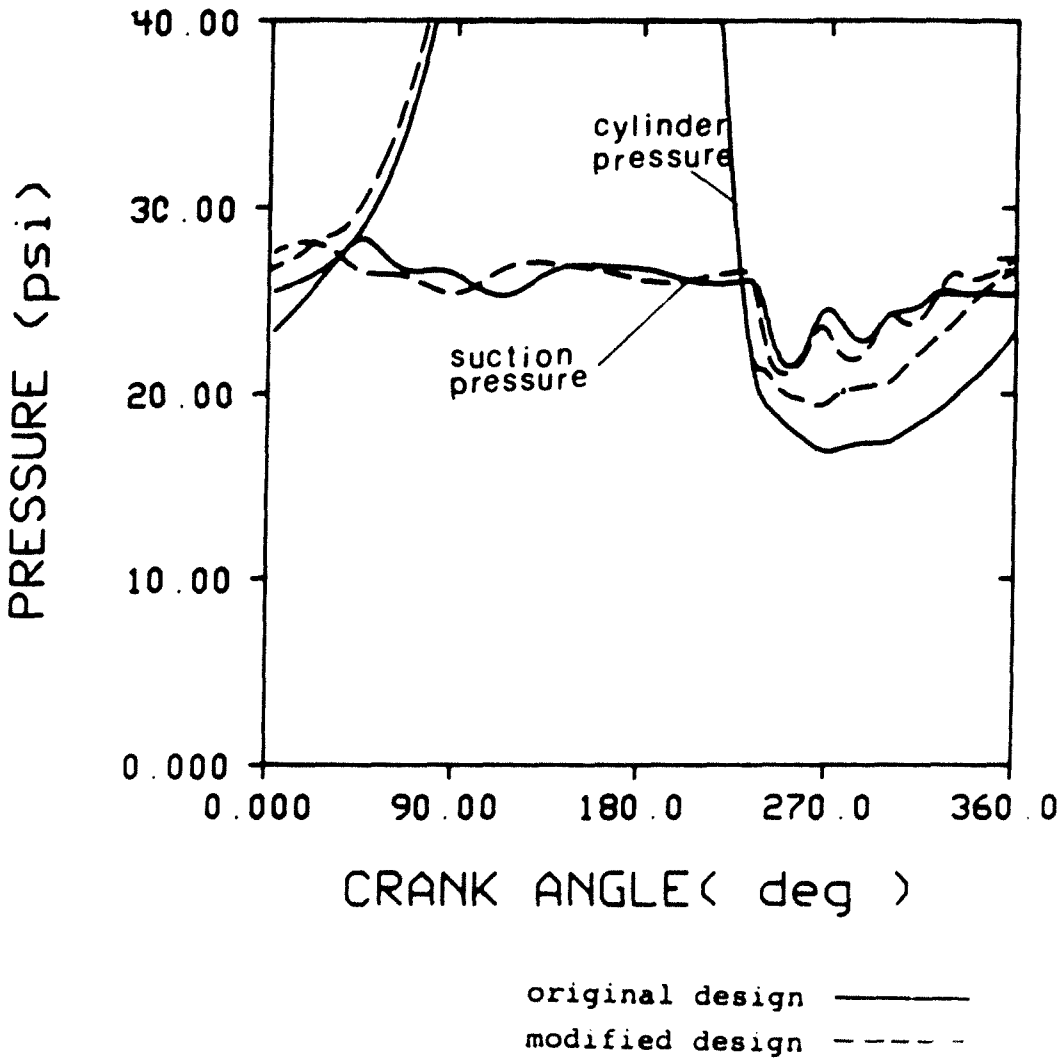

Figure 6.14 - Effect of Decreased Suction Port Area on the Suction and Cylinder Pressure

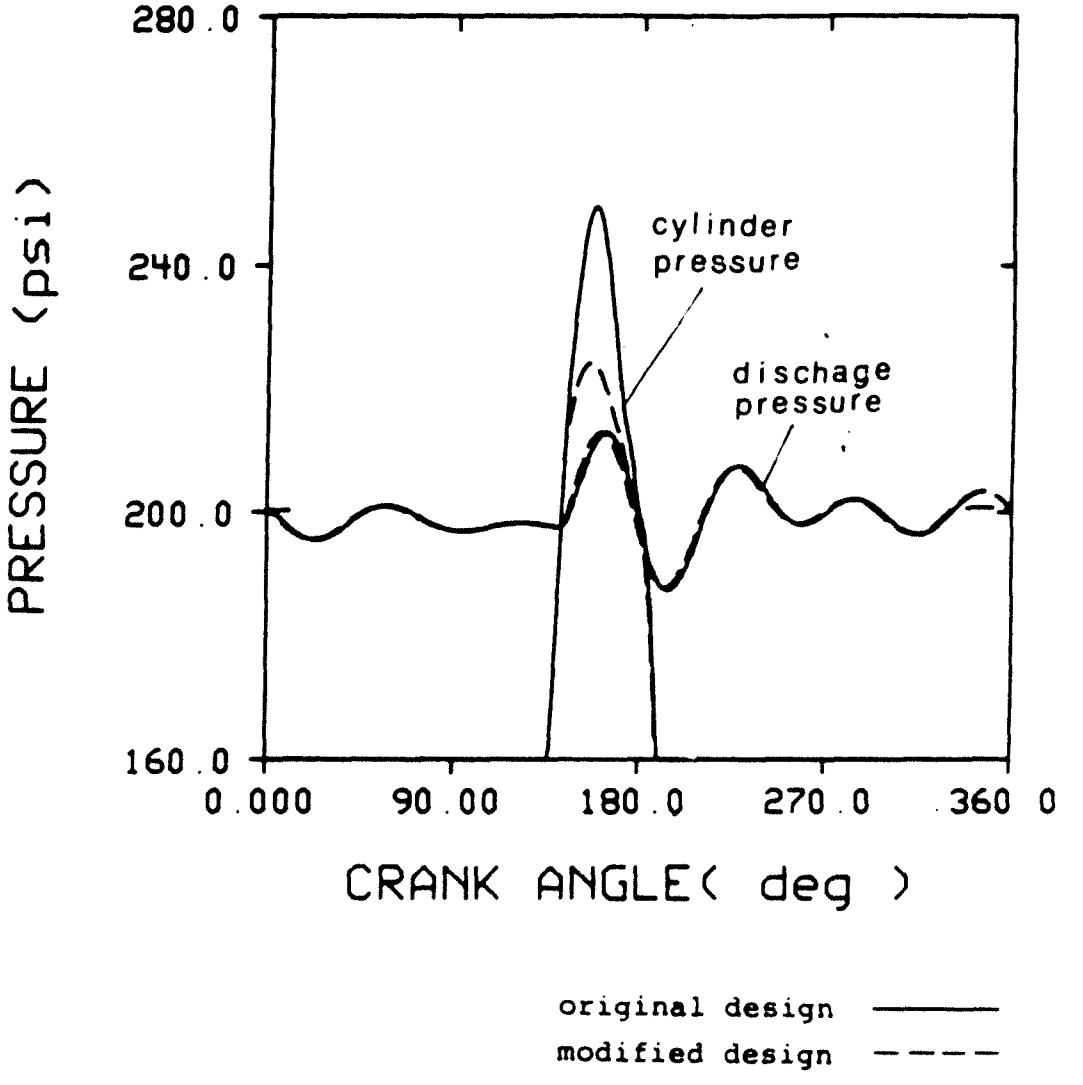

Figure 6.15 - Effect of Increased Discharge Port Area on the Discharge and Cylinder Pressure

pressures. Therefore, this effect is thought to be a potentially important factor only in noise reduction.

6.2.4 Effect of the Suction Muffler Volume

As it can be expected, the muffler volume had virtually no effect on the performance and the mass flow rates. The main effect was on the volume flow spectrum at the suction muffler exit, which is the main excitation of the shell cavity resonance. The flow spectra at muffler exit showed lower amplitude levels due to the increased volume of the suction muffler.

CHAPTER 7 - CONCLUSIONS

7.1 Summary

A computer simulation model of a hermetic, reciprocating compressor has been developed. The simulation program not only calculates basic compressor performances such as thermodynamic efficiencies, losses, and gas pulsations in suction and discharge gas paths but also the pressure pulsations in the compressor shell cavity. Special techniques were developed for the analysis of complex acoustic systems utilizing four pole concepts. Especially, the three dimensional annular shaped shell cavity was included in the acoustic model of the suction system for the first time in compressor research. For the stable convergence of the program, a modified integration scheme was introduced.

Fundamental measurements of the pressures, valve motions and temperatures were done to support the development of theoretical models. The main objective of the experimental work was to obtain necessary information for theoretical formulations. Pressure volume diagrams are the most important of all measurements from a practical viewpoint. The cylinder pressure and gas pulsation

pressures at the suction and discharge cavity were also measured. A new technique to construct the pressure volume diagram was suggested and possible errors of the procedure were estimated.

A general method to formulate four pole parameters of three dimensional acoustic cavities was established in chapter 4. Four pole parameters of an acoustic system were formulated from pressure response solutions of the system. An annular cylindrical compressor shell cavity was taken as an application example. The pressure response of the cavity was formulated using the eigenfunction expansion method. Acoustic characteristics of the annular cavity were studied in terms of the volume flow transfer function and excited pressures.

In chapter 5, the theory was further generalized for more complex acoustic systems which have multiply connected three dimensional continuous parameter cavities. The acoustic properties of the annular cylindrical cavity doubly connected to a small lumped parameter volume were investigated as an application example. The developed theory was applied to some novel designs of suction gas return systems.

In chapter 6, design improvements were explored. At first, various suction return systems and suction muffler designs were compared with each other. Especially the

application of the side branch resonator and special designs of suction return systems were investigated in depth. Also, important design parameters for the thermodynamic performances of the compressor were identified and their influence on the efficiency of the compressor was studied.

7.2 Achievements

Major contributions of this research to the state of art are believed to be the following :

1. Development of new modeling techniques for the compressor simulation, especially the extension of acoustic modeling capability to the three dimensional cavity and the modified iteration scheme for better convergence of the integration ;

2. Development of a new experimental technique for the construction of P-V diagrams and quantitative estimation of possible experimental errors involved in the process ;

3. Generalization of the advanced gas pulsation analysis techniques, especially the development of a new technique to formulate four pole parameters for general three dimensional cavities ;

4. Development of a general analysis method of an acoustic system composed of multiply connected

continuous parameter elements ;

5. Study of gas pulsations and their passive control in the shell cavity of a hermetic compressor.

7.2.1 Further Research Potential

The following are some areas which can be or need to be extended beyond the present study.

1. The shell cavity model that was used as an application example needs to be refined. A more realistic shell cavity model which deviates from the annular cylindrical geometry needs to be developed.

2. The structural interactions needs to be studied. Simulation of the shell vibrations due to pressure pulsation excitation is needed to provide better understanding of shell vibration behaviors. A sound radiation model is also feasible.

3. The optimal design theory can be applied to gas path design.

4. The computer simulation model needs to be further refined. There could be many possible directions. One of them is to combine the mathematical model based on the thermodynamics first law with the polytropic process based model to utilize the advantages of both methods.

LIST OF REFERENCES

LIST OF REFERENCES

[1] W. Soedel, "Gas Pulsations in Compressor and Engine Manifolds," Short Course Text Book of Purdue Compressor Technology Conference, Ray W. Herrick Lab., Purdue University, 1978.

[2] W. Soedel, "Design and Mechanics of Compressor Valves," Short Course Text Book of Purdue Compressor Technology Conference, Ray W. Herrick Lab., Purdue University, 1984.

[3] J. Brablik, "Gas Pulsations as Factor Affecting Operation of Automatic Valves in Reciprocating Compressors," Proc. of Purdue Compressor Technology Conference, pp 188-195, July 1972

[4] C. Johnson, "Fractional Horse Power, Rotary Vane Refrigerating Compressor Sound Source Investigation," Ph.D Thesis, Ray W. Herrick Lab., School of Mechanical Engineering, Purdue University, August 1969

[5] C. Johnson, J. F. Hamilton, "Noise Study of Fractional Horse Power, Rotary Vane, Refrigerent Compressor," Proc. of Purdue Compressor Technology Conference, pp 83-89, July 1972

[6] M. Noguchi, K. Sano, S. Takeshita, "Cavity Resonance and Noise Reduction in a Rotary Compressor," IEEE Trans. on Industry Applications, Vol IA-19, No. 6, pp 1118-1123, Nov/Dec 1983

[7] B. Roys and W. Soedel, "On the Acoustics of Shell Enclosed Compressors with Special Attention to Gas Pulsations on the Suction Side," Herrick Lab Report HL86-16P.

[8] R. Singh and W. Soedel, "A Review of Compressor Lines Pulsation Analysis and Muffler Design Research," Part I, II, Proc. of Purdue Compressor Technology Conference, pp 101-123, July 1974.

[9] M.D. Wambsganss, "Mathematical Modeling and Design Evaluation of High-Speed Reciprocating Compressors," Ph.D Thesis, Ray W. Herrick Lab., School of Mechanical Engineering, Purdue University, June 1966.

[10] J.P. Elson and W. Soedel, "Simulation of the Interaction of Compressor Valves with Acoustic Back Pressures in Long Discharge Lines," Journal of Sound and Vibration, Vol. 34(2), pp 211-220, 1974.

[11] R. Singh, "Modeling of Multicylinder Compressor Discharge System," Ph.D Thesis, Ray W. Herrick Lab., School of Mechanical Engineering, Purdue University, December 1975

[12] J.F.T. MacLahren and A.B. Tramscheck, "A Model of a Single Stage Reciprocating Gas Compressor Accounting for Flow Pulsations," Proc. of Purdue Compressor Technology Conference, pp 144-150, July 1974.

[13] W. Soedel, E. Padilla-Navas, B. D. Kotalik, "On Helmholtz resonator Effects in the Discharge System of a Two Cylinder Compressor", Journal of Sound and Vibration, Vol 30(3), pp263-277, 1973

[14] B.R.C. Mutyala, W. Soedel, "A Mathematical Model of Helmholtz Resonator Type Gas Oscillation Discharges of Two-Stroke Cycle Engines," Journal of Sound and Vibration, Vol. 44(4), pp479-491, 1976

[15] R.Singh and W. Soedel, "Interpretation of Gas Oscillations in Multicylinder Fluid Machinery Manifolds by Using Lumped Parameter Descriptions," Journal of Sound and Vibrations, Vol. 63(1), pp 125-143, 1979

[16] R. Singh and W. Soedel, "Assessment of Fluid-Induced Damping in Refrigeration Machinery Manifold," Journal of Sound and Vibrations, Vol. 57(3), pp 449-452, 1978.

[17] J.F. Hamilton, "Extensions of Mathematical Modeling of Positive Displacement Type Compressors," Short Course Text Book of Purdue Compressor Technology Conference, Ray W. Herrick Lab., Purdue University, 1974.

[18] W. Soedel, "Introduction to Computer Simulations of Positive Displacement Type Compressors," Short Course Text Book of Purdue Compressor Technology Conference, Ray W. Herrick Lab., Purdue university, 1972.

[19] W. Soedel and S. Wolverton, "Anatomy of a Compressor Simulation Programs," Ray W. Herrick Lab., Purdue University, 1974

[20] M. Dhar, and W. Soedel, "Compressor Simulation Program with Gas Pulsations," Ray W. Herrick Lab.,Purdue University, 1978

[21] D. Miller, B. Hatten, "Muffler Analysis by Digital Computer," ASHRAE Trans., Vol. 66, pp 202-216, 1960

[22] T. Abe, T. Fujikawa, S. Ito, "A Calculating Method of Pulsation in a Piping System," JSME Bulletin Vol. 13(59), pp 678-687, 1970.

[23] C. H. Kung, R. Singh, "Experimental Modal Analysis Technique for Three-Dimensional Acoustic Cavities," Journal of Acoustic Soc. of Am., Vol. 77 (2), pp 731-738, Feb. 1985

[24] W. Soedel, "On the Simulation of Anechoic Pipes in Helmholtz Resonator Models of Compressor Discharge Systems," Proc. of Purdue Compressor Technology Conference, pp136-139, 1974.

[25] J.F.T. MacLahren, A.B. Tramschek, "Prediction of Valve Behavior with Pulsating Flow in Reciprocating Compressors," Proc. of Purdue Compressor Technology Conference, pp203-211, 1972.

[26] D. Schwerzler, "Mathematical Modeling of Multiple Cylinder Refrigeration Compressor," Ph.D Thesis, Ray W. Herrick Lab., School of Mechanical Engineering, Purdue University, May 1971.

[27] T. J. Trella, "Computer Simulation of the Vibratory and Acoustic Behavior of a Reciprocating Compressor Discharge Valve," Ph.D Thesis, Ray W. Herrick Lab., School of Mechanical Engineering, Purdue University, Jan 1972.

[28] W. Thornton, "Noise Identification and Reduction for a Rotary Vane Compressor," Ph. D. Thesis, Ray W. Herrick labs., School of Mechanical Engineering, Purdue University, Dec. 1972.

[29] T. Matsuzaka, T. Hayashi, H. Shinto, "Analysis of Cavity Resonance in Fractional Horse Power Hermetic Reciprocating Compressor with Elliptic Shell," Proc. of Purdue compressor technology Conference, pp 338-344, 1980

[30] C. H. Kung, Singh, R., "Finite Element Modeling of Annular-Like Acoustic Cavities," Trans. of ASME, J. of Vibration,Acoustics, Stress, and Reliability in Design. 1984

[31] M. K. Au-Yang, "Free Vibration of Fluid-coupled Coaxial Cylindrical Shells of Different Lengths," Journal of Applied Mechanics, ASME , Sept. 1976, pp480-484

[32] M. K. Au-Yang, "Pump-Induced Acoustic Pressure Distribution in an Annular Cavity Bounded by Rigid Walls," Journal of Sound and Vibration, Vol. 62(4), pp 577-591, 1979.

[33] D.C. Gazig, "Three-Dimensional Investigation of the Propagation of Waves in Hollow Circular Cylinders," Journal of Acoustic society of America. Vol. 31, pp568-577.

[34] A.J. Pretlov,"A Simple approach to coupled Panel-Cavity Vibrations," Journal of Sound and Vibrations, Vol. 11(2), pp207-215, 1970.

[35] A.J. Pretlov,"Forced Vibration of a Rectangular Panel Backed by a Closed Rectangular Cavity," Journal of Sound and Vibrations, Vol. 3(3), pp252-261, 1966

[36] Proximity Probe User's manual, TW8019410. Bently-Nevada Co.

[37] J. Kim and W. Soedel, "Experimental Indicator Diagrams, Valve Motions and Gas Pulsations, with Interpretations from the Viewpoint of Thermodynamic Efficiency," Herrick Lab. Report HL86-14P

[38] M. Murata, M. Fujitani, "Improvement of P-V Diagram Measurement", Proc. of Purdue Compressor Technology Conference, pp 460 - 467, Aug. 1984.

[39] R.E. Sonntag and G.T.V. Wylen, "Introduction to Thermodynamics," John Wiley and Sons, New York, 1973

[40] J.C. Snowdon, "Mechanical Four Pole Parameters and Their Applications," Journal of Sound and Vibrations, Vol. 15(3), pp307-323, 1970.

[41] M.L. Munjal, A.V. Sreenath, and M.V. Narasimhan, "Velocity Ratio in the Analysis of Linear Dynamical Systems," Journal of Sound and Vibrations , Vol.26(2), pp 173-191, 1973

[42] W. Soedel, "Development of Method for the Analytical and Experimental Investigation of Large Axisymmetrical Deflection of Shallow Thin Shells of Revolution," Ph.D. Thesis, Ray W. Herrick lab., School of Mechanical Engineering, Purdue Universitv, June 1976.

[43] V. Chlumski, "Reciprocating and Rotary Compressors", E&FN, London, 1965.

[44] P.E. Doak, "Analysis of Internally Generated Sound in Continuous Materials," Journal of Sound and Vibrations, Vol. 2, pp 53-73, 1965

[45] W. Soedel, "Vibration of Shells and Plates", Marcel Dekker, New York, 1982.

[46] L.E. Penzes, "Theory of Pump-Induced Pulsating Coolant Pressure in Pressurized Water Jacket," Nuclear Engineering and Design, Vol. 27, pp 176-188, 1974

[47] J. Kim and W. Soesel, "Analytic Four Pole Parameters for Gas Filled Cylindrical Annular Cavity," Proc. of 20th Midwestern Mechanics Conference, pp 813-818, Aug. 1987.

[48] S. Price, "Identification of High Frequency Noise Path and Noise Source Mechanisms in Reciprocating Hermetic Compressors", M.S.M.E Thesis, Ray W. Herrick Lab., School of Mechanical Engineering, Purdue University, Aug. 1985

[49] L. Kinsler, A. Frey, A. Coppens, J. Sanders, "Fundamentals of Acoustics," John Wiley and Sons, NewYork, 1982

[50] W.A. Myer, "An Investigation into Heat Transfer Processes in a Small Hermetic Referigeration Compressor," M.S.M.E Thesis, Ray W. Herrick Lab., School of Mechanical Engineering, Purdue University, May 1987

[51] R. Srikanth, "How the Design of the Suction Return Affects Compressor Efficiency" M.S.M.E Thesis, Ray W. Herrick Lab., School of Mechanical Engineering, Purdue University, May 1987

VITA

VITA

Mr. Kim, Jonghyuk was born in Kimchon, Korea, on June 14 1955. He received his B.S. degree in Mechanical Engineering from Seoul National University, Korea in 1977 and his M.S. degree in Mechanical Engineering from the Korea Advanced Institute of Science in 1979. Since then, he worked as a structural design engineer for Samsung Heavy Indusrties, Korea for four and half year. He is married to Chula Kim in 1982 and they have a daughter Chris Soyoung.

In January 1985, he joined the Ray W. Herrick Laboratory, Purdue University for his Ph.D. study in the area of the compressor research.